FUNCTIONAL GENETIC SCREENING AND THERAPEUTIC TARGETING OF RECURRENT GLIOBLASTOMA

FUNCTIONAL GENETIC SCREENING AND THERAPEUTIC TARGETING OF RECURRENT GLIOBLASTOMA

BY CHIRAYU RAJENDRA CHOKSHI, (H)B.Sc.

A Thesis Submitted to the School of Graduate Studies in Partial Fulfillment of the Requirements for the Degree Doctor of Philosophy

DOCTOR OF PHILOSOPHY (2022)
Biochemistry and Biomedical Sciences
McMaster University
Hamilton, ON Canada

TITLE: Functional genetic screening and therapeutic targeting of recurrent glioblastoma

AUTHOR: Chirayu Rajendra Chokshi, (H)B.Sc. (McMaster)
SUPERVISOR: Dr. Sheila K. Singh
NUMBER OF PAGES: TBD

LAY ABSTRACT

Glioblastoma remains the most lethal and prevalent primary brain tumor in adults. Standard of care for patients remains unchanged since 2005, consisting of surgery to remove visible tumor at diagnosis (primary tumor), followed by radiation therapy and chemotherapy to treat remaining tumor cells. Despite these therapeutic efforts, tumor relapse (recurrent tumor) is inevitable with no standardized second-line therapy. Patients succumb to recurrent disease with a median overall survival of 14.6 months and only 5.5-6.8% of patients survive five years post diagnosis.

Therapy failure and tumor relapse are explained by immense diversity among tumor cells at the DNA and protein levels, giving rise to a subset of tumor cells with abilities to resist therapy and seed the recurrent tumor. Previous studies have presented evolution of tumor cells through therapy, with recurrent tumor cells harboring novel changes at the DNA and protein levels. However, the impact of these changes on tumor cell function has not been evaluated.

In this thesis, we developed and applied a genetic screening technique to determine the functional role of thousands of genes in primary and recurrent tumor cells from the same patient. This analysis revealed numerous genes that exhibit differential effects on survival of primary and recurrent tumor cells, including genes that drive recurrent tumor cell growth but are dispensable in primary tumor cells.

Functional remodeling of these genes and pathways revealed a new functional role of multiple proteins belonging to a process called axonal guidance in recurrent tumor cells. To evaluate the therapeutic potential of these findings, we deeply interrogated the mechanism by which axonal

guidance drives recurrent tumor cells and targeted crucial molecular players using chemical and immunological therapies. Using models that predict clinical effectiveness, we engineered and tested a novel therapy that redirects immune cells to target recurrent tumor cells driven by dysfunctional axonal guidance activity. The goal of this thesis was to discover the functional differences between primary and recurrent tumor cells, thereby leveraging this information to engineer candidate therapies for treatment of recurrent glioblastoma.

ABSTRACT

Glioblastoma (GBM) remains the most aggressive and prevalent malignant primary brain tumor in adults. Unchanged since 2005, standard of care (SoC) consists of surgical resection, followed by radiation therapy (RT) with concurrent and adjuvant chemotherapy with temozolomide (TMZ). Despite these therapeutic efforts, patients succumb to recurrent disease with a median overall survival of 14.6 months and a five-year survival rate of 5.5-6.8%. Therapeutic failure is largely explained by ITH and the presence of treatment-resistant GBM stem-like cells (GSCs). Given the lack of understanding of recurrent GBM and absence of second line therapies patients, I hypothesize that genome-scale functional genetic interrogation will unravel recurrent GBM-specific tumor biology and inform development of novel therapeutics.

First, I compared primary and recurrent GBM at the genetic, transcriptomic, proteomic and functional genetic levels. These analyses map a multilayered genetic response to drive tumor recurrence, identifying protein tyrosine phosphatase 4A2 (*PTP4A2)* as a novel modulator of self-renewal, proliferation and tumorigenicity at GBM recurrence. Mechanistically, genetic perturbation and a small molecule inhibitor of PTP4A2 repress axon guidance activity through a dephosphorylation axis with roundabout guidance receptor 1 (ROBO1) and exploit a genetic dependency on ROBO signaling. Importantly, engineered anti-ROBO1 single-domain antibodies also mimic the effects of PTP4A2 inhibition.

Given the genetic dependency on ROBO signaling and enrichment of ROBO1 expression in GBM tissues, I undertook a campaign to evaluate ROBO1 as a therapeutic target in recurrent GBM and develop anti-ROBO1 chimeric antigen receptor T (CAR-T) cells using camelid single-domain

antibodies targeting human ROBO1. I optimized the design of anti-ROBO1 CAR-T cells and tested the anti-tumor activity of these modalities in in vitro using patient-derived recurrent GBM lines and orthotopic patient-derived xenograft models. I present data to expand the repertoire of GBM-enriched antigens suitable for effective CAR-T cell therapy. Given that resistance to SoC and disease relapse are inevitable for GBM patients, pre-clinical and clinical advancement of immunotherapeutic modalities, combined with recent insights into the tumor immune microenvironment, are poised to improve clinical outcomes for this patient population.

ACKNOWLEDGEMENTS

My graduate studies would not have been as rewarding and successful without the unwavering support and guidance from my supervisor, Dr. Sheila K. Singh. You provided an enriching platform to grow as a scientist, establish a high level of scientific rigor, provided opportunities to expand my research beyond convention, and taught me to always ask clinically-relevant questions. I would also like to thank my graduate supervisory committee members (Drs. Kristin Hope and Jason Moffat) for their guidance, support and encouragement. I was fortunate enough to complete a research rotation in the Jason Moffat Lab, an experience that I will always cherish.

Beyond my supervisory committee, I would like to thank Dr. Chitra Venugopal, Dr. Kevin Brown, David Tieu and Benjamin Brakel who were my guides and allies through the day-to-day struggles and successes. To all members of the Sheila Singh and Jason Moffat lab – thank you for your support and guidance!

Most importantly, I would like to thank my parents, Rajendra and Usha Chokshi. I am eternally grateful that you took the risk of immigrating halfway across the world to provide me with opportunities beyond my dreams. Your love and dedication to my growth and success is second to none!

I dedicate this thesis to patients and their families whose courage, perseverance and dedication to scientific research will remain my largest source of motivation!

Table of Contents

List of Figures and Tables

List of Abbreviations and Symbols

+7/-10	Gain of chromosome 7/loss of chromosome 10
AC	Astrocyte-like
APC	Antigen presenting cell
α-KG	α-ketoglutarate
B7-H3	B7 family member B7-H3
BBB	Blood brain barrier
BF	Bayes Factor
BLI	Bioluminescence
BTIC	Brain tumor initiating cell
BTSC	Brain tumor stem cells
CAR-T	Chimeric antigen receptor T
CEG	Core essential genes
CGGA	Chinese Glioma Genome Atlas
cGI	Conditional genetic interaction
CNS	Central nervous system
CT	Computerized tomography
CTLA-4	Cytotoxic T lymphocyte antigen 4
CTNNB1	β-catenin
D-2-HG	D-2-hydroxyglutarate
DC	Dendritic cell
DEG	Differentially expressed genes
ECD	Extracellular domain
FA	Fanconi anemia
FDR	False discovery rate
FLAIR	Fluid-attenuated inversion recovery
GATK	Genome Analysis Toolkit
GBM	Glioblastoma
gRNA	Guide RNA
GSC	Glioblastoma stem-like cell
GSEA	Gene set enrichment analysis
HER2	Human epidermal growth factor receptor 2
ICI	Immune checkpoint inhibitor
IL13Rα2	Interleukin-13 receptor subunit alpha-2
ITH	Intratumoral heterogeneity
KPNA2	Karyopherin subunit alpha 2
LFC	Log fold change
LGG	Low grade glioma
MES	Mesenchymal

MGMT	O6-methylguanine-DNA methyltransferase
MMP2	Matrix metallopeptidase 2
MRI	Magnetic resonance imaging
MSI	Microsatellite instability
NES	Nestin
NES	Normalized enrichment score
NKG2D	NKG2-D type II integral membrane protein
NPC	Neural progenitor
NSC	Neural stem cell
OPC	Oligodendrocyte
OXA1L	Mitochondrial gene oxidase (cytochrome C) assembly 1-like
PBMC	Peripheral blood mononuclear cells
PD-1	Programmed cell death protein 1
PDGFA	Platelet-derived growth factor α
PDX	Patient-derived xenograft
PFS	Progression free survival
PTP4A2	Protein tyrosine phosphatase 4A2
RB	Retinoblastoma-associated protein
ROBO1	Roundabout guidance receptor 1
RT	Radiation therapy
RTK	Receptor tyrosine kinase
scRNA-seq	Single cell RNA sequencing
SF	Sphere formation
SIRPα	Signal regulatory protein α
SLIT2	Slit guidance ligand 2
SoC	Standard of care
SOX2	SRY-Box transcription factor 2
TCGA	The Cancer Genome Atlas
TIME	Tumor immune microenvironment
TM	Transmembrane
TMZ	Temozolomide
VEGF	Vascular endothelial growth factor
WHO	World Health Organization

Declaration of Academic Achievement

I contributed to the design and execution of the work presented in this thesis. I designed and executed experiments, performed data analysis, interpretation and writing of all sections. Dr. Sheila K. Singh supervised all research projects and aided in project planning and data interpretation. Contributions of co-authors to each publication are noted in preamble for Chapters 2-4. This thesis is presented in the format of a "sandwich" thesis as outlined in the "guide for preparation of Master's and Doctoral Theses" (v2016).

Chapter 1 gives an overview of the field of glioblastoma research and emerging immunotherapies. It contains excerpts from the following published work:

> **Chokshi, C. R.**, Brakel, B. A., Tatari, N., Savage, N., Salim, S. K., Venugopal, C., & Singh, S. K. (2021). Advances in Immunotherapy for Adult Glioblastoma. Cancers, 13(14), 3400.

Chapter 2 is an original manuscript describing insights into treatment resistance and disease recurrence in glioblastoma using genome-scale CRISPR-Cas9 screening:

> **Chokshi, C. R.,** Tieu, D., Brown, K. R., Venugopal, C., Liu, L., Kuhlmann, L., Rossotti, M.A., Chan, K., Tong, A. H. Y., Savage, N., McKenna, D., Aghaei, N., Subapanditha, M., Shaikh, V.M., Tatari, N., Brakel, B., Nachmani, O., Ignatchenko, V., Salamoun, J. M., Wipf, P., Sharlow, E. R., Provias, J. P., Lu, J. Q., Murty, N. K., Lazo, J. S., Kislinger, T., Henry, K. A., Lu, Y., Moffat, J., & Singh, S. K. Functional mapping reveals widespread remodelling in recurrent glioblastoma. (manuscript in preparation)

Chapter 3 is an original manuscript describing the development and testing of a novel chimeric antigen receptor (CAR) T cell therapy for recurrent glioblastoma:

Chokshi, C. R., Brakel, B. A., Rossotti, M. A., Venugopal, C., Salim, S. K., Henry, K. A., Singh, S. K. Anti-ROBO1 CAR T cells effectively target pediatric and adult malignant brain cancer. (manuscript in preparation)

Chapter 5 discusses the implications of the research presented in this thesis and explores future research directions to improve understanding of glioblastoma and effectively target this deadly disease.

CHAPTER 1: Introduction

Preamble

This chapter presents an introduction into glioblastoma (GBM), including clinical characteristics and prognosis of GBM patients, current standard of care and approved therapies, molecular characterisation and classification of GBM, intratumoral heterogeneity and the cancer stem cell hypothesis in GBM, the inevitability of treatment resistance and tumor recurrence, and emerging therapeutics that modulate the tumor immune microenvironment (TIME). Lastly, I present the hypothesis and overall aims of this thesis.

This chapter contains excerpts from the following published review:

> **Chokshi, C. R.**, Brakel, B. A., Tatari, N., Savage, N., Salim, S. K., Venugopal, C., & Singh, S. K. (2021). Advances in Immunotherapy for Adult Glioblastoma. Cancers, 13(14), 3400.

This chapter also contains excerpts from the following original manuscript:

> **Chokshi, C. R.,** Tieu, D., Brown, K. R., Venugopal, C., Liu, L., Kuhlmann, L., Rossotti, M.A., Chan, K., Tong, A. H. Y., Savage, N., McKenna, D., Aghaei, N., Subapanditha, M., Shaikh, V.M., Tatari, N., Brakel, B., Nachmani, O., Ignatchenko, V., Salamoun, J. M., Wipf, P., Sharlow, E. R., Provias, J. P., Lu, J. Q., Murty, N. K., Lazo, J. S., Kislinger, T., Henry, K. A., Lu, Y., Moffat, J., & Singh, S. K. Functional mapping reveals widespread remodelling and unrecognized pathway dependencies in recurrent glioblastoma. (manuscript in preparation)

1.1 Glioblastoma

1.1.1 Clinical characteristics and prognosis

Glioblastoma (GBM) remains the most common malignant primary brain tumor in adults (Vargas Lopez, 2021; Weller et al., 2021; Wen et al., 2020). Following diagnosis, patients undergo an aggressive standard of care (SoC) that consists of surgical resection of the bulk tumor, followed by chemoradiotherapy. However, tumor recurrence is inevitable with a median overall survival of <15 months post-diagnosis and a five-year survival rate of only 6.8% (Ostrom et al., 2021; Stupp et al., 2009). GBM has an incidence rate of 3.23 per 100,000 individuals, with a higher incidence in males (4.04) compared to females (2.53), and accounts for 14.3% of all primary brain and other CNS tumors and 49.1% of primary malignant tumors . Incidence rates were highest in individuals age 75-84 years (Ostrom et al., 2021). Despite substantial progress in understanding tumor biology, there have been no changes to SoC since the addition of alkylating agent temozolomide (TMZ) to radiotherapy in 2005 (Stupp et al., 2009; Stupp et al., 2005).

According to the World Health Organization (WHO) classification of central nervous system (CNS) tumors, GBM is a grade 4 tumor histologically-characterized by florid microvascular proliferation, necrosis with or without pseudopalisading, abnormal cellular and nuclear atypia, and poor differentiation with sparse mitotic activity (Louis et al., 2021; Whitfield and Huse, 2022). In addition to histological features, the 2021 WHO classification requires at least one of the following criteria to classify an *IDH*-wildtype diffuse and astrocytic glioma as GBM: *TERT* promoter mutation, *EGFR* amplification, and gain of chromosome 7/loss of chromosome 10 (+7/-10) (Louis et al., 2021; Whitfield and Huse, 2022). *TERT* promoter mutations lead to telomerase reactivation that maintains telomere length, while *EGFR* amplification increases downstream signaling

promoting survival and cellular proliferation. However, the biological significance of +7/-10 is poorly understood, with the exception that gain of chromosome 7 leads to increased expression of secreted platelet-derived growth factor α (*PDGFA*) (Ozawa et al., 2014).

Between 2014 to 2018 in the USA, GBM accounted for 14.3% of all brain and other CNS tumors and 49.1% of malignant tumors, of which 74.2% were *IDH*-wildtype, 2.0% *IDH*-mutant and 21.1% with *IDH* status unknown (Ostrom et al., 2021). Missense IDH mutations are found in >80% of grade II/III gliomas, and prior to recent reclassification by the WHO (Louis et al., 2021), *IDH*-mutant low grade astrocytic and oligodendroglial gliomas that recurred as grade IV tumors were diagnosed as secondary GBM (Louis et al., 2016). Under normal conditions, isocitrate dehydrogenase or IDH enzymes function as homodimers to convert isocitrate to α-ketoglutarate (α-KG), participating in multiple metabolic processes such as the Krebs cycle, glutamine and lipid metabolism, and redox regulation (Koh et al., 2004; Lee et al., 2004). Heterozygous mutations of arginine residues within the IDH catalytic site (R132 for IDH1, R140 or R172 for IDH2) lead to neomorphic enzymatic activity by mutant IDH, which further converts α-KG to D-2-hydroxyglutarate (D-2-HG) in an NADPH-dependent manner (Dang et al., 2009; Yan et al., 2009). Accumulation of D-2-HG in tumor cells depletes α-KG and shifts carbohydrate sources to glutamine, glutamate and branched-chain amino acids (Dang et al., 2009; McBrayer et al., 2018; Reitman et al., 2011; Waitkus et al., 2018). In addition, mutant IDH reduces glycolysis, shifts tumor cells to glutamine-derived lipogenesis and leads to global CpG island DNA hypermethylation and histone methylation, which may explain the relatively slow growth of IDH-mutant GBM (Christensen et al., 2011; Noushmehr et al., 2010; Reitman et al., 2014).

GBM tumors harbouring an IDH mutation doubled median patient survival to 31 months compared to 15 months for IDH wildtype tumors (Cancer Genome Atlas Research et al., 2015; Eckel-Passow et al., 2015; Yan et al., 2009). Despite identical histological features, these survival differences supported a reclassification of IDH-mutant GBM tumors as grade IV IDH-mutant astrocytoma, whereas all IDH-wildtype grade IV tumors with EGFR amplification, +7/-10, or *TERT* promoter mutation are now considered GBM (Louis et al., 2021). This introduction and subsequent chapters will largely focus on exploring the biology and therapeutically-targeting IDH-wildtype GBM.

1.1.2 Standard of care and approved therapies

In the clinic, GBM patients initially present with non-specific neurological symptoms stemming from raised intracranial pressure due to tumor formation and include general symptoms (e.g. headache, fatigue, nausea, etc.), motor and sensory symptoms (e.g. ataxia, speech deficit, visual impairment, etc.), otoneurological symptoms (e.g. dizziness, vertigo), and neuropsychological symptoms (e.g. depression, anxiety, cognitive impairment, etc.) (Lyratzopoulos et al., 2013; Walter et al., 2019).

Following a magnetic resonance imaging (MRI) or computerized tomography (CT) scan suggestive of a high grade glioma, patients undergo maximum safe resection of the tumor (Weller et al., 2021). Following a GBM diagnosis, patients under 70 years of age with a Karnofsky performance status ≥70 undergo SoC that includes daily fractionated radiation therapy with concurrent TMZ over six weeks, and additional cycles of adjuvant TMZ for up to six months (2021; Lapointe et al., 2018; Stupp et al., 2005; Weller et al., 2021). In addition to SoC, two therapeutics have received approval from the Food and Drug Administration, including (1) an anti-vascular endothelial growth factor (VEGF) monoclonal antibody bevacizumab, and (2) tumor-

treating fields that target proliferating tumor cells. However, these therapies have yet to be incorporated into SoC for GBM patients.

1. Maximal safe surgical resection

   The preferred initial intervention is maximal safe surgical resection of the gadolinium-enhancing tumor and is aimed to reduce gross tumor volume (cytoreduction) and tumor-mediated immune suppression, provide diseased tissue for pathology, relieve neurological symptoms and intracranial pressure, and increase efficacy of subsequent chemoradiotherapy (Brown et al., 2016b; Lacroix et al., 2001; Sanai et al., 2011). Considering the highly invasive nature of GBM, supratotal resection of the tumor is an emerging approach that includes the T1 gadolinium-enhanced region and the FLAIR (fluid-attenuated inversion recovery) abnormal region to increase tumor cytoreduction, prolonging GBM patient median survival to 18.5 months compared to 14 months for conventional gross total resection (Eyupoglu et al., 2016; Li et al., 2016; Pessina et al., 2017). Building on this approach, a retrospective study by Roh et al. (2019) presented a greater significant survival benefit for GBM patients that underwent a lobectomy to safely remove tumor-containing nondominant frontal or temporal lobes (PFS: 30.7 months), compared to conventional gross total resection (PFS: 11.5 months). These advances in surgical resection, including the use of tumor visualization agents such as 5-ALA (Schupper et al., 2021), continue to increase the extent of safe maximal tumor resection and directly correlate with improved patient survival and a better quality of life.

2. Radiation therapy (RT)

   Following surgical resection and a GBM diagnosis, the gold standard SoC protocol recommends daily fractionated radiation therapy with a dosage of 60 Gy over 30 fractions

for six weeks with concurrent TMZ (Cabrera et al., 2016). Next to surgical resection, radiation therapy continues to increase overall survival in the vast majority of GBM patients and has been a cornerstone of GBM therapy for ~50 years (Sheline, 1977; Walker et al., 1979).

3. Temozolomide (TMZ)

TMZ is a DNA alkylating agent that is administered concurrently with radiation therapy (75 mg/m^2) followed by 6-12 cycles of adjuvant TMZ (150-200 mg/m^2). Addition of TMZ to radiation therapy improved median GBM patient survival by approximately 2.5 months (Stupp et al., 2005). At the molecular level, TMZ is a prodrug that belongs to a class of bicyclic aromatic heterocycles called imidazotetrazines. Under neutral or alkaline conditions, the hydrolytic ring opens and yields the open chain trizene MTIC as the first significant intermediate. This activated intermediate further separates to liberate AIC and methyl diazonium ions. These methyl diazonium ions elicit the pharmacological activity of TMZ by methylating nucleophilic sites on DNA, predominantly methylating N3 and N7 nucleophilic sites on adenine (10-20%) and guanine (60-80%), respectively. However, these methylation sites are efficiently repaired by base excision repair. Aside from sites of major activity, TMZ methylates the O6 site on guanine (10%; O6-meG) which leads to a wobble base mispairing of O6-meG with thymine. Although the DNA mismatch repair pathway recognizes this defect and replaces the mismatched thymine, this cyclical process eventually leads to thymine depletion, genomic instability, long-lived double strand DNA breaks and eventual apoptosis (Danson and Middleton, 2001; Moody and Wheelhouse, 2014). Unfortunately, O6-meG is actively removed by O6-methylguanine-DNA methyltransferase (*MGMT*) , and consequently, a greater benefit of TMZ treatment on

patient survival is seen with a methylated *MGMT* promoter (48.5% of all patients) (Hegi et al., 2005; Parsons et al., 2008). TMZ treatment remains as part of SoC for all eligible GBM patients irrespective of *MGMT* promoter methylation status; however, removal of TMZ therapy for patients with an unmethylated *MGMT* promoter (>50%) may allow for addition of other therapeutic agents and avoidance of TMZ-induced hypermutation (Alexander et al., 2018; Hegi et al., 2005; Stupp et al., 2009).

1.2 Molecular characterization and classification of GBM

1.2.1 Molecular landscape of GBM

Although GBM has a lower tumor mutational burden than other solid tumors (Alexandrov et al., 2013), the molecular landscape of GBM exhibits a wide variety of genetic, epigenetic and transcriptomic events that contribute to intra- and inter-tumoral heterogeneity. Chromosomal changes commonly observed in GBM include amplification of chromosomes 4 (*PDGFRA*), 7 (*EGFR/MET/CDK6*), 12 (*CDK4/MDM2*), and deletion of chromosome 10 (*PTEN*) (Brennan et al., 2013). At a gene level, frequent mutations include *TP53* (34.4%), *EGFR* (32.6%), *PTEN* (32%), *NF1* (13.7%), *PIK3CA* (11.7%), *PIK3R1* (11.7%), *RB1* (9.3%), *SPTA1* (9%), *ATRX* (6%), *IDH1* (5.2%), *KEL* (5%), *PDGFRA* (4.5%) and *GABRA6* (4%) (Brennan et al., 2013; Cancer Genome Atlas Research, 2008; Parsons et al., 2008; Verhaak et al., 2010).

In addition to genomic aberrations, changes at the epigenetic level, including DNA methylation, correlate with tumor biology and patient survival (Etcheverry et al., 2010; Hegi et al., 2005; Romani et al., 2018). Frequently methylated genes include *GATA6* (68.4%), *CASP8* (56.8%), *MGMT* (48.5%), *CD81* (46.1%) and *DR4* (41.3%) (Brennan et al., 2013; Parsons et al., 2008; Skiriute et al., 2012). Of these, one of the most clinically-relevant change is correlation of a

methylated *MGMT* gene promoter with greater TMZ efficacy and longer overall patient survival (Hegi et al., 2005). Genome-wide analysis of DNA methylation separated tumors into distinct subtypes (M1 – M4, G-CIMP and M6), with the G-CIMP phenotype correlating with the proneural transcriptomic subtype (described in section 1.2.2), a survival advantage, *MGMT* promoter methylation, and *IDH* mutation (Brennan et al., 2013).

1.2.2 Subtyping GBM via bulk tumor transcriptomics

A collection of groups have utilized gene expression profiles to classify GBM tumors into subtypes using microarray technology (Nutt et al., 2003; Phillips et al., 2006; Rickman et al., 2001), followed by next-generation sequencing (Park et al., 2019; Parsons et al., 2008; Verhaak et al., 2010), and further delineated using single-cell sequencing technology (Neftel et al., 2019; Patel et al., 2014). Here, we will discuss four major transcriptomic subtypes introduced by the Cancer Genome Atlas (TCGA) in Verhaak et al. (2010), namely proneural, neural, classical and mesenchymal. Further insights into GBM subtyping and heterogeneity are summarized in section 1.3.1.

The proneural subtype of GBM is characterized by expression of *PDGFRA*, *OLIG2*, *DDL3*, *SOX2* and *NKX2-2*, with identifying mutations in *TP53*, *PI3K*, *IDH1* and *PDGFRA*. Notably, proneural GBM with *IDH* mutations, largely stemming from lower grade *IDH*-mutant gliomas, may be reclassified as grade IV *IDH*-mutant astrocytoma given the recent tumor reclassification by the WHO (Louis et al., 2021). Compared to other subtypes, patients with predominantly proneural GBM tumors tend to be younger and may have better survival rates, with a median overall survival of 17.0 months (Verhaak et al., 2010). However, these differences do not correlate with a

significant difference in sensitivity to SoC chemotherapy or radiation therapy (Colman et al., 2010).

The neural subtype of GBM is characterized by expression of *MBP/MAL*, *NEFL*, *SLC12A5*, *SYT1*, and *GABRA1*. Unlike the other three subtypes, neural GBM tumors are not associated with a distinct mutation signature and tend to be more sensitive to SoC chemotherapy and radiation therapy as compared to other subtypes. However, subsequent analyses revealed that this subtype predominantly represents non-tumor brain cells in the tumor microenvironment and is no longer used for subtyping (Verhaak et al., 2010; Wang et al., 2017).

The classical subtype of GBM is characterized by expression of *EGFR*, *AKT2*, *SMO*, *GAS1*, *GLI2*, *NOTCH3*, *JAG1*, and *LFNG*, with identifying mutations in *PTEN*, *CHKN2*, and *PDGFRA*. In addition, classical GBM tumors are accompanied by +7/-10, inactivation of the retinoblastoma-associated protein (RB) pathway, and homozygous focal deletion of 9p21.3. In addition to these gene-level aberrations, classical GBM tumors are driven by fundamental neurodevelopment pathways such as Sonic hedgehog pathways (*SMO*, *GLI2*, *GAS1*), Notch signaling pathways (*NOTCH3*, *JAG1*, *LFNG*), and enrichment of neural precursor and stem cell marker Nestin (*NES*) (Colman et al., 2010; Verhaak et al., 2010). Unlike other subtypes, patients with classical GBM tumors respond favourably to aggressive SoC radiation therapy and chemotherapy (Verhaak et al., 2010).

Considered the most aggressive subtype, mesenchymal GBM tumors are characterized by widespread tumor necrosis, a relatively inflamed microenvironment, and angiogenesis. This

subtype is identified by expression of *YKL40*, *MET*, *CD44*, *MERTYK*, *TRADD*, *RELB*, and *TNFRSF1A*, with frequent mutations in *NF-KB* and *NF1*. Mesenchymal GBM tumors are also accompanied by +7/-10, frequent deletion of tumor suppressor genes *TP53* and *PTEN*, and respond objectively to aggressive SoC radiation therapy and chemotherapy. Despite a favourable response, predominantly mesenchymal GBM tumors are associated with the worst prognosis among other subtypes (Colman et al., 2010).

Interestingly and unlike subtyping efforts in other solid tumors (e.g. medulloblastoma, breast cancer), transcriptomic-based subtyping of GBM tumors does not lead to predictable prognostic differences or customized treatment regimens. However, some partial associations were noted in a study by Cho et al. (2019). In this study, prognosis-led subtyping based on gene expression identified three functional subtypes: poor, intermediate, and favorable. The 'poor' prognosis subset of GBM patients displayed highly invasive tumors, as compared to a relatively 'favorable' subset with a mitotic signature and focal tumors. Predictably, the 'invasive' subtype overlapped with the mesenchymal and classical subtypes, whereas the 'favorable' subtype was largely comprised of neural and proneural tumors that responded well to TMZ treatment. Inconsistency of the relationship between tumor subtyping and patient prognosis is explained by the heterogeneous presence of tumor cells of multiple subtypes in a single tumor, as first introduced by Patel et al. (2014) and confirmed later by multiple groups (Couturier et al., 2020; Darmanis et al., 2017; Jacob et al., 2020; Neftel et al., 2019; Patel et al., 2014; Yu et al., 2020).

Since the adaptation of TCGA subtypes in GBM research, a recent single cell RNA sequencing (scRNA-seq) study by Neftel et al. (2019) expanded on subtyping efforts by introducing meta-

signatures to identify four plastic cellular states present across 28 GBM specimens: astrocyte-like (AC-like), mesenchymal-like (MES-like), oligodendrocyte progenitor-like (OPC-like), and neural progenitor-like (NPC-like). With the greatest fractions of cycling cells, NPC-like and OPC-like tumors correlated with *CDK4* and *PDGFRA* amplification, respectively. AC-like tumors harboured *EGFR* amplification mutations whereas MES-like tumors were often associated with chromosome 5q deletion, *NF1* alteration, immune infiltration and hypoxic regions (Neftel et al., 2019). In comparison to TCGA subtypes (Verhaak et al., 2010), proneural tumors were predominantly composed of NPC-like and OPC-like tumor cells whereas neural tumors were largely composed of non-cancerous oligodrocytes, further supporting removal of the neural subtype as a tumor classification. In addition, classical tumors were composed of AC-like cells, and mesenchymal tumors were composed of infiltrating macrophages and MES-like cells. Despite the increased resolution of scRNA-seq, subtyping efforts stop short of informing patient prognosis due to intratumoral heterogeneity.

1.3 Intratumoral heterogeneity and cancer stem cells

1.3.1 Molecular heterogeneity in pre-treatment primary GBM

As described by GBM's previous name 'glioblastoma multiforme', tumor regions within a single specimen and across patients have revealed histological variations prior to molecular profiling (Burger and Green, 1987). More recently, Reinartz et al. (2017) showed that single cell-derived subclones of freshly-resection GBM specimens led to differential drug response, tumorigenicity and histological features upon xenotransplantation, and distinct genetic identities. Development of whole genome sequencing methods revealed heterogeneity among and within GBM specimens, including chromosome alterations (Nobusawa et al., 2010), somatic mutations (Kumar et al., 2014), gene amplification (Snuderl et al., 2011), and extrachromosomal DNA (deCarvalho et al.,

2018). Similar to other solid tumors, dysregulation of receptor tyrosine kinases (RTKs; e.g. EGFR, PDGFRA) and their downstream effectors (e.g. PI3K, PTEN) is ubiquitous in GBM (Brennan et al., 2013). Complementary studies by Snuderl et al. (2011) and Szerlip et al. (2012) revealed amplification of different RTKs in distinct cell subpopulations of GBM specimens, and functionally, poly-targeting of multiple RTKs (EGFR and PDGFRA) was necessary to inhibit downstream PI3K signaling and tumor growth. Additionally, variants of EGFR (EGFRvIII and other carboxy-terminal deletions) have been found to be subclonal events and present in mutually exclusive tumor cell populations (Francis et al., 2014). The recent discovery of extrachromosomal DNA in GBM highlighted its association with oncogene amplification and tumor growth, further confounded by its uneven inheritance between daughter cells (Kim et al., 2020). In fact, non-coding epigenetic enhancer regions interact with extrachromosomal EGFR loci to upregulate expression and impact tumor cell fitness (Morton et al., 2019). Although numerous clinical studies have tried to inhibit GBM progression using RTK-targeting modalities (Hegi et al., 2011; Weller et al., 2017), these approaches have yet to significantly impact patient survival due to limited penetration of agents across the blood brain barrier (BBB), tumor heterogeneity, and stochastic tumor evolution.

Following the introduction of molecular GBM subtypes by the TCGA (Verhaak et al., 2010), presence of multiple subtypes was shown in a single tumor. By analyzing distinct tumor regions from 11 patients with GBM, Sottoriva et al. (2013) found that regions from the same patient tumor specimen classify into distinct GBM subtypes, harbour different driver gene aberrations and copy number alterations. Using phylogenetic reconstruction of tumor fragments, this study also proposed that loss of *CDKN2A/B* and amplification of *CDK6, EGFR* and *MET* are early events in

tumor formation and are followed by later-stage alterations in *PDGFRA*, *PTEN* and *TP53* (Sottoriva et al., 2013). A study by Patel et al. (2014) was the first to capture tumor cells belonging to all TCGA subtypes (neural, proneural, classical and mesenchymal) within a single GBM using scRNA-seq. In addition, further analyses by Patel et al. (2014) explained contaminant normal brain cells as the source of neural GBMs, revealed 'hybrid' transcriptomic states in which a single tumor cell exhibited transcriptomic characteristics of more than one TCGA subtype, and posited that a greater amount of intratumoral heterogeneity (ITH) was associated with decreased patient survival. Not only do GBM patients harbour unique distributions of GBM subtypes within their tumor, but also harbour miscellaneous genomic aberrations such as patient-specific copy number variations (Couturier et al., 2020; Darmanis et al., 2017; Jacob et al., 2020; Neftel et al., 2019; Patel et al., 2014; Yu et al., 2020). A study by Lee et al. (2017) sampled multi-sector tumor regions from GBM patients to reveal spatially-distinct and -shared driver genetic alterations, such as clonal mutations in *PIK3CA* that were shared by all tumor regions whereas alterations in *PTEN* and *EGFR* represented subclonal events exclusive to certain tumor regions. These findings were further supported by unbiased molecular profiling of anatomically-defined regions of GBM tumors by the Ivy Glioblastoma Atlas Project (Puchalski et al., 2018). Microdissection of anatomically-informed tumor regions (e.g. leading edge, infiltration tumor, cellular tumor, etc.) showed similarity across GBM patients but failed to associate regions with mutational signatures. At the functional level, studies by Meyer et al. (2015) and Reinartz et al. (2017) show that single-cell derived clonal subpopulations from GBM specimens respond differentially to small molecule inhibitors and cells resistant to SoC may pre-exist in primary *de novo* GBM. These studies posit that pre-existing subclonal or therapy-driven events may drive treatment resistance and subsequent tumor recurrence in GBM.

1.3.2 Molecular heterogeneity at tumor recurrence

Exposure to pressures of stochastic tumor-intrinsic events, the tumor microenvironment and SoC likely leads to positive selection of resistant tumor subpopulations during GBM progression. A study by Johnson et al. (2014) conducted exome sequencing of 23 initial and patient-matched recurrent low-grade *IDH*-mutant gliomas. In 43% of all cases, greater than 50% of mutations seen in the primary tumors were lost at tumor recurrence, and in 6 of 10 patients treated with SoC chemotherapy agent TMZ, recurrent tumors were hypermutated and characterized by a TMZ-induced mutation signature. In a recent study by the Glass consortium of initial and patient-matched recurrent diffuse gliomas from 222 patients, of which 134 were *IDH*-wildtype, 70% of recurrent tumors harboured an increased mutational burden at recurrence (Barthel et al., 2019). Similar to changes at recurrence seen in lower grade gliomas, whole-genome and multisector exome sequencing of patient-matched pre- and post-SoC GBM specimens revealed that few recurrent tumors harboured *TP53* driver mutations seen in their predecessors, whilst the vast majority of recurrent tumors exhibited subclonal divergent events undetected in the primary tumor (Kim et al., 2015a). In fact, another study by Wang et al. (2016) showed that 66% of post-SoC recurrent tumors undergo a change in their dominant TCGA GBM subtype compared to their patient-matched primary tumor. Characterization of post-SoC tumor recurrences showed that, in contrast to locally adjacent tumors, geographically separated mutifocal tumors are driven by subclonal events and are genetically distinct from their primary predecessor (Lee et al., 2017). These studies and others (Favero et al., 2015; Korber et al., 2019; Mazor et al., 2015) continue to support large scale shifts in the genomic and transcriptomic landscape of GBM at recurrence, with SoC and additional unrealized pressures increasing entropy of this deadly disease over time.

1.3.3 The cancer stem cell hypothesis in GBM

At the cellular level, ITH can be explained by the existence of multiple cellular subpopulations of cancer cells that have acquired stem cell properties, variably labeled in the literature as brain tumor initiating cells (BTICs) or glioblastoma initiating cells (GICs) (Clarke and Fuller, 2006; Dalerba et al., 2007; Singh et al., 2003; Singh et al., 2004). Since cell surface markers allow sorting of bulk GBM into cellular subpopulations, much research has focused on the application of proteins such as CD133 (Singh et al., 2003; Singh et al., 2004), CD15 (Son et al., 2009), integrin alpha 6 (Lathia et al., 2010), and L1CAM (Bao et al., 2008) to define functional BTIC subgroups. In addition, intracellular proteins such as RNA binding protein MSI1 (Kaneko et al., 2000), transcription factors SOX2 (Graham et al., 2003), OCT4 (Suva et al., 2014) and FOXG1 (Manoranjan et al., 2013), and polycomb repressor BMI1 (Abdouh et al., 2009; Venugopal et al., 2012) that have a characterized functional role in driving normal neural stem cell (NSC) self-renewal, have also been investigated as putative BTIC markers. Although data suggests that GBM BTICs are chemo- (Beier et al., 2011) and radioresistant (Bao et al., 2006), no study has prospectively identified whether such BTICs are causal of tumor relapse, and which targetable genes and pathways within these treatment-resistant BTIC populations drive tumor recurrence.

1.4 Modulating the GBM tumor immune microenvironment (TIME)

1.4.1 Emerging therapeutics to modulate the tumor immune microenvironment

A major contributor to treatment failure is intra-tumoral heterogeneity that gives rise to tumor cell populations distinct at the genomic, transcriptomic, proteomic and functional levels (Kim et al., 2015b; Meyer et al., 2015; Neftel et al., 2019; Patel et al., 2014; Wang et al., 2016). In addition to SoC, two therapeutics have received approval from the Food and Drug Administration, including (1) an anti-vascular endothelial growth factor (VEGF) monoclonal antibody bevacizumab, and (2)

tumor-treating fields that target proliferating tumor cells. However, these therapies have yet to be incorporated into SoC for GBM patients. Emerging therapeutics for GBM have shifted towards reconfiguring the patient's immune system to generate an anti-tumor response.

1.4.2 Vaccines

Cancer vaccines function by exposing tumor-associated antigens to antigen-presenting cells (APCs) which activate immune effector cells to achieve an anti-cancer immune response. Several promising vaccines targeting both single and multiple antigens have shown varying degrees of clinical promise, however, vaccines for GBM have yet to translate to SoC. While GBM-specific targets are sparse, several have been identified that are expressed on the cell surface. Perhaps the most explored to date, EGFR variant III (EGFRvIII) is a mutant receptor specific to GBM which has been targeted extensively through a variety of immunotherapeutic efforts including vaccination. Similarly, the cytomegalovirus (CMV) tegument phosphoprotein 65 (pp65) and IDH1(R132H)-mutant peptides are frequently and specifically expressed in GBM, in contrast to healthy brain (Bleeker et al., 2009; Mitchell et al., 2008). Vaccinations targeting these proteins have shown efficacy in clinical trials and often elicit strong responses, however, no targets identified to date are expressed on all GBM cells, allowing clonally driven recurrence to evade such treatments. In contrast, multi-targeted vaccines mediating the presentation of multiple tumor-associated antigens better address the heterogeneity of the tumor by reducing the population of cells not expressing a target and thus reducing clonally driven resistance, however, these treatments have shown little success.

Antigen presentation and the following activation and regulation of effector cells is another important process in achieving an effective immune response, which involves several proteins

such as those mediating suppression of T cells, macrophages, and other tumor infiltrating lymphocytes. Current efforts acting on this front, such as antibodies against these suppressors, have shown preclinical promise but have fallen short in clinical trials. Additionally, success seems to vary greatly upon combination of these inhibitors, underlining the importance of understanding and enhancing synergistic interactions between treatments.

1.4.3 Immune checkpoint inhibitors

A complex system of stimulatory and inhibitory regulators functions to maintain immune homeostasis. An important part of this system is immune checkpoints, which regulate activation to avoid autoimmunity. Upon activation or exhaustion, several immune cells upregulate these inhibitory checkpoints thus suppressing the immune response. Cancer cells express immune checkpoint proteins as well, allowing them to suppress the anti-cancer response. As a result, antibodies against these checkpoints known as immune checkpoint inhibitors (ICI) have been developed and have shown success in several cancers such as melanoma and non-small-cell lung cancer (Vaddepally et al., 2020), and several are underway for GBM (Table 2). Of these antibodies, the most advanced group are those blocking programmed cell death protein 1 (PD-1) and cytotoxic T lymphocyte antigen 4 (CTLA-4), which are expressed on T cells and prevent T cell stimulation and killing of glioma cells (Contardi et al., 2005; Davidson et al., 2019).

1.4.4 Chimeric antigen receptor T (CAR-T) cells

Chimeric antigen receptor (CAR) T cells represent an efficacious form of adoptive T cell therapy, in which peripheral T cells are genetically engineered to express a fusion receptor protein (i.e. CAR) that recognizes and targets a tumor-specific or -enriched antigen. Rapid and rational evolution of receptor design has transformed a first-generation CAR – composed of a ligand-binding domain, extracellular spacer, transmembrane domain and an intracellular signaling

domain – that suffered from limited signaling strength to highly efficacious second- and third-generation CARs that incorporate one or more intracellular co-stimulatory domains, respectively, to initialize and sustain T cell signaling (Finney et al., 2004; Finney et al., 1998; Imai et al., 2004; Sadelain et al., 2013). Irrespective of design principles, an antigen-bound CAR T cell activates a potent cytokine release and cytolytic degranulation response that kills antigen-expressing tumor cells and results in T cell proliferation (Hombach et al., 2001). CAR T cell therapy has been highly effective against hematological malignancies, achieving remission rates of up to 90% in patients with relapsed or refractory B cell malignancies with anti-CD19 CAR T cells (Maude et al., 2014). However, widespread clinical responses of CAR T cells have yet to be seen for solid tumors, including GBM.

Unlike hematological malignancies, CAR T cell therapy design and administration require unique considerations in the context of GBM, including factors such as intratumoral antigen heterogeneity, bypassing the blood-brain barrier (BBB) and exerting a potent anti-tumor response in a highly immunosuppressive microenvironment (Bagley et al., 2018). Two schools of thought have guided delivery of CAR T cell therapy to the brain thus far, one which supports systemic intravenous administration, and the other prefers intracavitary or intraventricular dosing to bypass the BBB. Supported by reports of a dysregulated BBB in GBM patients (Sarkaria et al., 2018; Watkins et al., 2014), investigators evaluating CAR T cell therapies targeting EGFRvIII and HER2 preferred intravenous delivery of their modality (Ahmed et al., 2010; O'Rourke et al., 2017). Although no dose-limiting toxicities were observed for either modality when delivered intravenously, three grade 2-4 adverse events were possibly associated with HER2 CAR T cell therapy, including headache (n = 1) and seizure (n = 2). In contrast, intracavitary (or intratumoral)

delivery of CAR T cells is not functionally restricted by the BBB. Using a reporter gene system, preliminary clinical evidence supports trafficking of intracerebrally-administered anti-IL13Rα2 CAR T cells to the tumor region using [^{18}F]FHBG PET-based imaging (Keu et al., 2017). Intracavitary treatment of GBM patients with anti-IL13Rα2 CAR T cells resulted in no dose-limiting toxicities (Brown et al., 2016a; Brown et al., 2015). However, similar to intravenous delivery of anti-EGFRvIII CAR T cells, two grade 3 adverse events were associated with the treatment, including headache (n = 1) and a neurologic event (n = 1). Unfortunately, an empirical and clinical comparison among CAR T cell delivery routes has yet to be performed for GBM. To varying extents, clinical studies have evaluated CAR T cells for GBM targeting interleukin-13 receptor subunit alpha-2 (IL13Rα2), human epidermal growth factor receptor 2 (HER2) and EGFRvIII, with follow-up studies targeting IL13Rα2 and HER2 underway. In addition, investigators have initiated clinical studies to evaluate CAR T cells targeting matrix metallopeptidase 2 (MMP2), B7 family member B7-H3, CD147 and NKG2-D type II integral membrane protein (NKG2D).

1.5 Understanding and therapeutically-targeting recurrent GBM

Although genetic and transcriptomic characterizations have provided static depictions of GSCs, targeting candidate driver pathways has yet to impact clinical outcome, likely because of dynamic evolution of GSCs and generation of their divergent progeny through therapy to recurrence. With the advent of CRISPR-Cas9 technology, efficacious and unbiased genome-wide functional genomic screens have provided insights into genes and pathways regulating tumor cell survival, invasion, and sensitivity to TMZ in primary tumor cells (Huang et al., 2019; MacLeod et al., 2019; Prolo et al., 2019; Toledo et al., 2015). In fact, not only does the genomic landscape at disease recurrence differ markedly from that of the primary tumor, these treatment-resistant cells continue

to deviate further by gathering additional mutations and adopting phenotypes that promote tumor proliferation (Favero et al., 2015; Johnson et al., 2014; Kim et al., 2015a; Kim et al., 2015b; Korber et al., 2019). This results in longitudinal heterogeneity of established therapeutic targets (e.g. PDGFR-β, FGFR-2, EGFR, etc.), wherein patient-matched primary and recurrent tumor specimens show significant expression changes for 90% of investigated targets (Schafer et al., 2019). Fundamental mechanisms of resistance to DNA-targeting agents may underlie treatment resistance in tumor cells, including enhanced DNA repair and drug efflux capacity, epigenetic modifications, and de-differentiation into a stem cell-like state. However, a comprehensive set of modulators governing treatment resistance and disease recurrence has yet to be determined in any cancer (Banelli et al., 2015; Bao et al., 2006; Lee et al., 2016; Lee et al., 2015).

Emerging therapeutics for GBM have shifted towards reconfiguring the patient's immune system to generate an anti-tumor response. However, immunotherapy has yet to significantly improve clinical outcomes for GBM patients and clinical studies have been disappointing thus far. Among the major hurdles to clinical efficacy are immense ITH (Neftel et al., 2019; Patel et al., 2014), parallel modes of immunosuppression by tumor cells (Jackson et al., 2019), and low mutational burden in GBM (Hodges et al., 2017). With these factors in mind, investigators and clinicians are shifting their focus to combinatorial treatment strategies to achieve synergistic effects, reduce treatment resistance and overcome immunosuppression.

Although CAR T cell therapy is a newer adaptation for GBM treatment, advancements to increase its clinical utility are rapidly progressing. While current trials are focused on targeting single tumor-associated antigens, this increased repertoire of targets will allow multiple antigens to be

targeted concurrently to overcome intertumoral heterogeneity as shown by Bielamowicz et al. (2018), who developed trivalent CAR T cells targeting HER2, IL13Rα2 and EphA2. In fact, these trivalent CAR T cells were able to eradicate nearly 100% of tumor cells from multiple GBM samples. Emerging trends towards rational combinatorial therapies are likely to include a systemic reignition of the tumor immune microenvironment. The continued discovery of novel tumor-associated and tumor-specific antigens, paired with the improvement of therapeutic modalities to increase efficacy and reduce toxicity, are necessary for the clinical efficacy of immunotherapies. Overall, a combinatorial therapy delivered at various stages throughout SoC may reliably improve clinical outcomes in GBM patients.

1.6 Summary of Intent

Glioblastoma (GBM) remains the most aggressive and prevalent malignant primary brain tumor in adults (Ostrom et al., 2016). Unchanged since 2005, standard of care (SoC) consists of surgical resection, followed by radiation therapy (RT) with concurrent and adjuvant chemotherapy with temozolomide (TMZ) (Lapointe et al., 2018; Stupp et al., 2005). Despite these therapeutic efforts, patients succumb to recurrent disease with a median overall survival of 14.6 months and a five-year survival rate of 5.5-6.8% (Ostrom et al., 2016; Stupp et al., 2009; Stupp et al., 2005). Therapeutic failure is largely explained by ITH and the presence of treatment-resistant GBM stem-like cells (GSCs) (Bao et al., 2006; Kim et al., 2015b; Neftel et al., 2019; Patel et al., 2014; Singh et al., 2004; Wang et al., 2016). GSCs initiate tumor formation, self-renew and differentiate to perpetuate intra-tumoral heterogeneity and, thus, drive resistance to multimodal therapies and seed disease recurrence (Chen et al., 2012; Lee et al., 2006; Li et al., 2009; Singh et al., 2004). However, research to identify functional genetic drivers of tumor relapse and the use this information to inform therapeutic development for GBM is rare. Given the lack of understanding of recurrent

GBM and absence of second line therapies patients, **I hypothesize that genome-scale functional genetic interrogation will unravel recurrent GBM-specific tumor biology and inform development of novel therapeutics.**

The aims of this thesis were to:

Aim 1: To adapt genome-scale CRISPR-Cas9 screening to patient-derived GBM models.

Aim 2: To identify functional genetic vulnerabilities enriched in recurrent GBM.

Aim 3: To develop and evaluate novel therapeutic strategies to inhibit recurrent GBM.

To achieve these aims, I first adapted genome-scale CRISPR-Cas9 gene knockout screening to patient-derived primary and recurrent GBM stem-like models (**Chapter 2**). By using patient-matched primary and recurrent GBM models, I compared these tumor cells at the genetic, transcriptomic, proteomic and functional genetic levels. These analyses map a multilayered genetic response to drive tumor recurrence, identifying protein tyrosine phosphatase 4A2 (*PTP4A2)* as a novel modulator of self-renewal, proliferation and tumorigenicity at GBM recurrence. Mechanistically, genetic perturbation and a small molecule inhibitor of PTP4A2 repress axon guidance activity through a dephosphorylation axis with roundabout guidance receptor 1 (ROBO1) and exploit a genetic dependency on ROBO signaling. Importantly, engineered anti-ROBO1 single-domain antibodies also mimic the effects of PTP4A2 inhibition. These findings provide a template for studying recurrence and support development of therapeutic regimens that are informed by therapy-driven or longitudinal shifts in the functional genomic landscape of recurrent tumors.

Given the genetic dependency on ROBO signaling and enrichment of ROBO1 expression in GBM tissues, I undertook a campaign to evaluate ROBO1 as a therapeutic target in recurrent GBM and develop anti-ROBO1 chimeric antigen receptor T (CAR-T) cells using camelid single-domain antibodies targeting human ROBO1 (**Chapter 3**). I optimized the design of anti-ROBO1 CAR-T cells and tested the anti-tumor activity of these modalities in *in vitro* using patient-derived recurrent GBM lines and orthotopic patient-derived xenograft models. I present data to expand the repertoire of GBM-enriched antigens suitable for effective CAR-T cell therapy.

To further contextualize my campaigns to evaluate small molecule and CAR-T therapies for recurrent GBM, I published a summary of clinical findings and highlighted promising pre-clinical studies of three major immunotherapeutic modalities in GBM: vaccines, antibodies, and chimeric antigen receptor (CAR) T cells (Chapter 4). Given that resistance to SoC and disease relapse are inevitable for GBM patients, pre-clinical and clinical advancement of immunotherapeutic modalities, combined with recent insights into the tumor immune microenvironment, are poised to improve clinical outcomes for this patient population.

Together, I present a deep dive into how the tumor biology at GBM recurrence differs from its primary predecessor. These novel insights validated that treatment-resistant GBM continues to deviate further by gathering additional mutations and adopting phenotypes that promote tumor proliferation. Using these data, I was able to propose and evaluate two novel therapeutic approaches to target recurrent GBM.

Chapter 2: Widespread functional remodeling at glioblastoma recurrence

Preamble

In this chapter, I first present an original manuscript describing functional genetic insights into disease recurrence in glioblastoma using genome-scale CRISPR-Cas9 screening:

> **Chokshi, C. R.,** Tieu, D., Brown, K. R., Venugopal, C., Liu, L., Kuhlmann, L., Rossotti, M.A., Chan, K., Tong, A. H. Y., Savage, N., McKenna, D., Aghaei, N., Subapanditha, M., Shaikh, V.M., Tatari, N., Brakel, B., Nachmani, O., Ignatchenko, V., Salamoun, J. M., Wipf, P., Sharlow, E. R., Provias, J. P., Lu, J. Q., Murty, N. K., Lazo, J. S., Kislinger, T., Henry, K. A., Lu, Y., Moffat, J., & Singh, S. K. Functional mapping reveals widespread remodelling in recurrent glioblastoma. (manuscript in preparation)

Author contributions are as follows for the aforementioned manuscript: Conceptualization: S.K.S, J.M, C.R.C and D.T; Resources: J.P.P, J.L, N.K.M, and S.K.S; Methodology, investigation and validation: C.R.C, D.T, L.L, L.K, M.A.R, K.C, A.H.Y.T, N.S, D.M, N.A and M.S; Software and formal analysis: C.R.C, D.T, S.K.S, J.M, K.R.B, C.V, O.N, V.I; Visualization: C.R.C, K.R.B, and K.A.H. Writing – original draft preparation: C.R.C; Writing – review and editing: C.R.C, K.R.B, J.M, and S.K.S with input from other authors; Project administration and supervision: S.K.S and J.M; Funding acquisition: S.K.S and J.M. All authors read and approved the manuscript.

Next, I present data summarizing our findings from genome-wide CRISPR-Cas9 screens in primary GBM treated with standard of care (SoC) radiation therapy and chemotherapy. These data are unrelated to any current manuscript.

Together, we explore the functional drivers of post-treatment recurrent GBM. By conducting genome-wide CRISPR-Cas9 screens in patient-derived GBM models, we uncover distinct genetic dependencies in recurrent tumor cells that were absent in their patient-matched primary predecessors, accompanied by increased mutational burden and differential transcript and protein expression. These analyses map a multilayered genetic response to resist chemoradiotherapy and drive tumor recurrence, identifying protein tyrosine phosphatase 4A2 (*PTP4A2)* as a novel driver of self-renewal, proliferation and tumorigenicity at GBM recurrence. Mechanistically, genetic perturbation and a small molecule inhibitor of PTP4A2 repress axon guidance activity through a dephosphorylation axis with roundabout guidance receptor 1 (ROBO1) and exploit a genetic dependency on ROBO signaling. Importantly, engineered anti-ROBO1 single-domain antibodies also mimic the effects of PTP4A2 inhibition. We conclude that functional reprogramming drives tumorigenicity and dependence on a PTP4A2-ROBO1 signaling axis at GBM recurrence.

Widespread functional remodelling at glioblastoma recurrence

Chirayu R. Chokshi[1], David Tieu[2,3], Kevin R. Brown[2], Chitra Venugopal[4], Lina Liu[1], Laura Kuhlmann[5], Martin A. Rossotti[6], Katherine Chan[2], Amy H. Y. Tong[2], Neil Savage[1], Dillon McKenna[4], Nikoo Aghaei[1], Minomi Subapanditha[4], Vaseem Shaikh[4], Benjamin Brakel[1], Omri Nachmani[4], Vladimir Ignatchenko[5], Joseph M. Salamoun[7], Peter Wipf[7], Elizabeth R. Sharlow[8], John P. Provias[9], Jian-Qiang Lu[9], Naresh K. Murty[4], John S. Lazo[8], Thomas Kislinger[5,10], Kevin A. Henry[6,11], Yu Lu[1], Jason Moffat[2,3,12,*, †] Sheila K. Singh[1,4,*, †]

Affiliations

[1]Department of Biochemistry and Biomedical Sciences, McMaster University, Hamilton, Ontario, Canada L8N 3Z5.

[2]Donnelly Centre, University of Toronto, Toronto, Ontario, Canada M5S 3E1.

[3]Department of Molecular Genetics, University of Toronto, Toronto, Ontario, Canada M5S 1A8.

[4]Department of Surgery, Faculty of Health Sciences, McMaster University, Hamilton, Ontario, Canada L8N 3Z5.

[5]Princess Margaret Cancer Centre, University Health Network, Toronto, Ontario, Canada M5G 2C1.

[6]Human Health Therapeutics Research Centre, Life Sciences Division, National Research Council Canada, Ottawa, Ontario, Canada K1A 0R6.

[7]Department of Chemistry, University of Pittsburgh, Pittsburgh, Pennsylvania, USA 15260.

[8]Department of Pharmacology, Fiske Drug Discovery Laboratory, University of Virginia, Charlottesville, Virginia, USA 22908-0735.

[9]Department of Pathology and Molecular Medicine, McMaster University, Hamilton, Ontario, Canada L8N 3Z5.

[10]Department of Medical Biophysics, University of Toronto, Ontario, Canada M5G 1L7.

[11]Department of Biochemistry, Microbiology and Immunology, Faculty of Medicine, University of Ottawa, Ottawa, Ontario, Canada K1H 8M5.

[12]Institute for Biomaterials and Biomedical Engineering, University of Toronto, Toronto, Ontario, Canada M5S 3G9.

*Lead Contact: Dr. Sheila K. Singh (ssingh@mcmaster.ca).

†Co-corresponding authors.

Abstract

Resistance to genotoxic therapies and tumor recurrence are hallmarks of glioblastoma (GBM), an aggressive brain tumor. Here, we explore the functional drivers of post-treatment recurrent GBM. By conducting genome-wide CRISPR-Cas9 screens in patient-derived GBM models, we uncover distinct genetic dependencies in recurrent tumor cells that were absent in their patient-matched primary predecessors, accompanied by increased mutational burden and differential transcript and protein expression. These analyses map a multilayered genetic response to drive tumor recurrence, identifying protein tyrosine phosphatase 4A2 (*PTP4A2)* as a novel modulator of self-renewal, proliferation and tumorigenicity at GBM recurrence. Mechanistically, genetic perturbation and a small molecule inhibitor of PTP4A2 repress axon guidance activity through a dephosphorylation axis with roundabout guidance receptor 1 (ROBO1) and exploit a genetic dependency on ROBO signaling. Importantly, engineered anti-ROBO1 single-domain antibodies also mimic the effects of PTP4A2 inhibition. We conclude that functional reprogramming drives tumorigenicity and dependence on a PTP4A2-ROBO1 signaling axis at GBM recurrence.

Keywords

Tumor recurrence, CRISPR-Cas9, brain cancer, glioblastoma, PTP4A2, ROBO1

Introduction

For decades, clinicians have administered radiation therapy and chemotherapy to treat cancer patients(DeVita, 1978). In parallel, resistance to these genotoxic treatments and tumor recurrence have become an inevitable reality for aggressive tumors. However, despite the clinical relevance and applications, functional drivers of disease recurrence remain poorly understood. Glioblastoma (GBM) remains the most aggressive and prevalent malignant primary brain tumor in adults(Ostrom et al., 2016). Unchanged since 2005, standard of care (SoC) consists of surgical resection, followed by radiation therapy (RT) plus concurrent and adjuvant chemotherapy with temozolomide (TMZ)(Lapointe et al., 2018; Stupp et al., 2005). Despite these therapeutic efforts, patients inevitably succumb to recurrent disease with a median overall survival of 14.6 months and a five-year survival rate of 5.5-6.8%(Ostrom et al., 2016; Stupp et al., 2009; Stupp et al., 2005). Unbiased genome-wide functional genomic screens have provided insights into genes and pathways regulating tumor cell survival, invasion, and sensitivity to TMZ in primary pre-treatment tumor cells(Huang et al., 2019; MacLeod et al., 2019; Prolo et al., 2019; Toledo et al., 2015). However, these studies do not examine changes at post-treatment tumor recurrence, and thus cannot explain treatment failure in ~70% of GBM patients(Norden et al., 2019). Here, we conduct a genome-scale comparison between patient-matched pre- and post-treatment GBM cells at the functional, transcriptomic, and proteomic levels. We uncover a therapeutic vulnerability for protein tyrosine phosphatase 4A2 (*PTP4A2)* at tumor recurrence, and introduce a modulatory role of PTP4A2 on axonal guidance members.

Comparing primary and recurrent GBM

We derived a pair of patient-matched GBM cultures, one obtained at initial diagnosis prior to chemoradiotherapy (BT594, primary tumor cells), and a second specimen at first disease

recurrence post-therapy (BT972, recurrent tumor cells) (Figure 1A). Consistent with previous observations(Orzan et al., 2017; Qazi et al., 2016), recurrent tumor cells showed a 25-fold increase in *in vitro* self-renewal capacity (P = 5.0e-09) and a 5-fold decrease in survival of xenografted mice (n = 5, P = 0.002), as compared to patient-matched primary tumor cells (Figures 1B and 1C). To explain enhanced stemness and tumorigenicity, we began by profiling the genomic, transcriptomic and proteomic changes at recurrence. Of an average of 15,444 canonical genomic variants per model, 2,019 variants were predicted to have high impact on protein function (e.g. frameshift variants) or classified as deleterious to protein function, collectively henceforth referred to as mutations (Figures 1D and 1E). Strikingly, tumor cells presented with 1,599 *de novo* mutations at recurrence, accounting for 79% of all mutations, including coding mutations in *MSH6*, *ARID1A*, *PTEN*, *TP53*, *EGFR* and *RB1*. These driver mutations emerging at recurrence likely represent subclonal therapy-driven or stochastic events, as previously observed in 77% of subclones in recurrent GBM specimens(Korber et al., 2019). In comparison, 186 mutations were exclusive to primary tumor cells and 234 mutations were shared.

Of genes mutated in >1% of tumor specimens representing 62 cancer types (MSK-IMPACT dataset, n = 10,336)(Zehir et al., 2017), recurrent tumor cells presented with *de novo* mutations impacting TP53 activity (including *TP53* and *CREBBP*), chromatin organization (including *ARID1A*, *KMT2C* and *KMT2D*), and PI3K/AKT signaling (including *PTEN*, *EGFR*, *MTOR*, *TSC2*, *IRS2*, *RICTOR* and *FOXO1*), among other processes. In keeping with the largest longitudinal analysis of GBM that showed transcriptional changes in 63% of GBM patients at recurrence(Wang et al., 2016), genomic events observed in recurrent tumor cells were accompanied by widespread differential expression at the transcript (n = 1,747 genes) and protein (n = 181 proteins) levels ($|LFC| > 2$, adjusted $P < 0.05$), most notably indicating a shift in subtype

from predominantly classical in primary tumor cells to a mesenchymal subtype at recurrence (Figure 1F). These data are consistent with the view that the root cause and result of therapy failure in GBM is an accumulation of driver mutations at recurrence that drastically reconfigure cellular processes and increase tumorigenicity.

Functional remodelling at recurrence

To understand how mutational patterns relate to functional dependencies, we conducted pooled, genome-wide CRISPR-Cas9 screens in patient-matched primary and recurrent GBM models using the TKOv3 library. After excluding core essential genes (CEGs)(Behan et al., 2019; Hart et al., 2017), 1,090 genes were specific to primary tumor cells, 995 genes specific to recurrent tumor cells and 1,172 were required in both cultures (FDR < 0.05). Given that ~2/3 of the detectable genetic dependencies are different between primary and recurrent models, we examined the extent to which *in vitro* treatment of primary tumor cells with SoC recapitulates dependencies observed at recurrence. To systematically identify genetic determinants of treatment resistance, we conducted CRISPR-Cas9 loss-of-function screens in treatment-naïve primary tumor cells treated with RT and/or TMZ. Applying the drugZ algorithm, we measured differential effects in recurrent tumor cells or drug-treated primary tumor cells (RT and/or TMZ) compared to untreated primary tumor cells (Table S4). Comparison of normalized Z scores, with and without filtering for significant genes (FDR < 0.05 in at least one screen), revealed weak to moderate positive correlation among recurrent tumor cells as compared to drug-treated primary tumor cells (Figure 2A; $R = 0.38–0.50$). Therefore, treatment-specific conditional genetic interactions in drug-treated primary tumor cells do not completely recapitulate differential dependencies at recurrence. Rather, these data suggest that treatment-evasive tumor cells continue to acquire novel dependencies post-treatment and into disease recurrence.

Focusing on functional differences at recurrence, we identified 406 genes that confer increased (n = 229) or decreased (n = 177) fitness upon knockout in recurrent tumor cells as compared to primary tumor cells (FDR < 0.5; Figure 2B). GO enrichment analysis of these fitness genes highlighted remodelling of cell cycle and signaling processes at recurrence (FDR < 0.026), including greater dependence on cyclin-dependent kinases (*CDK2*, *CDK4, CCND1*), loss of p53-dependent DNA damage response (*TP53*), and increased reliance on the 26S proteasome (*PSMD11*, *PSMD13*) (Figure 2C). In addition, while primary tumor cells show strong dependence on Fanconi Anemia pathway genes, this dependence is lost at recurrence (FDR < 0.002; *FANCA*, *FANCB*, *FANCC*, *FANCD2*, *FANCF*). Combined with p53 loss, this likely sets the stage for increased accumulation of genomic mutations in recurrent tumors. Along with increased dependence on nucleotide metabolism and glycolysis, these findings are indicative of a shift towards a more proliferative state, with increased proteotoxic stress and loss of key DNA repair pathways in recurrent GBM.

To identify additional genetic dependencies in recurrent GBM, we performed a CRISPR-Cas9 knockout screen in a second patient-derived recurrent tumor model, BT241 (Figure S4A-S4C). To identify genes functionally unique to recurrent tumor cells (FDR < 0.05 and Bayes Factor (BF) score > 5), we compared our screening results to the Cancer Dependency Map (DepMap) data (Behan et al., 2019; Dempster et al., 2019; Lenoir et al., 2018; Meyers et al., 2017), and further refined our list to genes that are highly expressed in GBM specimens compared to normal brain tissue (The Cancer Genome Atlas (TCGA) GBM dataset (Tang et al., 2017); adjusted $P < 0.01$). This prioritized a list of 13 candidate genes (Figure 3A), including the master stemness regulator SRY-Box transcription factor 2 (*SOX2*; FDR = 0) (Basu-Roy et al., 2015; Gangemi et al., 2009; Mao et al., 2015). The remaining genes are largely uninvestigated in GBM stemness and disease

recurrence, such as protein tyrosine phosphatase 4A2 (*PTP4A2*), metabolic reprogramming gene Karyopherin subunit alpha 2 (*KPNA2*) and mitochondrial gene oxidase (cytochrome C) assembly 1-like (*OXA1L*). Examination of these genes across our CRISPR-Cas9 screening data and those from previous studies (MacLeod et al., 2019; Toledo et al., 2015), we find *PTP4A2* ($P_{primary} = 0.016$, $P_{NSCs} = 0.022$), *KPNA2* ($P_{primary} = 1.3e\text{-}06$; $P_{NSCs} = 0.003$), *CCDC47* ($P_{primary} = 2e\text{-}06$; $P_{NSCs} = 0.0049$), *DCAF13* ($P_{primary} = 5.1e\text{-}05$; $P_{NSCs} = 0.013$), *NFIB* ($P_{primary} = 0.0059$; $P_{NSCs} = 0.0017$) and *SLC25A19* ($P_{primary} = 0.03$; $P_{NSCs} = 0.051$) to be more functionally required in recurrent tumor cells relative to primary tumor cells or fetal neural stem cells (NSCs), respectively (pairwise unpaired T test). Of these genes, *PTP4A2* has the greatest mRNA expression in GBM samples and shows substantial mRNA enrichment in tumor specimens compared to non-tumor tissue (adjusted $P = 2.8e\text{-}30$, genome-scale moderated contrast T-test; TCGA GBM dataset (Tang et al., 2017)).

PTP4A2 vulnerability at recurrence

PTP4A2 is a poorly characterized member of the 4A family of dual-specificity protein tyrosine phosphatases that dephosphorylate tyrosine, serine and threonine residues on target peptides (Bessette et al., 2008). Whereas invertebrates (i.e. *C. elegans*, *D. melanogaster*, *S. purpuratus* and *B. floridae*) express a single phosphatase encoded by *PTP4A*, all vertebrate species have three genes (*PTP4A1*, *PTP4A2*, *PTP4A3*) with more than 80% amino acid sequence similarity (Lin et al., 2013). Notably, *Ptp4a2* knockout leads to defects in spermatogenesis and self-renewal of hematopoietic stem cells in mice (Dong et al., 2014; Kobayashi et al., 2014).

In the context of gliomas, we observe that *PTP4A2* expression correlates with tumor grade, and higher expression is also associated with poor overall patient survival ($P < 0.0001$). To support our genomic observations, we validated the effects of *PTP4A2* perturbation in six patient-derived GBM models including 3 primary and 3 recurrent models. No detectable effects on cell

proliferation (PR) or secondary sphere formation (SF) (i.e. a measure of stemness) were seen in primary tumor cells following perturbation of *PTP4A2* (Figures 3B and 3C; $P > 0.05$, unpaired T-test). In contrast, significant effects were observed on PR or SF upon perturbation of *PTP4A2* in recurrent tumor cells ($P < 0.05$, unpaired T-test). To further explore the effects of *PTP4A2* perturbation, we created an inducible *PTP4A2* knockout construct using CRISPR-Cas9 and observed an increase in survival of immunocompromised mice engrafted orthotopically with recurrent tumor cells following treatment with the inducer doxycycline (Figure 3D; n = 8, $P < 0.0001$). In order to determine if essential cellular processes at recurrence are modulated by PTP4A2 phosphatase activity, we engineered a potent chemical inhibitor of the phosphatase(McQueeney et al., 2018; Salamoun et al., 2016). *In vitro* treatment of cells with the pan-PTP4A phosphatase inhibitor JMS-053 was found to be lethal in recurrent tumor cells, while patient-matched primary tumor cells and unmatched fetal NSCs (NSC201) showed little effect over a wide range of drug concentrations (Figure 3E). In a preliminary study, intraperitoneal treatment with 10 mg/kg JMS-053 for 14 days led to increased median overall survival in an orthotopic patient-derived xenograft (PDX) model of recurrent GBM ($P = 0.00059$; Figure 3F). In addition, recent toxicity studies indicate that JMS-053 is well tolerated up to 40 mg/kg for three weeks (data not shown).

PTP4A2 influences axon guidance

Given that small molecule inhibition of PTP4A2 phosphatase activity phenocopied genetic knockout, we examined the phosphorylation landscape to identify substrates that could be driving *PTP4A2* dependence. Patient-matched primary and recurrent tumor cells were treated with JMS-053 or control compound prior to phospho-proteomic profiling. Phospho-proteomic profiling identified 11,182 phospho-peptides belonging to 3,677 phospho-proteins, with short-term

enrichment of 508 phospho-peptides (5 min; 431 proteins) and long-term enrichment of 1,154 phospho-peptides (30 min; 831 proteins) (treatment/control phospho-peptide intensity ratio > 1.5). Moreover, only ~20% of phospho-peptide and ~23% of phospho-protein enrichments were shared between primary and recurrent tumor cells following short-term treatment with JMS-053. GO term analysis of phospho-proteins enriched in recurrent tumor cells finds an over-abundance of proteins from the cell periphery ($P = 0.01$), whereas phospho-proteins elevated in primary tumor cells are enriched for the nuclear lumen ($P = 0.03$). Specifically, the greatest differential enrichment at recurrence was observed in the axon guidance member Roundabout Guidance Receptor 1 (ROBO1) (Figure 4A; ROBO1 p-Ser1162 fold change = 1.8). Initially discovered for its role in axon pathfinding during neurodevelopment (Brose et al., 1999), ROBO1 mediates cell migration in glioma and is upregulated in tumor specimens (Mertsch et al., 2008), whereas its inhibitory ligand SLIT2 is often hypermethylated and down-regulated (Dallol et al., 2003). Correspondingly, GO term analysis annotated phospho-proteins enriched in short-term, pan-PTP4A inhibition in recurrent tumor cells to axon development (Figure 4B; FDR = 0.04). Given that neither *PTP4A1* nor *PTP4A3* are essential for survival of recurrent tumor cells (*PTP4A1* FDR = 0.213 and *PTP4A3* FDR = 0.412) or primary tumor cells (*PTP4A1* FDR = 0.390 and *PTP4A3* FDR = 0.426), we reasoned that the effect of pan-PTP4A inhibition on axon guidance may be occurring via a PTP4A2-ROBO1 axis. To support our hypothesis, we profiled the transcriptome of primary and recurrent tumor cells with knockout of *PTP4A2* (two gRNAs) or *AAVS1* control (Figure 4C). A total of 1,283 differentially expressed genes (DEGs) were identified following *PTP4A2* knockout ($|\text{fold change}| > 2$ and adjusted $P < 0.05$), with 818 DEGs exclusive to recurrent tumor cells. In agreement with the phosphoproteomic analysis, gene set enrichment analysis (GSEA) revealed a depletion of axon guidance members at the transcriptomic level in recurrent tumor cells with

PTP4A2 knockout (adjusted $P = 0.04$); however, no such effect was seen in primary tumor cells (adjusted $P = 1$) (Figure 4D).

In accordance with previous immunohistochemical studies of glioma specimens (Mertsch et al., 2008), we find that *ROBO1* is over-expressed in GBM tissues profiled by TCGA as compared to normal brain (Figure S8A; LFC > 1.5 and $P < 0.01$). Moreover, GSEA pathway analyses of our genome-wide functional screens supports a striking dependence on ROBO signaling in recurrent GBM models (BT241 and BT972 adjusted $P = 0.004$). Notably, none of *ROBO1-4* were identified as genetic dependencies in our functional screens, suggesting that single-gene knockout of any of *ROBO1-4* may not be sufficient to phenocopy *PTP4A2* perturbation. During normal neurodevelopment, binding of secreted SLIT2 to ROBO1 leads to axon repulsion and inhibition of cell migration via SRGAP-mediated CDC42 inactivation(Hu et al., 2005; Wong et al., 2001), in parallel to weakening N-cadherin-mediated cell adhesion via phosphorylation of β-catenin by ABL(Rhee et al., 2007; Rhee et al., 2002). In a neoplastic context, SLIT2 promoter methylation and inactivation is frequently observed in gliomas(Dallol et al., 2003), whereas ROBO1 is highly expressed at transcript and protein levels (Liu et al., 2016b). In other solid tumor contexts, SLIT/ROBO interactions have been shown to regulate quintessential oncogenic pathways, including signaling by EGFR, VEGFR, mTOR and HER2(Gara et al., 2015). Although the role of ROBO1-mediated signaling in GBM is yet to be resolved, our observations reveal a context-specific vulnerability on axon guidance through a PTP4A2-ROBO axis in recurrent GBM (Figure 4I). In recurrent GBM, PTP4A2 may support ROBO1/CDC42-mediated tumor cell invasion via dephosphorylation of SRGAP1, SRGAP3 and CDC42 effector proteins. In addition, direct dephosphorylation of β-catenin (CTNNB1) may support WNT signaling-mediated tumor cell stemness and proliferation. Our identification of this axis is also supported by previous studies

that link Ptp4a1 expression with axon synaptogenesis in the central nervous system of *Drosophila*, the genome of which includes a single *Ptp4a* gene (Urwyler et al., 2019).

Given the above findings and our previous success targeting axon guidance through the ephrin family members EPHA2 and EPHA3 in recurrent GBM using a bispecific antibody (Qazi et al., 2018), we developed a panel of camelid single-domain antibodies targeting human ROBO1. Of these antibodies, MKRo-20 showed high affinity and specificity for human ROBO1 (K_D = 12.1±0.06 nM) among other members of the ROBO family (ROBO2, ROBO3, and ROBO4) (Figures 4G, 4H). To determine whether antibody-based modulation of ROBO1 mimics PTP4A2 inhibition, we treated recurrent GBM spheroids immersed in Matrigel with JMS-053 and/or anti-ROBO1 MKRo20. Both treatment with MKRo20 and/or JMS-053 mediated inhibition of PTP4A2 led to robust decreases in tumor cell invasion and spheroid size (Figure 4J). These results propose that modulation of ROBO1 function using antibodies could be a viable and novel strategy to target recurrent GBM.

Discussion

We conducted the first set of unbiased functional genetic screens in patient-derived GBM models to reveal functional modulators of disease recurrence. Not only do recurrent tumor cells rely on a distinct set of functional drivers when compared to their primary predecessors, therapeutic avenues to treat recurrent disease cannot be predicted without profiling tumors at recurrence. The surprising loss of ~30% of genetic dependencies in primary tumor cells at recurrence (e.g. *RUNX1*, *ZEB1* and *RHOA*), gain of an additional ~30% new functional dependencies (e.g. *FASN* and *CD151*), and further loss of crucial replicative checkpoints (e.g. *TP53*, *PTEN*, *NF1*, and *NF2*), highlight the dramatic remodelling from primary to recurrent disease. Therapy-driven events, along with continuous temporal evolution at the genetic and

cellular levels, may select for a sub-clonal and treatment-resistant GSC population that redefines the functional genetic landscape of the recurrent tumor.

Collectively, these results support a model in which therapy-driven and stochastic events lead to a functionally distinct tumor at recurrence. Our analysis of the genomic, transcriptomic, proteomic and functional genetic landscapes of patient-matched primary and recurrent tumor cells supports parallel tumor-intrinsic mechanisms of treatment resistance which rely on acquisition of immunosuppressive capacity. Not only are recurrent GBM cells burdened by greater stem-like properties and tumorigenic potential, presence of *de novo* driver mutations such as a defective MMR pathway (*MSH6* A1179V and T1219I) may drive hypermutation and shield recurrent GBM cells from the host immune system and anti-PD-1 blockade(Touat et al., 2020). In stark contrast, anti-PD-1 blockade is a tractable therapeutic strategy in other aggressive cancers (i.e. non-small cell lung cancer, colorectal cancer and melanoma) with a hypermutated profile (Le et al., 2015; McGranahan et al., 2016; Rizvi et al., 2015). In addition, MMR-deficiency in recurrent GBM cells may predispose to a higher mutational burden but, unlike other cancers, these additional mutations may support an immunosuppressive microenvironment.

We observe that MMR-deficient recurrent GBM cells also harbour a deleterious mutation in *PTEN* (H123Y), previously shown to ablate phosphatase activity and prevent PTEN-mediated cell cycle arrest in breast cancer cells (Hlobilkova et al., 2000). In addition, MMR-deficiency and microsatellite instability (MSI) has been associated with truncal *PTEN* loss in gliomas, and likewise, *PTEN* loss occurs in 90% of human MSI endometrial carcinomas (Cancer Genome Atlas Research et al., 2013a; Touat et al., 2020). In addition to MMR deficiency, significant enrichment of *PTEN* mutations at recurrence has been associated with immunosuppressive expression

signatures in GBM patients who were classified as non-responders to immune checkpoint blockade in clinical trials with nivolumab and pembrolizumab (Zhao et al., 2019).

Altogether, our mutational, proteomic and functional characterization of the remodelled landscape in recurrent GBM reveals novel mechanisms of treatment resistance, warranting therapeutic approaches that exploit synthetic lethal vulnerabilities that emerge at recurrence. By performing the first genome-wide CRISPR-Cas9 gene knockout screens in patient-derived post-treatment recurrent tumor cells, we report an example of a context-specific vulnerability of *PTP4A2*. Pharmacological inhibition of PTP4A2 phosphatase activity revealed modulation of axon guidance via ROBO1 as a downstream effector of PTP4A2, further supported by a global enrichment and dependence on ROBO signaling. To develop a therapeutic approach targeting ROBO signaling, we present evidence supporting the use of an anti-ROBO1 single-domain antibody for treatment of recurrent tumor cells. These findings provide a template for studying recurrence and support development of therapeutic regimens that are informed by therapy-driven or longitudinal shifts in the functional genomic landscape of recurrent tumors.

Acknowledgements

We thank all members of laboratories led by Drs. Sheila K. Singh, Jason Moffat, Yu Lu, Kevin Henry, Thomas Kislinger, John S. Lazo and Elizabeth R. Sharlow. We thank Dr. Kristin Hope for her guidance and support. This research was supported by the Terry Fox Research Institute Program Project Grant (1065) and C.R.C was supported by MITACS Accelerate scholarships (IT15477 and IT11823). S.K.S holds a Senior Canadian Research Chair in Human Cancer Stem Cell Biology and J.M holds a Canada Research Chair in Functional Genomics of Cancer.

Author contributions

Conceptualization: S.K.S, J.M, C.R.C and D.T; Resources: J.P.P, J.L, N.K.M, and S.K.S; Methodology, investigation and validation: C.R.C, D.T, L.L, L.K, M.A.R, K.C, A.H.Y.T, N.S, D.M, N.A and M.S; Software and formal analysis: C.R.C, D.T, S.K.S, J.M, K.R.B, C.V, O.N, V.I; Visualization: C.R.C, K.R.B, and K.A.H. Writing – original draft preparation: C.R.C; Writing – review and editing: C.R.C, K.R.B, J.M, and S.K.S with input from other authors; Project administration and supervision: S.K.S and J.M; Funding acquisition: S.K.S and J.M. All authors read and approved the manuscript.

Declaration of interests

The authors declare no competing interests.

Figures

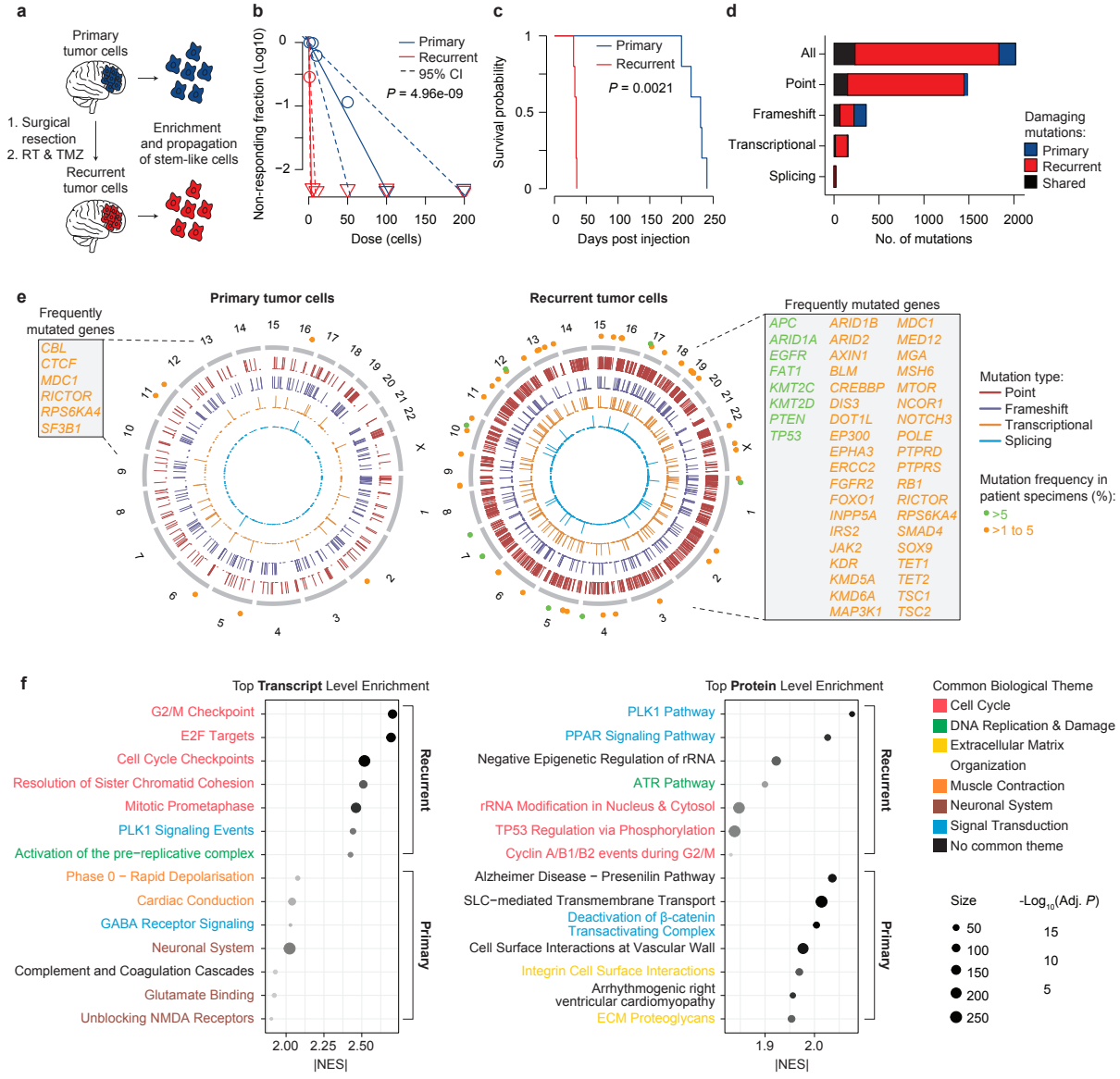
a
Primary tumor cells
1. Surgical resection
2. RT & TMZ
Recurrent tumor cells
Enrichment and propagation of stem-like cells
b
Non-responding fraction (Log10)
Primary
Recurrent
95% CI
P = 4.96e-09
Dose (cells)
c
Survival probability
Primary
Recurrent
P = 0.0021
Days post injection
d
All
Point
Frameshift
Transcriptional
Splicing
Damaging mutations:
Primary
Recurrent
Shared
No. of mutations
e
Primary tumor cells
Recurrent tumor cells
Frequently mutated genes
CBL
CTCF
MDC1
RICTOR
RPS6KA4
SF3B1
Frequently mutated genes
APC ARID1A EGFR FAT1 KMT2C KMT2D PTEN TP53
ARID1B ARID2 AXIN1 BLM CREBBP DIS3 DOT1L EP300 EPHA3 ERCC2 FGFR2 FOXO1 INPP5A IRS2 JAK2 KDR KMD5A KMD6A MAP3K1
MDC1 MED12 MGA MSH6 MTOR NCOR1 NOTCH3 POLE PTPRD PTPRS RB1 RICTOR RPS6KA4 SMAD4 SOX9 TET1 TET2 TSC1 TSC2
Mutation type:
Point
Frameshift
Transcriptional
Splicing
Mutation frequency in patient specimens (%):
>5
>1 to 5
f
Top Transcript Level Enrichment
G2/M Checkpoint
E2F Targets
Cell Cycle Checkpoints
Resolution of Sister Chromatid Cohesion
Mitotic Prometaphase
PLK1 Signaling Events
Activation of the pre−replicative complex
Phase 0 − Rapid Depolarisation
Cardiac Conduction
GABA Receptor Signaling
Neuronal System
Complement and Coagulation Cascades
Glutamate Binding
Unblocking NMDA Receptors
Recurrent
Primary
|NES|
Top Protein Level Enrichment
PLK1 Pathway
PPAR Signaling Pathway
Negative Epigenetic Regulation of rRNA
ATR Pathway
rRNA Modification in Nucleus & Cytosol
TP53 Regulation via Phosphorylation
Cyclin A/B1/B2 events during G2/M
Alzheimer Disease − Presenilin Pathway
SLC−mediated Transmembrane Transport
Deactivation of β-catenin Transactivating Complex
Cell Surface Interactions at Vascular Wall
Integrin Cell Surface Interactions
Arrhythmogenic right ventricular cardiomyopathy
ECM Proteoglycans
Recurrent
Primary
|NES|
Common Biological Theme
Cell Cycle
DNA Replication & Damage
Extracellular Matrix Organization
Muscle Contraction
Neuronal System
Signal Transduction
No common theme
Size
-Log10(Adj. P)
50
100
150
200
250
15
10
5

Figure 1. Genome-scale genetic and proteomic comparison of patient-matched, pre-treatment primary and post-treatment recurrent tumor cells.

(A) Schematic of patient-matched primary (BT594) and recurrent (BT972) tumor cell derivation.

(B) Limiting dilution assay to assess *in vitro* sphere formation in patient-matched primary (blue) and recurrent (red) tumor cells. Data are presented as means with 95% confidence interval (CI); *P* value from chi-squared likelihood ratio test.

(C) Kaplan-Meier survival analysis of immunocompromised mice engrafted with tumor cells, indicating death when mice reach endpoint. Primary (blue), $n = 5$; recurrent (red), $n = 5$; *P* value from log-rank (Mantel-Cox) test.

(D) Tally of damaging mutations in primary and recurrent tumor cells, separated by mutation type. Mutations were called using the Genome Analysis Toolkit (GATK) and filtered to include canonical variants with predicted high impact on protein function and/or classified as deleterious by Condel, SIFT and PolyPhen.

(E) Circos plots of deleterious mutations in primary and recurrent tumor cells separated by mutation type (i.e. point, frameshift, transcriptional and splicing variants). Mutations are aligned to their chromosomal position. For each mutation, gene-level mutation frequency (% of total patients) was obtained from 10,000 patient tumor specimens profiled by Zehir et al. (2017). Mutations present in >1% of patients are highlighted for primary and recurrent tumor cells.

(F) Fast gene set enrichment analysis (fGSEA) was performed on differentially-expressed transcripts (RNA sequencing) and proteins (whole cell proteomics) in recurrent tumor cells as compared to primary tumor cells (recurrent/primary). Integrated pathway gene sets (March 2021 version) were obtained from the Bader Lab (www.baderlab.org/Software). The top seven enriched gene sets in recurrent tumor cells (normalized enrichment score (NES) > 0) and primary tumor

cells (NES < 0) are highlighted, with dot size and color representing gene set size and adjusted *P* value, respectively. Gene sets with common biological themes are indicated by text color.

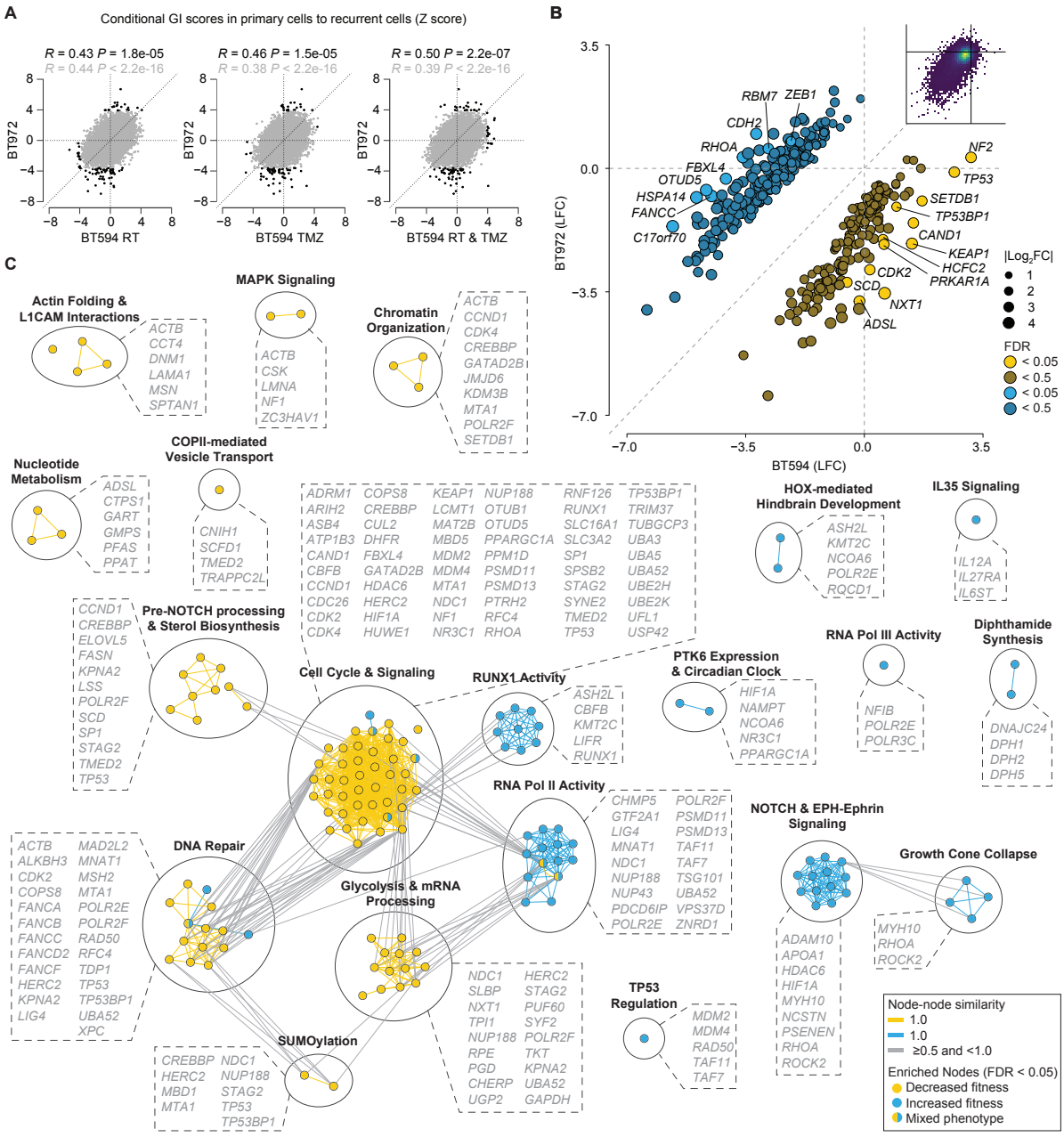
A
Conditional GI scores in primary cells to recurrent cells (Z score)
R = 0.43 P = 1.8e-05
R = 0.44 P < 2.2e-16
R = 0.46 P = 1.5e-05
R = 0.38 P < 2.2e-16
R = 0.50 P = 2.2e-07
R = 0.39 P < 2.2e-16
BT972
BT594 RT
BT594 TMZ
BT594 RT & TMZ
B
BT972 (LFC)
BT594 (LFC)
RBM7
ZEB1
CDH2
RHOA
FBXL4
OTUD5
HSPA14
FANCC
C17orf70
NF2
TP53
SETDB1
TP53BP1
CAND1
KEAP1
HCFC2
PRKAR1A
CDK2
SCD
NXT1
ADSL
|Log2FC|
FDR
C
Actin Folding & L1CAM Interactions
ACTB CCT4 DNM1 LAMA1 MSN SPTAN1
MAPK Signaling
ACTB CSK LMNA NF1 ZC3HAV1
Chromatin Organization
ACTB CCND1 CDK4 CREBBP GATAD2B JMJD6 KDM3B MTA1 POLR2F SETDB1
Nucleotide Metabolism
ADSL CTPS1 GART GMPS PFAS PPAT
COPII-mediated Vesicle Transport
CNIH1 SCFD1 TMED2 TRAPPC2L
ADRM1 ARIH2 ASB4 ATP1B3 CAND1 CBFB CCND1 CDC26 CDK2 CDK4
COPS8 CREBBP CUL2 DHFR FBXL4 GATAD2B HDAC6 HERC2 HIF1A HUWE1
KEAP1 LCMT1 MAT2B MBD5 MDM2 MDM4 MTA1 NDC1 NF1 NR3C1
NUP188 OTUB1 OTUD5 PPARGC1A PPM1D PSMD11 PSMD13 PTRH2 RFC4 RHOA
RNF126 RUNX1 SLC16A1 SLC3A2 SP1 SPSB2 STAG2 SYNE2 TMED2 TP53
TP53BP1 TRIM37 TUBGCP3 UBA3 UBA5 UBA52 UBE2H UBE2K UFL1 USP42
HOX-mediated Hindbrain Development
ASH2L KMT2C NCOA6 POLR2E RQCD1
IL35 Signaling
IL12A IL27RA IL6ST
CCND1 CREBBP ELOVL5 FASN KPNA2 LSS POLR2F SCD SP1 STAG2 TMED2 TP53
Pre-NOTCH processing & Sterol Biosynthesis
Cell Cycle & Signaling
RUNX1 Activity
ASH2L CBFB KMT2C LIFR RUNX1
PTK6 Expression & Circadian Clock
HIF1A NAMPT NCOA6 NR3C1 PPARGC1A
RNA Pol III Activity
NFIB POLR2E POLR3C
Diphthamide Synthesis
DNAJC24 DPH1 DPH2 DPH5
RNA Pol II Activity
CHMP5 GTF2A1 LIG4 MNAT1 NDC1 NUP188 NUP43 PDCD6IP POLR2E
POLR2F PSMD11 PSMD13 TAF11 TAF7 TSG101 UBA52 VPS37D ZNRD1
NOTCH & EPH-Ephrin Signaling
Growth Cone Collapse
ADAM10 APOA1 HDAC6 HIF1A MYH10 NCSTN PSENEN RHOA ROCK2
MYH10 RHOA ROCK2
ACTB ALKBH3 CDK2 COPS8 FANCA FANCB FANCC FANCD2 FANCF HERC2 KPNA2 LIG4
MAD2L2 MNAT1 MSH2 MTA1 POLR2E POLR2F RAD50 RFC4 TDP1 TP53 TP53BP1 UBA52 XPC
DNA Repair
Glycolysis & mRNA Processing
NDC1 SLBP NXT1 TPI1 NUP188 RPE PGD CHERP UGP2
HERC2 STAG2 PUF60 SYF2 POLR2F TKT KPNA2 UBA52 GAPDH
TP53 Regulation
MDM2 MDM4 RAD50 TAF11 TAF7
SUMOylation
CREBBP HERC2 MBD1 MTA1
NDC1 NUP188 STAG2 TP53 TP53BP1
Node-node similarity
1.0
1.0
≥0.5 and <1.0
Enriched Nodes (FDR < 0.05)
Decreased fitness
Increased fitness
Mixed phenotype

Figure 2. Functional screens reveal relative fitness trends at GBM recurrence.

(A) Gene-level cGI Z scores from screens performed in a treated primary tumor cell line relative to patient-matched recurrent cells. Pearson correlation coefficients and *P* values shown for each pairwise comparison with (black) and without (grey) filtering for genes that meet FDR < 0.05 in at least one screen. Conditional scores compute normalized difference of Z-scores between the condition indicated on the axis and BT594 DMSO control cells.

(B) Differential fitness genes between patient-matched primary and recurrent tumor cells. Genes that confer significantly increased (blue/dark blue; LFC > 0) or decreased (yellow/dark yellow; LFC < 0) tumor cell fitness in recurrent tumor cells relative to primary tumor cells are shown (FDR < 0.5). Node shade and size correspond to FDR and mean LFC (recurrent/primary), respectively. (Inset) Density plot with all data points shown.

(C) Network map of Reactome gene sets (Jassal et al., 2020) enriched in genes that exhibit differential fitness in recurrent GBM (BT972), with genes responsible for gene set enrichment listed alphabetically for each cluster. Network is designed using the Enrichment Map plugin in Cytoscape, and nodes are clustered using Auto Annotate (MCL Cluster algorithm, cluster cut off = 1.0). Nodes represent enriched pathways, while edges connect related pathways.

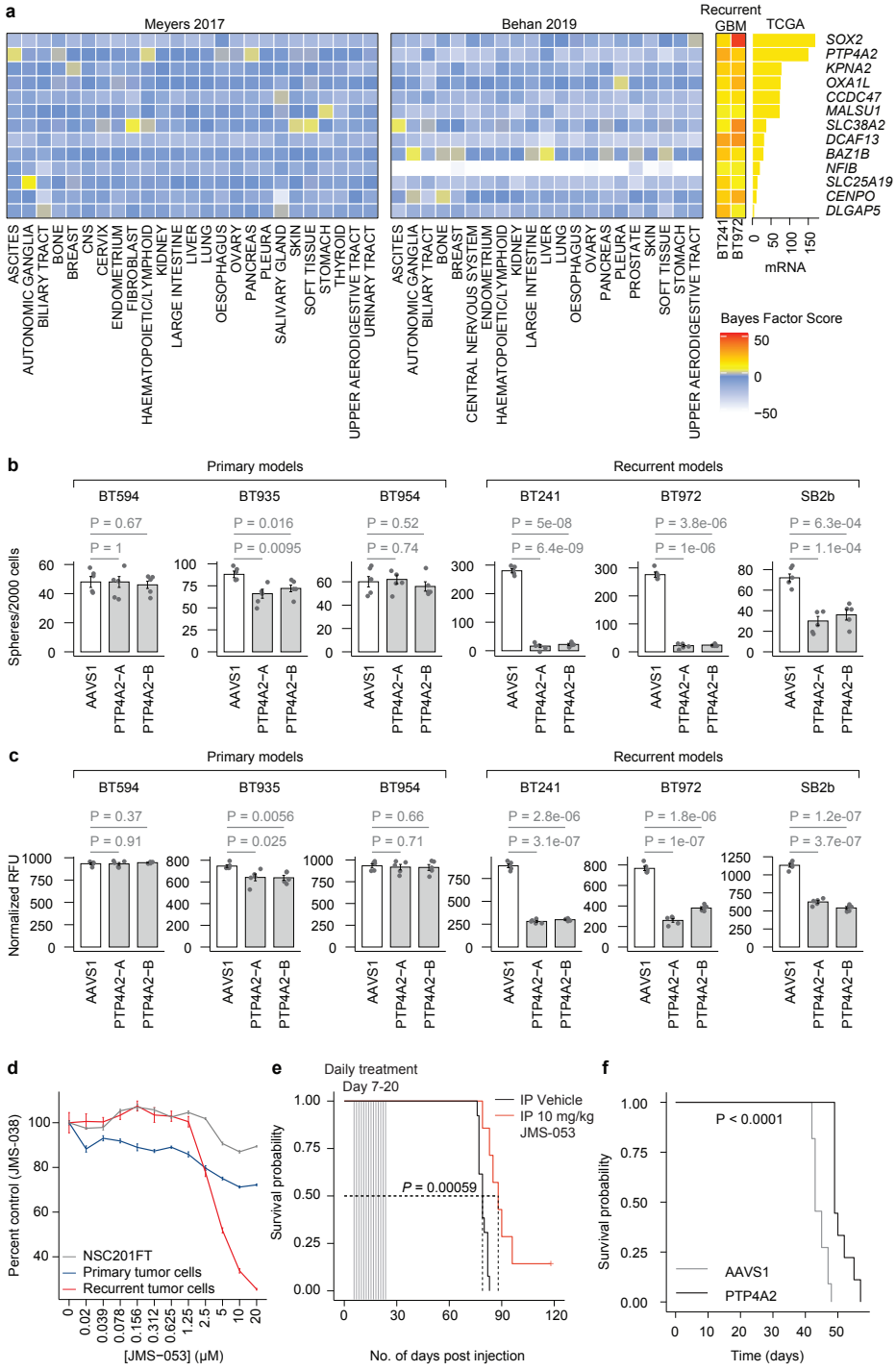
a
Meyers 2017
Behan 2019
Recurrent GBM
TCGA
SOX2
PTP4A2
KPNA2
OXA1L
CCDC47
MALSU1
SLC38A2
DCAF13
BAZ1B
NFIB
SLC25A19
CENPO
DLGAP5
mRNA
Bayes Factor Score
b
Primary models
Recurrent models
BT594
BT935
BT954
BT241
BT972
SB2b
Spheres/2000 cells
AAVS1
PTP4A2-A
PTP4A2-B
c
Normalized RFU
d
Percent control (JMS-038)
NSC201FT
Primary tumor cells
Recurrent tumor cells
[JMS−053] (μM)
e
Daily treatment
Day 7-20
IP Vehicle
IP 10 mg/kg
JMS-053
P = 0.00059
Survival probability
No. of days post injection
f
P < 0.0001
AAVS1
PTP4A2
Time (days)

Figure 3. Functional interrogation of patient-derived and post-treatment recurrent tumor cells.

(A) BF scores of recurrent tumor-specific essential genes (BF score > 5) as compared to CRISPR-Cas9 screens in human cancer cell lines from the Cancer Dependency Map (DepMap) (Behan et al., 2019; Meyers et al., 2017). Bar plot on right presents median mRNA level in primary GBM specimens, with all genes significantly upregulated in Cancer Genome Atlas (TCGA) GBM specimens as compared to non-tumor tissue (FDR < 0.05).

(B,C) Evaluation of protein tyrosine phosphatase 4A2 (*PTP4A2)* knockout (2 gRNAs, A and B) on (B) secondary sphere formation and (C) proliferation of primary and recurrent tumor cells, compared with a gRNA targeting *AAVS1* (control). All data are represented as mean +/- s.d.; *n* = 5 experimental replicates; *P* values are from unpaired Student's t-tests.

(D) Survival analysis of immunocompromised mice engrafted with recurrent tumor cells with an inducible *PTP4A2*- or *AAVS1*- knockout (n = 8 per knockout).

(E) Cell viability assays of patient-matched primary (BT594) and recurrent (BT972) tumor cells, and an unmatched fetal neural stem cell line (NSC201FT), exposed to increasing doses of JMS-053 over the course of 168 hours. Data presented as mean +/- s.d., *n* = 5 experimental replicates.

(F) Kaplan-Meier survival analysis of JMS-053-treated orthotopic patient-derived xenograft model (PDX) of recurrent GBM. Mice were treated with JMS-053 or vehicle control from days 7 to 20 post-injection (n = 8). Vehicle (black), *n* = 8; JMS-053 (red), *n* = 8; *P* value from log-rank (Mantel-Cox) test.

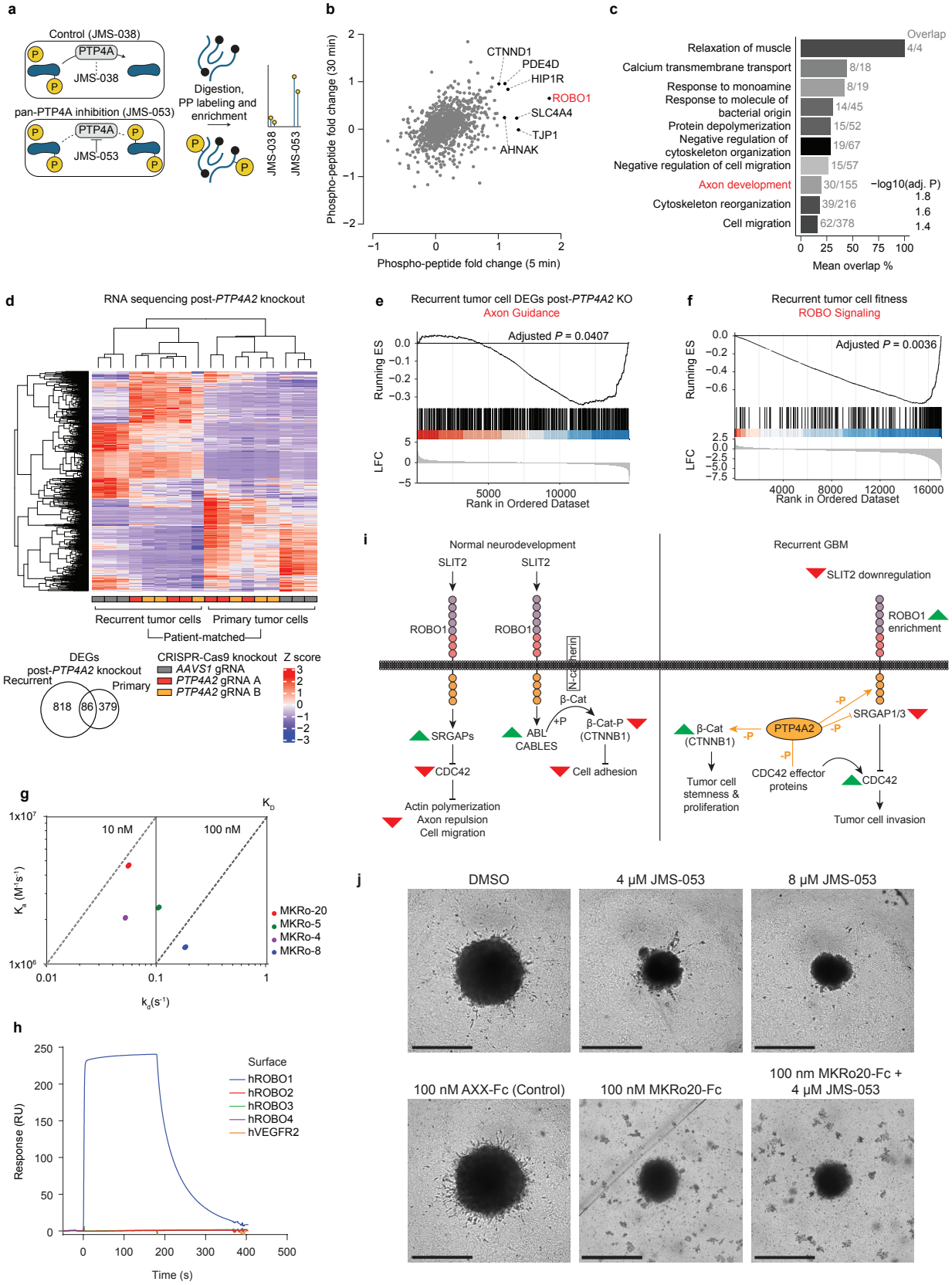
a
Control (JMS-038)
PTP4A
JMS-038
pan-PTP4A inhibition (JMS-053)
JMS-053
Digestion, PP labeling and enrichment
JMS-038
JMS-053
b
CTNND1
PDE4D
HIP1R
ROBO1
SLC4A4
TJP1
AHNAK
Phospho-peptide fold change (30 min)
Phospho-peptide fold change (5 min)
c
Overlap
Relaxation of muscle 4/4
Calcium transmembrane transport 8/18
Response to monoamine 8/19
Response to molecule of bacterial origin 14/45
Protein depolymerization 15/52
Negative regulation of cytoskeleton organization 19/67
Negative regulation of cell migration 15/57
Axon development 30/155
Cytoskeleton reorganization 39/216
Cell migration 62/378
−log10(adj. P)
Mean overlap %
d
RNA sequencing post-PTP4A2 knockout
Recurrent tumor cells
Primary tumor cells
Patient-matched
DEGs post-PTP4A2 knockout
Recurrent
Primary
818
86
379
CRISPR-Cas9 knockout
AAVS1 gRNA
PTP4A2 gRNA A
PTP4A2 gRNA B
Z score
e
Recurrent tumor cell DEGs post-PTP4A2 KO
Axon Guidance
Adjusted P = 0.0407
Running ES
LFC
Rank in Ordered Dataset
f
Recurrent tumor cell fitness
ROBO Signaling
Adjusted P = 0.0036
Running ES
LFC
Rank in Ordered Dataset
g
K_D
10 nM
100 nM
K_a (M⁻¹s⁻¹)
k_d(s⁻¹)
MKRo-20
MKRo-5
MKRo-4
MKRo-8
h
Surface
hROBO1
hROBO2
hROBO3
hROBO4
hVEGFR2
Response (RU)
Time (s)
i
Normal neurodevelopment
SLIT2
SLIT2
ROBO1
ROBO1
N-cadherin
β-Cat
+P
ABL
CABLES
β-Cat-P
(CTNNB1)
SRGAPs
CDC42
Actin polymerization
Axon repulsion
Cell migration
Cell adhesion
Recurrent GBM
SLIT2 downregulation
ROBO1
enrichment
SRGAP1/3
-P
β-Cat
(CTNNB1)
PTP4A2
Tumor cell
stemness &
proliferation
CDC42 effector
proteins
CDC42
Tumor cell invasion
j
DMSO
4 μM JMS-053
8 μM JMS-053
100 nM AXX-Fc (Control)
100 nM MKRo20-Fc
100 nm MKRo20-Fc +
4 μM JMS-053

Figure 4. Phospho-proteomic analysis reveals a PTP4A2-ROBO1 phosphorylation axis.

(A) Schematic of phospho-proteomic profiling of primary and recurrent tumor cells treated JMS-053 (active compound) or JMS-038 (inactive control).

(B) Fold change of enriched phospho-proteins annotated to the cell periphery. Protein-level fold change of enrichment ratios (recurrent/primary), following treatment with JMS-053 for 5 min compared to JMS-038.

(C) Enrichment for GO bioprocesses and Reactome terms among phospho-proteins enriched in recurrent tumor cells treated with JMS-053 for 5 min (ratio > 1.5 and %CV < 50%). Average number of genes intersecting with each term and term size indicated next to each bar. Bar color indicates the adjusted *P* values calculated by gProfileR.

(D) Row-normalized mRNA expression from primary (BT594) or recurrent (BT972) tumor cells with *PTP4A2* (2 gRNAs, A or B) or *AAVS1* knockout (1 gRNA, control). Data from three independent biological replicates are shown. Rows and columns are sorted by hierarchical clustering. On bottom left, Venn diagram of significantly differentially expressed genes (DEGs; adjusted $P < 0.05$) in primary or recurrent tumor cells with *PTP4A2* (2 gRNAs) or *AAVS1* knockout (1 gRNA, control). On right, top DEGs ($|LFC| > 2$ and adjusted $P < 0.05$) in recurrent tumor cells are highlighted.

(E) Gene Set Enrichment Analysis (GSEA) enrichment of axon guidance pathway gene expression in recurrent tumor cells following *PTP4A2* knockout, as compared to gRNA targeting *AAVS1* (control). Adjusted *P* values derived by ClusterProfiler.

(F) GSEA enrichment of Roundabout Guidance Receptor (ROBO) signaling pathway genes in CRISPR-Cas9 screen in recurrent tumor cells. Adjusted *P* value derived by ClusterProfiler.

(G) Multi-cycle kinetic analysis of the interaction between single domain antibodies and human ROBO1. Kinetic rate plot with iso-affinity diagonals for all antibodies.

(H) Binding of MKRo-20 (500 nM) to human ROBO1-4 and VEGFR2 by surface plasmon resonance.

(I) During normal neurodevelopment (left), SLIT2-ROBO1 interactions lead to axon repulsion and inhibition of cell migration via SRGAP-mediated CDC42 inactivation and to weakening N-cadherin-mediated cell adhesion via phosphorylation of β-catenin by ABL(Hu et al., 2005; Rhee et al., 2007; Rhee et al., 2002; Wong et al., 2001). In recurrent GBM, PTP4A2 may support CDC42-mediated tumor cell invasion via dephosphorylation of SRGAP1, SRGAP3 and CDC42 effector proteins. In addition, direct dephosphorylation of β-catenin (CTNNB1) may support WNT signaling-mediated tumor cell stemness and proliferation.

(J) Invasion of recurrent BT972 GSCs was evaluated by exposure to JMS-053 (4μM or 8μM), 100nM anti-ROBO1 MKRo20, or a combination (4μM JMS-053 with 100 nM MKRo20). Tumor spheroids were immersed in 12.5% Matrigel followed by drug exposure for 4 days.

Methods

Derivation and culture of patient-derived glioblastoma stem cell models

Primary glioblastoma (GBM) specimens and whole fetal brain samples were obtained from consenting patients and families as approved by the Hamilton Health Sciences and McMaster Health Sciences Research Ethics Board. After washing with PBS, specimens were mechanically dissociated followed by enzymatic dissociation in PBS containing 0.013 mg/mL Liberase Thermolysin Research Grade (Millipore Sigma no. 5401020001) at 37°C for 15 minutes. Dissociated cells were isolated by filtration through a 70 μm cell strainer (Millipore Sigma no. CLS431751-50EA), centrifuges and subjected to red blood cell lysis using 0.8% ammonium chloride solution (STEMCELL Technologies no. 07850). SB2b was a kind gift from Professor Bryan Day (Sid Faithfull Brain Cancer Laboratory) and Dr. Brett Stringer from Royal Brisbane Hospital in Herston, Australia. Tumor cells and fetal human neural stem cells (NSCs) were grown and maintained in NeuroCult NS-A proliferation kit (Human) (STEMCELL Technologies no. 05751), supplemented with 20 ng/mL EGF (STEMCELL Technologies no. 78006), 10 ng/mL FGF (STEMCELL Technologies no. 78003.2), 0.002% Heparin (w/v) (STEMCELL Technologies no. 07980), 1X antibiotic/antimycotic solution (Wisent Bio Products no. 450-115-EL). For the first two weeks of culture, patient-derived cells were treated for potential mycoplasma infection using 1X MycoZap Prophylactic (Lonza no. VZA-2031). Cells were cultured on tissue culture-treated dishes, cell-repellent dishes (Greiner Bio no. 628979), or tissue culture-treated dishes coated with Poly-L-ornithine (Millipore Sigma no. P4957) and mouse Laminin (Corning no. 354232). All cells were maintained at 37 °C and 5% CO_2. All cell lines were frequently tested for mycoplasma infection and, if needed, treated with additional 1X MycoZap for two weeks.

Library virus production and determination of multiplicity of infection

HEK293T (ATCC CRL-3216) cells were seeded (8 million per 15 cm dish) in DMEM containing glucose, pyruvate and 10% FBS. Twenty-four hours after seeding, a mix of 8μg of the Toronto KnockOut version 3.0 (TKOv3) guide RNA (gRNA) library (Hart et al., 2017) (Addgene no. 90294), viral packaging/envelope vectors (4.8 μg psPAX2 and 3.2 μg pMD2.G), 48 μL X-treme gene transfection reagent (Roche) and 1.4 mL Opti-MEM medium was transfected into cells. Twenty-four hours post transfection, the medium was replaced with DMEM high glucose supplemented with 0.011 g/mL BSA, 1% penicillin-streptomycin. Forty-eight hours post transfection, virus-containing media was separated by centrifugation, aliquoted and frozen at -80°C.

To determine multiplicity of infection, tumor cells were plated on 15 cm tissue culture-treated dishes with or without poly-L-ornithine/laminin coating at ~25-50% density depending on cell line-specific doubling time, in a total of 25-30 mL of media. Twenty-four hours after plating, cells were infected with different dilutions of the TKOv3 library lentivirus. Twenty-four hours after infection, the virus-containing media was replaced with 25-30 mL of fresh medium containing puromycin (1-3 μg/mL) and cells were incubated for an additional 24-72 hours. Multiplicity of infection (MOI) was determined by calculating the fraction of infected cells that survived puromycin selection as compared to infected cells that were not selected.

Genome-wide CRISPR-Cas9 screens in GBM models

Tumor cells were plated on 15 cm tissue culture-treated dishes with or without poly-L-ornithine/laminin coating at ~25-50% density depending on cell line-specific doubling time, in a total of 25-30 mL of media. Twenty-four hours after plating, cells were infected with the TKOv3

library lentivirus at an MOI of ~0.3, ensuring that each gRNA was present in 200-500 cells. Twenty-four hours after infection, the virus-containing media was replaced with 25-30 mL of fresh medium containing puromycin (1-3 μg/mL) and cells were incubated for an additional 24-72 hours. Cells that survived puromycin selection were pooled together, and 30 million cells were collected as an initial reference timepoint (T0).

For dropout screens (BT241 and BT972), infected and puromycin-selected cells were split into three experimental replicates, with each replicate containing 15+ million cells (>200-fold library coverage). Cells were passaged every 2-3 doublings and maintained at >200-fold library coverage for 15-18 doublings. Cell pellets were collected during passaging from each replicate for downstream analysis. For screens involving drug treatment (BT594 and BT935), infected and puromycin-selected cells were split into one of four treatment arms: control DMSO treatment, sublethal IC_{20-30} radiotherapy (RT), sublethal IC_{20-30} temozolomide (TMZ), or sublethal IC_{20-30} RT and TMZ. For combined RT and TMZ therapy, each plate was treated with TMZ (Millipore Sigma no. T2577) one hour prior to RT (Faxitron RX-650). For the entire duration of the screen, treatments were administered in cycles of 5 days on and 2 days off to allow for recovery and passaging. Passaging and collection of cell pellets was performed as described above.

Library preparation and Illumina sequencing

Genomic DNA (gDNA) was extracted from cell pellets collected at the beginning (T0) and end of each screen (Tn) using the Wizard Genomic DNA Purification Kit (Promega). Following resuspension in TE buffer, gDNA concentration was determined by Qubit using double-stranded DNA (dsDNA) Broad Range Assay reagents (Invitrogen). For each sample, 50 μg of extracted DNA was subjected to two PCR reactions, the first of which enriched gRNA-containing regions

and the second step amplified gRNAs and attached Illumina TruSeq adapters with i5 and i7 indices, as described previously Barcoded libraries were gel purified and concentrations were determined by qRT-PCR. Sequencing of libraries was performed on an Illumina HiSeq2500 using standard primers for dual indexing with HiSeq SBS Kit v4 reagents. The single-end sequencing run consisted of 21 dark cycles (base additions without imaging), followed by 36-base reads containing 2 index reads, first with i7 and the second with i5 sequences. The beginning (T0) and endpoints (Tn) were sequenced at 400- and 200-fold coverage, respectively.

Mapping and quantification of gRNAs

Following completion of Illumina sequencing, 20-bp gRNA sequences were extracted from FASTQ files by trimming reads according to constant sequence anchors. Trimmed reads were aligned to a FASTA file of gRNA sequences from TKOv3 using Bowtie (v0.12.8) (Langmead et al., 2009). Two mismatches and 1 exact alignment were allowed during alignment (specific parameters: -v2 -m1 -p4 –sam-nohead). Processed reads were tallied for each sample and merged into a matrix.

Quality control analysis and scoring of gRNAs

To begin quantifying the gene fitness in each screen, LFC of each gRNA was quantified by comparing read-depth-normalized gRNA counts at the beginning of each screen (T0) to the end of each screen (Tn). To perform quality control analysis, the LFC for all gRNAs targeting a single gene were averaged, with four gRNAs targeting each gene in TKOv3 (Hart et al., 2017). Established gene sets of core essential genes (reference) (Behan et al., 2019; Hart et al., 2015; Hart

et al., 2017) and non-essential genes (background) (Hart et al., 2015; Hart et al., 2017) were compared for dropout using LFC values and by computing precision over true positive statistics.

For all pooled CRISPR-Cas9 screens, LFC values of core essential genes and non-essential genes were used to apply the Bayesian Analysis of Gene Essentiality (BAGEL) algorithm (Hart and Moffat, 2016) to determined fitness of all genes. A Bayes Factor (BF) score of 5 and FDR<0.05 were used to identify genes essential for cell survival. For drug-treated CRISPR-Cas9 screens (BT594 and BT935), LFC values for gRNAs targeting each gene were compared between a drug-treated arm (treatment) and the DMSO-treated arm (control) for each cell line by applying the DrugZ algorithm (Colic et al., 2019). For each drug-treated arm (RT, TMZ, or combined RT and TMZ), positive and negative conditional genetic interactions (GIs) were identified using normalized Z scores combined with synthetic/suppressor FDR values.

Gene set enrichment analysis of conditional gRNA distributions

For all primary GBM CRISPR-Cas9 screens, normalized gene-level LFC values from each arm (DMSO, RT, TMZ, or combined RT and TMZ) were used to conduct gene set enrichment analysis (Subramanian et al., 2005) (GSEA) using fgsea (v1.14.0) (Korotkevich et al., 2020). For each screen, GSEA of Reactome (Jassal et al., 2020) canonical pathways (c2.cp.reactome.v7.1) was conducted with a minimum of 1 and maximum of 1000 genes in each gene set, a total of 10,000 permutations, and an adjusted $P<0.05$. GSEA results were collapsed into parent gene sets using the collapsePathways() function from fgsea. Normalized enrichment scores (NESs) from all screens were compiled in a matrix (Supplementary Table 4).

Functional gene enrichment analysis

Shared essential genes in primary and recurrent tumor cells. A set of shared essential genes with BF scores > 5 in primary BT594 (DMSO-treated) and recurrent BT972 tumor cells was determined. Genes belonging to core essential gene sets (Behan et al., 2019; Hart et al., 2017) were filtered out and remaining shared essential genes were subjected to functional enrichment analysis using gProfiler2 (Reimand et al., 2007) (v0.1.9). Using all genes targeted by TKOv3 (Hart et al., 2017) as background, the gost() function was applied to determine enriched gene sets from Reactome, gene ontology (GO) biological processes and GO molecular function with FDR<0.05. Using Cytoscape (v3.8.0), enriched gene sets with a similarity of >50% were collapsed using the Enrichment Map function (v3.3.0) and the AutoAnnotate function (v1.3.3) was used to determine themes of overlapping gene sets.

Shared essential genes in recurrent tumor cells. A set of shared essential genes with BF scores > 5 in recurrent BT241 and BT972 tumor cells was determined. Genes belonging to core essential gene sets (Behan et al., 2019; Hart et al., 2017) were filtered out and remaining shared essential genes were subjected to functional enrichment analysis using gProfiler2 (Reimand et al., 2007) (v0.1.9). Using all genes targeted by TKOv3 (Hart et al., 2017) as background, the gost() function was applied to determine enriched gene sets from Reactome, GO biological processes with FDR<0.05. Using Cytoscape (v3.8.0), enriched gene sets with a similarity of >50% were collapsed using the Enrichment Map function (v3.3.0) and the AutoAnnotate function (v1.3.3) was used to determine themes of overlapping gene sets.

<u>*In vitro* assays for self-renewal and proliferation</u>

Cell preparation. Tumor cells, with or without genetic knockout, were dissociated into a single cell suspension using TrypLE (ThermoFisher Scientific no. 12605028) for adherent cultures, or a

combination of Liberase Thermolysin Research Grade (Millipore Sigma no. 5401020001) and DNase I (Worthington Biochemical Corporation no. 9003-98-9) for suspension spherical cultures. Cells were incubated with dissociation agent for 5 minutes at 37°C. After washing dissociated cells twice with PBS, the cell suspension was filtered through a 35μm cell strainer prior to plating for assays. All assays were performed using NeuroCult NS-A proliferation kit (Human), supplemented as described above. All experiments were conducted with five experimental replicates per sample.

Limiting dilution assay. Tumor cells were plated at varying densities (1, 5, 10, 50, 100, 200 cells/well) in cell-repellent 96-well, flat-bottom microplate (Greiner Bio no. 655970). Cells were cultured in 200 μL of media and incubated for 3-5 days at 37°C and 5% CO_2. Following incubation, cell spheres were counted by microscopy. For each sample, the frequency of sphere-forming cells in each cell line was determined using the elda() function from statmod (v.1.4.34). A single-hit model with a log-log binomial regression was applied to determine confidence intervals for sphere-forming cell frequency. A chisquare likelihood ratio test statistic was applied to signify difference between samples.

Secondary sphere formation assay. Tumor cells were plated at 200 or 300 cells/well in cell-repellent 96-well, flat-bottom microplate (Greiner Bio no. 655970). Cells were cultured in 200 μL of media and incubated for 3-5 days at 37°C and 5% CO_2. Following incubation, cell spheres were counted by microscopy. An unpaired T-test was used to compare between samples.

Proliferation assay. Tumor cells were plated at 1000 cells/well in flat-bottom tissue culture-treated 96-well microplates. Cells were cultured in 200 μL of media and incubated for 3-5 days at 37°C and 5% CO_2. To quantify proliferation, 20 μL of PrestoBlue Cell Viability Reagent was added to each well followed by incubation for 4 hours at 37°C and 5% CO_2. Fluorescence was measured on

a FLUOstar Omega Fluorescence 566 Microplate reader (BMG LABTECH) (excitation 540 nm and emission 570 nm) and analyzed using Omega software. An unpaired T-test was used to compare between samples.

In vivo engraftment of tumor cells

All animal experimental protocols were approved by the McMaster University Animal Research Ethics Board. Tumor cells were injected orthotopically into immunocompromised mice as described previously (Singh et al., 2004). In brief, 10-12 week old NSG mice were anaesthetized using isofluorane gas (5% induction, 2.5% maintenance). A total of 250,000 tumor cells were injected per mouse into the right frontal lobes, suspended in 5 μL PBS. All mice were euthanized at endpoint and survival analysis was conducted using the survfit() and Surv() functions from the package survival (v.3.2-3), and plotted using the package survminer (v.0.4.8).

In vivo inducible knockout of *PTP4A2*

Recurrent BT241 tumor cells were infected with lentivirus containing an doxycycline-inducible Cas9 (iCas9) construct (Mair et al., 2019). Validated BT241-iCas9 cells were treated with doxycycline (DOX; 1.5μg/mL, Sigma) for 48 hours to induce Cas9 and BFP2 expression. DOX-induced and uninduced samples were run on a MoFlo XDP Cell Sorter (Beckman Coulter). After excluding dead cells using 7AAD (1/100, Beckman Coulter), BFP2+ cells were sorted into tubes containing NeuroCult NS-A proliferation kit (Human), supplemented as described above.

BT241-iCas9 cells were infected with a modified pLCKO vector (no Cas9) (Mair et al., 2019) containing gRNA sequences targeting *AAVS1* or *PTP4A2*, obtained from TKOv3 (Hart et al.,

2017) and cloned as described previously (Mair et al., 2019). Following selection with puromycin (3 μg/mL for 72 hours), 250,000 gRNA-expressing BT241-iCas9 were injected in immunocompromised NSG mice as described above. Two weeks after injection, mice were treated with DOX in their water (2 mg/mL DOX with 1% sucrose) and feed (625 mg/kg DOX-supplemented Envigo no. 7004 feed) for 2 weeks. Following DOX treatment, mice were put back on normal water and feed. All mice were euthanized at endpoint and survival analysis was conducted as described above.

RNA sequencing

Sample preparation. Five million tumor cells (BT594 or BT972) were plated in cell-repellent dishes (Grenier Bio no. 628979) and infected with lentivirus containing single-gRNA lentiCRISPRv2 constructs targeting *AAVS1* or *PTP4A2* (2 gRNAs), with gRNA sequences obtained from TKOv3 (Hart et al., 2017). Twenty-four hours post-infection, virus-containing media was replaced with fresh media containing puromycin (1-2 μg/mL) for 48-72 hours. Each cell line was cultured and processed in three experimental replicates. Following antibiotic selection, RNA was extracted using the RNeasy Kit (Qiagen), according to manufacturer's instructions. All samples were treated with DNase using RNase-free DNase Set (Qiagen no. 79254). Samples were submitted for mRNA-Seq at the Donnelly Sequencing Centre at the University of Toronto, Toronto, Canada (http://ccbr.utoronto.ca/donnelly-sequencing-centre). 300ng per sample was processed according to NEBNext Ultra II Directional RNA Library Prep sample preparation protocol (Part # E7760L) with the NEBNext Poly(A) mRNA Magnetic Isolation Module (Part # E7490). 1μL top stock of each purified final library was run on an Agilent TapeStation HS D1000 tape (Agilent). The libraries were quantified using Quant-

iT dsDNA HS Assay Kit (ThermoFisher Scientific) and were pooled at equimolar ratios after size adjustment. The final pool was run on an Agilent Bioanalyzer dsDNA High Sensitivity chip and quantified using NEBNext Library Quant Kit for Illumina (NEB). The quantified pool was hybridized at a final concentration of 2.75pM and sequenced paired-end 2x50 bp on the Illumina NovaSeq6000 platform using an S2 flowcell to obtain an average of 28M reads per sample.

Data processing. Read pairs shorter than 36bp on either read1 or read2 were filtered out prior to mapping. Reads were aligned to reference genome hg38 and Gencode V25 gene models using the STAR short-read aligner (v2.6.1b) (Dobin et al., 2013). An average of 86.9% of the filtered reads mapped uniquely. Gene-level read counts, determined by STAR, were merged along with gene annotations into a single matrix using a bespoke R script.

Differential expression. Differentially expressed genes (DEGs) were identified using the Bioconducter packages limma (Ritchie et al., 2015) (v3.44.3) and edgeR (McCarthy et al., 2012) (v3.30.3). The read count matrix was filtered to remove low-expressed genes using the function filterByExpr() using default parameters. Principal component analysis (PCA) allowed for visualization of treatment effects and adjustment for batch-to-batch differences. Normalization was performed using calcNormFactors (method = 'TMM') and log2-transformed using voom(). A linear model was fit to account for differences between BT594 and BT972 cells (main effect) as well as among knockouts for *AAVS1*, *PTP4A2* (first gRNA) and *PTP4A2* (second gRNA). DEGs were extracted using treat() (limma) and determined using $\log_2$(fold change)>1 and adjusted $P<0.05$.

Variant calling. Genomic variants affecting protein-coding genes were identified from the RNAseq data using the Genome Analysis Toolkit (GATK) version 3.1 following the recommended "Best Practices". Briefly, beginning with the BAM output file from STAR, the steps included

AddOrReplaceReadGroups, MarkDuplicates, ReorderSam, SplitNCigarReads, HaplotypeCaller, and finally VariantFiltration. Variant consequences were classified using the Variant Effect Predictor (VEP) release 89, which includes predictions from SIFT, PolyPhen and Condel.

Whole cell proteomics.

Sample preparation. Five million patient-derived tumor cells (BT594 and BT972) were cultured in cell-repellent 10 cm dishes (Greiner Bio no. 628979) with 10 mL of NeuroCult NS-A proliferation kit (Human) (STEMCELL Technologies no. 05751), supplemented as described above. Cells were incubated for 96 hours at 37°C and 5% CO_2 to enrich for sphere formation. Following incubation, cells were washed thrice with cold PBS, centrifuged into pellets and snap frozen using liquid nitrogen. Cell pellets were stored at -80°C until further processing.

Cells were lysed in PBS:2,2,2-trifluoroethanol (TFE) (1:1 v:v)) as previously described (Cogger et al (PMID: 28835709)). Protein concentration was determined using the BCA kit (Thermo) according to the manufacturer's instruction. Cysteins were reduced with Dithiothreitol (DTT, 5mM final concentration) at 60°C for 30 minutes and subsequently alkylated using iodoacetamide (25mM final concentration) in the dark at room temperature for 30 minutes. Samples were diluted with four volumes 100 mM ammonium bicarbonate (pH 8.0), supplemented with calcium chloride (2mM final concentration) and digested for 16 h at 37°C with Trypsin:LysC (Thermo) added at a 1:50 ratio. The digestion was quenched using 0.5% formic acid (FA) and tryptic peptides were fractionated using a basic C18 fractionation method. Briefly, tryptic peptides were loaded on four 45 mm C18 extraction disks (Empore™, Fischer Scientific) and eluted in five fractions using increasing acetonitrile (ACN) (5%, 7.5%, 10%, 12.5%, 15%, 17.5%, 20%, 50%) concentration solutions prepared in 0.1% ammonium hydroxide. Fractions were pooled as follows:

fractions 3+6; 4+7; 5+8. Fractions 1 and 2 were not pooled. The five resulting fractions were lyophilised and reconstituted in 21µL 3% ACN 0.1% FA. Peptide concentration was determined using a NanoDrop 2000 (Thermo) spectrophotometer and were loaded on a 50 cm ES803 column (Thermo). Peptides were separated using a 4h gradient, at 250 nL/min flow, using the Thermo Scientific EasyLC1000 nano-liquid-chromatography system. The chromatography system was coupled to an Orbitrap Fusion Mass Spectrometer (Thermo) and MS/MS data were acquired in a data dependent mode with full scans (350-1800 m/z) acquired using the ion trap mass analyser at a mass resolution of 120,000 m/z. Fifteen most intense precursors from a survey scan were selected for MS/MS from each cycle and detected at a mass resolution of 15,000 m/z. Tandem mass spectra were produced by high energy dissociation (HCD) method. Dynamic exclusion was set for 60 s. The automatic gain control for full MS was set to $1e^5$ ions and $1e^2$ ions for MS/MS with maximum ion injection times of 55 ms and 50 ms respectively.

Data analysis. The acquired raw data were analysed using the Max Quant software (version 1.6.1.0) using the complete human proteome (version 2016.07.13 containing 42,041 sequences). Search parameters were defined as follow: a maximum of two missed cleavages; carbamido-methylation of cysteine was specified as fixed modification and oxidation of methionine as variable modifications. Peptide length was specified to be 8-25 amino acids. The mass error was set to 10 p.p.m. for precursor ions and 0.5 Da for fragment ions. The false discovery rate (controlled using a target-decoy approach based on reversed sequences) was defined as 1% at peptide and protein levels. The Maxquant output was compiled into a matrix for further analysis.

Recurrent GBM-enriched gene essentiality and expression

Bayes factor (BF) scores for a total of 666 genome-wide CRISPR-Cas9 screens in human cancer cell lines were acquired from the PICKLES database (Lenoir et al., 2018), which included the Behan 2019 (Behan et al., 2019) and Avana 2018 q4 (Meyers et al., 2017) datasets. For each data set, BF scores were averaged by sample collection site and merged into a single matrix and merged with BF scores from recurrent GBM screens (BT241 and BT972). To incorporate differentially expressed genes (DEGs) in GBM, the GEPIA2 interface was utilized to compare genome-scale gene expression between Cancer Genome Atlas (TCGA) GBM specimens and GTEX normal brain specimens, as described previously (Tang et al., 2017). To determine a set of recurrent GBM-specific essential genes, a stringent cut-off of BF score > 5 was used to classify an essential gene. By filtering for genes with BF>5 in recurrent tumor cell lines and BF≤5 in all 666 screens from the PICKLES database (Lenoir et al., 2018), we determined a set of recurrent GBM-specific essential genes. This subset of genes were further filtered to include those genes that are enriched for expression in GBM tissues (TCGA) as compared to normal brain tissue (GTEX), with a $\log_2$ fold change > 1 and an adjusted $P < 0.01$.

Gene expression and survival analysis from TCGA and CGGA

Gene expression and patient survival data was obtained for all low grade glioma and GBM patients profiled by TCGA (GBMLGG RNA-seq dataset from Gliovis, www.gliovis.bioinfo.cnio.es) and the Chinese Glioma Genome Atlas (CGGA; mRNAseq_693 dataset from www.cgga.org.cn). To profile PTP4A2 gene expression in each dataset, *PTP4A2* gene expression values were $\log_2$-transformed and stratified according to WHO (World Health Organization) grading. Pairwise comparisons among WHO grades were conducted using the Wilcoxon rank sum test. To determine the effect of *PTP4A2* expression on patient survival, patient specimen expression values were

stratified into 'high *PTP4A2'* and 'low *PTP4A2'* groups according to the median expression value in each dataset. Data was plotted using the package survminer (v.0.4.8).

In vitro treatment of cells with pan-PTP4A inhibitor

Briefly, the pan-PTP4A inhibitor JMS-053 and an inactive control compound (JMS-038) were synthesized as described previously (Salamoun et al., 2016) and resuspended at 5 mM in 100% DMSO. To test for cytotoxicity, cells (tumor cells or fetal NSCs) were plated at 1000 cells/well in flat-bottom tissue culture-treated 96-well microplates. Cells were treated once with various concentrations (20 nM to 20 μM) of JMS-038 or JMS-053. Cells were cultured in 200 μL of media and incubated for 7 days at 37°C and 5% CO_2. To quantify proliferation, 20 μL of PrestoBlue Cell Viability Reagent was added to each well followed by incubation for 4 hours at 37°C and 5% CO_2. Fluorescence was measured on a FLUOstar Omega Fluorescence 566 Microplate reader (BMG LABTECH) (excitation 540 nm and emission 570 nm) and analyzed using Omega software.

Phospho-proteomic profiling of PTP4A-inhibited tumor cells

Sample preparation. 2.5 million tumor cells (BT594 and BT972) were plated at a density of 0.5 million cells/mL of NeuroCult NS-A proliferation kit (Human), supplemented as described above. Cells were either treated with 1 μM JMS-053 (active pan-PTP4A inhibitor) or 1μM JMS-038 (inactive control compound) for 5 minutes or 30 minutes at 37°C and 5% CO_2. Following incubation, samples were immediately washed with cold PBS containing 1X Halt Protease and Phosphatase Inhibitor (Thermo Fisher Scientific no. 78442). Following three cycles of centrifugation and washing with HALT-containing PBS, samples were pelleted. Except for BT594 tumor cells treated with JMS-053 for 30 minutes, all samples were cultured, treated and processed

in experimental duplicates. Cell pellets were suspended in 200μL of lysis buffer composing of 8M urea (Sigma-Aldrich) and 100mM ammonium bicarbonate (Sigma-Aldrich) each. Cells were then vortexed at 2,800rpm using Mini S-2 Vortex Mixer (Fisher Scientific) for ten seconds, followed by ten seconds of incubation on ice. This procedure was repeated six times. The lysate was then centrifuged at 21,000xg for five minutes at 4°C. Protein reduction was conducted using 5mM of tris (2-carboxyethyl) phosphine (Sigma-Aldrich) for 45 minutes at 37°C. Subsequently, 10mM of iodoacetamide (Sigma-Aldrich) was added for protein alkylation for 45 minutes at room temperature (dark). Following alkylation, cell lysate was diluted five-fold with 100mM of ammonium bicarbonate to lower urea concentration. Based on protein amount, Sequencing Grade Modified Trypsin (Promega) was then added in (trypsin: protein(w:w) at 1:50) for overnight digestion at 37°C. Trifluoroacetic acid (Thermo Scientific) was added to reduce pH, and desalting was conducted with SOLA Solid Phase Extraction 10mg 96-well plates (Thermo Scientific). Peptides were eluted using 400④L 80% Acetonitrile - 0.1% trifluoroacetic acid. Eluted peptides were speed-vacuum dried using Labconco CentriVap Benchtop Vacuum Concentrator (Kansas City, MO).

Labeling, phospho-peptide enrichment and LC/MS/MS. Tandem Mass Tag (TMT)11-plex Isobaric Label Reagent Set (Thermo Fisher) were used to label peptides form each condition following manufacturer's protocol. Briefly, dried peptide samples were resuspended in 100mM of triethylammonium bicarbonate (TEAB) (Sigma-Aldrich) to 1μg/μL. Then, 0.2mg TMT reagents were mixed with 50μg of peptide samples at 4:1 (wt/wt) ratio and incubated at room temperature for one hour. Following incubation, each TMT reaction was quenched with 2μL of 5% hydroxylamine (Sigma-Aldrich) for 15 minutes at room temperature. Labeled samples were pooled together at equal ratio and then speed-vacuum dried. Desalting was then performed to

purify salt-free TMT-label peptide samples. Phosphopeptides-enrichment were conducted using Ni-NTA magnetic agarose beads (Qiagen). Briefly, 138μl of Ni-NTA magnetic agarose beads were washed three times with 400μl of ultrapure nuclease-free water, and then incubate with 400μl of 100nM EDTA for 30 minutes. After three times wash with 400μl of ultrapure nuclease-free water, the beads were incubated with 100nM $FeCl_3$ for 30 minutes. Then beads were washed three times with 400μl of ultrapure nuclease-free water and one time with 400μl of 80% Acetonitrile - 0.1% trifluoroacetic acid. 550μg TMT-labeled peptides were resuspended in 550μl of 80% Acetonitrile - 0.1% trifluoroacetic acid and added to the Fe-activated beads, rotating for 30 minutes. After capture, the supernatant was saved for analysis of unphosphorylated peptides and phosphopeptides were eluted using 50μl of 1.4% of ammonia hydroxide solution followed by another 50 μl of ultrapure nuclease-free water.

Enriched phosphopeptides were separated into 9 fractions by high pH reverse phase liquid chromatography (RPLC) using a home-made C18 column (200 μm x 30cm bed volume, Waters BEH 130 5μm resin) from 11%-32% acenotritile-20mM ammonium formate (pH=10) at flow rate of 5μl/minute. Each fraction was then loaded onto a home-made trap column (200 μm x 5 cm bed volume) packed with POROS 10R2 10μm resin (Applied Biosystems), followed by a home-made analytical column (75μm x 25cm bed volume) packed with Reprosil-Pur 120 C18-AQ 1.9μm particles (Dr. Maisch) with integrated Picofrit nanospray emitter (New Objective). LC-MS experiments were performed on a Thermo Fisher Ultimate 3000 RSLCNano UPLC system that ran a 3hr gradient (11%-38% acetonitrile-0.1% formic acid) at 70nl/min, coupled to a Thermo QExactive HF quadrupole-Orbitrap mass spectrometer. A parent ion scan was performed using a resolving power of 120,000 and then up to the 30 most intense peaks were selected for MS/MS

(minimum ion counts of 1000 for activation), using higher energy collision induced dissociation (HCD) fragmentation. Dynamic exclusion was activated such that MS/MS of the same m/z (within a range of 10ppm; exclusion list size=500) detected twice within 5s were excluded from analysis for 30s.

Data analysis. LC-MS data were searched against a UniProt human protein database (Ver 2017-06, 42,173 entries) for protein identification and quantification by Protein Discover software (Thermo). From 300,970 MS/MS spectra acquired in all 9 fractions, 84,496 peptide-to-spectrum matches (PSMs), 20,443 unique peptide groups (with Peptide FDR < 0.01), and 4,732 unique proteins (Protein FDR < 0.01) were identified. Among the identified peptide groups, 17,127 hits were phosphopeptides. The density of these phosphopeptides was normalized by total TMT reporter intensity values from a separate LC/MS/MS run of the phosphoenrichment flow-through. Phosphopeptide fold change between JMS-053 and JMS-038 for both cell lines was calculated, and the mean value of TMT reporter intensity for each phosphopeptide was calculated as well. These values were then uploaded to Perseus software to generate Significance B values.

Functional enrichment analysis of enriched phospho-proteins

Phospho-peptide intensities for all samples were filtered for <50% coefficient of variation (Rfast v.1.9.9). Phospho-peptides enriched after short-term treatment with JMS-053, with a treatment/control phospho-peptide intensity fold change > 1.5, were determined and the corresponding phospho-proteins were subjected to functional enrichment analysis. Using the package gProfiler2 (v0.1.9), The gost() function was applied to determine enriched gene sets from GO cellular component processes with FDR<0.05.

Development of anti-ROBO1 antibodies

Generation of anti-ROBO1 single-domain antibodies. Camelid single-domain antibodies were raised by llama immunization and phage display essentially as previously described (Arbabi Ghahroudi et al., 1997; Baral et al., 2013). A phage-displayed heavy chain (V_HH) library was constructed from the peripheral blood B-cell repertoire of a llama immunized with recombinant human ROBO1-Fc (8975-RB-050, R&D Systems, Minneapolis, MN). Antigen-reactive V_HH-phage were enriched by panning against ROBO1-Fc with subtraction on Fc alone.

Antibody expression, purification and validation. Monomeric single-domain antibodies bearing His_6 and biotin acceptor peptide tags were expressed in the periplasm of *Escherichia coli* BL21 (DE3) cells, enzymatically biotinylated *in vitro* using BirA(Fairhead and Howarth, 2015), and purified by immobilized metal affinity chromatography followed by size exclusion chromatography (Superdex 75 Increase 10/300 GL, GE Healthcare, Chicago, IL). ROBO1 extracellular domain (NP_598334.1 aa 1–858) and ROBO1 Ig1-Ig2 domains (NP_002932.1 aa 61–266) were produced by transient transfection of HEK293-6E cells with pTT3/pTT5 vectors and antibody binding to these proteins was assessed by indirect titration ELISA. The affinities and kinetics of the interactions between monomeric single domain antibodies and human ROBO1 (25°C, pH 7.4) were determined using surface plasmon resonance. ROBO1 and other proteins were immobilized on a sensor chip CM5 (GE Healthcare) by amine coupling and antibodies were flowed over the antigen surfaces on a Biacore T200 instrument (GE Healthcare). Data from multi-cycle kinetic analysis were fit to a 1:1 binding model.

Generation of human Fc-linked MKRo-20 (MKRo-20-hFc). The encoding sequence of MKRo20 was codon optimized (Gene Art, ThermoFisher Scientific) and cloned into pTT5-hIgG1. Bivalent V_HH-human IgG1 Fc fusions were produced by transient transfection of HEK293-6E cells

followed by protein A affinity chromatography as described previously (Durocher et al., 2002; Zhang et al., 2009). The same procedure was applied for the generation of A20.1 (AXX-hFc), a V_HH specific for clostridium difficile toxin A (Hussack et al., 2011) used as negative control (Durocher et al., 2002; Zhang et al., 2009). The same procedure was applied for the generation of A20.1 (AXX-hFc), a V_HH specific for clostridium difficile toxin A (Hussack et al., 2011) used as negative control.

Flow cytometry validation of MKRo-20-hFc binding to recurrent tumor cells. Cells were dissociated using Liberase (Millipore Sigma no. 5401127001) and DNase I (Worthington Biochemical Corporation no. 9003-98-9) into a single cell suspension. After washing once with PBS, cells were resuspended in PBS. To quantify ROBO1 expression on the cell surface, 500,000 live cells were stained with 0.002 mg/mL anti-ROBO1 mouse-anti-human IgG1-AF647 (R&D Systems no. FAB71181R) or various concentrations of MKRo-20-hFc (3.4e-05 to 1.1e-03 mg/mL) for 15 minutes at room temperature. Equivalent concentrations of the isotypic control (AXX-hFc) for MKRo-20-hFc were also used to stain cells. Following staining, cells were washed with PBS, followed by staining with 1/1000 dilution of anti-human IgG Fcγ-specific AF488 (Jackson ImmunoResearch no. 109-545-008) for 30 minutes on ice. After washing with PBS, cells were stained with 1/100 7-AAD viability dye (Beckman Coulter no. B88526). Samples were run on a CytoFLEX LX (Beckman Coulter), and data was analyzed using analysis software Kaluza 2.0 (Beckman Coulter). Forward scatter (FSC)-Area vs. side scatter (SSC)-Area is used as the initial gate to exclude debris. Viability gate is set to exclude non-viable cells by gating on the 7-AAD negative population. Isotype control AXX-hFc is used to set the gate for expression of ROBO1, where gate is drawn to separate ROBO1-positive cells from non-specific binding of AXX-hFc.

In vivo validation of MKRo-20 in recurrent GBM

Immunocompromised mice were intracranially injected with 250,000 live cells/mouse of recurrent BT241 tumor cells. Six days post injection, mice were administered four intracranial treatments of 40 μg tetrameric MKRo-20 (n = 4) or 40 μg tetrameric control (n = 4) spaced evenly over 2 weeks. One week after the last treatment (27 days post injection), mice were euthanized, brains were collected, fixed with formalin and subjected to paraffin-embedding for hematoxylin and eosin (H&E) staining.

Statistical analysis

All experimental data is accompanied by number of experimental experiments in the figure legends or text. Unless stated otherwise, statistical significance was assessed using an unpaired Student's t-test. In all cases otherwise states, *** $p<0.0001$, ** $p<0.001$, *$p<0.05$. Statistical analyses were performed using the R language programming environment.

Data and code availability statement

All processed data is included in the manuscript and supplemental materials. Raw sequencing data (i.e. FASTQ files) will be uploaded to an appropriate online database prior to publication. All custom code will be made available via GitHub.

Biological material availability statement

All unique biological materials are available upon request from corresponding authors.

Supplementary Figures

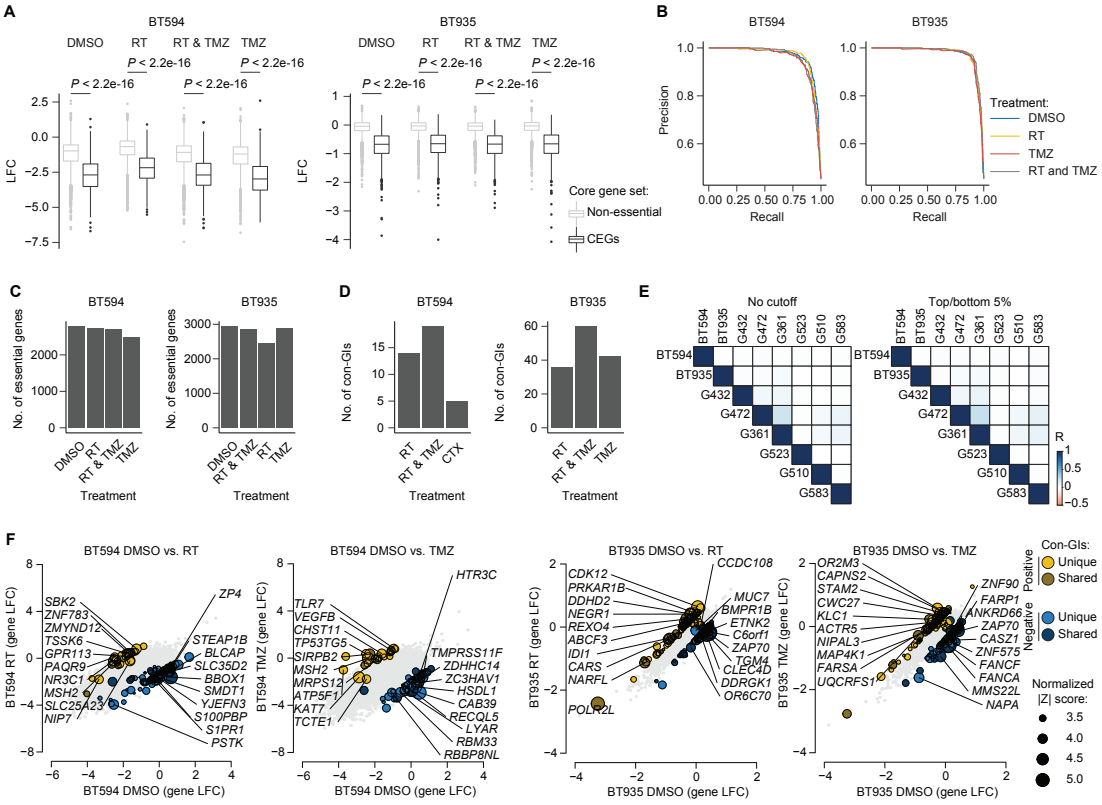

Figure S1. Quality control analysis of screens in primary GBM models, Related to Figure 1.

(A) Gene-level LFC of CEGs (Behan et al., 2019; Hart et al., 2017) and non-essential genes (Hart et al., 2017) across screens in primary tumor cells. All data presented from $n = 3$ biologically independent replicates. *P* values are from unpaired Student's t tests.

(B) Precision-recall plots indicate high performance of screens in primary tumor cells.

(C) Number of essential genes (FDR < 0.05) identified in primary GBM screens.

(D) Number of cGIs identified in BT594 (left) or BT935 (right) cells treated with RT and/or TMZ (FDR < 0.05).

(E) Pearson correlation matrices of cGI Z scores between TMZ-treated screens on primary tumor cells, as well as screens from (Toledo et al., 2015) and (MacLeod et al., 2019). Data presented with (left) and without (right) filtering for genes that fall into the top or bottom 5% of Z scores in least one screen.

(F) Negative and positive cGIs of mono therapy (RT or TMZ) identified in BT594 (left 2 panels) and BT935 (right 2 panels) cells. Significant positive (yellow) and negative (blue) cGIs (FDR < 0.1) highlighted. Node color represents the overlap of significant cGIs between monotherapy-treated screens (sublethal RT or TMZ), while node size corresponds to the absolute normalized Z score of cGIs of combination treatment. Top 10 positive and negative cGIs, according to normalized Z score, are labelled.

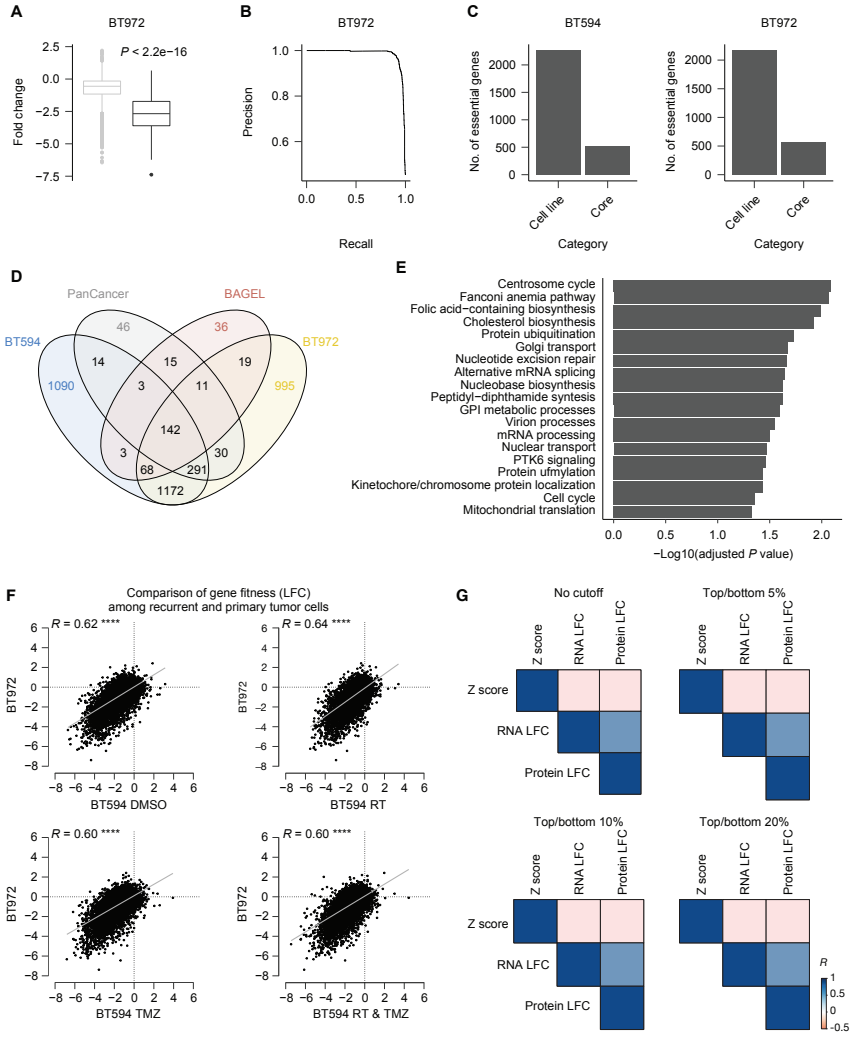
A
BT972
P < 2.2e−16
Fold change
2.5
0.0
−2.5
−5.0
−7.5
B
BT972
Precision
1.0
0.8
0.6
0.0
0.5
1.0
Recall
C
BT594
BT972
No. of essential genes
2000
1500
1000
500
0
Cell line
Core
Category
D
PanCancer
BAGEL
BT594
BT972
1090
995
46
36
14
15
19
3
11
142
3
30
68
291
1172
E
Centrosome cycle
Fanconi anemia pathway
Folic acid−containing biosynthesis
Cholesterol biosynthesis
Protein ubiquitination
Golgi transport
Nucleotide excision repair
Alternative mRNA splicing
Nucleobase biosynthesis
Peptidyl−diphthamide syntesis
GPI metabolic processes
Virion processes
mRNA processing
Nuclear transport
PTK6 signaling
Protein ufmylation
Kinetochore/chromosome protein localization
Cell cycle
Mitochondrial translation
0.0
0.5
1.0
1.5
2.0
−Log10(adjusted P value)
F
Comparison of gene fitness (LFC)
among recurrent and primary tumor cells
R = 0.62 ****
R = 0.64 ****
R = 0.60 ****
R = 0.60 ****
BT972
BT594 DMSO
BT594 RT
BT594 TMZ
BT594 RT & TMZ
G
No cutoff
Top/bottom 5%
Top/bottom 10%
Top/bottom 20%
Z score
RNA LFC
Protein LFC
R
1
0.5
0
-0.5

Figure S2. Quality control analysis of screens in patient-matched primary and recurrent GBM models, Related to Figure 2.

(A) Gene-level LFC of CEGs and non-essential genes from CRISPR screen in BT972 tumor cells. All data presented as the mean of three biologically independent replicates. *P* values are from unpaired Student's t tests.

(B) Precision-recall plots indicate performance of CRISPR screen in BT972 tumor cells.

(C) Number of cell-line-specific and core essential genes (FDR < 0.05) in patient-matched tumor cells.

(D) Venn diagram of essential genes (FDR < 0.05) in BT594 and BT972 tumor cells. Overlap with CEG sets shown.

(E) Enrichment of GO biological process, molecular function and Reactome terms among genes that show decreased or increased level of essentiality in BT972 tumor cells(FDR < 0.05), relative to DMSO-treated BT594 tumor cells. FDR-adjusted *P* values derived from gProfiler (Reimand et al., 2007).

(F) Gene-level LFC in BT972 tumor cells compared to drug-treated or DMSO-treated BT594 tumor cells. Data presented as the mean from three biologically independent replicates; Pearson correlation coefficients and resulting *P* values indicated with linear correlation line.

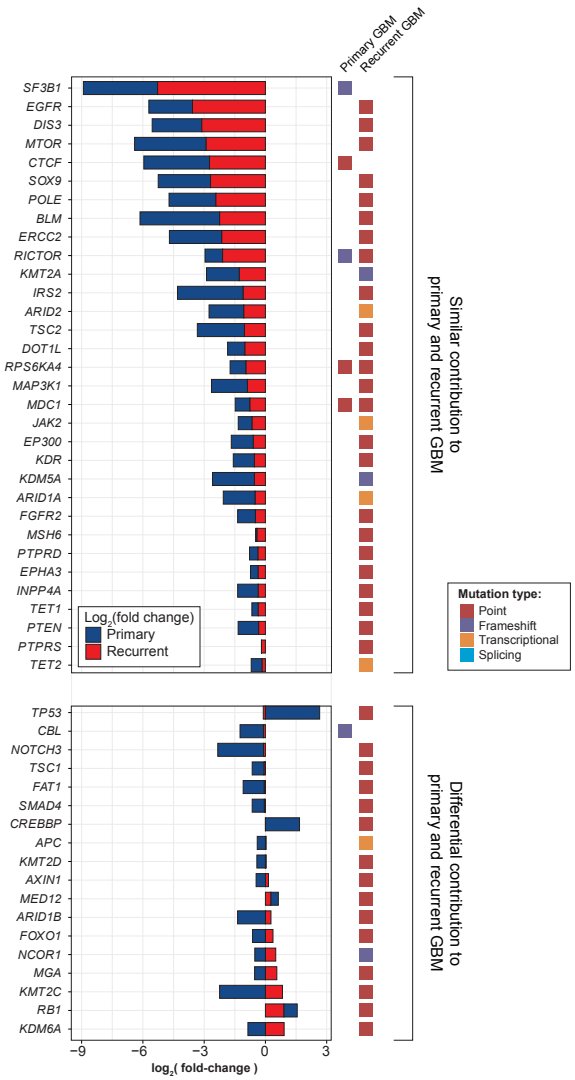
Primary GBM
Recurrent GBM
SF3B1
EGFR
DIS3
MTOR
CTCF
SOX9
POLE
BLM
ERCC2
RICTOR
KMT2A
IRS2
ARID2
TSC2
DOT1L
RPS6KA4
MAP3K1
MDC1
JAK2
EP300
KDR
KDM5A
ARID1A
FGFR2
MSH6
PTPRD
EPHA3
INPP4A
TET1
PTEN
PTPRS
TET2
Log2(fold change)
Primary
Recurrent
Similar contribution to primary and recurrent GBM
Mutation type:
Point
Frameshift
Transcriptional
Splicing
TP53
CBL
NOTCH3
TSC1
FAT1
SMAD4
CREBBP
APC
KMT2D
AXIN1
MED12
ARID1B
FOXO1
NCOR1
MGA
KMT2C
RB1
KDM6A
−9
−6
−3
0
3
log2(fold-change)
Differential contribution to primary and recurrent GBM

Figure S3. Impact of driver mutations on tumor cell fitness in primary and recurrent GSCs, Related to Figure 2.

Superimposed gene-level LFC values from functional genetic screens on primary (blue) and recurrent (red) GSCs. Mutational status shown on right with color indicating type of mutation (point, frameshift, transcriptional or splicing variant). Genes separated into two sections according to their functional contribution to primary and recurrent GSCs.

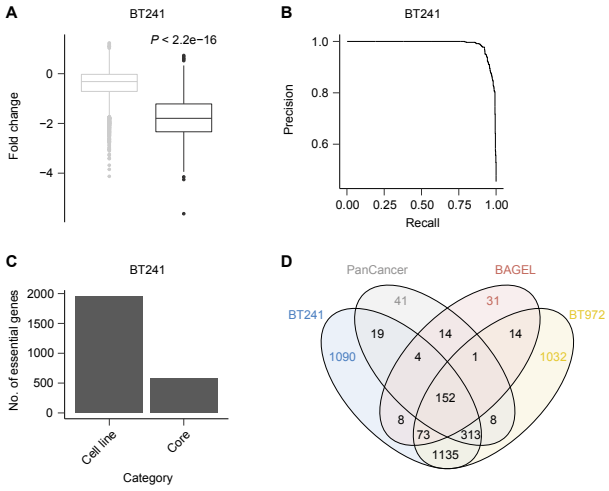
A
BT241
P < 2.2e−16
Fold change
0
−2
−4
B
BT241
Precision
1.0
0.8
0.6
0.00
0.25
0.50
0.75
1.00
Recall
C
BT241
No. of essential genes
2000
1500
1000
500
0
Cell line
Core
Category
D
PanCancer
BAGEL
BT241
BT972
41
31
19
14
14
1090
4
1
1032
152
8
8
73
313
1135

Figure S4. Quality control and overlap analyses of screens in recurrent GBM models, Related to Figure 4.

(A) Gene-level LFC of CEGs (Behan et al., 2019; Hart et al., 2017) and non-essential genes (Hart et al., 2017) from a CRISPR screen in BT241 tumor cells. All data presented as means from three biologically independent replicates. *P* values are from unpaired Student's t tests.

(B) Precision-recall plots indicate performance of CRISPR screen in BT241 tumor cells.

(C) Number of cell line-specific and core essential genes (FDR < 0.05) in BT241 tumor cells.

(D) Venn diagram of essential genes (FDR < 0.05) in recurrent tumor cells, stratified into essential genes specific to each cell line or belonging to CEG sets.

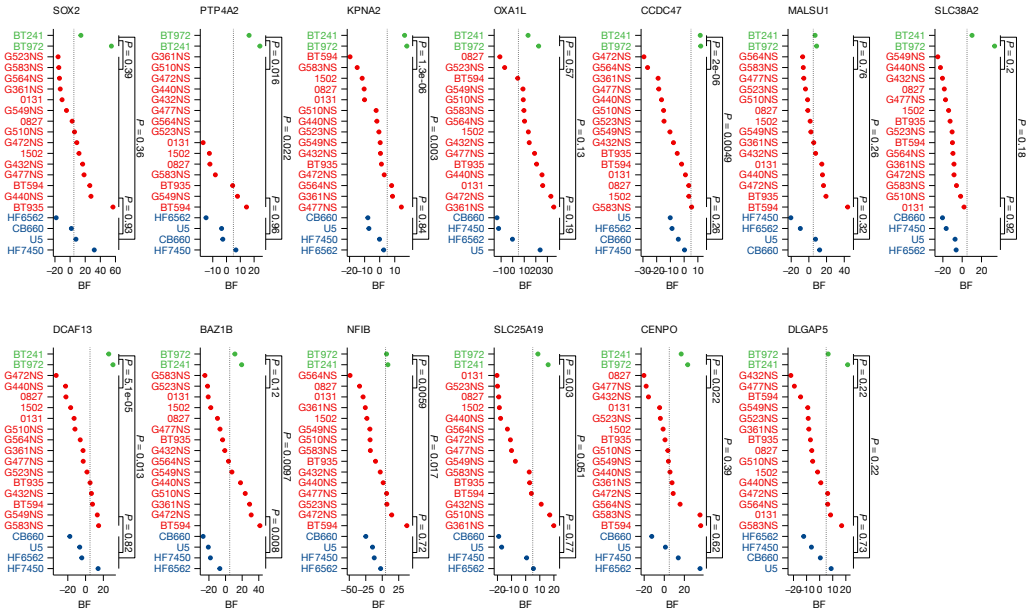
SOX2
PTP4A2
KPNA2
OXA1L
CCDC47
MALSU1
SLC38A2
DCAF13
BAZ1B
NFIB
SLC25A19
CENPO
DLGAP5
BF

Figure S5. Essentiality of 13 top genes in primary GBM, recurrent GBM and neural stem cell models, Related to Figure 4.

For each labelled gene, dot plots of cell line BF scores are presented from recurrent tumor cells (green), primary tumor cells (red) and neural stem cells (blue). Data are presented as means from three biologically independent replicates; pairwise cell-type comparisons conducted using unpaired Student's T-tests.

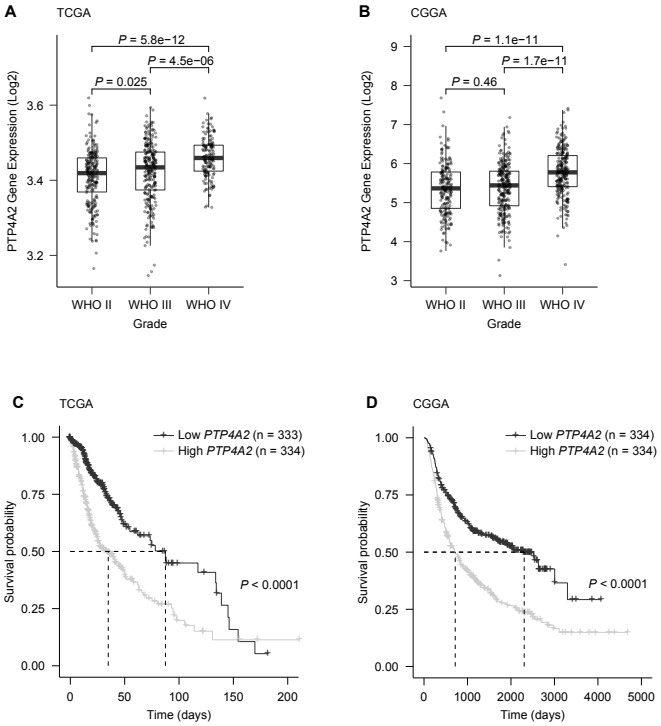
A
TCGA
P = 5.8e−12
P = 4.5e−06
P = 0.025
PTP4A2 Gene Expression (Log2)
3.2
3.4
3.6
WHO II
WHO III
WHO IV
Grade
B
CGGA
P = 1.1e−11
P = 1.7e−11
P = 0.46
PTP4A2 Gene Expression (Log2)
3
4
5
6
7
8
9
WHO II
WHO III
WHO IV
Grade
C
TCGA
Low PTP4A2 (n = 333)
High PTP4A2 (n = 334)
Survival probability
0.00
0.25
0.50
0.75
1.00
P < 0.0001
0
50
100
150
200
Time (days)
D
CGGA
Low PTP4A2 (n = 334)
High PTP4A2 (n = 334)
Survival probability
0.00
0.25
0.50
0.75
1.00
P < 0.0001
0
1000
2000
3000
4000
5000
Time (days)

Figure S6. Impact of *PTP4A2* expression on tumor grade and patient survival, Related to Figure 4.

(A, B) *PTP4A2* expression in (A) The Cancer Genome Atlas (TCGA) and (B) the Chinese Glioma Genome Atlas (CGGA), stratified by tumor grade. Boxes indicate 25th, 50th and 75th percentile while the whiskers extend to 1.4 times the IQR; *P* values from unpaired Wilcoxon Rank-Sum test. (C, D) Kaplan-Meier survival analysis of glioma patients stratified by median *PTP4A2* expression from (C) TCGA and (D) CGGA. *P* value from log-rank (Mantel-Cox) test.

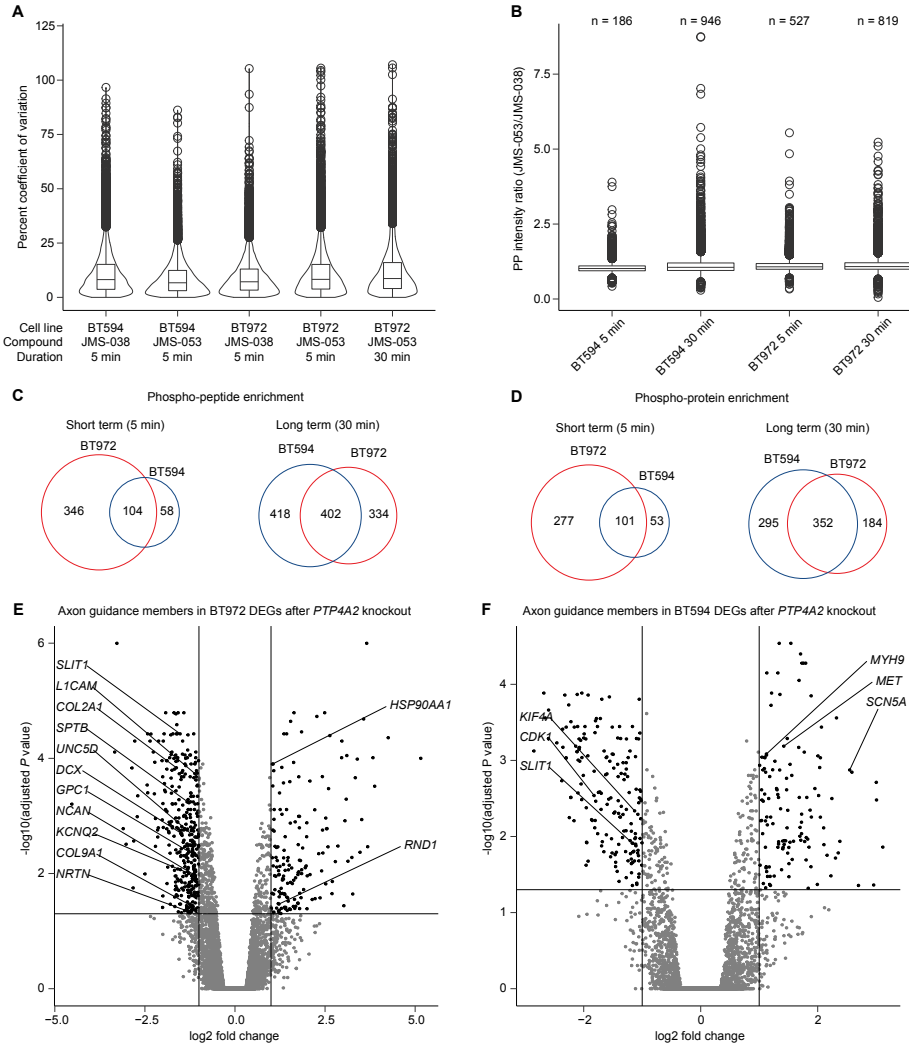
A
Percent coefficient of variation
125
100
75
50
25
0
Cell line
Compound
Duration
BT594
JMS-038
5 min
BT594
JMS-053
5 min
BT972
JMS-038
5 min
BT972
JMS-053
5 min
BT972
JMS-053
30 min
B
n = 186
n = 946
n = 527
n = 819
PP intensity ratio (JMS-053/JMS-038)
7.5
5.0
2.5
0.0
BT594 5 min
BT594 30 min
BT972 5 min
BT972 30 min
C
Phospho-peptide enrichment
Short term (5 min)
BT972
BT594
346
104
58
Long term (30 min)
BT594
BT972
418
402
334
D
Phospho-protein enrichment
Short term (5 min)
BT972
BT594
277
101
53
Long term (30 min)
BT594
BT972
295
352
184
E
Axon guidance members in BT972 DEGs after PTP4A2 knockout
-log10(adjusted P value)
SLIT1
L1CAM
COL2A1
SPTB
UNC5D
DCX
GPC1
NCAN
KCNQ2
COL9A1
NRTN
HSP90AA1
RND1
log2 fold change
F
Axon guidance members in BT594 DEGs after PTP4A2 knockout
-log10(adjusted P value)
KIF4A
CDK1
SLIT1
MYH9
MET
SCN5A
log2 fold change

Figure S7. Phospho-proteomic and transcriptomic analysis supporting data, Related to Figures 5 and 6.

(A) Violin plot depicting percent coefficient of variance (%CV) in phospho-peptide intensities from replicates of BT594 and BT972 tumor cells treated with JMS-053 for 5 or 30 min, as compared to JMS-038 treatment.

(B) Phospho-peptide intensity ratios (JMS-053/JMS-038) from BT594 and BT972 tumor cells treated with JMS-053 for 5 or 30 min, as compared to JMS-038 treatment. Data presented for phospho-peptides with ratio > 1.5 and %CV < 50; number of enriched phospho-peptides indicated for each sample.

(C-D) Venn diagrams of phospho-peptides (C) and corresponding phospho-proteins (D) enriched in JMS-053-treated tumor cells (5 or 30 min) as compared to JMS-038 treatment. A JMS-053/JMS-038 phospho-peptide intensity ratio > 1.5 is used to classify enrichment.

(E-F) Volcano plots of LFC (knockout/control) in (E) BT972 and (F) BT594 tumor cells with *PTP4A2* knockout (2 gRNAs) as compared to *AAVS1* knockout (1 gRNA, control). DEGs with |fold change| > 2 and adjusted $P < 0.05$ considered significant. Genes annotated to axon guidance that overlap with significant DEGs in each cell line are highlighted.

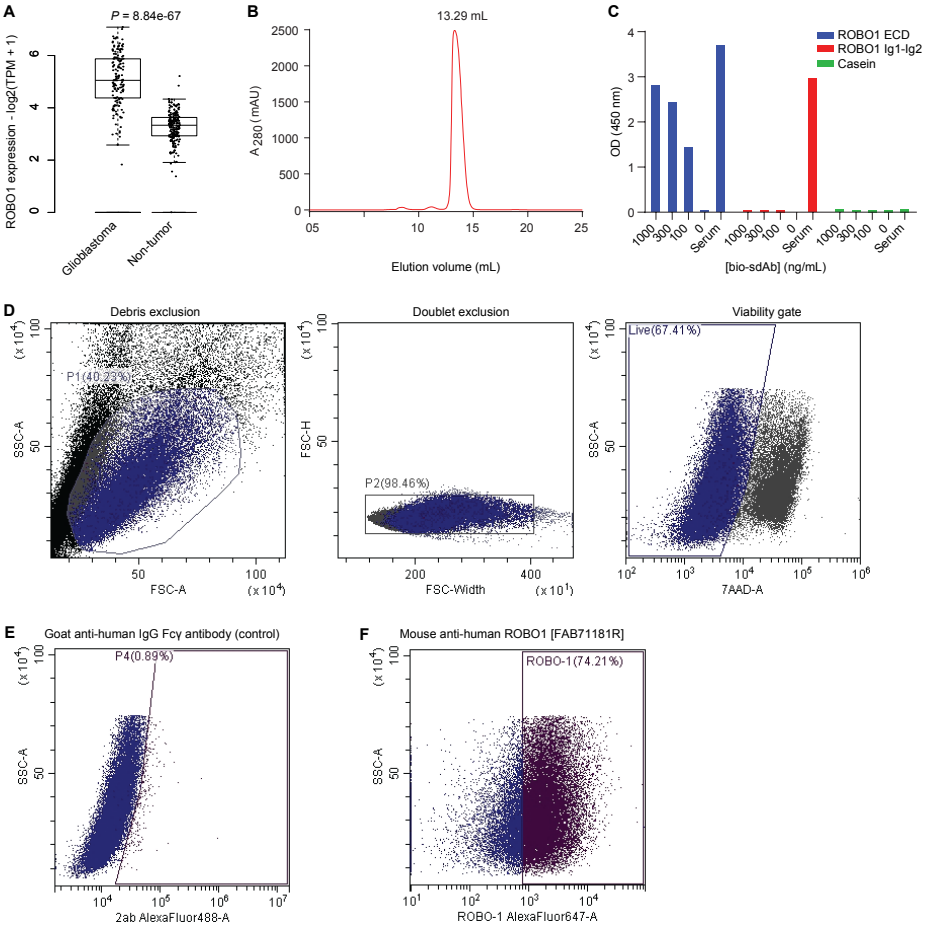
A
P = 8.84e-67
ROBO1 expression - log2(TPM + 1)
Glioblastoma
Non-tumor
B
13.29 mL
A280 (mAU)
Elution volume (mL)
C
ROBO1 ECD
ROBO1 Ig1-Ig2
Casein
OD (450 nm)
[bio-sdAb] (ng/mL)
D
Debris exclusion
P1(40.23%)
SSC-A
FSC-A
Doublet exclusion
P2(98.46%)
FSC-H
FSC-Width
Viability gate
Live(67.41%)
7AAD-A
E
Goat anti-human IgG Fcγ antibody (control)
P4(0.89%)
2ab AlexaFluor488-A
F
Mouse anti-human ROBO1 [FAB71181R]
ROBO-1(74.21%)
ROBO-1 AlexaFluor647-A

Figure S8. ROBO1 in patient tissue specimens and MKRo-20 validation, Related to Figure 7.

(A) Comparison of ROBO1 expression (transcripts per million, TPM) in GBM tumor specimens (TCGA) and non-tumor specimens (Genotype-Tissue Expression, GTEx). Adjusted *P* value is from genome scale LIMMA comparison of all protein coding genes.

(B) Size exclusion chromatography profile (Superdex 75 Increase 10/300 GL) of MKRo-20.

(C) Binding of MKRo-20 to full-length ROBO1 extracellular domain (ECD) and Ig1-Ig2 domains. Polyclonal llama immune serum (1:16000 dilution, detected using a goat anti-llama-HRP secondary antibody) served as a positive control.

(D) Gating parameters for flow cytometric analysis of MKRo-20-hFc binding to recurrent GBM cells, including debris exclusion, doublet exclusion and gating for live cells using 7-AAD viability dye.

(E) Non-specific binding analysis of a secondary anti-human IgG Fcγ-specific AF488 antibody to recurrent GBM cells.

(F) Anti-ROBO1 staining analysis of a commercial anti-ROBO1-AF647 antibody to recurrent GBM cells.

Table S1. Clinical and mutational analysis of GBM models.

Table S2. Normalized gRNA read counts for all 10 genome-wide CRISPR-Cas9 screens (n = 10).

Table S3. Bayes Factor (BF) scores of gRNAs for all untreated primary and recurrent GBM models (n = 4).

Table S4. DrugZ scores for all drug-treated screens in primary GBM models (n = 6).

Table S5. Results of enrichment analyses presented in Figures 1, 2, and 3.

Table S6. Mutational analysis of primary (BT594) and recurrent (BT972) GSCs.

Table S7. Differential expression analysis at transcript and protein levels in primary (BT594) and recurrent (BT972) GSCs.

Table S8. Gene-level fitness effects of fitness trends in primary (BT594) and recurrent (BT972) GSCs.

Table S9. Phospho-proteomic analyses of primary (BT594) and recurrent (BT972) GSCs treated with JMS-038 or JMS-053.

Table S10. Transcript-level differential expression analyses in primary (BT594) and recurrent (BT972) GSCs with knockout of *AAVS1* (control) and *PTP4A2*.

References

1 DeVita, V. T., Jr. The evolution of therapeutic research in cancer. *The New England journal of medicine* **298**, 907-910, doi:10.1056/NEJM197804202981610 (1978).

2 Ostrom, Q. T. *et al.* CBTRUS Statistical Report: Primary Brain and Other Central Nervous System Tumors Diagnosed in the United States in 2009-2013. *Neuro-oncology* **18**, v1-v75, doi:10.1093/neuonc/now207 (2016).

3 Stupp, R. *et al.* Radiotherapy plus concomitant and adjuvant temozolomide for glioblastoma. *The New England journal of medicine* **352**, 987-996, doi:10.1056/NEJMoa043330 (2005).

4 Lapointe, S., Perry, A. & Butowski, N. A. Primary brain tumours in adults. *Lancet* **392**, 432-446, doi:10.1016/S0140-6736(18)30990-5 (2018).

5 Stupp, R. *et al.* Effects of radiotherapy with concomitant and adjuvant temozolomide versus radiotherapy alone on survival in glioblastoma in a randomised phase III study: 5-year analysis of the EORTC-NCIC trial. *The Lancet. Oncology* **10**, 459-466, doi:10.1016/S1470-2045(09)70025-7 (2009).

6 Toledo, C. M. *et al.* Genome-wide CRISPR-Cas9 Screens Reveal Loss of Redundancy between PKMYT1 and WEE1 in Glioblastoma Stem-like Cells. *Cell reports* **13**, 2425-2439, doi:10.1016/j.celrep.2015.11.021 (2015).

7 MacLeod, G. *et al.* Genome-Wide CRISPR-Cas9 Screens Expose Genetic Vulnerabilities and Mechanisms of Temozolomide Sensitivity in Glioblastoma Stem Cells. *Cell reports* **27**, 971-986 e979, doi:10.1016/j.celrep.2019.03.047 (2019).

8 Prolo, L. M. *et al.* Targeted genomic CRISPR-Cas9 screen identifies MAP4K4 as essential for glioblastoma invasion. *Scientific reports* **9**, 14020, doi:10.1038/s41598-019-50160-w (2019).

9 Huang, K. *et al.* Genome-Wide CRISPR-Cas9 Screening Identifies NF-kappaB/E2F6 Responsible for EGFRvIII-Associated Temozolomide Resistance in Glioblastoma. *Adv Sci (Weinh)* **6**, 1900782, doi:10.1002/advs.201900782 (2019).

10 Norden, A. D. *et al.* A Real-World Claims Analysis of Costs and Patterns of Care in Treated Patients with Glioblastoma Multiforme in the United States. *J Manag Care Spec Pharm* **25**, 428-436, doi:10.18553/jmcp.2019.25.4.428 (2019).

11 Orzan, F. *et al.* Genetic Evolution of Glioblastoma Stem-Like Cells From Primary to Recurrent Tumor. *Stem cells* **35**, 2218-2228, doi:10.1002/stem.2703 (2017).

12 Qazi, M. A. *et al.* A novel stem cell culture model of recurrent glioblastoma. *Journal of neuro-oncology* **126**, 57-67, doi:10.1007/s11060-015-1951-6 (2016).

13 Korber, V. *et al.* Evolutionary Trajectories of IDH(WT) Glioblastomas Reveal a Common Path of Early Tumorigenesis Instigated Years ahead of Initial Diagnosis. *Cancer cell* **35**, 692-704 e612, doi:10.1016/j.ccell.2019.02.007 (2019).

14 Zehir, A. *et al.* Mutational landscape of metastatic cancer revealed from prospective clinical sequencing of 10,000 patients. *Nature medicine* **23**, 703-713, doi:10.1038/nm.4333 (2017).

15 Wang, J. *et al.* Clonal evolution of glioblastoma under therapy. *Nature genetics* **48**, 768-776, doi:10.1038/ng.3590 (2016).

16 Hart, T. *et al.* Evaluation and Design of Genome-Wide CRISPR/SpCas9 Knockout Screens. *G3 (Bethesda)* **7**, 2719-2727, doi:10.1534/g3.117.041277 (2017).

17 Behan, F. M. *et al.* Prioritization of cancer therapeutic targets using CRISPR-Cas9 screens. *Nature* **568**, 511-516, doi:10.1038/s41586-019-1103-9 (2019).

18 Meyers, R. M. *et al.* Computational correction of copy number effect improves specificity of CRISPR-Cas9 essentiality screens in cancer cells. *Nature genetics* **49**, 1779-1784, doi:10.1038/ng.3984 (2017).

19 Dempster, J. M. *et al.* Agreement between two large pan-cancer CRISPR-Cas9 gene dependency data sets. *Nat Commun* **10**, 5817, doi:10.1038/s41467-019-13805-y (2019).

20 Lenoir, W. F., Lim, T. L. & Hart, T. PICKLES: the database of pooled in-vitro CRISPR knockout library essentiality screens. *Nucleic acids research* **46**, D776-D780, doi:10.1093/nar/gkx993 (2018).

21 Tang, Z. *et al.* GEPIA: a web server for cancer and normal gene expression profiling and interactive analyses. *Nucleic acids research* **45**, W98-W102, doi:10.1093/nar/gkx247 (2017).

22 Gangemi, R. M. *et al.* SOX2 silencing in glioblastoma tumor-initiating cells causes stop of proliferation and loss of tumorigenicity. *Stem cells* **27**, 40-48, doi:10.1634/stemcells.2008-0493 (2009).

23 Mao, D. D. *et al.* A CDC20-APC/SOX2 Signaling Axis Regulates Human Glioblastoma Stem-like Cells. *Cell reports* **11**, 1809-1821, doi:10.1016/j.celrep.2015.05.027 (2015).

24 Basu-Roy, U. *et al.* Sox2 antagonizes the Hippo pathway to maintain stemness in cancer cells. *Nature communications* **6**, 6411, doi:10.1038/ncomms7411 (2015).

25 Bessette, D. C., Qiu, D. & Pallen, C. J. PRL PTPs: mediators and markers of cancer progression. *Cancer Metastasis Rev* **27**, 231-252, doi:10.1007/s10555-008-9121-3 (2008).

26 Lin, M. D. *et al.* Expression of phosphatase of regenerating liver family genes during embryogenesis: an evolutionary developmental analysis among Drosophila, amphioxus, and zebrafish. *BMC Dev Biol* **13**, 18, doi:10.1186/1471-213X-13-18 (2013).

27 Kobayashi, M. *et al.* PRL2/PTP4A2 phosphatase is important for hematopoietic stem cell self-renewal. *Stem cells* **32**, 1956-1967, doi:10.1002/stem.1672 (2014).

28 Dong, Y. *et al.* Phosphatase of regenerating liver 2 (PRL2) deficiency impairs Kit signaling and spermatogenesis. *The Journal of biological chemistry* **289**, 3799-3810, doi:10.1074/jbc.M113.512079 (2014).

29 Salamoun, J. M. *et al.* Photooxygenation of an amino-thienopyridone yields a more potent PTP4A3 inhibitor. *Organic & biomolecular chemistry* **14**, 6398-6402, doi:10.1039/c6ob00946h (2016).

30 McQueeney, K. E. *et al.* Targeting ovarian cancer and endothelium with an allosteric PTP4A3 phosphatase inhibitor. *Oncotarget* **9**, 8223-8240, doi:10.18632/oncotarget.23787 (2018).

31 Brose, K. *et al.* Slit proteins bind Robo receptors and have an evolutionarily conserved role in repulsive axon guidance. *Cell* **96**, 795-806, doi:10.1016/s0092-8674(00)80590-5 (1999).

32 Mertsch, S. *et al.* Slit2 involvement in glioma cell migration is mediated by Robo1 receptor. *Journal of neuro-oncology* **87**, 1-7, doi:10.1007/s11060-007-9484-2 (2008).

33 Dallol, A. *et al.* Frequent epigenetic inactivation of the SLIT2 gene in gliomas. *Oncogene* **22**, 4611-4616, doi:10.1038/sj.onc.1206687 (2003).

34 Wong, K. *et al.* Signal transduction in neuronal migration: roles of GTPase activating proteins and the small GTPase Cdc42 in the Slit-Robo pathway. *Cell* **107**, 209-221 (2001).

35 Hu, H. *et al.* Cross GTPase-activating protein (CrossGAP)/Vilse links the Roundabout receptor to Rac to regulate midline repulsion. *Proceedings of the National Academy of Sciences of the United States of America* **102**, 4613-4618, doi:10.1073/pnas.0409325102 (2005).

36 Rhee, J., Buchan, T., Zukerberg, L., Lilien, J. & Balsamo, J. Cables links Robo-bound Abl kinase to N-cadherin-bound beta-catenin to mediate Slit-induced modulation of adhesion and transcription. *Nature cell biology* **9**, 883-892, doi:10.1038/ncb1614 (2007).

37 Rhee, J. *et al.* Activation of the repulsive receptor Roundabout inhibits N-cadherin-mediated cell adhesion. *Nature cell biology* **4**, 798-805, doi:10.1038/ncb858 (2002).

38 Liu, L. *et al.* Slit2 and Robo1 expression as biomarkers for assessing prognosis in brain glioma patients. *Surg Oncol* **25**, 405-410, doi:10.1016/j.suronc.2016.09.003 (2016).

39 Gara, R. K. *et al.* Slit/Robo pathway: a promising therapeutic target for cancer. *Drug discovery today* **20**, 156-164, doi:10.1016/j.drudis.2014.09.008 (2015).

40 Urwyler, O. *et al.* Branch-restricted localization of phosphatase Prl-1 specifies axonal synaptogenesis domains. *Science* **364**, doi:10.1126/science.aau9952 (2019).

41 Qazi, M. A. *et al.* Cotargeting Ephrin Receptor Tyrosine Kinases A2 and A3 in Cancer Stem Cells Reduces Growth of Recurrent Glioblastoma. *Cancer research* **78**, 5023-5037, doi:10.1158/0008-5472.CAN-18-0267 (2018).

42 Touat, M. *et al.* Mechanisms and therapeutic implications of hypermutation in gliomas. *Nature* **580**, 517-523, doi:10.1038/s41586-020-2209-9 (2020).

43 Rizvi, N. A. *et al.* Cancer immunology. Mutational landscape determines sensitivity to PD-1 blockade in non-small cell lung cancer. *Science* **348**, 124-128, doi:10.1126/science.aaa1348 (2015).

44 Le, D. T. *et al.* PD-1 Blockade in Tumors with Mismatch-Repair Deficiency. *The New England journal of medicine* **372**, 2509-2520, doi:10.1056/NEJMoa1500596 (2015).

45 McGranahan, N. *et al.* Clonal neoantigens elicit T cell immunoreactivity and sensitivity to immune checkpoint blockade. *Science* **351**, 1463-1469, doi:10.1126/science.aaf1490 (2016).

46 Hlobilkova, A. *et al.* Cell cycle arrest by the PTEN tumor suppressor is target cell specific and may require protein phosphatase activity. *Experimental cell research* **256**, 571-577, doi:10.1006/excr.2000.4867 (2000).

47 Cancer Genome Atlas Research, N. *et al.* Integrated genomic characterization of endometrial carcinoma. *Nature* **497**, 67-73, doi:10.1038/nature12113 (2013).

48 Zhao, J. *et al.* Immune and genomic correlates of response to anti-PD-1 immunotherapy in glioblastoma. *Nature medicine* **25**, 462-469, doi:10.1038/s41591-019-0349-y (2019).

49 Jassal, B. *et al.* The reactome pathway knowledgebase. *Nucleic acids research* **48**, D498-D503, doi:10.1093/nar/gkz1031 (2020).

50 Langmead, B., Trapnell, C., Pop, M. & Salzberg, S. L. Ultrafast and memory-efficient alignment of short DNA sequences to the human genome. *Genome biology* **10**, R25, doi:10.1186/gb-2009-10-3-r25 (2009).

51 Hart, T. *et al.* High-Resolution CRISPR Screens Reveal Fitness Genes and Genotype-Specific Cancer Liabilities. *Cell* **163**, 1515-1526, doi:10.1016/j.cell.2015.11.015 (2015).

52 Hart, T. & Moffat, J. BAGEL: a computational framework for identifying essential genes from pooled library screens. *BMC Bioinformatics* **17**, 164, doi:10.1186/s12859-016-1015-8 (2016).

53 Colic, M. *et al.* Identifying chemogenetic interactions from CRISPR screens with drugZ. *Genome Med* **11**, 52, doi:10.1186/s13073-019-0665-3 (2019).

54 Subramanian, A. *et al.* Gene set enrichment analysis: a knowledge-based approach for interpreting genome-wide expression profiles. *Proceedings of the National Academy of Sciences of the United States of America* **102**, 15545-15550, doi:10.1073/pnas.0506580102 (2005).

55 Korotkevich, G., Sukhov, V. & Sergushichev, A. Fast gene set enrichment analysis. *bioRxiv*, doi:https://doi.org/10.1101/060012 (2020).

56 Reimand, J., Kull, M., Peterson, H., Hansen, J. & Vilo, J. g:Profiler--a web-based toolset for functional profiling of gene lists from large-scale experiments. *Nucleic acids research* **35**, W193-200, doi:10.1093/nar/gkm226 (2007).

57 Singh, S. K. *et al.* Identification of human brain tumour initiating cells. *Nature* **432**, 396-401, doi:10.1038/nature03128 (2004).

58 Mair, B. *et al.* Essential Gene Profiles for Human Pluripotent Stem Cells Identify Uncharacterized Genes and Substrate Dependencies. *Cell reports* **27**, 599-615 e512, doi:10.1016/j.celrep.2019.02.041 (2019).

59 Dobin, A. *et al.* STAR: ultrafast universal RNA-seq aligner. *Bioinformatics* **29**, 15-21, doi:10.1093/bioinformatics/bts635 (2013).

60 Ritchie, M. E. *et al.* limma powers differential expression analyses for RNA-sequencing and microarray studies. *Nucleic acids research* **43**, e47, doi:10.1093/nar/gkv007 (2015).

61 McCarthy, D. J., Chen, Y. & Smyth, G. K. Differential expression analysis of multifactor RNA-Seq experiments with respect to biological variation. *Nucleic acids research* **40**, 4288-4297, doi:10.1093/nar/gks042 (2012).

62 Arbabi Ghahroudi, M., Desmyter, A., Wyns, L., Hamers, R. & Muyldermans, S. Selection and identification of single domain antibody fragments from camel heavy-chain antibodies. *FEBS letters* **414**, 521-526, doi:10.1016/s0014-5793(97)01062-4 (1997).

63 Baral, T. N., MacKenzie, R. & Arbabi Ghahroudi, M. Single-domain antibodies and their utility. *Curr Protoc Immunol* **103**, 2 17 11-12 17 57, doi:10.1002/0471142735.im0217s103 (2013).

64 Fairhead, M. & Howarth, M. Site-specific biotinylation of purified proteins using BirA. *Methods in molecular biology* **1266**, 171-184, doi:10.1007/978-1-4939-2272-7_12 (2015).

65 Durocher, Y., Perret, S. & Kamen, A. High-level and high-throughput recombinant protein production by transient transfection of suspension-growing human 293-EBNA1 cells. *Nucleic acids research* **30**, E9, doi:10.1093/nar/30.2.e9 (2002).

66 Zhang, J. *et al.* Transient expression and purification of chimeric heavy chain antibodies. *Protein Expr Purif* **65**, 77-82, doi:10.1016/j.pep.2008.10.011 (2009).

67 Hussack, G. *et al.* Neutralization of Clostridium difficile toxin A with single-domain antibodies targeting the cell receptor binding domain. *The Journal of biological chemistry* **286**, 8961-8976, doi:10.1074/jbc.M110.198754 (2011).

Conditional genetic interactions are treatment- and model-specific in primary GBM

To systematically identify genetic determinants of treatment resistance, we conducted pooled, genome-wide CRISPR-Cas9 loss-of-function screens in treatment-naïve and patient-derived primary GSC (BT594 and BT935) models that were treated with RT and/or TMZ (Figure 5A, Table S1). We infected cells with the genome-wide Toronto KnockOut version 3.0 (TKOv3) pooled guide RNA (gRNA) library targeting 18,053 human protein-coding genes with an average of four gRNAs per gene (Hart et al., 2017). Following infection and selection of transduced populations, in which each gRNA was represented in ~250 distinct cells, we subjected cells to the following four conditions: vehicle control (DMSO); sublethal RT; sublethal TMZ; or sublethal combination therapy. Populations were sampled over ~15-18 doublings and genomic DNA from these samples was subjected to gRNA barcode sequencing (Table S2). Strong depletion of gRNA barcodes targeting reference core essential genes (CEGs) (Behan et al., 2019; Hart et al., 2017) and lack of depletion of guides targeting non-essential genes (Hart et al., 2017) indicate high precision and recall for each of the treatment conditions, with an average of ~2,700 essential genes identified per condition (Figures S9A-S9C, Table S2; false discovery rate (FDR) < 0.05).

Application of the drugZ algorithm (Colic et al., 2019) identified an average of 29 **c**onditional **G**enetic **I**nteraction**s** (cGIs) that significantly altered sensitivity to RT, TMZ or combination therapy in primary tumor cells (Figure S9D, Table S4; FDR < 0.05). Comparison of gene-level $\log_2$(fold change) (LFC) and drugZ values revealed little correlation among the top hits between different primary GBM models (Pearson correlation coefficient $|R| \leq 0.4$), whereas drugZ scores correlated moderately across conditions within a model (Figures 5B and 5C; $R = 0.64–0.81$, FDR < 0.05). Less than 25% of cGIs were shared across different treatment arms within each cell line, indicating that condition-specific dependency profiles are relatively unique to both condition

and model (Figure 5D; FDR < 0.05). To determine if the lack of correlation across models was unique to BT594 and BT935, we compared our results to published data from six additional primary GSC models treated with sublethal doses of TMZ (MacLeod et al., 2019) and found little overlap among all eight cell lines with and without filtering for the top and bottom 5% of drugZ scores ($R < 0.2$; Figure S9E).

Given the uniqueness of cGI profiles, we performed functional enrichment analysis (Yu et al., 2012) to determine if changes in gene fitness showed similar trends at the pathway level. Enrichment analysis categorized treatment- and model-specific cGIs into largely distinct gene sets, with a single instance of overlap between models (Figure 5E, Table S5; Adjusted $P < 0.05$). Response to combination treatment in both primary GBM models highlight cGIs involved in DNA repair (BT594: *MSH2*, *PPP5C* and *TP53*; BT935: *POLR2L*, *FANCA*, *FANCD2*, *FANCF*, *FANCM* and *SLX4*), supported by known roles of mismatch repair (MMR) deficiency (Touat et al., 2020) and a reliance on Fanconi anemia (FA) pathway (MacLeod et al., 2019) in acquired chemotherapy resistance. In keeping with pathway-level analysis, drugZ analysis of individual genes largely distinguishes the response to combination treatment from either monotherapy (RT or TMZ), with 43/46 cGIs in BT594 and 67/99 cGIs in BT935 unique to combination treatment (Figures 5F, 5G and S9F; FDR < 0.1). These cGIs highlight well-established members of DNA repair pathways and cell cycle checkpoints (*TP53*, *PMS2*, *CDC25A*, *CENPA*), ATP-binding cassette drug transporter *ABCC2*, and other genes previously investigated in GBM progression (*B4GALT3*, *EDN3*, *PHIP*, *RARRES1*, *UPF1*, *ABCC2*, *CD59*, *DIRAS3*, *DYNC1*, *EIF2AK3*, *LOXL1*, *MXD1*). However, the vast majority of cGIs (129/145) from combination treatment have not previously been reported in GBM, including the E3 ligase *HUWE1*, Wnt ligand *WNT9A*, complement *C5*, and members of the spliceosome complex (*LSM4*, *THOC7*). In line with previous data, loss-of-function

of *MSH2* is a precursor to combination therapy resistance, in keeping with frequent hypermutation and downregulation of MMR genes in gliomas and their association with a poor prognosis (Touat et al., 2020). A strong *TP53* dependency was observed in BT594 tumor cells in response to combination treatment, wherein targeting of *TP53* leads to treatment resistance, likely by increasing MYC activity to dedifferentiate to a stem-like state (Zheng et al., 2008). BT935 tumor cells, on the other hand, showed strong negative cGIs following TMZ monotherapy or combination treatment with members of the FA pathway (*FANCA*, *FANCC*, *FANCD2*, *FANCF*, and *FANCM*), indicating a reliance on the FA core complex to resolve stalled DNA replication forks induced by TMZ (Kim and D'Andrea, 2012). Thus, cGIs responding strongly to combination treatment are partially represented in responses to either monotherapy and implicate novel genes that have not been previously annotated in GBM, warranting further investigation of their role in treatment resistance and recurrence.

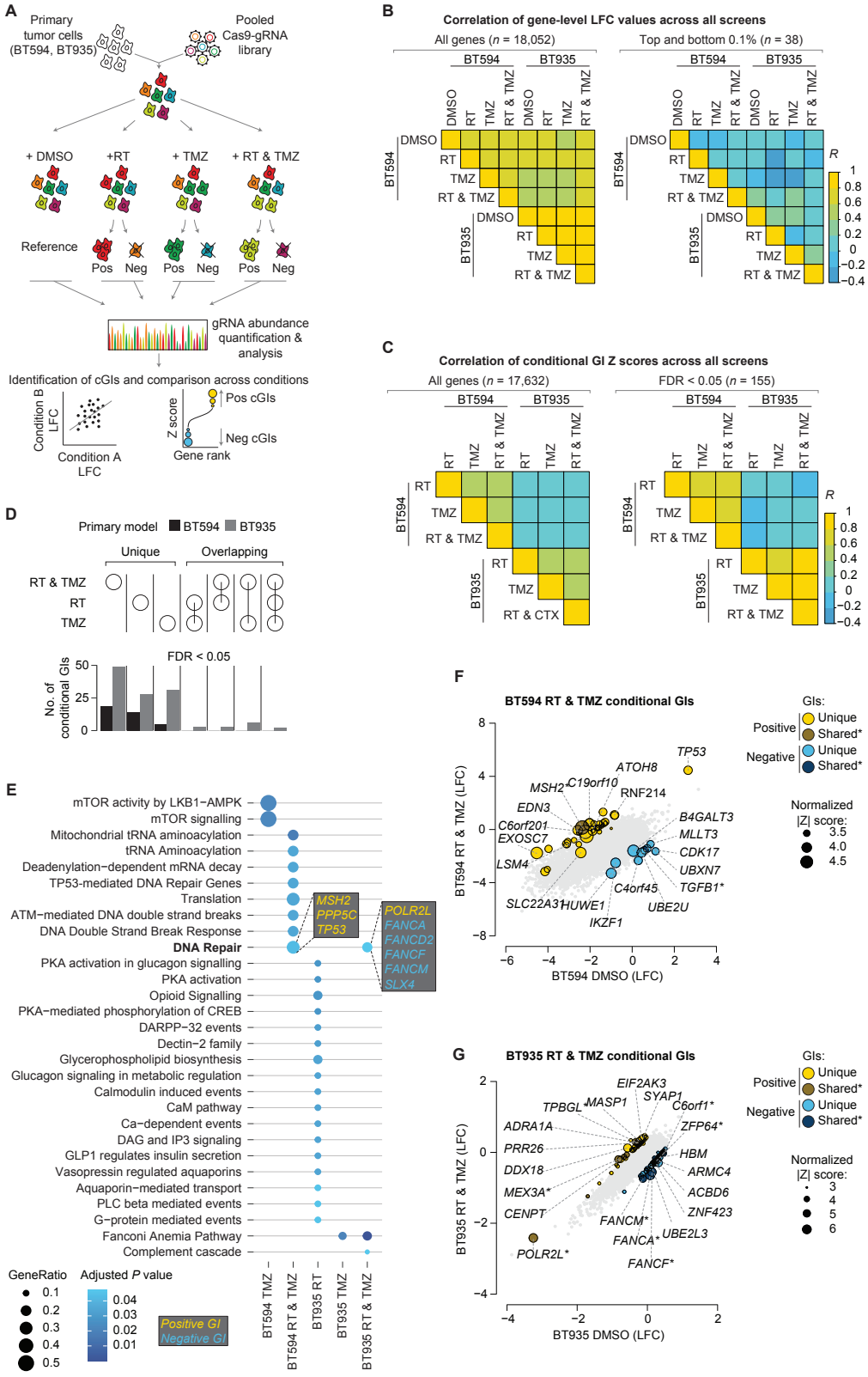
A
Primary tumor cells (BT594, BT935)
Pooled Cas9-gRNA library
+ DMSO
+RT
+ TMZ
+ RT & TMZ
Reference
Pos Neg Pos Neg Pos Neg
gRNA abundance quantification & analysis
Identification of cGIs and comparison across conditions
Condition B LFC
Condition A LFC
Z score
Pos cGIs
Neg cGIs
Gene rank
B
Correlation of gene-level LFC values across all screens
All genes (n = 18,052)
Top and bottom 0.1% (n = 38)
BT594
BT935
DMSO
RT
TMZ
RT & TMZ
R
1
0.8
0.6
0.4
0.2
0
−0.2
−0.4
C
Correlation of conditional GI Z scores across all screens
All genes (n = 17,632)
FDR < 0.05 (n = 155)
RT & CTX
D
Primary model BT594 BT935
Unique
Overlapping
RT & TMZ
RT
TMZ
FDR < 0.05
No. of conditional GIs
50
25
0
E
mTOR activity by LKB1−AMPK
mTOR signalling
Mitochondrial tRNA aminoacylation
tRNA Aminoacylation
Deadenylation−dependent mRNA decay
TP53-mediated DNA Repair Genes
Translation
ATM−mediated DNA double strand breaks
DNA Double Strand Break Response
DNA Repair
PKA activation in glucagon signalling
PKA activation
Opioid Signalling
PKA−mediated phosphorylation of CREB
DARPP−32 events
Dectin−2 family
Glycerophospholipid biosynthesis
Glucagon signaling in metabolic regulation
Calmodulin induced events
CaM pathway
Ca−dependent events
DAG and IP3 signaling
GLP1 regulates insulin secretion
Vasopressin regulated aquaporins
Aquaporin−mediated transport
PLC beta mediated events
G−protein mediated events
Fanconi Anemia Pathway
Complement cascade
MSH2
PPP5C
TP53
POLR2L
FANCA
FANCD2
FANCF
FANCM
SLX4
GeneRatio
0.1
0.2
0.3
0.4
0.5
Adjusted P value
0.04
0.03
0.02
0.01
Positive GI
Negative GI
BT594 TMZ
BT594 RT & TMZ
BT935 RT
BT935 TMZ
BT935 RT & TMZ
F
BT594 RT & TMZ conditional GIs
BT594 RT & TMZ (LFC)
BT594 DMSO (LFC)
TP53
ATOH8
C19orf10
MSH2
RNF214
EDN3
C6orf201
EXOSC7
LSM4
B4GALT3
MLLT3
CDK17
UBXN7
TGFB1*
C4orf45
UBE2U
SLC22A3
HUWE1
IKZF1
GIs:
Positive
Negative
Unique
Shared*
Normalized |Z| score:
3.5
4.0
4.5
G
BT935 RT & TMZ conditional GIs
BT935 RT & TMZ (LFC)
BT935 DMSO (LFC)
EIF2AK3
SYAP1
TPBGL
MASP1
C6orf1*
ADRA1A
ZFP64*
PRR26
HBM
DDX18
ARMC4
MEX3A*
ACBD6
CENPT
ZNF423
FANCM*
FANCA*
UBE2L3
POLR2L*
FANCF*
3
4
5
6

Figure 5. Genome-scale identification of conditional genetic interactions (cGIs) with radiation therapy (RT) and/or temozolomide (TMZ) in primary tumor cells.

(A) Schematic for the identification of cGIs in treatment-naïve and patient-derived primary glioblastoma (GBM) models. For each cell line, tumor cells were infected with a genome-wide CRISPR-Cas9 gene knockout library (TKOv3) and exposed to DMSO, sublethal RT, sublethal TMZ or combination treatment (RT & TMZ) over 15-18 doublings. Guide RNA (gRNA) fold-change and Z scores within cell populations at the beginning and end of each screen identified cGIs.

(B) Pearson correlation of gene-level $\log_2$ fold change (ΔLFC) from all treated screens, presented with (right) and without (left) filtering for genes in the top and bottom 0.1%.

(C) Pearson correlation of cGI (drugZ) scores from all treated screens, presented with (right) and without (left) filtering for genes with false discovery rate (FDR) < 0.05 in at least one screen.

(D) Overlap of cGI subsets from all screens (drugZ FDR < 0.05). Combination of circles in top matrix indicate intersecting gene sets.

(E) ClusterProfiler analysis of cGIs (drugZ FDR < 0.05) from all screens. Reactome gene sets enriched at an adjusted $P < 0.05$ are shown in the dot plot, with dot size corresponding to gene ratio and dot color indicating adjusted P values. Positive and negative cGIs responsible for the only overlapping enriched pathway (DNA Repair) are listed for each model.

(F,G) Negative and positive cGIs of combination treatment (RT & TMZ) identified in (F) BT594 and (G) BT935 tumor cells. The gene-level LFC in DMSO-treated and combination treatment-treated primary tumor cells are shown, with significant positive (yellow) and negative (blue) cGIs (FDR < 0.1) highlighted. Node color represents the overlap of significant cGIs between monotherapy-treated screens (sublethal RT or TMZ), while node size corresponds to absolute

normalized Z score of cGIs of combination treatment. Top 10 positive and negative cGIs, according to normalized Z score, are indicated.

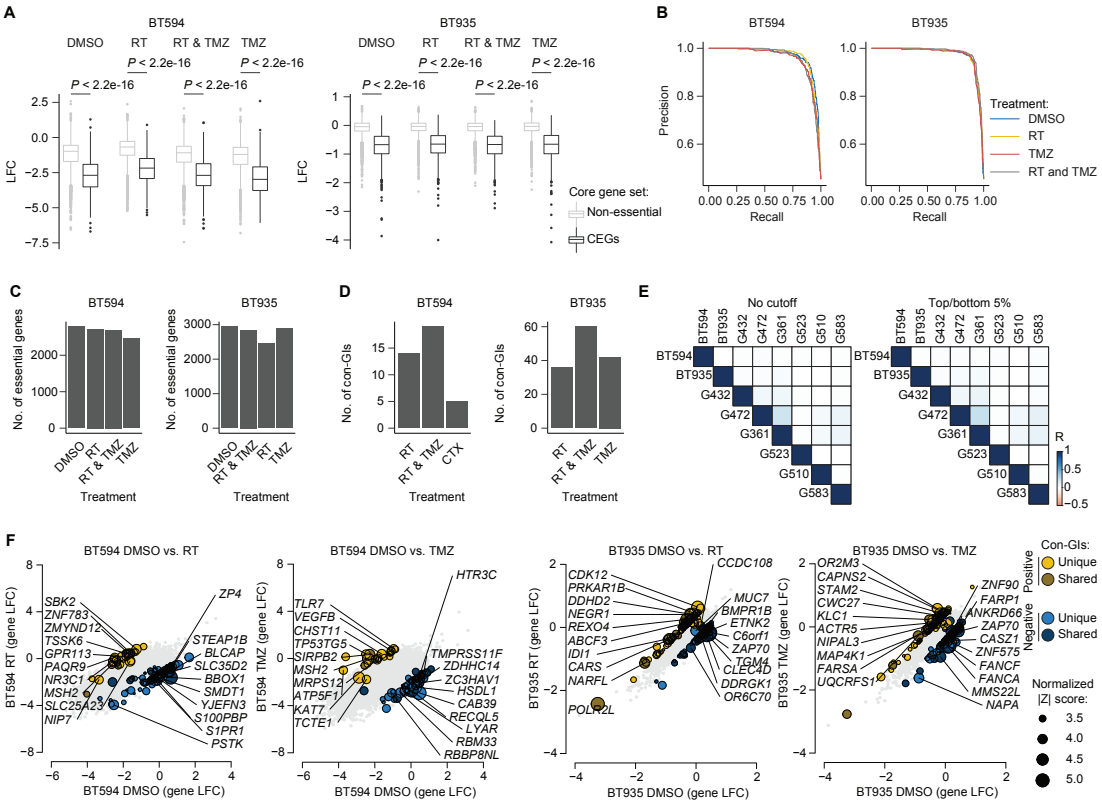
A
BT594
BT935
DMSO
RT
RT & TMZ
TMZ
P < 2.2e-16
LFC
Core gene set:
Non-essential
CEGs
B
Precision
Recall
Treatment:
DMSO
RT
TMZ
RT and TMZ
C
No. of essential genes
Treatment
D
No. of con-GIs
RT
RT & TMZ
CTX
E
No cutoff
Top/bottom 5%
R
F
BT594 DMSO vs. RT
BT594 DMSO vs. TMZ
BT935 DMSO vs. RT
BT935 DMSO vs. TMZ
BT594 RT (gene LFC)
BT594 TMZ (gene LFC)
BT935 RT (gene LFC)
BT935 TMZ (gene LFC)
BT594 DMSO (gene LFC)
BT935 DMSO (gene LFC)
SBK2
ZNF783
ZMYND12
TSSK6
GPR113
PAQR9
NR3C1
MSH2
SLC25A23
NIP7
ZP4
STEAP1B
BLCAP
SLC35D2
BBOX1
SMDT1
YJEFN3
S100PBP
S1PR1
PSTK
TLR7
VEGFB
CHST11
TP53TG5
SIRPB2
MSH2
MRPS12
ATP5F1
KAT7
TCTE1
HTR3C
TMPRSS11F
ZDHHC14
ZC3HAV1
HSDL1
CAB39
RECQL5
LYAR
RBM33
RBBP8NL
CDK12
PRKAR1B
DDHD2
NEGR1
REXO4
ABCF3
IDI1
CARS
NARFL
POLR2L
CCDC108
MUC7
BMPR1B
ETNK2
C6orf1
ZAP70
TGM4
CLEC4D
DDRGK1
OR6C70
OR2M3
CAPNS2
STAM2
CWC27
KLC1
ACTR5
NIPAL3
MAP4K1
FARSA
UQCRFS1
ZNF90
FARP1
ANKRD66
ZAP70
CASZ1
ZNF575
FANCF
FANCA
MMS22L
NAPA
Con-GIs:
Unique
Shared
Positive
Negative
Normalized |Z| score:

Figure S9. Quality control analysis of screens in primary GBM models, Related to Figure 5.

(A) Gene-level LFC of CEGs (Behan et al., 2019; Hart et al., 2017) and non-essential genes (Hart et al., 2017) across screens in primary tumor cells. All data presented from $n = 3$ biologically independent replicates. *P* values are from unpaired Student's t tests.

(B) Precision-recall plots indicate high performance of screens in primary tumor cells.

(C) Number of essential genes (FDR < 0.05) identified in primary GBM screens.

(D) Number of cGIs identified in BT594 (left) or BT935 (right) cells treated with RT and/or TMZ (FDR < 0.05).

(E) Pearson correlation matrices of cGI Z scores between TMZ-treated screens on primary tumor cells, as well as screens from (Toledo et al., 2015) and (MacLeod et al., 2019). Data presented with (left) and without (right) filtering for genes that fall into the top or bottom 5% of Z scores in least one screen.

(F) Negative and positive cGIs of mono therapy (RT or TMZ) identified in BT594 (left 2 panels) and BT935 (right 2 panels) cells. Significant positive (yellow) and negative (blue) cGIs (FDR < 0.1) highlighted. Node color represents the overlap of significant cGIs between monotherapy-treated screens (sublethal RT or TMZ), while node size corresponds to the absolute normalized Z score of cGIs of combination treatment. Top 10 positive and negative cGIs, according to normalized Z score, are labelled.

References

Behan, F.M., Iorio, F., Picco, G., Goncalves, E., Beaver, C.M., Migliardi, G., Santos, R., Rao, Y., Sassi, F., Pinnelli, M.*, et al.* (2019). Prioritization of cancer therapeutic targets using CRISPR-Cas9 screens. Nature *568*, 511-516.

Bhat, K.P.L., Balasubramaniyan, V., Vaillant, B., Ezhilarasan, R., Hummelink, K., Hollingsworth, F., Wani, K., Heathcock, L., James, J.D., Goodman, L.D.*, et al.* (2013). Mesenchymal differentiation mediated by NF-kappaB promotes radiation resistance in glioblastoma. Cancer cell *24*, 331-346.

Colic, M., Wang, G., Zimmermann, M., Mascall, K., McLaughlin, M., Bertolet, L., Lenoir, W.F., Moffat, J., Angers, S., Durocher, D.*, et al.* (2019). Identifying chemogenetic interactions from CRISPR screens with drugZ. Genome Med *11*, 52.

DePristo, M.A., Banks, E., Poplin, R., Garimella, K.V., Maguire, J.R., Hartl, C., Philippakis, A.A., del Angel, G., Rivas, M.A., Hanna, M.*, et al.* (2011). A framework for variation discovery and genotyping using next-generation DNA sequencing data. Nature genetics *43*, 491-498.

Hart, T., Tong, A.H.Y., Chan, K., Van Leeuwen, J., Seetharaman, A., Aregger, M., Chandrashekhar, M., Hustedt, N., Seth, S., Noonan, A.*, et al.* (2017). Evaluation and Design of Genome-Wide CRISPR/SpCas9 Knockout Screens. G3 (Bethesda) *7*, 2719-2727.

Kim, H., and D'Andrea, A.D. (2012). Regulation of DNA cross-link repair by the Fanconi anemia/BRCA pathway. Genes & development *26*, 1393-1408.

Korber, V., Yang, J., Barah, P., Wu, Y., Stichel, D., Gu, Z., Fletcher, M.N.C., Jones, D., Hentschel, B., Lamszus, K.*, et al.* (2019). Evolutionary Trajectories of IDH(WT) Glioblastomas Reveal a Common Path of Early Tumorigenesis Instigated Years ahead of Initial Diagnosis. Cancer cell *35*, 692-704 e612.

MacLeod, G., Bozek, D.A., Rajakulendran, N., Monteiro, V., Ahmadi, M., Steinhart, Z., Kushida, M.M., Yu, H., Coutinho, F.J., Cavalli, F.M.G.*, et al.* (2019). Genome-Wide CRISPR-Cas9 Screens Expose Genetic Vulnerabilities and Mechanisms of Temozolomide Sensitivity in Glioblastoma Stem Cells. Cell reports *27*, 971-986 e979.

Orzan, F., De Bacco, F., Crisafulli, G., Pellegatta, S., Mussolin, B., Siravegna, G., D'Ambrosio, A., Comoglio, P.M., Finocchiaro, G., and Boccaccio, C. (2017). Genetic Evolution of Glioblastoma Stem-Like Cells From Primary to Recurrent Tumor. Stem cells *35*, 2218-2228.

Qazi, M.A., Vora, P., Venugopal, C., McFarlane, N., Subapanditha, M.K., Murty, N.K., Hassell, J.A., Hallett, R.M., and Singh, S.K. (2016). A novel stem cell culture model of recurrent glioblastoma. Journal of neuro-oncology *126*, 57-67.

Toledo, C.M., Ding, Y., Hoellerbauer, P., Davis, R.J., Basom, R., Girard, E.J., Lee, E., Corrin, P., Hart, T., Bolouri, H.*, et al.* (2015). Genome-wide CRISPR-Cas9 Screens Reveal Loss of Redundancy between PKMYT1 and WEE1 in Glioblastoma Stem-like Cells. Cell reports *13*, 2425-2439.

Touat, M., Li, Y.Y., Boynton, A.N., Spurr, L.F., Iorgulescu, J.B., Bohrson, C.L., Cortes-Ciriano, I., Birzu, C., Geduldig, J.E., Pelton, K.*, et al.* (2020). Mechanisms and therapeutic implications of hypermutation in gliomas. Nature *580*, 517-523.

Wang, J., Cazzato, E., Ladewig, E., Frattini, V., Rosenbloom, D.I., Zairis, S., Abate, F., Liu, Z., Elliott, O., Shin, Y.J.*, et al.* (2016). Clonal evolution of glioblastoma under therapy. Nature genetics *48*, 768-776.

Wang, Q., Hu, B., Hu, X., Kim, H., Squatrito, M., Scarpace, L., deCarvalho, A.C., Lyu, S., Li, P., Li, Y.*, et al.* (2018). Tumor Evolution of Glioma-Intrinsic Gene Expression Subtypes Associates with Immunological Changes in the Microenvironment. Cancer cell *33*, 152.

Yu, G., Wang, L.G., Han, Y., and He, Q.Y. (2012). clusterProfiler: an R package for comparing biological themes among gene clusters. OMICS *16*, 284-287.

Zehir, A., Benayed, R., Shah, R.H., Syed, A., Middha, S., Kim, H.R., Srinivasan, P., Gao, J., Chakravarty, D., Devlin, S.M.*, et al.* (2017). Mutational landscape of metastatic cancer revealed from prospective clinical sequencing of 10,000 patients. Nature medicine *23*, 703-713.

Zheng, H., Ying, H., Yan, H., Kimmelman, A.C., Hiller, D.J., Chen, A.J., Perry, S.R., Tonon, G., Chu, G.C., Ding, Z.*, et al.* (2008). p53 and Pten control neural and glioma stem/progenitor cell renewal and differentiation. Nature *455*, 1129-1133.

CHAPTER 3: ROBO1-specific CAR-T cells effectively target recurrent glioblastoma

Preamble

This chapter is an original manuscript describing the development and testing of a novel chimeric antigen receptor (CAR) T cell therapy for recurrent glioblastoma:

> **Chokshi, C. R.**, Brakel, B. A., Rossotti, M. A., Venugopal, C., Salim, S. K., Henry, K. A., Singh, S. K. Anti-ROBO1 CAR T cells effectively target pediatric and adult malignant brain cancer. (manuscript in preparation)

Author contributions are as follows for the aforementioned manuscript: Conceptualization: S.K.S, K.A.H, and C.R.C; Resources: S.K.S, K.A.H; Methodology, investigation and validation: C.R.C, B.A.B and C.V.; Software and formal analysis: C.R.C and B.A.B; Visualization: C.R.C. Writing – original draft preparation: C.R.C; Writing – review and editing: C.R.C, B.A.B, K.A.H., V.C, and S.K.S with input from other authors; Project administration and supervision: S.K.S; Funding acquisition: S.K.S and K.A.H. All authors read and approved the manuscript.

ROBO1-specific CAR-T cells effectively target recurrent glioblastoma

Chirayu Chokshi[1], Benjamin Brakel[1], Martin Rossotti[2], Chitra Venugopal[3], Vaseem Sheikh[3], William Maich[1], Daniel Mobilio[1], Sabra K. Salim[1], Kevin A. Henry[2,4], Sheila K. Singh[1,2,5,*]

Affiliations

[1]Department of Biochemistry and Biomedical Sciences, McMaster University, Hamilton, Ontario, Canada L8N 3Z5.
[2]Human Health Therapeutics Research Centre, Life Sciences Division, National Research Council Canada, Ottawa, Ontario, Canada K1A 0R6.
[3]Department of Surgery, Faculty of Health Sciences, McMaster University, Hamilton, Ontario, Canada L8N 3Z5.
[4]Department of Biochemistry, Microbiology and Immunology, Faculty of Medicine, University of Ottawa, Ottawa, Ontario, Canada K1H 8M5.
[5]McMaster Centre for Discovery in Cancer Research, McMaster University, Hamilton, Ontario, Canada L8N 3Z5.

*Lead Contact and corresponding author: Dr. Sheila K. Singh (ssingh@mcmaster.ca).

Abstract

Over 1/3 of current clinical trials for glioblastoma (GBM) are evaluating efficacy of immune-modulating agents. However, immunotherapies have yet to impact survival for the vast majority of GBM patients. Here, we show that axonal guidance member roundabout receptor 1 (ROBO1) is enriched at transcript- and protein-levels in GBM specimens, and shows consistent expression on the cell surface of GSC models. To target this GBM-enriched antigen, we developed anti-ROBO1 CAR-T cells using camelid single-domain antibodies targeting human ROBO1. We developed a panel of novel camelid monomeric single-domain antibodies that specifically bind to human ROBO1 with high affinity, and these binders are translatable to an efficacious and ROBO1-specific CAR-T modality. Our ROBO1-targeted CAR-T cell modality can be added to the existing and emerging repertoire of tumor-targeted immunotherapies.

Introduction

Glioblastoma (GBM) remains the most common primary malignant brain tumor in adults. Despite advances in surgical resection in addition to aggressive chemoradiotherapy as standard of care (SoC), GBM patients inevitably relapse with a median overall survival of 12-18 months post-diagnosis (Ostrom et al., 2021). Unchanged since the introduction of the alkylating agent Temozolomide (TMZ) as part of SoC (Stupp et al., 2005), conventional therapy fails to prevent tumor relapse with no standardized second-line therapy for recurrent GBM patients.

One of the foremost therapeutics under development for GBM is immunotherapies, with 34% of current GBM clinical trials evaluating immune-modulating agents (Bagley et al., 2022). Of these immunotherapies, chimeric antigen receptor T (CAR-T) cells combine antibody-based recognition of tumor antigens with the cytotoxic activity of T lymphocytes, thereby mounting an anti-tumor response and circumventing antigen priming and presentation by major histocompatibility complex (Choi et al., 2018; Sampson et al., 2017). Although CAR-T cell therapies have achieved widespread clinical success against hematological malignancies (Maude et al., 2014), this is not the case for solid tumors including GBM due to tumor heterogeneity (Neftel et al., 2019; Patel et al., 2014), immune evasion by tumor cells (Jackson et al., 2019), and low mutational burden (Hodges et al., 2017). Despite these hurdles, the potential for CAR-T cell therapy for GBM was realized during an initial clinical trial of IL13Rα2-directed CAR-T cells that led to 77-100% decrease in tumor burden and 7.5 months of progression-free survival in a single patient with multifocal relapsed GBM (Brown et al., 2016a). In a separate study, EGFRvIII-directed CAR-T cells led to 59 months of overall survival in a patient with recurrent GBM (Goff et al., 2019). However, the vast majority of GBM patients have yet to benefit from CAR-T cell

efficacy largely due to target antigen heterogeneity, as noted in clinical studies (Brown et al., 2016a; O'Rourke et al., 2017).

Roundabout (ROBO) receptors and their inhibitory secreted slit guidance ligands (SLITs) were identified for their role in providing repulsive cues for axonal extension during neurodevelopment (Seeger et al., 1993; Wu et al., 1999). In addition to axonal guidance and repulsion, SLIT/ROBO signaling also governs cellular polarity, cell adhesion via interactions between E-cadherin and β-catenin, and cell death during the development of the central nervous system (CNS) (Dickinson and Duncan, 2010; Ypsilanti et al., 2010). We and others have previously reported that glioblastoma stem cells (GSCs) drive tumorigenesis and treatment resistance by hijacking neurodevelopmental processes, and in turn, these GBM-enriched processes can be successfully targeted using small molecules and immunotherapies (Bao et al., 2006; Bruggeman et al., 2007; Manoranjan et al., 2020; Qazi et al., 2018; Singh et al., 2004; Venugopal et al., 2015; Vora et al., 2020; Zbinden et al., 2010). In keeping with this premise, ROBO/SLIT signaling has been shown to be dysregulated in GBM (Geraldo et al., 2021; Mertsch et al., 2008; Nguemgo Kouam et al., 2018; Yiin et al., 2009). During normal neurodevelopment, binding of secreted SLIT2 to ROBO1 leads to axon repulsion and inhibition of cell migration via SRGAP-mediated CDC42 inactivation (Hu et al., 2005; Wong et al., 2001), in parallel to weakening N-cadherin-mediated cell adhesion via phosphorylation of β-catenin by ABL (Rhee et al., 2007; Rhee et al., 2002). In a neoplastic context, SLIT2 promoter methylation and inactivation is frequently observed in gliomas (Dallol et al., 2003), whereas ROBO1 is highly expressed at transcript and protein levels (Liu et al., 2016b). In other solid tumor contexts, SLIT/ROBO interactions have been shown to regulate quintessential oncogenic pathways, including signaling by EGFR, VEGFR, mTOR and HER2 (Gara et al., 2015). Although the role of ROBO1-mediated signaling in GBM

is yet to be resolved, downregulation of SLIT2 may allow for aberrant ROBO1 expression that can be therapeutically advantageous for development of tumor antigen-specific immunotherapies.

Here, we sought to develop anti-ROBO1 CAR-T cells using camelid single-domain antibodies targeting human ROBO1. We optimized the design of anti-ROBO1 CAR-T cells and tested the anti-tumor activity of these modalities in *in vitro* using patient-derived recurrent GBM lines and orthotopic patient-derived xenograft models. Together, we present data to expand the repertoire of GBM-enriched antigens suitable for effective CAR-T cell therapy.

Materials and Methods

Derivation and culture of patient-derived brain tumour tissue

Primary glioblastoma (GBM) specimens and whole fetal brain samples were obtained from consenting patients and families as approved by the Hamilton Health Sciences and McMaster Health Sciences Research Ethics Board. After washing with PBS, specimens were mechanically dissociated followed by enzymatic dissociation in PBS containing 0.013 mg/mL Liberase Thermolysin Research Grade (Millipore Sigma no. 5401020001) at 37°C for 15 minutes. Dissociated cells were isolated by filtration through a 70 µm cell strainer (Millipore Sigma no. CLS431751-50EA), centrifuges and subjected to red blood cell lysis using 0.8% ammonium chloride solution (STEMCELL Technologies no. 07850). SB2b was a kind gift from Professor Bryan Day (Sid Faithfull Brain Cancer Laboratory) and Dr. Brett Stringer from Royal Brisbane Hospital in Herston, Australia. Tumor cells and fetal human neural stem cells (NSCs) were grown and maintained in NeuroCult NS-A proliferation kit (Human) (STEMCELL Technologies no. 05751), supplemented with 20 ng/mL EGF (STEMCELL Technologies no. 78006), 10 ng/mL FGF (STEMCELL Technologies no. 78003.2), 0.002% Heparin (w/v) (STEMCELL Technologies no. 07980), 1X antibiotic/antimycotic solution (Wisent Bio Products no. 450-115-EL). For the first

two weeks of culture, patient-derived cells were treated for potential mycoplasma infection using 1X MycoZap Prophylactic (Lonza no. VZA-2031). Cells were cultured on tissue culture-treated dishes, cell-repellent dishes (Greiner Bio no. 628979), or tissue culture-treated dishes coated with Poly-L-ornithine (Millipore Sigma no. P4957) and mouse Laminin (Corning no. 354232). All cells were maintained at 37 °C and 5% CO_2. All cell lines were frequently tested for mycoplasma infection and, if needed, treated with additional 1X MycoZap for two weeks.

Flow cytometric analysis of malignant and normal cells

Cells were dissociated using TrypLE (ThermoFisher no. 12605010), resuspended in PBS with 2mM EDTA (ThermoFisher no. AM9260G), and stained with AF647-conjugated mouse-anti-human ROBO1 antibody (R&D Systems no. FAB71181R) or mouse IgG1 isotype control (R&D Systems no. IC002R). After incubation at room temperature for 15 minutes, samples were run on a CytoFLEX flow cytometer (Beckman Coulter). Dead cells were excluded using 7AAD the viability dye (1:10; Beckman Coulter, A07704). Compensation was performed using mouse IgG CompBeads (BD Biosciences, Cat#552843).

ROBO1 knockout in GBM cells

Guide RNAs targeting AAVS1 (5'-GGGGCCACTAGGGACAGGAT-3') or ROBO1 (5'-GAAGAAAGATGGCTCTCCAC-3') were obtained from TKOv3(Hart et al., 2017) and cloned into the single-gRNA lentiCRISPRv2 construct (Addgene no. 52961). Sequences were verified using Sanger sequencing. Each construct was packaged independently into lentivirus using second-generation packaging constructs. Briefly, HEK293T cells were seeded into T-75 cm^2 flasks at a density of 10 million cells per flask and cultured in high-glucose DMEM with 2mM L-glutamine and 1mM sodium pyruvate supplemented with 1% non-essential amino acid solution and 10% fetal bovine serum. The following day, media was replaced with viral harvesting media

(HEK culture media supplemented with 10mM HEPES and 1mM sodium butyrate). Next, 8µg of transfer plasmid (lentiCRISPRv2, AAVS1 or ROBO1), 4.8µg of psPAX2 (Addgene), and 3.8µg of pMD2.G (Addgene) were mixed with polyethylenimin at a 1:3 ratio (m:m) in 1.3mL of Opti-MEM. After complexing for 15 minutes at room temperature, the PEI/DNA mixture was transferred dropwise into the HEK293T-containing flasks. Viral supernatants were collected 24, 48 and 72 hours after transfection, concentrated using ultracentrifugation (41832 x *g* for 2 hours at 4°C) and aliquoted and stored at -80°C.

Development of anti-ROBO1 single domain antibodies

Generation of anti-ROBO1 single-domain antibodies. Camelid single-domain antibodies were raised by llama immunization and phage display essentially as previously described (Arbabi Ghahroudi et al., 1997; Baral et al., 2013). A phage-displayed heavy chain (V_HH) library was constructed from the peripheral blood B-cell repertoire of a llama immunized with recombinant human ROBO1-Fc (8975-RB-050, R&D Systems, Minneapolis, MN). Antigen-reactive V_HH-phage were enriched by panning against ROBO1-Fc with subtraction on Fc alone.

Antibody expression, purification and validation. Monomeric single-domain antibodies bearing His_6 and biotin acceptor peptide tags were expressed in the periplasm of *Escherichia coli* BL21 (DE3) cells, enzymatically biotinylated *in vitro* using BirA(Fairhead and Howarth, 2015), and purified by immobilized metal affinity chromatography followed by size exclusion chromatography (Superdex 75 Increase 10/300 GL, GE Healthcare, Chicago, IL). ROBO1 extracellular domain (NP_598334.1 aa 1–858) and ROBO1 Ig1-Ig2 domains (NP_002932.1 aa 61–266) were produced by transient transfection of HEK293-6E cells with pTT3/pTT5 vectors and antibody binding to these proteins was assessed by indirect titration ELISA. The affinities and kinetics of the interactions between monomeric single domain antibodies and human ROBO1

(25°C, pH 7.4) were determined using surface plasmon resonance. ROBO1 and other proteins were immobilized on a sensor chip CM5 (GE Healthcare) by amine coupling and antibodies were flowed over the antigen surfaces on a Biacore T200 instrument (GE Healthcare). Data from multi-cycle kinetic analysis were fit to a 1:1 binding model.

Design and cloning of CAR-T constructs

Human anti-ROBO1 (XRo and MKRo20) single domain binder sequences were cloned into a second-generation lentiviral CAR vector. The CAR construct consisted of a human EF1α promoter followed by a CD8a signaling domain, human ROBO1 scFv, 45 or 50 amino acid CD8a hinge region, CD28 transmembrane/costimulatory domain, CD3ζ cytoplasmic signalling domain, T2A self-cleavage peptide sequence, and truncated human EGFR sequence.

Lentivirus packaging, production and enrichment of CAR-T cells

Generation of CAR lentivirus. Each CAR construct was packaged independently into lentivirus using third-generation packaging constructs. Briefly, HEK293T cells were seeded into T-75 cm^2 flasks at a density of 10 million cells per flask and cultured in high-glucose DMEM with 2mM L-glutamine and 1mM sodium pyruvate supplemented with 1% non-essential amino acid solution and 10% fetal bovine serum. The following day, media was replaced with viral harvesting media (HEK culture media supplemented with 10mM HEPES and 1mM sodium butyrate). Next, 10.6µg of transfer plasmid (XRo-50 or MKRo20-50 CAR vector), 5.3µg of Gag/Pol (Addgene), 2.6µg of Rev (Addgene) and 2.6µg of VSVg (Addgene) plasmids were mixed with polyethylenimin at a 1:3 ratio (m:m) in 1.3mL of Opti-MEM. After complexing for 15 minutes at room temperature, the PEI/DNA mixture was transferred dropwise into the HEK293T-containing flasks. Viral supernatants were collected 24, 48 and 72 hours after transfection, concentrated using ultracentrifugation (41832 x *g* for 2 hours at 4°C), aliquoted into XSFM () and stored at −80°C.

Generation of CAR-T cells. Peripheral blood mononuclear cells (PBMCs) from consenting healthy blood donors in XSFM media (Irvine Scientific, Cat#91141) were activated with human T cell Transact (Miltenyi Biotec no. 130-111-160) in a 96-well round bottom plate with 100U/mL rhIL-2 (Peprotech, Cat#200-02). Twenty-four hours after activation, T cells were transduced with lentivirus at an MOI of ~1. T cell cultures were expanded into fresh media (XSFM media supplemented with 100U/mL rhIL-2) as required for 12–15 days prior to experimentation. Untransduced T cells were used as controls.

Enrichment of CAR-T cells. 10-12 days after activation, CAR-T cells were isolated using a biotin-conjugated human EGFR antibody (R&D Systems no. FAB9577B) and magnetic positive selection (STEMCELL Technologies no. 17663) according to the manufacturers protocol. Efficiency of transduction was determined using flow cytometry for EGFR expression. T cells were stained with AF488-conjugated mouse-anti-human EGFR antibody (R&D Systems no. FAB9577G) or mouse IgG1 isotype control (R&D Systems no. IC002G). After incubation at room temperature for 15 minutes, samples were run on a CytoFLEX flow cytometer (Beckman Coulter). Dead cells were excluded using 7AAD the viability dye (1:10; Beckman Coulter, A07704). Compensation was performed using mouse IgG CompBeads (BD Biosciences, Cat#552843).

CAR-T cell cytotoxicity, activation, proliferation and cytokine release assays

Bioluminescence cytotoxicity. Luciferase-expressing GBM cells at a concentration of 20,000 cells/well were plated in flat-bottom, tissue culture-treated 96–well plates in triplicates. In order to establish the bioluminescence (BLI) baseline reading and to ensure equal distribution of target cells, D-firefly luciferin potassium salt (100 mg/mL) was added to the wells and measured with a luminometer for 10s (Omega). Subsequently, effector cells were added at 2:1, 1:1, 0.5:1, 0.25:1 and 0:1 effector-to-target (E:T) ratios. Cell lysis controls were treated with 1% Nonidet P-40

(NP40, ThermoFisher no. 8379) to measure maximal lysis, while target cells incubated without effector cells were used to measure spontaneous death. Cells were incubated at 37 °C, 5% CO_2, and BLI was measured for 10s every 6 hours over a span of 72 hours with a luminometer as relative luminescence units (RLU). The readings from triplicates were averaged and percent viability was normalized to the UTD controls.

Fluorescence cytotoxicity and microscopy. Assays were set up similar to bioluminescence cytotoxicity. Wild type GBM cells were used as target cells, and a fluorescent nucleic acid stain (SYTOX green nucleic acid stain, ThermoFisher no. S7020) was added to coculture media according to the manufacturer's instructions. Cells were incubated at 37 °C, 5% CO_2 in a fluorescent and microscopy imaging incubator (Incucyte, Sartorius) for 24 hours, imaging every 4 hours. The fluorescent signal was used as a measure of cell death.

Activation. CAR-T cells (XRo or MKRo20) or untransduced T cells were co-cultured with target cells at a 1:1 ratio for 24 hours. T cells were stained for CD3 with PE-Cy7-conjugated mouse-anti-human CD3 antibody (BD Biosciences no. 563423), and CD3+ T cells were analyzed for activation markers CD25 (PE-conjugated mouse-anti-human CD25 antibody, BD Biosciences no. 555432) and CD69 (APC-conjugated mouse-anti-human CD25 antibody, BD Biosciences no. 555533) by flow cytometry using a CytoFLEX flow cytometer (Beckman Coulter). Dead cells were excluded using 7AAD the viability dye (1:10; Beckman Coulter, A07704). Compensation was performed using mouse IgG CompBeads (BD Biosciences, Cat#552843).

Proliferation. CAR-T cells (XRo or MKRo20) or untransduced T cells were co-cultured with target cells at a 1:1 ratio for 24 hours. Cells were then collected and CD3+ T cells were sorted into flat-bottom, TC-treated 96 well plates in XSFM and incubated for 3 days at 37 °C, 5% CO_2.

Proliferation was analyzed using the Presto Blue assay (ThermoFisher no. A13261) according to the manufacturer's instructions.

Cytokine release. CAR-T cells (XRo or MKRo20) or untransduced T cells were co-cultured with target cells at a 1:1 ratio for 24 hours. Supernatants were collected and stored at -80 °C. The DuoSet ELISA human IFN-gamma (R&D Systems no. DY285B) and human TNF-alpha (R&D Systems no. DY210) kits were used for quantification of cytokines, according to manufacturer's descriptions.

Results

ROBO1 is enriched on the cell surface of GBM cells

In accordance with previous histological and transcriptomic studies (Liu et al., 2016b), we find that *ROBO1* expression is enriched in GBM and low grade glioma specimens profiled by The Cancer Genome Atlas (TCGA) (Cancer Genome Atlas Research et al., 2013b), as compared to region-matched normal brain tissue (Figures 1A and 1B; Log_2 fold change or LFC > 1.5 and $P < 0.01$). In addition, ROBO1 expression is also enriched in diffuse large B-cell lymphoma, thymomas, liver hepatocellular carcinoma, and adenocarcinomas of the pancreas and stomach (Figure 1A; Log_2 fold change or LFC > 1.5 and $P < 0.01$). To corroborate these findings at the protein level, we queried expression of ROBO receptors (ROBO1, ROBO2, ROBO3 and ROBO4) and SLIT ligands (SLIT1, SLIT2 and SLIT3) in a dataset of 52 primary and 65 recurrent GBM specimens analyzed using whole cell proteomics (Tatari et al., Under revision at *Acta Neuropathologica*). Protein levels of ROBO1, ROBO2 and SLIT1 were detected in GBM specimens, with the greatest enrichment seen in ROBO1 levels (ROBO1-ROBO2 P = 1.1E-13, ROBO1-SLIT1 P = 1.7E-11). Other ROBO receptors and SLIT ligands were undetected in this dataset, which is consistent with previous literature on *SLIT2* promoter methylation in glioma

tissues (Dallol et al., 2003). Comparison between primary (n = 52) and recurrent (n = 65) GBM specimens showed no significant difference in protein levels of ROBO1, ROBO2 and SLIT1 (Figure 1D; $P > 0.05$). Using patient-derived GSC models, we found that ROBO1 is enriched on the cell surface of pre-treatment primary GSCs (54.08-98.52% ROBO1+; n = 6) and post-SoC recurrent GSCs (46.88-96.57% ROBO1+; n = 6), as compared to normal human astrocytes (9.38% ROBO1+; Figures 1E and 1F).

Given the consistent expression across GSC models, we wondered whether ROBO1 expression is enriched in other malignant brain tumors. Surprisingly, ROBO1 is expressed on the cell surface of adult lung-to-brain metastases initiating cells (43.67-98.73% ROBO1+; n = 2) and pediatric group 3 medulloblastoma initiating cells (37.18-91.48% ROBO1+; n = 3). Transcript- and protein-level enrichment in tumor specimens in addition to consistent expression on the cell surface of GSC models present ROBO1 as a candidate therapeutic target for immunotherapy for GBM, and potentially other malignant brain tumor models.

Camelid-derived single domain antibodies bind human ROBO1

To target human ROBO1, we constructed a phage-displayed heavy chain (V_HH) library from the peripheral blood B-cell repertoire of a llama immunized with the extracellular domain of human ROBO1. Compared to commercial cell lines MCF7 and HeLa, patient-derived primary GSC model BT428 cells have the greatest expression of ROBO1 as assayed by a commercial anti-ROBO1 antibody (Figure 2A). Monomeric anti-ROBO1 single-domain antibodies bound to human ROBO1 in a expression dependent manner, with binders MKRo20 and XRo showing the greatest affinities for ROBO1 in BT428 (Figure 2B). XRo showed similar antigen ROBO1 binding dynamics in HeLa cells, and neither MKRo20 nor XRo bound to MCF7 cells with negligible ROBO1 expression (Figure 2C and 2D).

Anti-ROBO1 CAR-T cells specifically eliminate ROBO1+ brain tumor cells

We next sought to transfer the ROBO1-binding monomeric single-domain antibodies MKRo20 and XRo into a second generation CAR construct. We designed CAR constructs with a CD8A signal peptide, a monomeric single-domain binder (MKRo20, XRo or control A20.1), an optional GGGGS linker, CD8A hinge region, CD28 transmembrane and co-stimulatory domains, and a CD3Z stimulatory domain (Figure 3A). Each CAR construct was introduced into donor-derived peripheral blood mononuclear cells (PBMCs) using lentivirus infection and grown *in vitro* for 10-14 days, resulting in enrichment efficiencies up to 95% (Figure 3B and 3C).

Using an *in vitro* CAR-T cell cytotoxicity assay with a tumor cell-specific bioluminescence readout, we compared cytotoxic potential of anti-ROBO1 CAR-T cells in three malignant BTSC lines with low (37%) and high (97%+) ROBO1 cell surface positivity (Group 3 medulloblastoma suMB002, lung-to-brain metastases BT530, primary GBM BT935; Figure 3D). Upon co-culture for 24 hours, MKRo20 and XRo CAR-T cells potently induced tumor cell cytotoxicity at effector:target (E:T) ratios of 0.5:1 in all tumor models (Figure 3E). Compared to MKRo20 CAR-T cells, XRo CAR-T cells elicited greater cytotoxicity in all models, irrespective of the E:T ratio. No significant differences in CAR-T cell mediated cytotoxicity was seen between CD8A hinge regions with or without a preceding GGGGS linker. Surprisingly, the control binder A20.1 showed non-specific binding at E:T ratios of 0.5:1 and 1:1 in suMB002 and BT530 models, but no such binding was seen in BT935. Given this inconsistency, we replaced this control with untransduced (UTD) T cells grown side-by-side to CAR-T cell modalities. In addition, we selected to further characterize XRo-based CAR-T cells given their enhanced affinity for ROBO1 in both antibody and CAR-T formats compared to MKRo20 (Figures 2 and 3).

Following optimization of the ROBO1-binding moiety, we evaluated the time course of XRo CAR-T cell cytotoxicity using two complementary assays, one which measures accumulation of tumor cell death using a fluorescent viability dye and the second which measured loss of tumor cell-specific bioluminescence, as described previously. Co-culture of XRo CAR-T cells with ROBO1-expressing GSCs led to complete tumor cell cytotoxicity at E:T ratios as low as 0.25:1, with ratios of 1:1 and above achieving 100% target cell death within 30 hours ($P < 0.01$; Figures 4A and 4B). To evaluate specificity of XRo CAR-T cells for ROBO1-expressing tumor cells, we evaluated T cell activation of upon antigen exposure by assaying cell surface levels of CD25 and CD69. Exposure to ROBO1-expressing GSCs (72% ROBO1+) led to robust increases in CD25 and CD69 levels in XRo CAR-T cells as compared to GSCs with an isogenic CRISPR-Cas9 knockout of *ROBO1* (5.78 to 34.98% CD25+, 22.87 to 43.3% CD69+; Figures 4C and 4D). No significant changes in CD25 or CD69 levels were seen in exposure of UTD T cells to GSCs, or with culture of either effector cell population alone. Together, these data show that XRo CAR-T cells can specifically recognize and eliminate ROBO1-expressing GBM cells.

Anti-ROBO1 CAR-T cells reduce tumor burden in orthotopic xenograft models

To test *in vivo* antitumor activity of ROBO1-targeted CAR-T cells, we established orthotopic xenografts using patient-derived recurrent BT241 GSCs with ~78% ROBO1+ cells (Figure 1F). Following confirmation of engraftment, mice were treated with a single dose of 500,000 XRo CAR-T cells (n = 8), MKRo20 CAR-T cells (n = 2), or UTD T cells (n = 7) (Figure 5A). Within 6 days post-imaging, all mice treated with XRo and MKRo20 CAR-T cells showed elimination of detectable tumor burden (Figures 5B and 5C). Tumor-bearing mice treated with UTD T cells showed robust increases in tumor burden post-treatment (post/pre fold change or FC 1.65 to 9.59), whereas mice treated with XRo CAR-T cells and MKRo20 CAR-T cells showed

significant reductions in tumor burden (XRo post/pre FC 0.16 to 0.21, MKRo20 post/pre FC 0.09 to 0.34; Figure 5B). Following repetition of these results in other malignant brain tumor models and predicted increases in survival, ROBO1-targeted CAR-T cells may provide robust and specific antitumor responses for brain cancer.

Discussion

Although CAR-T cell therapy is a newer adaptation for GBM treatment, advancements to increase its clinical utility are rapidly progressing. Here, we present a novel CAR-T cell therapy targeting ROBO1 in GBM. We present that ROBO1 expression in enriched in primary and recurrent GBM specimens at the transcript and protein levels, including on the cell surface of brain tumor stem cells (BTSCs). We developed a panel of novel camelid monomeric single-domain antibodies that specifically bind to human ROBO1 with high affinity, and these binders are translatable to an efficacious and ROBO1-specific CAR-T modality. Our study establishes anti-ROBO1 CAR-T cells as a potent immunotherapy for GBM.

Intratumoral heterogeneity, accumulation of mutations over time and a remodeled tumor recurrence limit selection of tumor-enriched or -specific antigens for immunotherapy in GBM. Exposure to pressures of stochastic tumor-intrinsic events, the tumor microenvironment and SoC likely lead to positive selection of resistant tumor subpopulations during GBM progression. A study by Johnson et al. (2014) conducted exome sequencing of 23 initial and patient-matched recurrent low-grade *IDH*-mutant gliomas. In 43% of all cases, greater than 50% of mutations seen in the primary tumors were lost at tumor recurrence, and in 6 of 10 patients treated with SoC chemotherapy agent TMZ, recurrent tumors were hypermutated and characterized by a TMZ-induced mutation signature. In a recent study by the Glass consortium of initial and patient-matched recurrent diffuse gliomas from 222 patients, of which 134 were *IDH*-wildtype, 70% of

recurrent tumors harboured an increased mutational burden at recurrence (Barthel et al., 2019). In fact, another study by Wang et al. (2016) showed that 66% of post-SoC recurrent tumors undergo a change in their dominant TCGA GBM subtype compared to their patient-matched primary tumor. The adaptation of CAR-T cell therapy for GBM is also impacted by temporal and spatial intratumoral heterogeneity. A recent clinical letter outlined administration of B7-H3 CAR-T cells to a 56-year-old woman with recurrent GBM, highlighting a potent but short-term anti-tumor response *in situ*, absent of grade 3 or higher toxicities associated with CAR-T cell infusion (Tang et al., 2021). Unfortunately, target antigen heterogeneity was predicted as the reason for treatment failure, as noted previously for CAR-T cell therapy targeting EGFRvIII and IL13Rα2 (Brown et al., 2016a; O'Rourke et al., 2017). Here, we present data to support broad enrichment of ROBO1 across primary and recurrent GBM and a potent GBM-targeting capability of anti-ROBO1 CAR-T cells in pre-clinical models. Our ROBO1-targeted CAR-T cell modality can be added to the existing and emerging repertoire of tumor-targeted immunotherapies. Currently, 12 clinical trials are recruiting GBM patients to evaluate CAR-T cell therapy against B7 family member B7-H3 (NCT04385173, NCT04077866), CD147, HER2 (NCT03389230), IL13Rα2 (NCT04003649, NCT04661384, NCT02208362), matrix metallopeptidase 2 (MMP2; NCT04214392), and NKG2D (NCT04717999). While current trials are focused on targeting single tumor-associated antigens, this increased repertoire of targets will allow multiple antigens to be targeted concurrently to overcome intertumoral heterogeneity.

Figures

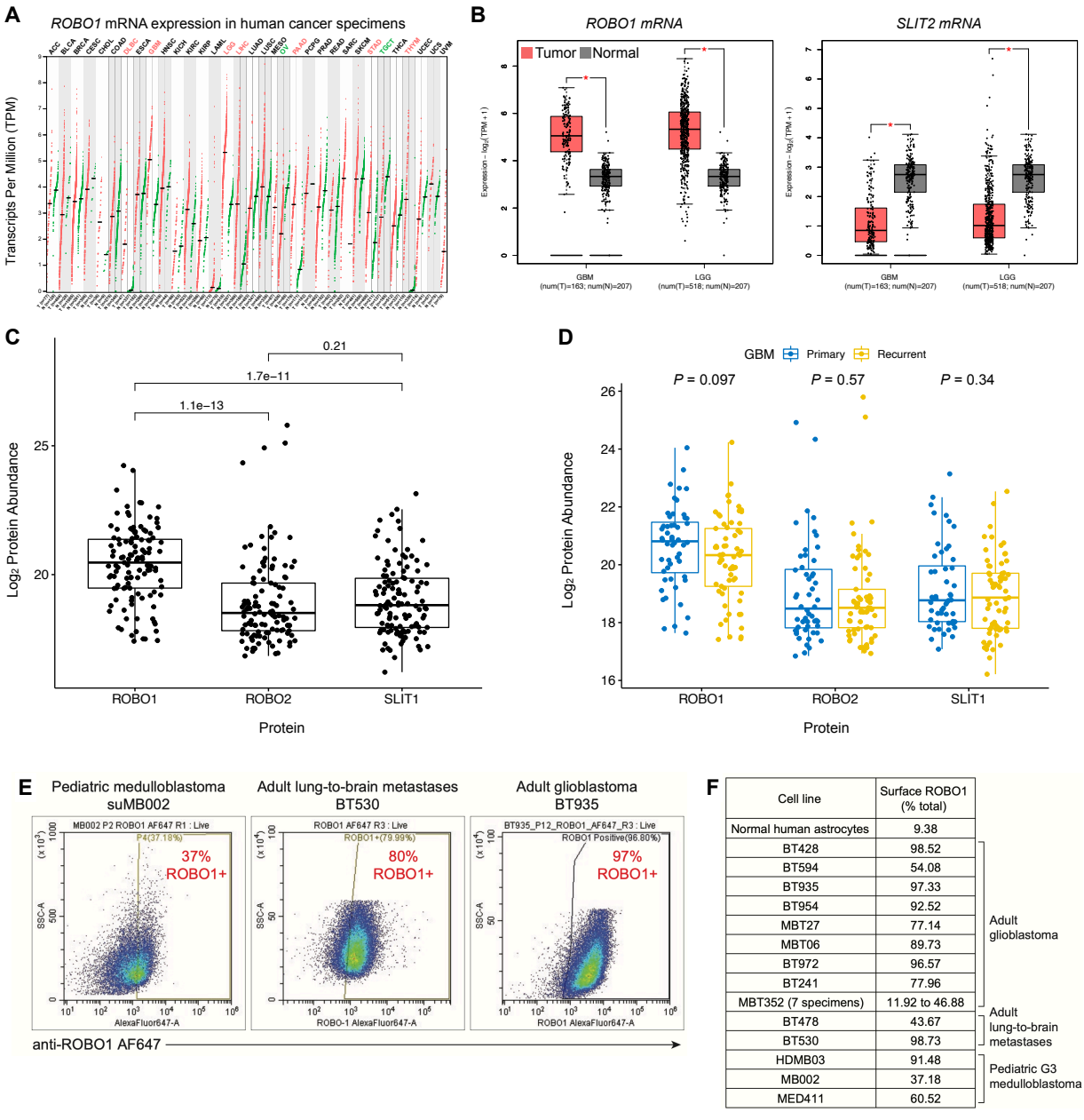

F

Cell line	Surface ROBO1 (% total)	
Normal human astrocytes	9.38	
BT428	98.52	Adult glioblastoma
BT594	54.08	
BT935	97.33	
BT954	92.52	
MBT27	77.14	
MBT06	89.73	
BT972	96.57	
BT241	77.96	
MBT352 (7 specimens)	11.92 to 46.88	
BT478	43.67	Adult lung-to-brain metastases
BT530	98.73	
HDMB03	91.48	Pediatric G3 medulloblastoma
MB002	37.18	
MED411	60.52	

Figure 1. ROBO1 is enriched in primary and recurrent GBM. (A) *ROBO1* mRNA expression was assayed in 33 human cancer specimens profiled by the TCGA (red dots) and in region-matched normal tissues (green dots). Enrichment in cancerous tissues (red label), normal tissues (green label) or no enrichment (black label) is indicated (LFC > |1.5| and $P < 0.01$). Sample numbers for tumor (T) and normal (N) tissue for each comparison are indicated at the bottom. Using the same dataset, **(B)** *ROBO1* and *SLIT2* mRNA expression was assayed in GBM and low grade glioma (LGG) specimens and their region-specific normal tissue counterparts. Enrichment or depletion in tumor (red) or normal (grey) tissue is indicated for each comparison (LFC > |1.5| and $P < 0.01$). **(C-D)** All ROBO receptors (ROBO1-ROBO4) and SLIT ligands (SLIT1-SLIT3) were assayed for expression in a dataset of 52 primary and 65 recurrent GBM specimens analyzed using whole cell proteomics (Tatari et al., Under revision at *Acta Neuropathologica*). **(C)** Comparison among ROBO1, ROBO2 and SLIT2 expression levels is indicated with *P* values from Student's t test. **(D)** Comparison of expression levels between primary and recurrent GBM specimens is indicated with *P* values from Student's t test. **(E-F)** Patient-derived brain tumor stem cells (BTSC) lines from pediatric Group 3 medulloblastoma, adult lung-to-brain metastases, and adult glioblastoma were immunostained for ROBO1 expression. Percentages of stained cells above isotype control are indicated in representative dot plots **(E)** and summary table **(F)**. Staining data for adult normal human astrocytes is also shown.

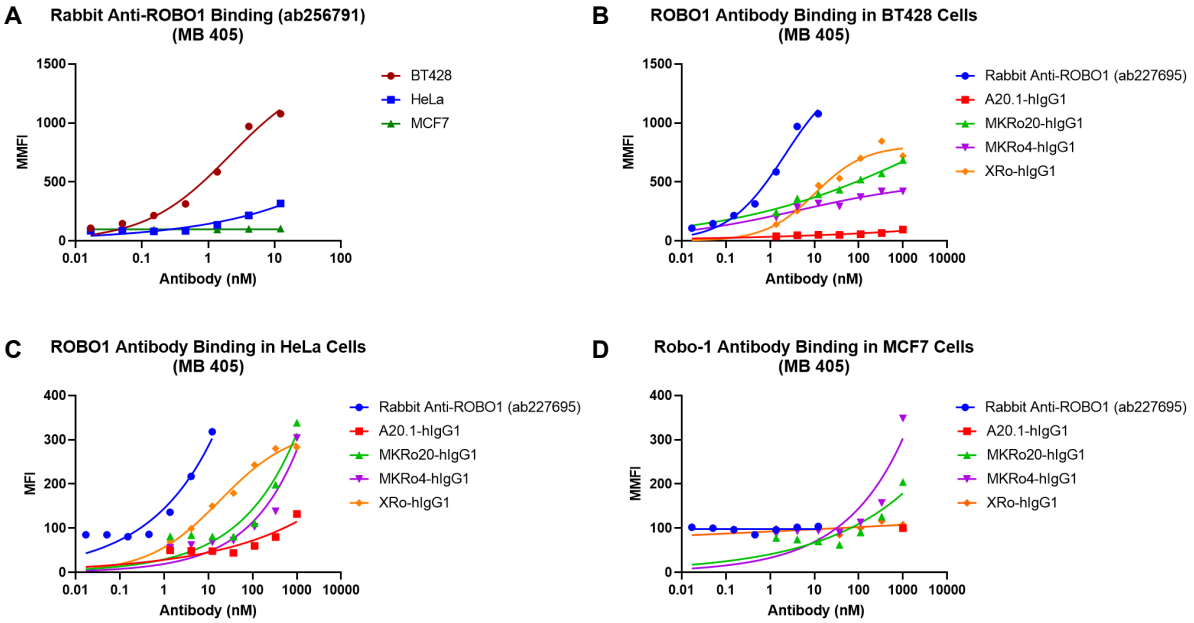
A
Rabbit Anti-ROBO1 Binding (ab256791)
(MB 405)
MMFI
Antibody (nM)
BT428
HeLa
MCF7
B
ROBO1 Antibody Binding in BT428 Cells
(MB 405)
MMFI
Antibody (nM)
Rabbit Anti-ROBO1 (ab227695)
A20.1-hIgG1
MKRo20-hIgG1
MKRo4-hIgG1
XRo-hIgG1
C
ROBO1 Antibody Binding in HeLa Cells
(MB 405)
MFI
Antibody (nM)
Rabbit Anti-ROBO1 (ab227695)
A20.1-hIgG1
MKRo20-hIgG1
MKRo4-hIgG1
XRo-hIgG1
D
Robo-1 Antibody Binding in MCF7 Cells
(MB 405)
MMFI
Antibody (nM)
Rabbit Anti-ROBO1 (ab227695)
A20.1-hIgG1
MKRo20-hIgG1
MKRo4-hIgG1
XRo-hIgG1

Figure 2. Camelid monomeric single-domain antibodies bind human ROBO1. (A) Immunostaining of patient-derived GSC line BT428 and commercial cell lines (HeLa and MCF4) for ROBO1 using a commercially-available ROBO1 antibody to establish models with a large range in ROBO1 expression. **(B-D)** Immunostaining of BT428 **(B)**, HeLA **(C)**, and MCF7 **(D)** cells with ROBO1-specific commercial antibody (ab227695) as well as camelid monomeric single-domain antibodies against ROBO1 (MKRo20-hIgG1, MKRo4-hIgG1, and XRo-hIgG1) or a control antigen (A20.1-hIgG1). Mean fluorescence values (MFI or MMFI) are indicated.

A

Construct	Signal	Binder	Hinge	TM	Co-stim	Stim
XRo_45	CD8A	XRo	CD8A 45	CD28	CD28	CD3Z
XRo_50	CD8A	XRo	CD8A 50	CD28	CD28	CD3Z
MKRo20_45	CD8A	MKRo20	CD8A 45	CD28	CD28	CD3Z
MKRo20_50	CD8A	MKRo20	CD8A 50	CD28	CD28	CD3Z
A20.1	CD8A	A20.1	CD8A 45	CD28	CD28	CD3Z
A20.1	CD8A	A20.1	CD8A 50	CD28	CD28	CD3Z

B

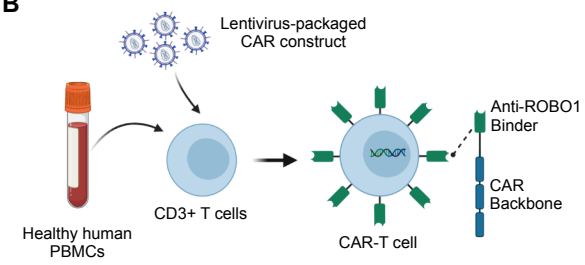

C

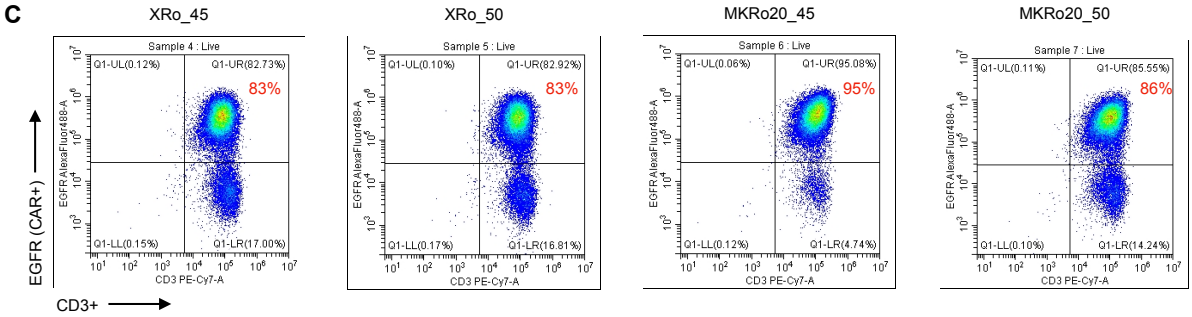

D

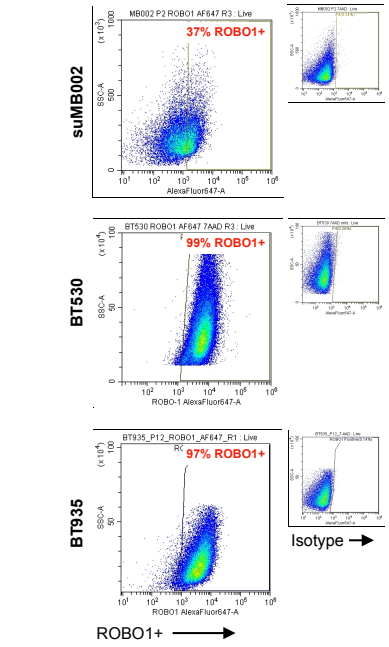

E

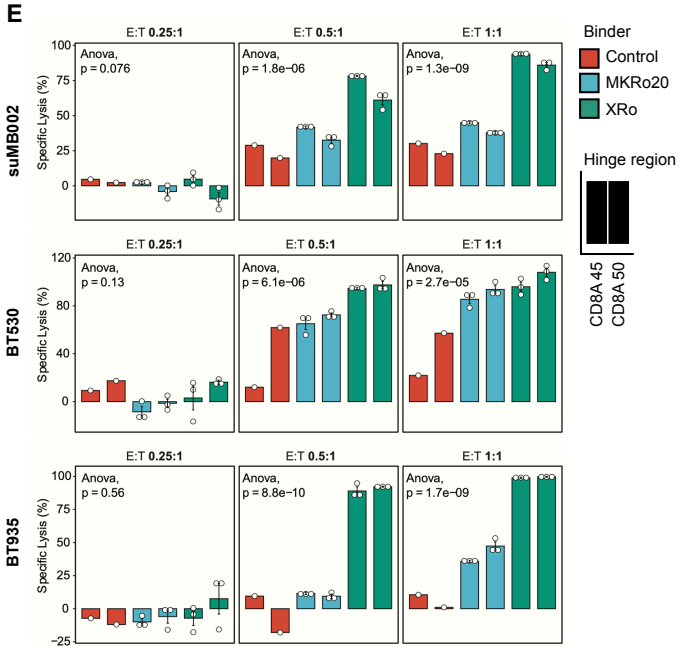

Figure 3. Design, production and optimization of anti-ROBO1 CAR-T cells. (A) Table of second generation CAR constructs incorporating a CD8A signal peptide, monomeric single-domain binders against ROBO1 (XRo and MKRo20) or a control antigen (A20.1), CD8A hinge region with (50) or without (45) a preceding optional GGGGS linker, CD28 transmembrane (TM) and co-stimulatory domains (Co-stim), and a CD3Z stimulatory domain (CD3Z). **(B)** Diagram of CAR-T cell production including isolation of CD3+ T cells from healthy human peripheral blood mononuclear cells (PBMCs), lentiviral infection of CAR constructs, and generation of CAR-T cells. **(C)** Combined efficiency of lentiviral transduction and enrichment of anti-ROBO1 CAR-T cells indicated by immunostaining with CD3 and EGFR. EGFR staining is a surrogate of CAR+ T cells as protein coding of the CAR is followed by a truncated EGFR marker. Percentages of stained CAR+ T cells above isotype control are indicated (red). **(D)** Immunostaining of patient-derived group 3 medulloblastoma (suMB002), lung-to-brain metastases (BT530) and adult glioblastoma (BT935) BTSC lines with ROBO1. Percentages of stained ROBO1+ cells above isotype control (small plots on right) are indicated (red). **(E)** Percent tumor cell killing of different BTSC lines co-cultured with control (A20.1) or anti-ROBO1 (MKRo20 and XRo) CAR-T cells at various E:T ratios (0.25:1 to 1:1) for 24 hours, normalized against the numbers of viable tumor cells when cultured in the absence of effector cells. Shown are means +/- SEM of % cell killing in triplicate wells. A one-way ANOVA test with Bonferroni's multiple comparison correction determined statistical significance with *P* values indicated.

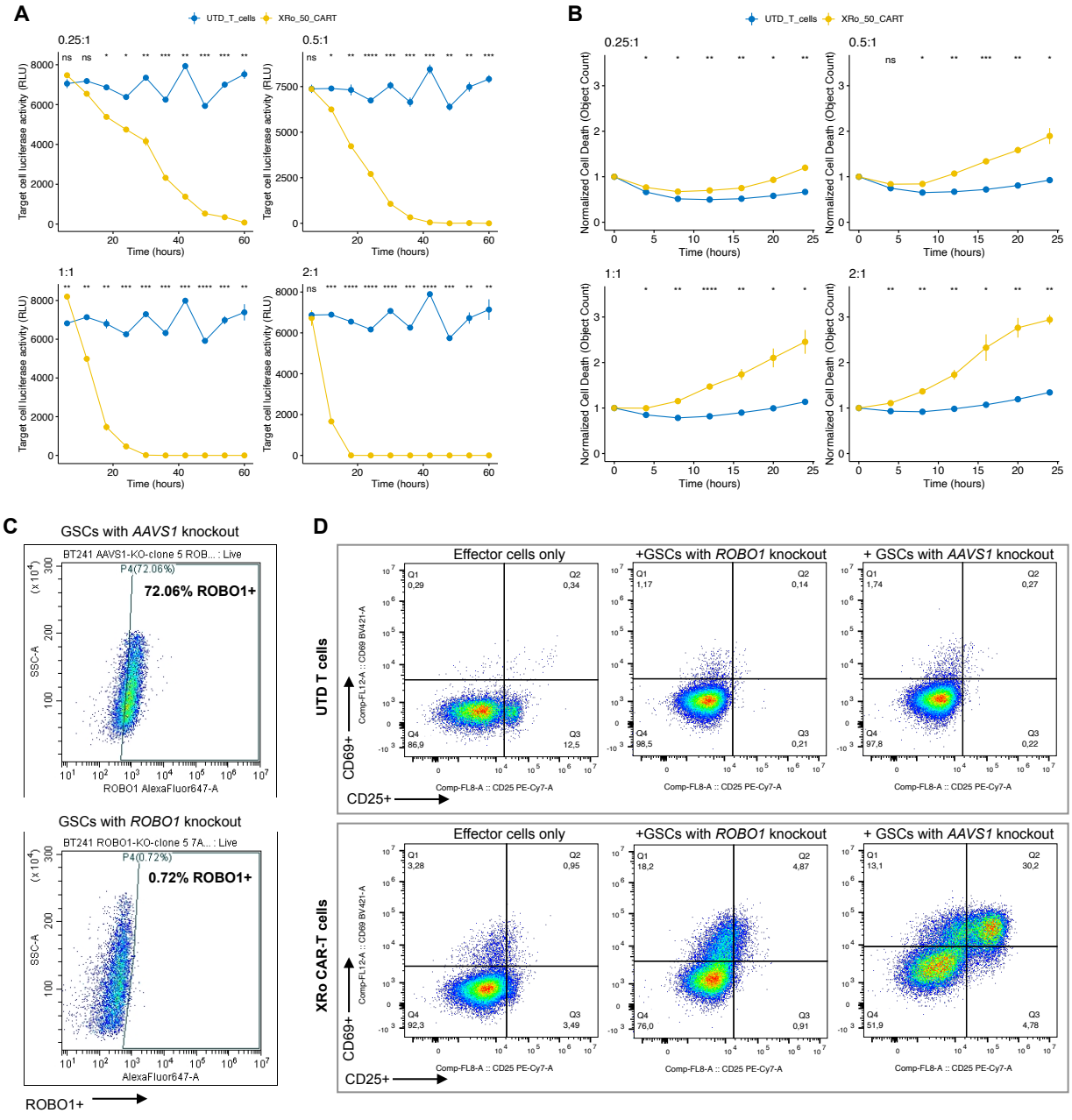
A
UTD_T_cells
XRo_50_CART
0.25:1
0.5:1
1:1
2:1
Target cell luciferase activity (RLU)
Time (hours)
B
Normalized Cell Death (Object Count)
C
GSCs with AAVS1 knockout
BT241 AAVS1-KO-clone 5 ROB... : Live
P4(72.06%)
72.06% ROBO1+
SSC-A
ROBO1 AlexaFluor647-A
GSCs with ROBO1 knockout
BT241 ROBO1-KO-clone 5 7A... : Live
P4(0.72%)
0.72% ROBO1+
AlexaFluor647-A
ROBO1+
D
Effector cells only
+GSCs with ROBO1 knockout
+ GSCs with AAVS1 knockout
UTD T cells
XRo CAR-T cells
CD69+
CD25+
Comp-FL12-A :: CD69 BV421-A
Comp-FL8-A :: CD25 PE-Cy7-A
Q1 0,29
Q2 0,34
Q4 86,9
Q3 12,5
Q1 1,17
Q2 0,14
Q4 98,5
Q3 0,21
Q1 1,74
Q2 0,27
Q4 97,8
Q3 0,22
Q1 3,28
Q2 0,95
Q4 92,3
Q3 3,49
Q1 18,2
Q2 4,87
Q4 76,0
Q3 0,91
Q1 13,1
Q2 30,2
Q4 51,9
Q3 4,78

Figure 4. Effector activity and activation of XRo CAR-T cells. (A-B) Time course of tumor cell killing of ROBO1-expressing BT241 GSCs co-cultured with untransduced (UTD) T cells or XRo CAR-T cells at various E:T ratios (0.25:1 to 1:1) for up to 60 hours. Target cell death was measured using **(A)** target cell luciferase activity (BLI) and **(B)** cell death (object count) normalized against number of viable cells at 0 hours. Shown are means +/- SEM in quintuplicate wells and E:T ratios are indicated above each plot. Student's *t* test was conducted for each timepoint (*$P < 0.05$; **$P < 0.01$; and ***$P < 0.001$ comparing XRo CAR versus UTD). **(C)** Immunostaining of BT241 GSCs with isogenic knockout of *AAVS1* (top) or *ROBO1* (bottom) with ROBO1. Percentages of stained ROBO1+ cells above isotype control are indicated (black). **(D)** Assessment of T cell activation by immunostaining UTD T cells (top) or XRo CAR-T cells (bottom) alone (left), or as co-cultures with GSCs with *ROBO1* knockout (middle) or ROBO1-expressing GSCs (*AAVS1* knockout; right) at an E:T ratio of 1:1 for 24 hours. Cultures were stained for CD3, CD25 and CD69. Percentages of CD3+CD25+ and/or CD3+CD69+ are indicates in respective quadrants.

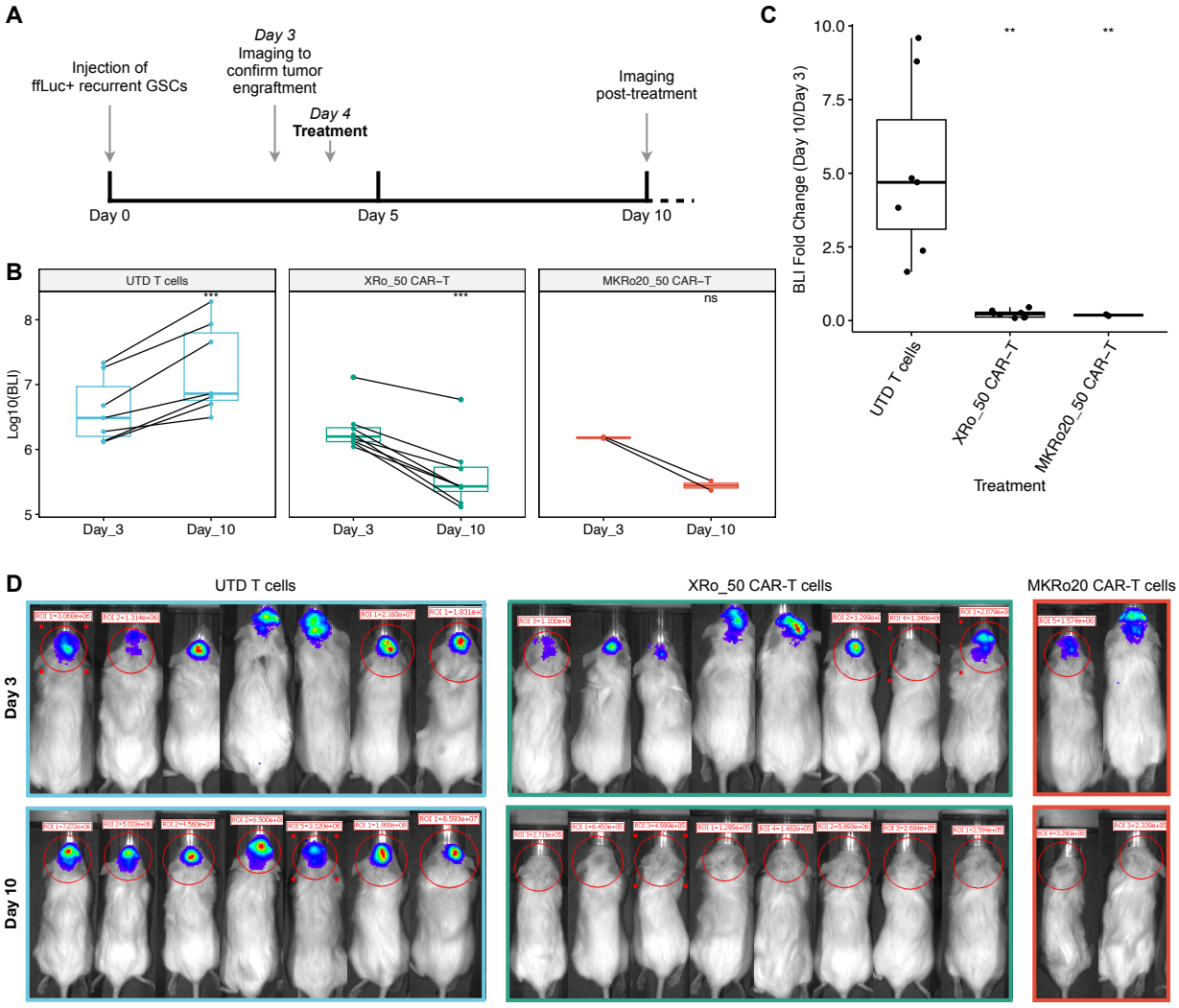
A
Injection of ffLuc+ recurrent GSCs
Day 3 Imaging to confirm tumor engraftment
Day 4 Treatment
Imaging post-treatment
Day 0
Day 5
Day 10
B
UTD T cells
XRo_50 CAR–T
MKRo20_50 CAR–T
Log10(BLI)
Day_3
Day_10
***
ns
C
BLI Fold Change (Day 10/Day 3)
10.0
7.5
5.0
2.5
0.0
**
UTD T cells
XRo_50 CAR–T
MKRo20_50 CAR–T
Treatment
D
UTD T cells
XRo_50 CAR-T cells
MKRo20 CAR-T cells
Day 3
Day 10

Figure 5. In vivo antitumor activity of anti-ROBO1 CAR-T cells. (A) Timeline of an on-going *in vivo* pre-clinical trial summarizing orthotopic injection of 50,000 ffLuc+ recurrent GSCs (Day 0) followed by imaging to confirm tumor engraftment (Day 3), treatment with 500,000 UTD T cells or anti-ROBO1 CAR-T cells (XRo or MKRo; Day 4), and post-treatment imaging of tumor burden (Day 10). **(B)** Bioluminescence (BLI) imaging of tumor-bearing mice before (Day 3) and after (Day 10) treatment with UTD T cells (left), XRo CAR-T cells (middle), or MKRo20 CAR-T cells (right). Paired data connections indicate a single mouse. Paired Student's *t* tested were conducted between Day 10 and Day 3 values for each treatment (ns not significant, ***$P < 0.001$). **(C)** Bioluminescence (BLI) images for each cohort on Day 3 (top) and Day 10 (bottom).

References

Arbabi Ghahroudi, M., Desmyter, A., Wyns, L., Hamers, R., and Muyldermans, S. (1997). Selection and identification of single domain antibody fragments from camel heavy-chain antibodies. FEBS letters *414*, 521-526.

Bagley, S.J., Kothari, S., Rahman, R., Lee, E.Q., Dunn, G.P., Galanis, E., Chang, S.M., Nabors, L.B., Ahluwalia, M.S., Stupp, R.*, et al.* (2022). Glioblastoma Clinical Trials: Current Landscape and Opportunities for Improvement. Clinical cancer research : an official journal of the American Association for Cancer Research *28*, 594-602.

Bao, S., Wu, Q., McLendon, R.E., Hao, Y., Shi, Q., Hjelmeland, A.B., Dewhirst, M.W., Bigner, D.D., and Rich, J.N. (2006). Glioma stem cells promote radioresistance by preferential activation of the DNA damage response. Nature *444*, 756-760.

Baral, T.N., MacKenzie, R., and Arbabi Ghahroudi, M. (2013). Single-domain antibodies and their utility. Curr Protoc Immunol *103*, 2 17 11-12 17 57.

Barthel, F.P., Johnson, K.C., Varn, F.S., Moskalik, A.D., Tanner, G., Kocakavuk, E., Anderson, K.J., Abiola, O., Aldape, K., Alfaro, K.D.*, et al.* (2019). Longitudinal molecular trajectories of diffuse glioma in adults. Nature *576*, 112-120.

Brown, C.E., Alizadeh, D., Starr, R., Weng, L., Wagner, J.R., Naranjo, A., Ostberg, J.R., Blanchard, M.S., Kilpatrick, J., Simpson, J.*, et al.* (2016). Regression of Glioblastoma after Chimeric Antigen Receptor T-Cell Therapy. The New England journal of medicine *375*, 2561-2569.

Bruggeman, S.W., Hulsman, D., Tanger, E., Buckle, T., Blom, M., Zevenhoven, J., van Tellingen, O., and van Lohuizen, M. (2007). Bmi1 controls tumor development in an Ink4a/Arf-independent manner in a mouse model for glioma. Cancer cell *12*, 328-341.

Cancer Genome Atlas Research, N., Weinstein, J.N., Collisson, E.A., Mills, G.B., Shaw, K.R., Ozenberger, B.A., Ellrott, K., Shmulevich, I., Sander, C., and Stuart, J.M. (2013). The Cancer Genome Atlas Pan-Cancer analysis project. Nature genetics *45*, 1113-1120.

Choi, B.D., Curry, W.T., Carter, B.S., and Maus, M.V. (2018). Chimeric antigen receptor T-cell immunotherapy for glioblastoma: practical insights for neurosurgeons. Neurosurg Focus *44*, E13.

Dallol, A., Krex, D., Hesson, L., Eng, C., Maher, E.R., and Latif, F. (2003). Frequent epigenetic inactivation of the SLIT2 gene in gliomas. Oncogene *22*, 4611-4616.

Dickinson, R.E., and Duncan, W.C. (2010). The SLIT-ROBO pathway: a regulator of cell function with implications for the reproductive system. Reproduction *139*, 697-704.

Fairhead, M., and Howarth, M. (2015). Site-specific biotinylation of purified proteins using BirA. Methods in molecular biology *1266*, 171-184.

Gara, R.K., Kumari, S., Ganju, A., Yallapu, M.M., Jaggi, M., and Chauhan, S.C. (2015). Slit/Robo pathway: a promising therapeutic target for cancer. Drug discovery today *20*, 156-164.

Geraldo, L.H., Xu, Y., Jacob, L., Pibouin-Fragner, L., Rao, R., Maissa, N., Verreault, M., Lemaire, N., Knosp, C., Lesaffre, C.*, et al.* (2021). SLIT2/ROBO signaling in tumor-associated microglia and macrophages drives glioblastoma immunosuppression and vascular dysmorphia. The Journal of clinical investigation *131*.

Goff, S.L., Morgan, R.A., Yang, J.C., Sherry, R.M., Robbins, P.F., Restifo, N.P., Feldman, S.A., Lu, Y.C., Lu, L., Zheng, Z.*, et al.* (2019). Pilot Trial of Adoptive Transfer of Chimeric Antigen Receptor-transduced T Cells Targeting EGFRvIII in Patients With Glioblastoma. Journal of immunotherapy *42*, 126-135.

Hart, T., Tong, A.H.Y., Chan, K., Van Leeuwen, J., Seetharaman, A., Aregger, M., Chandrashekhar, M., Hustedt, N., Seth, S., Noonan, A.*, et al.* (2017). Evaluation and Design of Genome-Wide CRISPR/SpCas9 Knockout Screens. G3 (Bethesda) *7*, 2719-2727.

Hodges, T.R., Ott, M., Xiu, J., Gatalica, Z., Swensen, J., Zhou, S., Huse, J.T., de Groot, J., Li, S., Overwijk, W.W.*, et al.* (2017). Mutational burden, immune checkpoint expression, and mismatch repair in glioma: implications for immune checkpoint immunotherapy. Neuro-oncology *19*, 1047-1057.

Hu, H., Li, M., Labrador, J.P., McEwen, J., Lai, E.C., Goodman, C.S., and Bashaw, G.J. (2005). Cross GTPase-activating protein (CrossGAP)/Vilse links the Roundabout receptor to Rac to regulate midline repulsion. Proceedings of the National Academy of Sciences of the United States of America *102*, 4613-4618.

Jackson, C.M., Choi, J., and Lim, M. (2019). Mechanisms of immunotherapy resistance: lessons from glioblastoma. Nature immunology *20*, 1100-1109.

Johnson, B.E., Mazor, T., Hong, C., Barnes, M., Aihara, K., McLean, C.Y., Fouse, S.D., Yamamoto, S., Ueda, H., Tatsuno, K.*, et al.* (2014). Mutational analysis reveals the origin and therapy-driven evolution of recurrent glioma. Science *343*, 189-193.

Liu, L., Li, W., Geng, S., Fang, Y., Sun, Z., Hu, H., Liang, Z., and Yan, Z. (2016). Slit2 and Robo1 expression as biomarkers for assessing prognosis in brain glioma patients. Surg Oncol *25*, 405-410.

Manoranjan, B., Chokshi, C., Venugopal, C., Subapanditha, M., Savage, N., Tatari, N., Provias, J.P., Murty, N.K., Moffat, J., Doble, B.W.*, et al.* (2020). A CD133-AKT-Wnt signaling axis drives glioblastoma brain tumor-initiating cells. Oncogene *39*, 1590-1599.

Maude, S.L., Frey, N., Shaw, P.A., Aplenc, R., Barrett, D.M., Bunin, N.J., Chew, A., Gonzalez, V.E., Zheng, Z., Lacey, S.F., *et al.* (2014). Chimeric antigen receptor T cells for sustained remissions in leukemia. The New England journal of medicine *371*, 1507-1517.

Mertsch, S., Schmitz, N., Jeibmann, A., Geng, J.G., Paulus, W., and Senner, V. (2008). Slit2 involvement in glioma cell migration is mediated by Robo1 receptor. Journal of neuro-oncology *87*, 1-7.

Neftel, C., Laffy, J., Filbin, M.G., Hara, T., Shore, M.E., Rahme, G.J., Richman, A.R., Silverbush, D., Shaw, M.L., Hebert, C.M., *et al.* (2019). An Integrative Model of Cellular States, Plasticity, and Genetics for Glioblastoma. Cell *178*, 835-849 e821.

Nguemgo Kouam, P., Rezniczek, G.A., Kochanneck, A., Priesch-Grzeszkowiak, B., Hero, T., Adamietz, I.A., and Buhler, H. (2018). Robo1 and vimentin regulate radiation-induced motility of human glioblastoma cells. PloS one *13*, e0198508.

O'Rourke, D.M., Nasrallah, M.P., Desai, A., Melenhorst, J.J., Mansfield, K., Morrissette, J.J.D., Martinez-Lage, M., Brem, S., Maloney, E., Shen, A., *et al.* (2017). A single dose of peripherally infused EGFRvIII-directed CAR T cells mediates antigen loss and induces adaptive resistance in patients with recurrent glioblastoma. Science translational medicine *9*.

Ostrom, Q.T., Cioffi, G., Waite, K., Kruchko, C., and Barnholtz-Sloan, J.S. (2021). CBTRUS Statistical Report: Primary Brain and Other Central Nervous System Tumors Diagnosed in the United States in 2014-2018. Neuro-oncology *23*, iii1-iii105.

Patel, A.P., Tirosh, I., Trombetta, J.J., Shalek, A.K., Gillespie, S.M., Wakimoto, H., Cahill, D.P., Nahed, B.V., Curry, W.T., Martuza, R.L., *et al.* (2014). Single-cell RNA-seq highlights intratumoral heterogeneity in primary glioblastoma. Science *344*, 1396-1401.

Qazi, M.A., Vora, P., Venugopal, C., Adams, J., Singh, M., Hu, A., Gorelik, M., Subapanditha, M.K., Savage, N., Yang, J.*, et al.* (2018). Cotargeting Ephrin Receptor Tyrosine Kinases A2 and A3 in Cancer Stem Cells Reduces Growth of Recurrent Glioblastoma. Cancer research *78*, 5023-5037.

Rhee, J., Buchan, T., Zukerberg, L., Lilien, J., and Balsamo, J. (2007). Cables links Robo-bound Abl kinase to N-cadherin-bound beta-catenin to mediate Slit-induced modulation of adhesion and transcription. Nature cell biology *9*, 883-892.

Rhee, J., Mahfooz, N.S., Arregui, C., Lilien, J., Balsamo, J., and VanBerkum, M.F. (2002). Activation of the repulsive receptor Roundabout inhibits N-cadherin-mediated cell adhesion. Nature cell biology *4*, 798-805.

Sampson, J.H., Maus, M.V., and June, C.H. (2017). Immunotherapy for Brain Tumors. Journal of clinical oncology : official journal of the American Society of Clinical Oncology *35*, 2450-2456.

Seeger, M., Tear, G., Ferres-Marco, D., and Goodman, C.S. (1993). Mutations affecting growth cone guidance in Drosophila: genes necessary for guidance toward or away from the midline. Neuron *10*, 409-426.

Singh, S.K., Hawkins, C., Clarke, I.D., Squire, J.A., Bayani, J., Hide, T., Henkelman, R.M., Cusimano, M.D., and Dirks, P.B. (2004). Identification of human brain tumour initiating cells. Nature *432*, 396-401.

Stupp, R., Mason, W.P., van den Bent, M.J., Weller, M., Fisher, B., Taphoorn, M.J., Belanger, K., Brandes, A.A., Marosi, C., Bogdahn, U.*, et al.* (2005). Radiotherapy plus concomitant and adjuvant temozolomide for glioblastoma. The New England journal of medicine *352*, 987-996.

Tang, X., Wang, Y., Huang, J., Zhang, Z., Liu, F., Xu, J., Guo, G., Wang, W., Tong, A., and Zhou, L. (2021). Administration of B7-H3 targeted chimeric antigen receptor-T cells induce regression of glioblastoma. Signal Transduct Target Ther *6*, 125.

Venugopal, C., Hallett, R., Vora, P., Manoranjan, B., Mahendram, S., Qazi, M.A., McFarlane, N., Subapanditha, M., Nolte, S.M., Singh, M.*, et al.* (2015). Pyrvinium Targets CD133 in Human Glioblastoma Brain Tumor-Initiating Cells. Clinical cancer research : an official journal of the American Association for Cancer Research *21*, 5324-5337.

Vora, P., Venugopal, C., Salim, S.K., Tatari, N., Bakhshinyan, D., Singh, M., Seyfrid, M., Upreti, D., Rentas, S., Wong, N.*, et al.* (2020). The Rational Development of CD133-Targeting Immunotherapies for Glioblastoma. Cell stem cell *26*, 832-844 e836.

Wang, J., Cazzato, E., Ladewig, E., Frattini, V., Rosenbloom, D.I., Zairis, S., Abate, F., Liu, Z., Elliott, O., Shin, Y.J.*, et al.* (2016). Clonal evolution of glioblastoma under therapy. Nature genetics *48*, 768-776.

Wong, K., Ren, X.R., Huang, Y.Z., Xie, Y., Liu, G., Saito, H., Tang, H., Wen, L., Brady-Kalnay, S.M., Mei, L.*, et al.* (2001). Signal transduction in neuronal migration: roles of GTPase activating proteins and the small GTPase Cdc42 in the Slit-Robo pathway. Cell *107*, 209-221.

Wu, W., Wong, K., Chen, J., Jiang, Z., Dupuis, S., Wu, J.Y., and Rao, Y. (1999). Directional guidance of neuronal migration in the olfactory system by the protein Slit. Nature *400*, 331-336.

Yiin, J.J., Hu, B., Jarzynka, M.J., Feng, H., Liu, K.W., Wu, J.Y., Ma, H.I., and Cheng, S.Y. (2009). Slit2 inhibits glioma cell invasion in the brain by suppression of Cdc42 activity. Neuro-oncology *11*, 779-789.

Ypsilanti, A.R., Zagar, Y., and Chedotal, A. (2010). Moving away from the midline: new developments for Slit and Robo. Development *137*, 1939-1952.

Zbinden, M., Duquet, A., Lorente-Trigos, A., Ngwabyt, S.N., Borges, I., and Ruiz i Altaba, A. (2010). NANOG regulates glioma stem cells and is essential in vivo acting in a cross-functional network with GLI1 and p53. The EMBO journal *29*, 2659-2674.

CHAPTER 4: Advances in immunotherapy for adult glioblastoma

Preamble

This is a pre-copyrighted, author-produced version of an article published in *Cancers (Basel)*. Chokshi, C. R., Brakel, B. A., Tatari, N., Savage, N., Salim, S. K., Venugopal, C., & Singh, S. K. (2021). Advances in Immunotherapy for Adult Glioblastoma. *Cancers*, *13* is available online at: https://www.mdpi.com/2072-6694/13/14/3400

CRC designed premise of this review and prepared the manuscript. CRC and BAB conducted literature searches, wrote the manuscript, prepared figures and edited the manuscript. NT, NS, SKS (Sabra) reviewed and edited the manuscript. CV and SKS (Sheila) provided critical intellectual comments and edited the manuscript. SKS (Sheila) supervised this effort in its entirety.

In this review, we will summarize clinical findings and highlight promising pre-clinical studies of three major immunotherapeutic modalities in GBM, including vaccines, antibodies, and chimeric antigen receptor (CAR) T cells. Common to all therapeutic modalities are fundamental mechanisms of therapy evasion by tumor cells, including immense intratumoral heterogeneity, suppression of the tumor immune microenvironment, and low mutational burden. These insights have led efforts to design rational combinations of therapeutics that can reignite the anti-tumor immune response, effectively and specifically target tumor cells, and reliably decrease tumor burden for GBM patients.

Sections of this review have also been used in Chapter 1 and Chapter 5 of this thesis.

Advances in immunotherapy for adult glioblastoma

Chirayu R. Chokshi[1], Benjamin A. Brakel[1], Nazanin Tatari[1], Neil Savage[1], Sabra K. Salim[1], Chitra Venugopal[2], Sheila K. Singh[1,2,*]

Affiliations

[1]Department of Biochemistry and Biomedical Sciences, McMaster University, Hamilton, Ontario, Canada L8N 3Z5.

[2]Department of Surgery, Faculty of Health Sciences, McMaster University, Hamilton, Ontario, Canada L8N 3Z5.

*Lead contact and corresponding author: Dr. Sheila K. Singh (ssingh@mcmaster.ca).

Abstract

Despite aggressive multimodal therapy, glioblastoma (GBM) remains the most common malignant primary brain tumor in adults. With the advent of therapies that revitalize the anti-tumor immune response, several immunotherapeutic modalities have been developed for the treatment of GBM. In this review, we summarize recent clinical and pre-clinical efforts to evaluate vaccination strategies, immune checkpoint inhibitors (ICIs) and chimeric antigen receptor (CAR) T cells. Although these modalities have shown long term tumor regression in subsets of treated patients, the underlying biology that may predict efficacy and therapy development to grow this cohort of treatment-responders are being actively investigated. Common to all therapeutic modalities are fundamental mechanisms of therapy evasion by tumor cells, including immense intratumoral heterogeneity, suppression of the tumor immune microenvironment, and low mutational burden. These insights have led efforts to design rational combinations of therapeutics that can reignite the anti-tumor immune response, effectively and specifically target tumor cells, and reliably decrease tumor burden for GBM patients.

Introduction

Glioblastoma (GBM) remains the most aggressive and prevalent malignant primary brain tumor in adults(Ostrom et al., 2016). Unchanged since 2005, patients undergo standard of care (SoC) that consists of gross total resection to remove the tumor bulk, followed by radiation therapy (RT) with concurrent and adjuvant chemotherapy with temozolomide (TMZ)(Lapointe et al., 2018; Stupp et al., 2005). Despite these aggressive therapeutic efforts, tumor relapse is inevitable, and patients face a median overall survival of 14.6 months and a five-year survival rate of 5.5-6.8%(Ostrom et al., 2016; Stupp et al., 2009; Stupp et al., 2005). A major contributor to treatment failure is intra-tumoral heterogeneity that gives rise to tumor cell populations distinct at the genomic, transcriptomic, proteomic and functional levels(Kim et al., 2015b; Meyer et al., 2015; Neftel et al., 2019; Patel et al., 2014; Wang et al., 2016). In addition to SoC, two therapeutics have received approval from the Food and Drug Administration, including (1) an anti-vascular endothelial growth factor (VEGF) monoclonal antibody bevacizumab, and (2) tumor-treating fields that target proliferating tumor cells. However, these therapies have yet to be incorporated into SoC for GBM patients.

Emerging therapeutics for GBM have shifted towards reconfiguring the patient's immune system to generate an anti-tumor response. Here, we will summarize clinical findings and highlight promising pre-clinical studies of three major immunotherapeutic modalities in GBM, including vaccines, antibodies, and chimeric antigen receptor (CAR) T cells. For a recent review of advances in oncolytic virotherapy for gliomas, refer to Rius-Rocabert et al. (2020). Given that resistance to SoC and disease relapse are inevitable for GBM patients, pre-clinical and clinical advancement of immunotherapeutic modalities, combined with recent insights into the tumor immune microenvironment, are poised to improve clinical outcomes for this patient population.

Vaccines

Cancer vaccines function by exposing tumor-associated antigens to antigen-presenting cells (APCs) which activate immune effector cells to achieve an anti-cancer immune response. Several promising vaccines targeting both single and multiple antigens have shown varying degrees of clinical promise (Table 1), however, vaccines for GBM have yet to translate to SoC. While GBM-specific targets are sparse, several have been identified that are expressed on the cell surface. Perhaps the most explored to date, EGFR variant III (EGFRvIII) is a mutant receptor specific to GBM which has been targeted extensively through a variety of immunotherapeutic efforts including vaccination. Similarly, the cytomegalovirus (CMV) tegument phosphoprotein 65 (pp65) and IDH1(R132H)-mutant peptides are frequently and specifically expressed in GBM, in contrast to healthy brain (Bleeker et al., 2009; Mitchell et al., 2008). Vaccinations targeting these proteins have shown efficacy in clinical trials and often elicit strong responses, however, no targets identified to date are expressed on all GBM cells, allowing clonally driven recurrence to evade such treatments. In contrast, multi-targeted vaccines mediating the presentation of multiple tumor-associated antigens better address the heterogeneity of the tumor by reducing the population of cells not expressing a target and thus reducing clonally driven resistance, however, these treatments have shown little success.

Antigen presentation and the following activation and regulation of effector cells is another important process in achieving an effective immune response, which involves several proteins such as those mediating suppression of T cells, macrophages, and other tumor infiltrating lymphocytes. Current efforts acting on this front, such as antibodies against these suppressors, have shown preclinical promise but have fallen short in clinical trials. Additionally, success seems

to vary greatly upon combination of these inhibitors, underlining the importance of understanding and enhancing synergistic interactions between treatments.

Single-Target Vaccines

Several vaccines have been developed for GBM using a single, tumor-specific antigen. One of the most advanced GBM vaccines to date is *Rindopepimut*, a peptide vaccine targeting EGFRvIII which has been identified as a tumor-specific mutant expressed in roughly one-third of GBMs (Heimberger et al., 2005). This protein also enhances GBM tumorigenicity (Batra et al., 1995; Nagane et al., 1996) and is highly immunogenic (Sampson et al., 2009), altogether providing a promising target for immunotherapy. Early preclinical studies have confirmed its immunogenicity and shown it to be effective in mice (Heimberger et al., 2003), however, the protein's heterogeneous and unstable expression leaves room for EGFRvIII-negative tumor cells to drive therapy resistance and recurrence. A series of phase II *Rindopepimut* trials, named "ACTIVATE, ACT II and ACT III," have shown promise (NCT00643097, NCT00458601), achieving median survivals between 22 and 26 months (Sampson et al., 2011; Sampson et al., 2010; Schuster et al., 2015). To validate the findings, a large phase III trial termed "ACT IV" was completed with 371 patients (NCT01480479), however, no survival benefit was seen among vaccinated patients compared to controls, with median survivals of 20.1 and 20 months, respectively (Weller et al., 2017). Interestingly, patients with significant residual disease received a greater benefit from the vaccine, perhaps due to the larger amount of tumor able to initiate a response. Patients in the trial also showed strong humoral immune responses, suggesting resistance to the therapy was enabled at least in part by the heterogeneity of EGFRvIII expression. Indeed, those who underwent post-treatment biopsies of the recurrent tumor in both control and vaccinated groups showed loss of EGFRvIII expression in a majority of patients. This spontaneous loss of

expression highlights the limitations of single-target therapies in such a heterogeneous tumor and underlines the importance polytherapy will have in the future (Schafer et al., 2019). Additionally, the improved survival of the placebo group compared to historical controls was surprising, and future trials should account for this difference or change in control performance over time.

The complex interplay between therapies and the immune response must also be considered. For instance, *Rindopepimut* was given along with TMZ which induces lymphopenia(Brock et al., 1998). While an accompanying increase in regulatory T cells suggests this may hinder the response to *Rindopepimut*, previous findings have shown it can enhance it (Sampson et al., 2011). An additional study on *Rindopepimut* was done in 72 recurrent GBM patients in a phase II trial termed "ReACT" (NCT01498328), combining the vaccine with bevacizumab, a monoclonal antibody against VEG-F that has been shown to enhance immune responses (Mansfield et al., 2013). The trial showed improvement upon the ACT IV trial, with treated patients having a 24-month survival of 20% compared to 3% for controls and showing potential for *Rindopepimut* when the limitations surrounding immunosuppression are concurrently addressed (Reardon et al., 2020b).

Another promising vaccination effort is the CMV dendritic cell (DC) vaccine. While rare in the healthy brain, viral proteins and nucleic acids of CMV are present in around 90% of GBM tumors (Mitchell et al., 2008). The implications of CMV in tumor initiation and therapy resistance are not understood, however, these viral antigens pose a potential immunotherapeutic target specific to cancerous cells. Of these antigens, CMV pp65 is highly expressed in glioma tumors and is the main target of current CMV vaccination as it elicits the majority of cytotoxic T lymphocyte responses following infection (Wills et al., 1996). The CMV pp65 DC vaccine consists of autologous DCs pulsed with pp65 RNA fused in frame with the human Lysosomal Associated

Membrane Protein (hLAMP) gene shown to enhance antigen processing (Arruda et al., 2006). A series of large phase II trials were recently completed with the vaccine in patients with newly diagnosed GBM following SoC treatment.

The initial "ATTAC" trial (NCT00639639) and subsequent "ATTAC-GM" trial (NCT00639639) both showed long-term survival in approximately one-third of patients. The initial trial also revealed that pre-conditioning with tetanus-diphtheria (Td) toxoid significantly increased DC migration to the lymph nodes which correlated with increased survival, leading to half of the pre-conditioned patients remaining progression-free >36.6 months from diagnosis (Mitchell et al., 2015). The second trial instead administered dose-intensified TMZ (DI-TMZ) with the vaccination, as DI-TMZ-induced lymphopenia has previously been shown to enhance both humoral and cellular immune responses (Mitchell et al., 2011). While DI-TMZ increased immunosuppressive regulatory T cells, the group had a median survival of 41.1 months, greatly exceeding matched historical controls (Batich et al., 2017). Excitingly, four patients remained progression-free at 59 to 64 months post-diagnosis, and overall, the trial showed the vaccine to be effective at targeting GBM based on the presence of CMV pp65. A subsequent phase II trial termed "ELEVATE" is ongoing to validate the benefit of Td toxoid pre-conditioning on DC migration, and to evaluate synergy between vaccination, Td toxoid pre-conditioning, and the anti-tumor antibody *basiliximab* (NCT02366728). To date, the trial has confirmed increased migration of DCs to the lymph nodes following pre-conditioning, however, analysis of the other aims is not yet complete (Batich et al., 2020).

Vaccines have also been developed targeting the IDH1 subtype of gliomas, consisting of the IDH1(R132H)-mutated peptide which is highly expressed in the subset of patients with the mutation (Bleeker et al., 2009). The vaccine was previously found to be effective in a mouse model

transgenic for human MHC class I and II with IDH1(R132H), showing MHC class II presentation of the epitope and mutation-specific T cell and antibody responses (Schumacher et al., 2014). A phase I clinical trial termed "NOA-16" (NCT02454634) was recently completed for the vaccine concurrently with topical imiquimod, a myeloid-activating TLR7 agonist. Results of the trial were extremely promising, with 93% of patients showing a vaccine-specific immune response and 84% surviving >3 years (Platten et al., 2021). A second phase II trial called "RESIST" is underway, adjuvating the vaccination with granulocyte-macrophage colony-stimulating factor (GM-CSF) in combination with TMZ and Td toxoid (NCT02193347).

Multi-Target Vaccines

To treat a heterogeneous disease such as GBM, targeting a single antigen can lead to clonal evolution and drive resistance. One way of overcoming this is by targeting multiple antigens concurrently. Interestingly, the majority of advanced, successful vaccination attempts are that of single antigen-targeting vaccines, likely due to the strong, specific response to these single antigens seen in most trials. Regardless, the importance of targeting the heterogeneity of GBM tumors is well established, and several multi-targeted GBM vaccines have shown promising results. One such multi-targeted vaccine is DCVax-L, a more personalized approach to peptide vaccination that uses autologous, or patient-derived, DCs pulsed with resected tumor lysate to target a variety of tumor antigens. In rat models, the vaccine was found to significantly increase survival and T cell infiltration (Liau et al., 1999), leading to several clinical trials. In a phase III trial (NCT00045968), 232 patients were vaccinated with concurrent TMZ while all 331 patients were allowed the vaccine upon recurrence. The overall study population had a median survival of 23.1 months, with a large group (n=100) having a particularly long median survival of 40.5 months unexplained by any prognostic factors suggesting clinical efficacy related to vaccination (Liau et al., 2018). A trial is

now ongoing in patients who were previously ineligible due to post-chemoradiotherapy progression or insufficient vaccine production (NCT02146066).

Vaccines relying on heat shock proteins (HSP) are also advancing for GBM. There have been several trials investigating HSP vaccines for glioma which consist of HSPs and tumor-associated peptides. These vaccines primarily rely on tumor-derived HSP glycoprotein 96 (gp96), which binds tumor antigens forming the HSP protein complex-96 (HSPPC-96). This complex mediates the presentation of antigens in antigen-presenting cells and can bind different peptides for a multi-targeted approach. An initial trial of a multi-peptide HSPPC-96 vaccine with TMZ (NCT00293423) confirmed strong peripheral and local immune responses specific to the HSPPC-96-bound antigens in 11 of 12 treated patients (Crane et al., 2013). These responders had a median survival of 11.8 months post-vaccination and surgery compared to 4 months for the single non-responder, and in the phase II portion of the trial, patients showed a median survival of 10.7 months, significantly exceeding controls (Bloch et al., 2014). Additionally, patients with pre-vaccination lymphopenia had decreased survival compared to those with higher lymphocyte counts, likely due to worsened immune function and thus decreased responses. Addressing this question and further validating the effectiveness of the vaccine, another trial (NCT02122822) revealed those with strong tumor-specific immune responses indeed had longer median survival than those with weak responses (>40.5 months and 14.6 months, respectively), with the overall patient population reaching a median survival of 31.4 months and again exceeding controls (Ji et al., 2018).

Another phase II trial was recently completed with the HSPPC-96 vaccine and TMZ following SoC (NCT00905060) achieving a median survival of 23.8 months, further validating the efficacy of the vaccine (Bloch et al., 2017). Interestingly, the trial found expression of the T cell

suppressing immune checkpoint PD-L1 in myeloid cells to be indicative of survival, with high expression leading to shorter survival than those with lower expression (18 months and 44.7 months, respectively). While a promising lead, no HSPPC-96 vaccines have been combined with anti-PD-L1 therapies to date. However, a trial is currently investigating the vaccine when combined with standard TMZ, radiotherapy, and the antibody *pembrolizumab* targeting the ligand of PD-L1, which is still ongoing (NCT03018288).

Table 1. Summary of clinical trials for vaccines against GBM.

NCT Number	Treatment	Summary of results	Indication	Reference
NCT00643097	EGFRvIII peptide vaccine + DI-TMZ	EGFRvIII-expressing cells eradicated and vaccine immunogenic, with DI-TMZ cohort having enhanced humoral response. Median overall survival of 23.6 months.	Primary GBM	Sampson, et al. (Sampson et al., 2010) Sampson et al. (Sampson et al., 2011)
NCT00458601	EGFRvIII Peptide Vaccine + TMZ	Median overall survival of 21.8 months and 36-month survival of 26%. Anti-EGFRvIII antibodies increased ≥4-fold in 85% of patients and with duration of treatment.	Primary GBM	Schuster et al. (Schuster et al., 2015)
NCT01480479	EGFRvIII peptide vaccine + TMZ	Strong humoral responses, however, no survival advantage and loss of EGFRvIII expression upon recurrence.	Primary GBM	Weller et al. (Weller et al., 2017)

NCT01498328	EGFRvIII peptide vaccine + bevacizumab	24-month survival of 20% compared to 3% for controls.	Recurrent GBM	Reardon et al. (Reardon et al., 2020b)
NCT00639639	CMV pp65 DC vaccine + Td Toxoid + TMZ	Td toxoid pre-conditioning enhanced DC migration to the lymph nodes and improved survival. 3/6 Td toxoid patients were alive and progression-free at time of survival analysis (>36.6 months), while controls had median overall survival of 18.5 months.	Primary GBM	Mitchell et al. (Mitchell et al., 2015)
NCT00639639	CMV pp65 DC vaccine + DI-TMZ	Antigen-specific immune responses and median overall survival of 41.1 months in DI-TMZ cohort. 36% survival five years from diagnosis, with four patients remaining progression-free at 59 to 64 months from diagnosis.	Primary GBM	Batich et al. (Batich et al., 2017)
NCT02366728	CMV pp65 DC vaccine + 111In-labeled DC vaccine + Td Toxoid + basiliximab	Ongoing, have reported increased DC migration to lymph nodes following Td toxoid pre-conditioning.	Primary GBM	Batich et al. (Batich et al., 2020)

NCT02454634	IDH1 peptide vaccine	93% vaccine-specific response rate, 84% survival >3 years.	High-grade glioma	Platten et al. (Platten et al., 2021)
NCT00045968	DCVax-L vaccine	Median overall survival of 23.1 months, with large group (n=100) reaching 40.5 months.	Primary GBM	Liau et al. (Liau et al., 2018)
NCT00293423	HSPPC-96 peptide vaccine	Specific immune response in 11 of the 12 patients, responders had median overall survival of 11.8 months.	Recurrent GBM	Crane et al. (Crane et al., 2013) Bloch et al. (Bloch et al., 2014)
NCT02122822	HSPPC-96 peptide vaccine + TMZ + radiotherapy	Median overall survival of 31.4 months. Patients with high tumor-specific immune responses had median overall survival of >40.5 months compared to 14.6 months for low responders.	Primary GBM	Ji et al. (Ji et al., 2018)

NCT00905060	HSPPC-96 vaccine + TMZ	Median overall survival of 23.8 months. Patients with low PD-L1 expression in myeloid cells had median overall survival of 44.7 months compared to 18 months for those with high expression.	Primary GBM	Bloch et al. (Bloch et al., 2017)

Immune Checkpoint Inhibitors

A complex system of stimulatory and inhibitory regulators functions to maintain immune homeostasis. An important part of this system is immune checkpoints, which regulate activation to avoid autoimmunity. Upon activation or exhaustion, several immune cells upregulate these inhibitory checkpoints thus suppressing the immune response. Cancer cells express immune checkpoint proteins as well, allowing them to suppress the anti-cancer response. As a result, antibodies against these checkpoints known as immune checkpoint inhibitors (ICI) have been developed and have shown success in several cancers such as melanoma and non-small-cell lung cancer(Vaddepally et al., 2020), and several are underway for GBM (Table 2). Of these antibodies, the most advanced group are those blocking programmed cell death protein 1 (PD-1) and cytotoxic T lymphocyte antigen 4 (CTLA-4), which are expressed on T cells and prevent T cell stimulation and killing of glioma cells(Contardi et al., 2005; Davidson et al., 2019).

Immune checkpoint inhibitors

PD-1 antibodies *pembrolizumab* and *nivolumab* have been approved to treat various solid tumors(Vaddepally et al., 2020), however, clinical efficacy in GBM has yet to be achieved. Combination therapy of an anti-PD-1 antibody and radiotherapy has shown preclinical success *in vivo*(Zeng et al., 2013) leading to the phase III CheckMate 143 trial of *nivolumab* (NCT02017717), comparing it to the approved VEGF-A inhibitor *bevacizumab* in recurrent GBM. The trial results showed a median survival of around 10 months for both groups and identical 12-month survival rates of 42%(Reardon et al., 2020a). Additionally, preliminary safety data of an earlier cohort of patients revealed high toxicity of a previously considered anti-PD-1/anti-CTLA-4 combination arm(Omuro et al., 2018), leading to the discontinuation of this dual ICI therapy. *Nivolumab* has also been explored in other combinations such as the phase III CheckMate 498 trial

(NCT02617589) using it with radiotherapy compared to TMZ and radiotherapy, however, the trial showed no survival advantage of *nivolumab* treatment with similar median survivals around 14 months for both groups. Another phase III trial CheckMate 548 (NCT02667587) is combining *nivolumab*, radiotherapy and TMZ. While still ongoing, an announcement was made that the trial failed to meet its primary endpoints of overall survival and progression-free survival(Squibb, 2020).

Pembrolizumab is another, less advanced PD-1 antibody currently in trials for gliomas. In a phase I trial of 24 recurrent high-grade glioma patients treated with *pembrolizumab*, *bevacizumab* and hypofractionated stereotactic irradiation (NCT02313272), more than half the patients achieved significant responses and median survival was 13.5 months(Sahebjam et al., 2021). However, another phase I trial of pembrolizumab with *bevacizumab* and *pembrolizumab* alone in recurrent GBM patients (NCT02337491) showed a median survival of 8.8 months and 10.3 months, respectively(Reardon, 2006). The reduced survival upon lack of radiotherapy emphasizes the synergistic effect radiotherapy seems to have with anti-PD-1 therapies.

Additional efforts have been made to enhance responses to anti-PD-1 ICIs including neoadjuvation prior to surgery, which has enhanced and prolonged the anti-tumor immune response and increased survival in other cancers(Blank et al., 2018; Liu et al., 2016a). A phase II trial of this technique with *pembrolizumab* in recurrent GBM patients showed lengthened survival with neoadjuvant compared to an adjuvant-only cohort (13.2 months and 6.3 months, respectively)(Cloughesy et al., 2019). Neoadjuvation also led to an upregulation of T cell- and interferon-γ-related genes and down-regulation of cell cycle-related genes in the tumor. In a similar phase II trial (NCT02550249), neoadjuvant *nivolumab* was shown to enhance chemokine expression, T cell receptor (TCR) clonal diversity among tumor infiltrating lymphocytes (TILs)

and immune cell infiltration of the tumor, however, the median survival of treated patients was only 7.3 months(Schalper et al., 2019). Interestingly, two patients in the neoadjuvant cohort had complete surgical resection and remained disease-free for 33.3 and 28.5 months which was not explainable by any recorded prognostic factors.

CTLA-4 (CD152) is another ICI that reduces CD28 co-stimulatory signaling by competitively binding to its natural ligands CD80 and CD86, suppressing T cell stimulation. Anti-CTLA-4 therapy has been approved for several cancers(Vaddepally et al., 2020), extended survival of glioma-bearing mice(Fecci et al., 2007), and in combination with anti-PD-1 therapy shown eradication of tumors in a majority of mice(Reardon et al., 2016). Clinical trials have recently begun assessing anti-CTLA-4 therapies in treating gliomas (NCT02311920, NCT02829931), though no trials have been completed with glioma patients to date.

PD-L1, the ligand of PD-1 regularly expressed on APCs, is also expressed on cancer cells and mediates the suppression of tumor-infiltrating T cells. Anti-PD-L1 antibodies have been approved in other cancers(Vaddepally et al., 2020), however, their efficacy in gliomas remains poor. An ongoing phase II trial is evaluating the anti-PD-L1 antibody *durvalumab* with radiotherapy and *bevacizumab* in GBM (NCT02336165), with preliminary results of the recurrent, *bevacizumab*-refractory cohort showing only 36% survival at 5.5 months(Reardon, 2017). Another phase I trial is looking at a different combination of ICIs, treating recurrent glioma patients with *durvalumab* and an anti-CTLA-4 antibody (NCT02794883), however, no updates have been given. Previous trials have found low expression of PD-L1 in GBM, with the CheckMate-143 trial finding only 10 of the 37 patients with evaluable PD-L1 expression showing ≥10%(Omuro et al., 2018). This inherently limits any PD-L1 therapy and may partially explain the poor outcomes thus far.

LAG-3 is another immune checkpoint receptor expressed on exhausted T cells that negatively regulates T cell responses. While anti-LAG-3 therapies have had preclinical success(Harris-Bookman et al., 2018), studies have shown LAG-3 expression to be present in a low portion of tumor-infiltrating lymphocytes(Mair et al., 2021), thus limiting the potential impact of these therapies on stimulating the immune response. Regardless, a phase I trial evaluating the anti-LAG-3 antibody "BMS 986016" is underway, assessing its efficacy alone and in combination with the anti-PD-1 antibody *nivolumab* in recurrent GBM (NCT02658981). A recent update revealed a median survival of 8 months for the anti-LAG-3 group and 7 months for the anti-LAG-3, anti-PD-1 combination group. The trial also assessed an agonistic antibody targeting the 4-1BB (CD137) immune checkpoint protein. 4-1BB is a costimulatory receptor expressed by T cells upon activation which augments activation signaling. The anti-4-1BB group had a promising median survival of 14 months(Lim et al., 2019), however, while preclinical investigations support this therapy(Kuhnol et al., 2013; Newcomb et al., 2010), other trials of anti-4-1BB antibodies are yet to occur.

TIM-3 is a receptor expressed on lymphocytes that can suppress the immune response by inducing T cell exhaustion, such that expression of TIM-3 in GBM has been linked with poorer prognoses(Zhang et al., 2020). Anti-TIM-3 antibody therapy for GBM has shown success preclinically in combination with anti-PD-1 therapy and stereotactic radiosurgery (SRS). SRS drives the release of antigens from the tumor, enhancing the immune response which is further stimulated by the concurrent checkpoint inhibitors. While neither anti-TIM-3 nor SRS alone prolonged survival of GBM-bearing mice, combining the two increased median survival from 22 to 100 days, an effect similarly obtained in the anti-TIM-3 and anti-PD-1 combination(Kim et al., 2017). When combining all three treatments, 100% of mice were alive 100 days post-engraftment,

revealing great synergy and prompting a phase I trial of this combinational therapy which is still underway (NCT03961971).

Macrophage-Targeted Antibodies

Response to ICIs varies between tumor types and may be dependent on immune infiltrates such as TILs. Recently, mass cytometry and single-cell RNA sequencing in patients with cancers that typically do not respond well to immune checkpoint therapy, such as GBM, and cancers that do, revealed an overexpression of CD73-high macrophages in GBM which persists through anti-PD-1 treatment and limits ICIs by inhibiting T cell infiltration(Goswami et al., 2020b). Prevalence of these cells correlated with a low response to ICIs, and genetic perturbation of CD73 in mice improved the efficacy of anti-CTLA-4 and anti–PD-1 combination therapy which was correlated with T cell infiltration. These results show a promising new immunotherapeutic target to enhance existing ICIs.

CD47 is an enzyme that suppresses macrophage activation through binding the signal regulatory protein α (SIRPα). It is overexpressed in many tumors(Willingham et al., 2012), allowing cancer cells to avoid phagocytosis. Anti-CD47 antibodies have been developed to shift macrophages to an immunostimulatory phenotype, promoting the anti-tumor response (Zhang et al., 2016) and effectively reducing the growth of several tumors (Edris et al., 2012; Zhang et al., 2017). Preclinical studies of anti-CD47 therapies for glioma have shown that while anti-CD47 therapy is sometimes effective at stimulating glioma cell phagocytosis (Li et al., 2018), chemotherapy and radiotherapy are synergistic with the treatment and may be required to enhance phagocytosis and extend survival in mice (Gholamin et al., 2020; von Roemeling et al., 2020). This enhanced phagocytosis also leads to increased antigen cross-presentation and T cell priming (von Roemeling et al., 2020), and anti-CD47 therapies have also shown synergy with autophagy

inhibition (Zhang et al., 2018a; Zhang et al., 2018b) and other ICIs and tumor-specific antibodies (Sockolosky et al., 2016). The potential for synergistic co-therapies makes treatment with CD47 antibodies more complex, and effective combinations should be compared in the future to guide rational therapeutic development efforts.

Table 2. Summary of clinical trials for immune checkpoint inhibitors against GBM.

NCT Number	Treatment	Summary of results	Indication	Reference
NCT02017717	Nivolumab (anti-PD-1) or bevacizumab	Median overall survival was around 10 months for both groups, 12-month survival rates were identical between treatments at 42%.	Recurrent GBM	Reardon et al. (Reardon et al., 2020a)
NCT02617589	Nivolumab (anti-PD-1) + radiotherapy or TMZ + radiotherapy	No survival advantage over TMZ, median overall survival of 13.4 months for nivolumab cohort and 14.88 months for TMZ.	Primary GBM	No Reference
NCT02667587	Nivolumab (anti-PD-1) + TMZ + radiotherapy	Nivolumab provided no survival advantage over placebo, trial still ongoing.	Primary GBM	Squibb et al. (Squibb, 2020)
NCT02313272	Hypofractionated stereotactic irradiation + pembrolizumab (anti-PD-1) + bevacizumab	>50% patients had significant response, median overall survival of 13.5 months.	Recurrent high-grade glioma	Sahebjam et al. (Sahebjam et al., 2021)

NCT02337491	Pembrolizumab (anti-PD-1) or pembrolizumab + bevacizumab	Median overall survival of 8.8 months for pembrolizumab with bevacizumab, 10.3 months for pembrolizumab alone.	Recurrent GBM	Reardon et al. (Reardon, 2006)
NCT02550249	Neoadjuvant nivolumab	Neoadjuvant nivolumab enhanced chemokine expression, TCR clonal diversity among TILs and immune cell infiltration of the tumor, however, median overall survival was only 7.3 months.	GBM	Schalper et al. (Schalper et al., 2019)
NCT02336165	Durvalumab (anti-PD-L1) alone, with bevacizumab, or with radiotherapy	Preliminary results of recurrent, bevacizumab-refractory cohort had 36% survival at 5.5 months. Trial still ongoing.	GBM	Reardon et al. (Reardon, 2017)
NCT02658981	Anti-LAG-3 or anti-CD137 alone or with anti-PD-1	Median overall survival of 8 months for anti-LAG-3, 7 months for anti-LAG-3, anti-PD-1 combination, and 14 months for anti-CD137. Trial still ongoing.	Recurrent GBM	Lim et al. (Lim et al., 2019)

Chimeric antigen receptor (CAR) T cells

Chimeric antigen receptor (CAR) T cells represent an efficacious form of adoptive T cell therapy, in which peripheral T cells are genetically engineered to express a fusion receptor protein (i.e. CAR) that recognizes and targets a tumor-specific or -enriched antigen. Rapid and rational evolution of receptor design has transformed a first-generation CAR – composed of a ligand-binding domain, extracellular spacer, transmembrane domain and an intracellular signaling domain – that suffered from limited signaling strength to highly efficacious second- and third-generation CARs that incorporate one or more intracellular co-stimulatory domains, respectively, to initialize and sustain T cell signaling(Finney et al., 2004; Finney et al., 1998; Imai et al., 2004; Sadelain et al., 2013). Irrespective of design principles, an antigen-bound CAR T cell activates a potent cytokine release and cytolytic degranulation response that kills antigen-expressing tumor cells and results in T cell proliferation(Hombach et al., 2001). CAR T cell therapy has been highly effective against hematological malignancies, achieving remission rates of up to 90% in patients with relapsed or refractory B cell malignancies with anti-CD19 CAR T cells(Maude et al., 2014). However, widespread clinical responses of CAR T cells have yet to be seen for solid tumors, including GBM. Here, we summarize lessons learned from clinical evaluation of CAR T cell therapies in GBM patients, highlight promising preclinical candidates and discuss approaches to improving clinical efficacy.

Unlike hematological malignancies, CAR T cell therapy design and administration require unique considerations in the context of GBM, including factors such as intratumoral antigen heterogeneity, bypassing the blood-brain barrier (BBB) and exerting a potent anti-tumor response in a highly immunosuppressive microenvironment(Bagley et al., 2018). Two schools of thought have guided delivery of CAR T cell therapy to the brain thus far, one which supports systemic

intravenous administration, and the other prefers intracavitary or intraventricular dosing to bypass the BBB. Supported by reports of a dysregulated BBB in GBM patients(Sarkaria et al., 2018; Watkins et al., 2014), investigators evaluating CAR T cell therapies targeting EGFRvIII and HER2 preferred intravenous delivery of their modality(Ahmed et al., 2010; O'Rourke et al., 2017). Although no dose-limiting toxicities were observed for either modality when delivered intravenously, three grade 2-4 adverse events were possibly associated with HER2 CAR T cell therapy, including headache (n = 1) and seizure (n = 2). In contrast, intracavitary (or intratumoral) delivery of CAR T cells is not functionally restricted by the BBB. Using a reporter gene system, preliminary clinical evidence supports trafficking of intracerebrally-administered anti-IL13Rα2 CAR T cells to the tumor region using [^{18}F]FHBG PET-based imaging(Keu et al., 2017). Intracavitary treatment of GBM patients with anti-IL13Rα2 CAR T cells resulted in no dose-limiting toxicities(Brown et al., 2016a; Brown et al., 2015). However, similar to intravenous delivery of anti-EGFRvIII CAR T cells, two grade 3 adverse events were associated with the treatment, including headache (n = 1) and a neurologic event (n = 1). Unfortunately, an empirical and clinical comparison among CAR T cell delivery routes has yet to be performed for GBM.

To varying extents, clinical studies have evaluated CAR T cells for GBM targeting interleukin-13 receptor subunit alpha-2 (IL13Rα2), human epidermal growth factor receptor 2 (HER2) and EGFRvIII (Table 3), with follow-up studies targeting IL13Rα2 and HER2 underway. In addition, investigators have initiated clinical studies to evaluate CAR T cells targeting matrix metallopeptidase 2 (MMP2), B7 family member B7-H3, CD147 and NKG2-D type II integral membrane protein (NKG2D). Here, we outline clinical advances in CAR T cell therapies for the treatment of GBM.

IL13Rα2-specific CAR T cells

IL13Rα2 is a monomeric high-affinity receptor for interleukin 13 (IL13) that is enriched in GBM specimens compared to normal brain tissue(Brown et al., 2013; Debinski et al., 1999). In fact, IL13Rα2 expression correlates moderately with the mesenchymal signature(Brown et al., 2013), a subtype of GBM associated with greater proliferation, tumorigenicity and resistance to conventional chemoradiotherapy as compared to other subtypes(Bhat et al., 2013; Wang et al., 2018b). Supported by these findings, IL13Rα2 CAR T cells were designed using using a mutated IL13-zetakine binding domain (IL13.E13K.R109K), engineered to provide greater specificity for IL13Rα2 over IL13Rα1/IL4Rα, and attached to a CD28 co-stimulation and CD3ζ signaling domain(Kong et al., 2012). These IL13-zetakine CAR T cells were specifically and potently activated in presence of IL13Rα2-expressing glioma cells, whereas no appreciable effect was seen in the absence of IL13Rα2 expression. Strikingly, a single intracranial injection of IL13-zetakine CAR T cells into mice with orthotopic glioma xenografts led to a robust decrease in tumor burden and increased median overall survival from 35-40 days in control mice to 88 days in IL13-zetakine CAR T cell-treated mice. These promising preclinical results led to the first-in-human pilot safety and feasibility study of IL13-zetakine CAR T cells in three patients with relapsed GBM(Brown et al., 2015). In the study, IL13-zetakine CAR T cells were administered via an implanted reservoir/catheter system and led to treatment-induced inflammation at the tumor site. Although this treatment was well tolerated and led to decreased expression of IL13Rα2, two grade 3 headaches and a grade 3 neurologic event were observed following CAR T cell administration. A mean survival of 11 months after relapse was noted for these three patients, with one patient surviving 14 months.

Following this study, the group engineered second-generation IL13-targeted CAR T cells with a 4-1BB (CD137) co-stimulation domain and a mutated IgG4-Fc linker to improve antitumor potency and increase T cell persistence, while improving the safety profile(Brown et al., 2018; Brown et al., 2016a). These reengineered IL13BBζ-CAR T cells were administered to a patient with highly aggressive recurrent GBM with multifocal leptomeningeal disease and high IL13Rα2 expression. Although intracavitary infusions of IL13BBζ-CAR T cells did not cause any grade 3 or higher toxic effects and inhibited disease progression locally, distal non-resected tumors and new tumors progressed. Prompted by distant disease progression, IL13BBζ-CAR T cells were delivered via intraventricular infusions and led to dramatic reductions of all tumors after the fifth infusion, with 77 to 100% decrease in tumor burden, a systemic anti-tumor inflammatory response and an absence of systemic toxic effects, allowing the patient to return to normal life and work activities. Unfortunately, disease recurrence was observed after 7.5 months with tumor formation in new locations and decreased expression of IL13Rα2, elucidating a common antigen loss response to targeted therapies and advocating for rational combinational or adjuvant therapies. Recently, preclinical efforts to improve IL13Rα2-directed CAR T cell therapy have included the incorporation of an IL13Rα2-specific single-chain variable fragment (scFv)(Krenciute et al., 2016), complementary IL15 expression to enhance T cell effector function(Krenciute et al., 2017), characterization of the tumor immune microenvironment following CAR T cell therapy(Pituch et al., 2018), and optimal selection of T cell subsets for sustained CAR activity(Wang et al., 2018a).

EGFRvIII-specific CAR T cells

Expressed heterogeneously in ~30% of GBM specimens(Padfield et al., 2015), investigators have engineered and evaluated EGFRvIII-targeted CAR T cells in two in-human trials. A phase 1 study of EGFRvIII-targeted CAR T cells, previously tested in orthotopic

xenograft models of EGFRvIII+ glioma for efficacy and specificity to EGFRvIII over EGFR(Johnson et al., 2015; Ohno et al., 2013), was conducted in 10 patients with EGFRvIII+ recurrent GBM to evaluate safety and feasibility as the primary end points(O'Rourke et al., 2017). Although no subjects experienced dose-limiting toxicities, including systemic cytokine release syndrome, tumor regression was not observed in any patients based on magnetic resonance (MR) imaging. A median overall survival of ~8 months was noted after CAR T cell infusion, with one long-term survivor exhibiting stable disease for >18 months. Of 10 treated patients, seven underwent tumor resection post-infusion and analysis of tumor tissue indicated a decrease or ablation of EGFRvIII expression.

A second phase I clinical trial leveraged a third-generation EGFRvIII-targeted CAR with 4-1BB and CD38 co-stimulation domains to conduct a dose-escalation study in 18 patients with EGFRvIII+ GBM(Goff et al., 2019). No dose-limiting toxicities were observed with EGFRvIII-targeted CAR T cells until the highest dose of $\geq 10^{10}$, at which point a patient developed acute dyspnea and experienced oxygen desaturation, eventually succumbing to severe hypotension. Despite efforts to increase CAR T cell persistence and tumor localization, no objective responses were noted using MR imaging, with 16 of 17 remaining patients showing signs of disease progression <3 months after infusion and a median survival of 6.9 months post-treatment. Interestingly, a single patient remained alive up to 59 months post-CAR therapy and an additional two patients survived >1 year. In addition to further preclinical studies on third-generation anti-EGFRvIII CAR T cells by multiple groups(Choi et al., 2014; Miao et al., 2014; Sampson et al., 2014), recent studies have augmented their approach to increase efficacy and decrease toxicity, including an approach to combine anti-EGFRvIII CAR T cells with anti-EGFR bispecific T cell engager (BiTE) antibodies to treat EGFR-positive/EGFRvIII-negative GBM(Choi et al., 2019). In

addition, investigators recently developed multi-antigen prime-and-kill synNotch-CAR T cells that use a dual receptor circuit, the first of which detects EGFRvIII or a brain-specific myelin oligodendrocyte glycoprotein to induce expression of CARs against EphA2 and IL13Rα2 (Choe et al., 2021). In comparison to constitutively-active anti-EGFRvIII/EphA2/IL13Rα2 CAR T cells, synNotch-CAR T cells showed greater antitumor efficacy without off-tumor toxicity.

HER2-specific CAR T cells

The human epidermal growth factor receptor 2 (HER2), originally discovered as a tumor-associated antigen in breast cancer, is a transmembrane glycoprotein with an intracellular tyrosine kinase domain(Ahmed et al., 2010). HER2 is a sparsely-expressed antigen in GBM, detected in up to 17% of specimens and indicative of poor prognosis(Haynik et al., 2007; Koka et al., 2003). With promising preclinical results of a second-generation anti-HER2 CAR engineered with a CD28 costimulatory domain(Ahmed et al., 2010), a clinical trial was undertaken to treat 17 patients with HER2-positive GBM with virus-specific anti-HER2 CAR T cells(Ahmed et al., 2017). Although no dose-limiting toxicity was observed and CAR T cell persistence was noted up to 12 months post-infusion, no significant survival benefit was noted for treated patients with a median overall survival of 11.1 months.

NCT Number	Treatment	Summary of results	Indication	Reference
NCT00730613	IL13(E13Y)-CD3ζ CAR T cells (first generation)	Transient inflammation at tumor site and a significant decrease in IL13Rα2 expression post-treatment were observed. Two grade 3 adverse events were observed. A median survival of 11 months after tumor relapse was noted.	Recurrent GBM	Brown et al. (2015)
NCT02208362	IL13(E13Y)-41BBζ CAR T cells (second generation)	A single patient with multifocal relapsed GBM was treated, resulting in 77- 100% decrease in tumor burden and 7.5 months of progression-free survival. Increased presence of inflammatory cytokines at tumor site with no adverse events related to CAR T cell therapy.	Recurrent GBM	Brown et al. (2016a)
NCT01109095	HER2-CD28ζ CAR T cells (second generation)	No dose-limiting toxicity was observed and CAR T cells persisted for 12 months post-infusion. No significant increase in survival was noted, with a median overall survival of 11.1 months.	GBM	Ahmed et al. (2017)
NCT02209376	EGFRvIII-41BBζ CAR T cells (second generation)	No dose-limiting toxicity was observed and EGFRvIII expression was reduced post-treatment. No significant	Recurrent GBM	O'Rourke et al. (2017)

		increase in survival was noted, with a median overall survival of 8 months post-treatment.		
NCT01454596	EGFRvIII-CD28-41BBζ CAR T cells (third generation)	At highest dose, 2 patients suffered dose-limiting toxicity. A median overall survival of 6.9 months was noted, with one patient alive at 59 months.	Recurrent GBM	Goff et al. (2019)

Table 3. Summary of clinical trials for CAR T cells against GBM.

Discussion and Conclusion

Immunotherapy has yet to significantly improve clinical outcomes for GBM patients and clinical studies have been disappointing thus far. Here, we detailed clinical and pre-clinical advances in immune checkpoint blockade, vaccination strategies, and emerging CAR T cell therapies for treatment of GBM (Figure 1). Among the major hurdles to clinical efficacy are immense intratumoral heterogeneity(Neftel et al., 2019; Patel et al., 2014), parallel modes of immunosuppression by tumor cells(Jackson et al., 2019), and low mutational burden in GBM(Hodges et al., 2017). With these factors in mind, investigators and clinicians are shifting their focus to combinatorial treatment strategies to achieve synergistic effects, reduce treatment resistance and overcome immunosuppression.

Given their effectiveness in other cancers such as melanoma(Wei et al., 2018), ongoing clinical studies are combining ICIs with conventional chemoradiotherapy and experimental therapeutics to increase efficacy. A rational advancement of ICI therapy is co-targeting multiple immune checkpoints, with clinical trials initiated to test the following combinations in GBM: anti-CTLA4 and/or anti-PD-1 with TMZ in newly diagnosed GBM (NCT02311920), anti-CTLA-4 and anti-PD-L1 in recurrent GBM (NCT02794883), anti-LAG-3 and anti-PD-1 in recurrent GBM (NCT02658981), anti-IDO with anti-CTLA4 or anti-PD-1 in GBM (NCT02327078). In addition, hypofractionated stereotactic radiotherapy (NCT0289931, NCT02313272, and NCT02530502) and MRI-guided laser ablation (NCT02311582) are also being combined with ICI. As reviewed by Rius-Rocabert et al. (2020), oncolytic viruses are another form of immunotherapy that preferentially infect tumor cells, thereby activating the innate immune system and increasing T cell trafficking to the tumor bed. Based on promising pre-clinical data(Chen et al., 2018; Cockle

et al., 2016; Jiang et al., 2017), clinical studies are evaluating a combination of adenovirus-based therapy DNX-2401 with anti-PD-1 blockade for recurrent GBM (NCT02798406).

Although CAR T cell therapy is a newer adaptation for GBM treatment, advancements to increase its clinical utility are rapidly progressing. Currently, 12 clinical trials are recruiting GBM patients to evaluate CAR T cell therapy against B7 family member B7-H3 (NCT04385173, NCT04077866), CD147, HER2 (NCT03389230), IL13Rα2 (NCT04003649, NCT04661384, NCT02208362), matrix metallopeptidase 2 (MMP2; NCT04214392), and NKG2D (NCT04717999). In fact, a recent clinical letter outlined administration of B7-H3 CAR T cells to a 56-year-old woman with recurrent GBM, highlighting a potent but short-term anti-tumor response *in situ*, absent of grade 3 or higher toxicities associated with CAR T cell infusion(Tang et al., 2021). Unfortunately, target antigen heterogeneity was predicted as the reason for treatment failure, as noted previously for CAR T cell therapy targeting EGFRvIII and IL13Rα2(Brown et al., 2016a; O'Rourke et al., 2017). Additionally, novel therapeutic targets for CAR T cell therapy are quickly emerging, including antigens such as the disialoganglioside GD2(Murty et al., 2020), CD70(Jin et al., 2018; Yang et al., 2020), CD133(Vora et al., 2020), carbonic anhydrase IX (CAIX)(Cui et al., 2019), EPHA2(Chow et al., 2013; Yi et al., 2018), podoplanin (PDPN)(Shiina et al., 2016), chondroitin sulfate proteoglycan 4 (CSPG4)(Beard et al., 2014; Geldres et al., 2014), and adhesion molecule L1-CAM (CD171)(Hong et al., 2014). While current trials are focused on targeting single tumor-associated antigens, this increased repertoire of targets will allow multiple antigens to be targeted concurrently to overcome intertumoral heterogeneity as shown by Bielamowicz et al. (2018), who developed trivalent CAR T cells targeting HER2, IL13Rα2 and EphA2. In fact, these trivalent CAR T cells were able to eradicate nearly 100% of tumor cells from multiple GBM samples.

Emerging trends towards rational combinatorial therapies are likely to include a systemic reignition of the tumor immune microenvironment. The continued discovery of novel tumor-associated and tumor-specific antigens, paired with the improvement of therapeutic modalities to increase efficacy and reduce toxicity, are necessary for the clinical efficacy of immunotherapies. Overall, a combinatorial therapy delivered at various stages throughout SoC may reliably improve clinical outcomes in GBM patients.

References

1 Ostrom, Q. T. *et al.* CBTRUS Statistical Report: Primary Brain and Other Central Nervous System Tumors Diagnosed in the United States in 2009-2013. *Neuro-oncology* **18**, v1-v75, doi:10.1093/neuonc/now207 (2016).

2 Stupp, R. *et al.* Radiotherapy plus concomitant and adjuvant temozolomide for glioblastoma. *The New England journal of medicine* **352**, 987-996, doi:10.1056/NEJMoa043330 (2005).

3 Lapointe, S., Perry, A. & Butowski, N. A. Primary brain tumours in adults. *Lancet* **392**, 432-446, doi:10.1016/S0140-6736(18)30990-5 (2018).

4 Stupp, R. *et al.* Effects of radiotherapy with concomitant and adjuvant temozolomide versus radiotherapy alone on survival in glioblastoma in a randomised phase III study: 5-year analysis of the EORTC-NCIC trial. *The Lancet. Oncology* **10**, 459-466, doi:10.1016/S1470-2045(09)70025-7 (2009).

5 Kim, J. *et al.* Spatiotemporal Evolution of the Primary Glioblastoma Genome. *Cancer cell* **28**, 318-328, doi:10.1016/j.ccell.2015.07.013 (2015).

6 Neftel, C. *et al.* An Integrative Model of Cellular States, Plasticity, and Genetics for Glioblastoma. *Cell* **178**, 835-849 e821, doi:10.1016/j.cell.2019.06.024 (2019).

7 Patel, A. P. *et al.* Single-cell RNA-seq highlights intratumoral heterogeneity in primary glioblastoma. *Science* **344**, 1396-1401, doi:10.1126/science.1254257 (2014).

8 Wang, J. *et al.* Clonal evolution of glioblastoma under therapy. *Nature genetics* **48**, 768-776, doi:10.1038/ng.3590 (2016).

9 Meyer, M. *et al.* Single cell-derived clonal analysis of human glioblastoma links functional and genomic heterogeneity. *Proceedings of the National Academy of Sciences of the United States of America* **112**, 851-856, doi:10.1073/pnas.1320611111 (2015).

10 Rius-Rocabert, S., Garcia-Romero, N., Garcia, A., Ayuso-Sacido, A. & Nistal-Villan, E. Oncolytic Virotherapy in Glioma Tumors. *Int J Mol Sci* **21**, doi:10.3390/ijms21207604 (2020).

11 Mitchell, D. A. *et al.* Sensitive detection of human cytomegalovirus in tumors and peripheral blood of patients diagnosed with glioblastoma. *Neuro Oncol* **10**, 10-18, doi:10.1215/15228517-2007-035 (2008).

12 Bleeker, F. E. *et al.* IDH1 mutations at residue p.R132 (IDH1(R132)) occur frequently in high-grade gliomas but not in other solid tumors. *Hum Mutat* **30**, 7-11, doi:10.1002/humu.20937 (2009).

13 Heimberger, A. B. *et al.* Prognostic effect of epidermal growth factor receptor and EGFRvIII in glioblastoma multiforme patients. *Clin Cancer Res* **11**, 1462-1466, doi:10.1158/1078-0432.CCR-04-1737 (2005).

14 Batra, S. K. *et al.* Epidermal growth factor ligand-independent, unregulated, cell-transforming potential of a naturally occurring human mutant EGFRvIII gene. *Cell Growth Differ* **6**, 1251-1259 (1995).

15 Nagane, M. *et al.* A common mutant epidermal growth factor receptor confers enhanced tumorigenicity on human glioblastoma cells by increasing proliferation and reducing apoptosis. *Cancer Res* **56**, 5079-5086 (1996).

16 Sampson, J. H. *et al.* An epidermal growth factor receptor variant III-targeted vaccine is safe and immunogenic in patients with glioblastoma multiforme. *Mol Cancer Ther* **8**, 2773-2779, doi:10.1158/1535-7163.MCT-09-0124 (2009).

17 Heimberger, A. B. *et al.* Epidermal growth factor receptor VIII peptide vaccination is efficacious against established intracerebral tumors. *Clin Cancer Res* **9**, 4247-4254 (2003).

18 Sampson, J. H. *et al.* Immunologic escape after prolonged progression-free survival with epidermal growth factor receptor variant III peptide vaccination in patients with newly diagnosed glioblastoma. *J Clin Oncol* **28**, 4722-4729, doi:10.1200/JCO.2010.28.6963 (2010).

19 Sampson, J. H. *et al.* Greater chemotherapy-induced lymphopenia enhances tumor-specific immune responses that eliminate EGFRvIII-expressing tumor cells in patients with glioblastoma. *Neuro Oncol* **13**, 324-333, doi:10.1093/neuonc/noq157 (2011).

20 Schuster, J. *et al.* A phase II, multicenter trial of rindopepimut (CDX-110) in newly diagnosed glioblastoma: the ACT III study. *Neuro Oncol* **17**, 854-861, doi:10.1093/neuonc/nou348 (2015).

21 Weller, M. *et al.* Rindopepimut with temozolomide for patients with newly diagnosed, EGFRvIII-expressing glioblastoma (ACT IV): a randomised, double-blind, international phase 3 trial. *Lancet Oncol* **18**, 1373-1385, doi:10.1016/S1470-2045(17)30517-X (2017).

22 Schafer, N. *et al.* Longitudinal heterogeneity in glioblastoma: moving targets in recurrent versus primary tumors. *J Transl Med* **17**, 96, doi:10.1186/s12967-019-1846-y (2019).

23 Brock, C. S. *et al.* Phase I trial of temozolomide using an extended continuous oral schedule. *Cancer Res* **58**, 4363-4367 (1998).

24 Mansfield, A. S., Nevala, W. K., Lieser, E. A., Leontovich, A. A. & Markovic, S. N. The immunomodulatory effects of bevacizumab on systemic immunity in patients with metastatic melanoma. *Oncoimmunology* **2**, e24436, doi:10.4161/onci.24436 (2013).

25 Reardon, D. A. *et al.* Rindopepimut with Bevacizumab for Patients with Relapsed EGFRvIII-Expressing Glioblastoma (ReACT): Results of a Double-Blind Randomized Phase II Trial. *Clin Cancer Res* **26**, 1586-1594, doi:10.1158/1078-0432.CCR-18-1140 (2020).

26 Wills, M. R. *et al.* The human cytotoxic T-lymphocyte (CTL) response to cytomegalovirus is dominated by structural protein pp65: frequency, specificity, and T-cell receptor usage of pp65-specific CTL. *J Virol* **70**, 7569-7579, doi:10.1128/JVI.70.11.7569-7579.1996 (1996).

27 Arruda, L. B. *et al.* Dendritic cell-lysosomal-associated membrane protein (LAMP) and LAMP-1-HIV-1 gag chimeras have distinct cellular trafficking pathways and prime T and B cell responses to a diverse repertoire of epitopes. *J Immunol* **177**, 2265-2275, doi:10.4049/jimmunol.177.4.2265 (2006).

28 Mitchell, D. A. *et al.* Tetanus toxoid and CCL3 improve dendritic cell vaccines in mice and glioblastoma patients. *Nature* **519**, 366-369, doi:10.1038/nature14320 (2015).

29 Mitchell, D. A. *et al.* Monoclonal antibody blockade of IL-2 receptor alpha during lymphopenia selectively depletes regulatory T cells in mice and humans. *Blood* **118**, 3003-3012, doi:10.1182/blood-2011-02-334565 (2011).

30 Batich, K. A. *et al.* Long-term Survival in Glioblastoma with Cytomegalovirus pp65-Targeted Vaccination. *Clin Cancer Res* **23**, 1898-1909, doi:10.1158/1078-0432.CCR-16-2057 (2017).

31 Batich, K. A., Mitchell, D. A., Healy, P., Herndon, J. E., 2nd & Sampson, J. H. Once, Twice, Three Times a Finding: Reproducibility of Dendritic Cell Vaccine Trials Targeting Cytomegalovirus in Glioblastoma. *Clin Cancer Res* **26**, 5297-5303, doi:10.1158/1078-0432.CCR-20-1082 (2020).

32 Schumacher, T. *et al.* A vaccine targeting mutant IDH1 induces antitumour immunity. *Nature* **512**, 324-327, doi:10.1038/nature13387 (2014).

33 Platten, M. *et al.* A vaccine targeting mutant IDH1 in newly diagnosed glioma. *Nature* **592**, 463-468, doi:10.1038/s41586-021-03363-z (2021).

34 Liau, L. M. *et al.* Treatment of intracranial gliomas with bone marrow-derived dendritic cells pulsed with tumor antigens. *J Neurosurg* **90**, 1115-1124, doi:10.3171/jns.1999.90.6.1115 (1999).

35 Liau, L. M. *et al.* First results on survival from a large Phase 3 clinical trial of an autologous dendritic cell vaccine in newly diagnosed glioblastoma. *J Transl Med* **16**, 142, doi:10.1186/s12967-018-1507-6 (2018).

36 Crane, C. A. *et al.* Individual patient-specific immunity against high-grade glioma after vaccination with autologous tumor derived peptides bound to the 96 KD chaperone protein. *Clin Cancer Res* **19**, 205-214, doi:10.1158/1078-0432.CCR-11-3358 (2013).

37 Bloch, O. *et al.* Heat-shock protein peptide complex-96 vaccination for recurrent glioblastoma: a phase II, single-arm trial. *Neuro Oncol* **16**, 274-279, doi:10.1093/neuonc/not203 (2014).

38 Ji, N. *et al.* Heat shock protein peptide complex-96 vaccination for newly diagnosed glioblastoma: a phase I, single-arm trial. *JCI Insight* **3**, doi:10.1172/jci.insight.99145 (2018).

39 Bloch, O. *et al.* Autologous Heat Shock Protein Peptide Vaccination for Newly Diagnosed Glioblastoma: Impact of Peripheral PD-L1 Expression on Response to Therapy. *Clin Cancer Res* **23**, 3575-3584, doi:10.1158/1078-0432.CCR-16-1369 (2017).

40 Vaddepally, R. K., Kharel, P., Pandey, R., Garje, R. & Chandra, A. B. Review of Indications of FDA-Approved Immune Checkpoint Inhibitors per NCCN Guidelines with the Level of Evidence. *Cancers (Basel)* **12**, doi:10.3390/cancers12030738 (2020).

41 Davidson, T. B. *et al.* Expression of PD-1 by T Cells in Malignant Glioma Patients Reflects Exhaustion and Activation. *Clin Cancer Res* **25**, 1913-1922, doi:10.1158/1078-0432.CCR-18-1176 (2019).

42 Contardi, E. *et al.* CTLA-4 is constitutively expressed on tumor cells and can trigger apoptosis upon ligand interaction. *Int J Cancer* **117**, 538-550, doi:10.1002/ijc.21155 (2005).

43 Zeng, J. *et al.* Anti-PD-1 blockade and stereotactic radiation produce long-term survival in mice with intracranial gliomas. *Int J Radiat Oncol Biol Phys* **86**, 343-349, doi:10.1016/j.ijrobp.2012.12.025 (2013).

44 Reardon, D. A. *et al.* Effect of Nivolumab vs Bevacizumab in Patients With Recurrent Glioblastoma: The CheckMate 143 Phase 3 Randomized Clinical Trial. *JAMA Oncol* **6**, 1003-1010, doi:10.1001/jamaoncol.2020.1024 (2020).

45 Omuro, A. *et al.* Nivolumab with or without ipilimumab in patients with recurrent glioblastoma: results from exploratory phase I cohorts of CheckMate 143. *Neuro Oncol* **20**, 674-686, doi:10.1093/neuonc/nox208 (2018).

46 Squibb, B. M. (Bristol Myers Squibb, Princeton, NJ, 2020).

47 Sahebjam, S. *et al.* Hypofractionated stereotactic re-irradiation with pembrolizumab and bevacizumab in patients with recurrent high-grade gliomas: results from a phase I study. *Neuro Oncol* **23**, 677-686, doi:10.1093/neuonc/noaa260 (2021).

48 Reardon, D. A. Phase II study of pembrolizumab or pembrolizumab plus bevacizumab for recurrent glioblastoma (rGBM) patients. *Journal of Clinical Oncology* **36**, doi:10.1200/JCO.2018.36.15_suppl.2006 (2006).

49 Liu, J. *et al.* Improved Efficacy of Neoadjuvant Compared to Adjuvant Immunotherapy to Eradicate Metastatic Disease. *Cancer Discov* **6**, 1382-1399, doi:10.1158/2159-8290.CD-16-0577 (2016).

50 Blank, C. U. *et al.* Neoadjuvant versus adjuvant ipilimumab plus nivolumab in macroscopic stage III melanoma. *Nat Med* **24**, 1655-1661, doi:10.1038/s41591-018-0198-0 (2018).

51 Cloughesy, T. F. *et al.* Neoadjuvant anti-PD-1 immunotherapy promotes a survival benefit with intratumoral and systemic immune responses in recurrent glioblastoma. *Nat Med* **25**, 477-486, doi:10.1038/s41591-018-0337-7 (2019).

52 Schalper, K. A. *et al.* Neoadjuvant nivolumab modifies the tumor immune microenvironment in resectable glioblastoma. *Nat Med* **25**, 470-476, doi:10.1038/s41591-018-0339-5 (2019).

53 Fecci, P. E. *et al.* Systemic CTLA-4 blockade ameliorates glioma-induced changes to the CD4+ T cell compartment without affecting regulatory T-cell function. *Clin Cancer Res* **13**, 2158-2167, doi:10.1158/1078-0432.CCR-06-2070 (2007).

54 Reardon, D. A. *et al.* Glioblastoma Eradication Following Immune Checkpoint Blockade in an Orthotopic, Immunocompetent Model. *Cancer Immunol Res* **4**, 124-135, doi:10.1158/2326-6066.CIR-15-0151 (2016).

55 Reardon, D. A. ATIM-12. PHASE 2 STUDY TO EVALUATE THE CLINICAL EFFICACY AND SAFETY OF MEDI4736 (DURVALUMAB [DUR]) IN PATIENTS WITH BEVACIZUMAB (BEV)-REFRACTORY RECURRENT GLIOBLASTOMA (GBM). *Neuro Oncol* **19**, doi:10.1093/neuonc/nox168.108 (2017).

56 Harris-Bookman, S. *et al.* Expression of LAG-3 and efficacy of combination treatment with anti-LAG-3 and anti-PD-1 monoclonal antibodies in glioblastoma. *Int J Cancer* **143**, 3201-3208, doi:10.1002/ijc.31661 (2018).

57 Mair, M. J. *et al.* LAG-3 expression in the inflammatory microenvironment of glioma. *J Neurooncol* **152**, 533-539, doi:10.1007/s11060-021-03721-x (2021).

58 Lim, M. *et al.* Updated phase I trial of anti-LAG-3 or anti-CD137 alone and in combination with anti-PD-1 in patients with recurrent GBM. *Journal of Clinical Oncology* **37**, 2017-2017, doi:10.1200/JCO.2019.37.15_suppl.2017 (2019).

59 Kuhnol, C., Herbarth, M., Foll, J., Staege, M. S. & Kramm, C. CD137 stimulation and p38 MAPK inhibition improve reactivity in an in vitro model of glioblastoma immunotherapy. *Cancer Immunol Immunother* **62**, 1797-1809, doi:10.1007/s00262-013-1484-9 (2013).

60 Newcomb, E. W. *et al.* Radiotherapy enhances antitumor effect of anti-CD137 therapy in a mouse Glioma model. *Radiat Res* **173**, 426-432, doi:10.1667/RR1904.1 (2010).

61 Zhang, J. *et al.* Tim-3 Expression and MGMT Methylation Status Association With Survival in Glioblastoma. *Front Pharmacol* **11**, 584652, doi:10.3389/fphar.2020.584652 (2020).

62 Kim, J. E. *et al.* Combination Therapy with Anti-PD-1, Anti-TIM-3, and Focal Radiation Results in Regression of Murine Gliomas. *Clin Cancer Res* **23**, 124-136, doi:10.1158/1078-0432.CCR-15-1535 (2017).

63 Goswami, S. *et al.* Immune profiling of human tumors identifies CD73 as a combinatorial target in glioblastoma. *Nat Med* **26**, 39-46, doi:10.1038/s41591-019-0694-x (2020).

64 Willingham, S. B. *et al.* The CD47-signal regulatory protein alpha (SIRPa) interaction is a therapeutic target for human solid tumors. *Proc Natl Acad Sci U S A* **109**, 6662-6667, doi:10.1073/pnas.1121623109 (2012).

65 Zhang, M. *et al.* Anti-CD47 Treatment Stimulates Phagocytosis of Glioblastoma by M1 and M2 Polarized Macrophages and Promotes M1 Polarized Macrophages In Vivo. *PLoS One* **11**, e0153550, doi:10.1371/journal.pone.0153550 (2016).

66 Zhang, X. *et al.* Targeting CD47 and Autophagy Elicited Enhanced Antitumor Effects in Non-Small Cell Lung Cancer. *Cancer Immunol Res* **5**, 363-375, doi:10.1158/2326-6066.CIR-16-0398 (2017).

67 Edris, B. *et al.* Antibody therapy targeting the CD47 protein is effective in a model of aggressive metastatic leiomyosarcoma. *Proc Natl Acad Sci U S A* **109**, 6656-6661, doi:10.1073/pnas.1121629109 (2012).

68 Li, F. *et al.* Blocking the CD47-SIRPalpha axis by delivery of anti-CD47 antibody induces antitumor effects in glioma and glioma stem cells. *Oncoimmunology* **7**, e1391973, doi:10.1080/2162402X.2017.1391973 (2018).

69 Gholamin, S. *et al.* Irradiation or temozolomide chemotherapy enhances anti-CD47 treatment of glioblastoma. *Innate Immun* **26**, 130-137, doi:10.1177/1753425919876690 (2020).

70 von Roemeling, C. A. *et al.* Therapeutic modulation of phagocytosis in glioblastoma can activate both innate and adaptive antitumour immunity. *Nat Commun* **11**, 1508, doi:10.1038/s41467-020-15129-8 (2020).

71 Zhang, X. *et al.* Disrupting CD47-SIRPalpha axis alone or combined with autophagy depletion for the therapy of glioblastoma. *Carcinogenesis* **39**, 689-699, doi:10.1093/carcin/bgy041 (2018).

72 Zhang, X. *et al.* Inhibition of autophagy potentiated the anti-tumor effects of VEGF and CD47 bispecific therapy in glioblastoma. *Appl Microbiol Biotechnol* **102**, 6503-6513, doi:10.1007/s00253-018-9069-3 (2018).

73 Sockolosky, J. T. *et al.* Durable antitumor responses to CD47 blockade require adaptive immune stimulation. *Proc Natl Acad Sci U S A* **113**, E2646-2654, doi:10.1073/pnas.1604268113 (2016).

74 Sadelain, M., Brentjens, R. & Riviere, I. The basic principles of chimeric antigen receptor design. *Cancer discovery* **3**, 388-398, doi:10.1158/2159-8290.CD-12-0548 (2013).

75 Finney, H. M., Lawson, A. D., Bebbington, C. R. & Weir, A. N. Chimeric receptors providing both primary and costimulatory signaling in T cells from a single gene product. *Journal of immunology* **161**, 2791-2797 (1998).

76 Finney, H. M., Akbar, A. N. & Lawson, A. D. Activation of resting human primary T cells with chimeric receptors: costimulation from CD28, inducible costimulator, CD134, and CD137 in series with signals from the TCR zeta chain. *Journal of immunology* **172**, 104-113, doi:10.4049/jimmunol.172.1.104 (2004).

77 Imai, C. *et al.* Chimeric receptors with 4-1BB signaling capacity provoke potent cytotoxicity against acute lymphoblastic leukemia. *Leukemia* **18**, 676-684, doi:10.1038/sj.leu.2403302 (2004).

78 Hombach, A. *et al.* Tumor-specific T cell activation by recombinant immunoreceptors: CD3 zeta signaling and CD28 costimulation are simultaneously required for efficient IL-2 secretion and can be integrated into one combined CD28/CD3 zeta signaling receptor molecule. *Journal of immunology* **167**, 6123-6131, doi:10.4049/jimmunol.167.11.6123 (2001).

79 Maude, S. L. *et al.* Chimeric antigen receptor T cells for sustained remissions in leukemia. *The New England journal of medicine* **371**, 1507-1517, doi:10.1056/NEJMoa1407222 (2014).

80 Bagley, S. J., Desai, A. S., Linette, G. P., June, C. H. & O'Rourke, D. M. CAR T-cell therapy for glioblastoma: recent clinical advances and future challenges. *Neuro-oncology* **20**, 1429-1438, doi:10.1093/neuonc/noy032 (2018).

81 Sarkaria, J. N. *et al.* Is the blood-brain barrier really disrupted in all glioblastomas? A critical assessment of existing clinical data. *Neuro-oncology* **20**, 184-191, doi:10.1093/neuonc/nox175 (2018).

82 Watkins, S. *et al.* Disruption of astrocyte-vascular coupling and the blood-brain barrier by invading glioma cells. *Nature communications* **5**, 4196, doi:10.1038/ncomms5196 (2014).

83 O'Rourke, D. M. *et al.* A single dose of peripherally infused EGFRvIII-directed CAR T cells mediates antigen loss and induces adaptive resistance in patients with recurrent glioblastoma. *Science translational medicine* **9**, doi:10.1126/scitranslmed.aaa0984 (2017).

84 Ahmed, N. *et al.* HER2-specific T cells target primary glioblastoma stem cells and induce regression of autologous experimental tumors. *Clinical cancer research : an official journal of the American Association for Cancer Research* **16**, 474-485, doi:10.1158/1078-0432.CCR-09-1322 (2010).

85 Keu, K. V. *et al.* Reporter gene imaging of targeted T cell immunotherapy in recurrent glioma. *Science translational medicine* **9**, doi:10.1126/scitranslmed.aag2196 (2017).

86 Brown, C. E. *et al.* Bioactivity and Safety of IL13Ralpha2-Redirected Chimeric Antigen Receptor CD8+ T Cells in Patients with Recurrent Glioblastoma. *Clinical cancer research : an official journal of the American Association for Cancer Research* **21**, 4062-4072, doi:10.1158/1078-0432.CCR-15-0428 (2015).

87 Brown, C. E. *et al.* Regression of Glioblastoma after Chimeric Antigen Receptor T-Cell Therapy. *The New England journal of medicine* **375**, 2561-2569, doi:10.1056/NEJMoa1610497 (2016).

88 Brown, C. E. *et al.* Glioma IL13Ralpha2 is associated with mesenchymal signature gene expression and poor patient prognosis. *PloS one* **8**, e77769, doi:10.1371/journal.pone.0077769 (2013).

89 Debinski, W., Gibo, D. M., Hulet, S. W., Connor, J. R. & Gillespie, G. Y. Receptor for interleukin 13 is a marker and therapeutic target for human high-grade gliomas. *Clinical cancer research : an official journal of the American Association for Cancer Research* **5**, 985-990 (1999).

90 Bhat, K. P. L. *et al.* Mesenchymal differentiation mediated by NF-kappaB promotes radiation resistance in glioblastoma. *Cancer cell* **24**, 331-346, doi:10.1016/j.ccr.2013.08.001 (2013).

91 Wang, Q. *et al.* Tumor Evolution of Glioma-Intrinsic Gene Expression Subtypes Associates with Immunological Changes in the Microenvironment. *Cancer cell* **33**, 152, doi:10.1016/j.ccell.2017.12.012 (2018).

92 Kong, S. *et al.* Suppression of human glioma xenografts with second-generation IL13R-specific chimeric antigen receptor-modified T cells. *Clinical cancer research : an official journal of the American Association for Cancer Research* **18**, 5949-5960, doi:10.1158/1078-0432.CCR-12-0319 (2012).

93 Brown, C. E. *et al.* Optimization of IL13Ralpha2-Targeted Chimeric Antigen Receptor T Cells for Improved Anti-tumor Efficacy against Glioblastoma. *Molecular therapy : the journal of the American Society of Gene Therapy* **26**, 31-44, doi:10.1016/j.ymthe.2017.10.002 (2018).

94 Krenciute, G. *et al.* Characterization and Functional Analysis of scFv-based Chimeric Antigen Receptors to Redirect T Cells to IL13Ralpha2-positive Glioma. *Molecular therapy : the journal of the American Society of Gene Therapy* **24**, 354-363, doi:10.1038/mt.2015.199 (2016).

95 Krenciute, G. *et al.* Transgenic Expression of IL15 Improves Antiglioma Activity of IL13Ralpha2-CAR T Cells but Results in Antigen Loss Variants. *Cancer immunology research* **5**, 571-581, doi:10.1158/2326-6066.CIR-16-0376 (2017).

96 Pituch, K. C. *et al.* Adoptive Transfer of IL13Ralpha2-Specific Chimeric Antigen Receptor T Cells Creates a Pro-inflammatory Environment in Glioblastoma. *Molecular therapy : the journal of the American Society of Gene Therapy* **26**, 986-995, doi:10.1016/j.ymthe.2018.02.001 (2018).

97 Wang, D. *et al.* Glioblastoma-targeted CD4+ CAR T cells mediate superior antitumor activity. *JCI Insight* **3**, doi:10.1172/jci.insight.99048 (2018).

98 Sigismund, S., Avanzato, D. & Lanzetti, L. Emerging functions of the EGFR in cancer. *Molecular oncology* **12**, 3-20, doi:10.1002/1878-0261.12155 (2018).

99 Verhaak, R. G. *et al.* Integrated genomic analysis identifies clinically relevant subtypes of glioblastoma characterized by abnormalities in PDGFRA, IDH1, EGFR, and NF1. *Cancer cell* **17**, 98-110, doi:10.1016/j.ccr.2009.12.020 (2010).

100 Saikali, S. *et al.* Expression of nine tumour antigens in a series of human glioblastoma multiforme: interest of EGFRvIII, IL-13Ralpha2, gp100 and TRP-2 for immunotherapy. *Journal of neuro-oncology* **81**, 139-148, doi:10.1007/s11060-006-9220-3 (2007).

101 An, Z., Aksoy, O., Zheng, T., Fan, Q. W. & Weiss, W. A. Epidermal growth factor receptor and EGFRvIII in glioblastoma: signaling pathways and targeted therapies. *Oncogene* **37**, 1561-1575, doi:10.1038/s41388-017-0045-7 (2018).

102 Padfield, E., Ellis, H. P. & Kurian, K. M. Current Therapeutic Advances Targeting EGFR and EGFRvIII in Glioblastoma. *Front Oncol* **5**, 5, doi:10.3389/fonc.2015.00005 (2015).

103 Johnson, L. A. *et al.* Rational development and characterization of humanized anti-EGFR variant III chimeric antigen receptor T cells for glioblastoma. *Science translational medicine* **7**, 275ra222, doi:10.1126/scitranslmed.aaa4963 (2015).

104 Ohno, M. *et al.* Expression of miR-17-92 enhances anti-tumor activity of T-cells transduced with the anti-EGFRvIII chimeric antigen receptor in mice bearing human GBM xenografts. *Journal for immunotherapy of cancer* **1**, 21, doi:10.1186/2051-1426-1-21 (2013).

105 Goff, S. L. *et al.* Pilot Trial of Adoptive Transfer of Chimeric Antigen Receptor-transduced T Cells Targeting EGFRvIII in Patients With Glioblastoma. *Journal of immunotherapy* **42**, 126-135, doi:10.1097/CJI.0000000000000260 (2019).

106 Choi, B. D. *et al.* Intracerebral delivery of a third generation EGFRvIII-specific chimeric antigen receptor is efficacious against human glioma. *Journal of clinical neuroscience : official journal of the Neurosurgical Society of Australasia* **21**, 189-190, doi:10.1016/j.jocn.2013.03.012 (2014).

107 Sampson, J. H. *et al.* EGFRvIII mCAR-modified T-cell therapy cures mice with established intracerebral glioma and generates host immunity against tumor-antigen loss. *Clinical cancer research : an official journal of the American Association for Cancer Research* **20**, 972-984, doi:10.1158/1078-0432.CCR-13-0709 (2014).

108 Miao, H. *et al.* EGFRvIII-specific chimeric antigen receptor T cells migrate to and kill tumor deposits infiltrating the brain parenchyma in an invasive xenograft model of glioblastoma. *PloS one* **9**, e94281, doi:10.1371/journal.pone.0094281 (2014).

109 Choi, B. D. *et al.* CAR-T cells secreting BiTEs circumvent antigen escape without detectable toxicity. *Nature biotechnology* **37**, 1049-1058, doi:10.1038/s41587-019-0192-1 (2019).

110 Choe, J. H. *et al.* SynNotch-CAR T cells overcome challenges of specificity, heterogeneity, and persistence in treating glioblastoma. *Science translational medicine* **13**, doi:10.1126/scitranslmed.abe7378 (2021).

111 Haynik, D. M., Roma, A. A. & Prayson, R. A. HER-2/neu expression in glioblastoma multiforme. *Appl Immunohistochem Mol Morphol* **15**, 56-58, doi:10.1097/01.pai.0000213133.09160.da (2007).

112 Koka, V. *et al.* Role of Her-2/neu overexpression and clinical determinants of early mortality in glioblastoma multiforme. *Am J Clin Oncol* **26**, 332-335, doi:10.1097/01.COC.0000020922.66984.E7 (2003).

113 Ahmed, N. *et al.* HER2-Specific Chimeric Antigen Receptor-Modified Virus-Specific T Cells for Progressive Glioblastoma: A Phase 1 Dose-Escalation Trial. *JAMA Oncol* **3**, 1094-1101, doi:10.1001/jamaoncol.2017.0184 (2017).

114 Jackson, C. M., Choi, J. & Lim, M. Mechanisms of immunotherapy resistance: lessons from glioblastoma. *Nature immunology* **20**, 1100-1109, doi:10.1038/s41590-019-0433-y (2019).

115 Hodges, T. R. *et al.* Mutational burden, immune checkpoint expression, and mismatch repair in glioma: implications for immune checkpoint immunotherapy. *Neuro-oncology* **19**, 1047-1057, doi:10.1093/neuonc/nox026 (2017).

116 Wei, S. C., Duffy, C. R. & Allison, J. P. Fundamental Mechanisms of Immune Checkpoint Blockade Therapy. *Cancer discovery* **8**, 1069-1086, doi:10.1158/2159-8290.CD-18-0367 (2018).

117 Cockle, J. V. *et al.* Combination viroimmunotherapy with checkpoint inhibition to treat glioma, based on location-specific tumor profiling. *Neuro-oncology* **18**, 518-527, doi:10.1093/neuonc/nov173 (2016).

118 Jiang, H. *et al.* Oncolytic Adenovirus and Tumor-Targeting Immune Modulatory Therapy Improve Autologous Cancer Vaccination. *Cancer research* **77**, 3894-3907, doi:10.1158/0008-5472.CAN-17-0468 (2017).

119 Chen, C. Y., Hutzen, B., Wedekind, M. F. & Cripe, T. P. Oncolytic virus and PD-1/PD-L1 blockade combination therapy. *Oncolytic Virother* **7**, 65-77, doi:10.2147/OV.S145532 (2018).

120 Tang, X. *et al.* Administration of B7-H3 targeted chimeric antigen receptor-T cells induce regression of glioblastoma. *Signal Transduct Target Ther* **6**, 125, doi:10.1038/s41392-021-00505-7 (2021).

121 Murty, S. *et al.* Intravital imaging reveals synergistic effect of CAR T-cells and radiation therapy in a preclinical immunocompetent glioblastoma model. *Oncoimmunology* **9**, 1757360, doi:10.1080/2162402X.2020.1757360 (2020).

122 Yang, M. *et al.* Tandem CAR-T cells targeting CD70 and B7-H3 exhibit potent preclinical activity against multiple solid tumors. *Theranostics* **10**, 7622-7634, doi:10.7150/thno.43991 (2020).

123 Jin, L. *et al.* CD70, a novel target of CAR T-cell therapy for gliomas. *Neuro-oncology* **20**, 55-65, doi:10.1093/neuonc/nox116 (2018).

124 Vora, P. *et al.* The Rational Development of CD133-Targeting Immunotherapies for Glioblastoma. *Cell stem cell* **26**, 832-844 e836, doi:10.1016/j.stem.2020.04.008 (2020).

125 Cui, J. *et al.* Targeting hypoxia downstream signaling protein, CAIX, for CAR T-cell therapy against glioblastoma. *Neuro-oncology* **21**, 1436-1446, doi:10.1093/neuonc/noz117 (2019).

126 Yi, Z., Prinzing, B. L., Cao, F., Gottschalk, S. & Krenciute, G. Optimizing EphA2-CAR T Cells for the Adoptive Immunotherapy of Glioma. *Mol Ther Methods Clin Dev* **9**, 70-80, doi:10.1016/j.omtm.2018.01.009 (2018).

127 Chow, K. K. *et al.* T cells redirected to EphA2 for the immunotherapy of glioblastoma. *Molecular therapy : the journal of the American Society of Gene Therapy* **21**, 629-637, doi:10.1038/mt.2012.210 (2013).

128 Shiina, S. *et al.* CAR T Cells Targeting Podoplanin Reduce Orthotopic Glioblastomas in Mouse Brains. *Cancer immunology research* **4**, 259-268, doi:10.1158/2326-6066.CIR-15-0060 (2016).

129 Beard, R. E. *et al.* Multiple chimeric antigen receptors successfully target chondroitin sulfate proteoglycan 4 in several different cancer histologies and cancer stem cells. *Journal for immunotherapy of cancer* **2**, 25, doi:10.1186/2051-1426-2-25 (2014).

130 Geldres, C. *et al.* T lymphocytes redirected against the chondroitin sulfate proteoglycan-4 control the growth of multiple solid tumors both in vitro and in vivo. *Clinical cancer research : an official journal of the American Association for Cancer Research* **20**, 962-971, doi:10.1158/1078-0432.CCR-13-2218 (2014).

131 Hong, H. *et al.* Diverse solid tumors expressing a restricted epitope of L1-CAM can be targeted by chimeric antigen receptor redirected T lymphocytes. *Journal of immunotherapy* **37**, 93-104, doi:10.1097/CJI.0000000000000018 (2014).

132 Bielamowicz, K. *et al.* Trivalent CAR T cells overcome interpatient antigenic variability in glioblastoma. *Neuro-oncology* **20**, 506-518, doi:10.1093/neuonc/nox182 (2018).

Figures

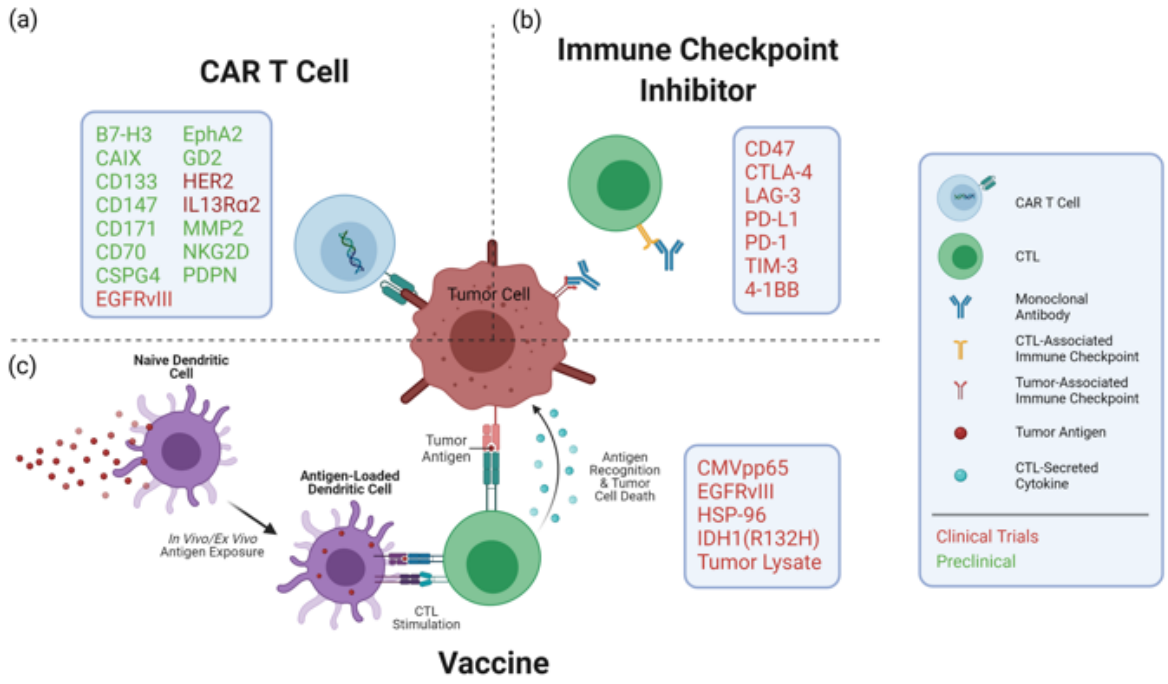

Figure 1. Overview of current modalities and therapeutic targets being investigated to treat GBM. (**a**) CAR T cells recognize antigens through a genetically engineered extracellular receptor which triggers intracellular T cell activation upon binding. (**b**) Inhibitors of immune checkpoint proteins prevent their attenuation of immune responses upon activation and exhaustion. (**c**) Vaccines expose antigen-presenting cells to tumoral antigens, stimulating a target-specific immune response. Boxes indicate therapeutic targets or mediators being pursued for each modality. CAR: chimeric antigen receptor; CTL: cytotoxic T lymphocyte.

CHAPTER 5: Discussion and future directions

5.1 Functional genetic insights into GBM recurrence

In Chapter 2, we conducted the first set of unbiased functional genetic screens in patient-derived GBM models to reveal functional modulators of SoC and disease recurrence. Not only do recurrent tumor cells rely on a distinct set of functional drivers when compared to their primary predecessors, therapeutic avenues to treat recurrent disease cannot be predicted without profiling tumors at recurrence. The surprising loss of ~30% of genetic dependencies in primary tumor cells at recurrence (e.g. *RUNX1*, *ZEB1* and *RHOA*), gain of an additional ~30% new functional dependencies (e.g. *FASN* and *CD151*), and further loss of crucial replicative checkpoints (e.g. *TP53*, *PTEN*, *NF1*, and *NF2*), highlight the dramatic remodelling from primary to recurrent disease. Therapy-driven events, along with continuous temporal evolution at the genetic and cellular levels, may select for a sub-clonal and treatment-resistant GSC population that redefines the functional genetic landscape of the recurrent tumor.

Collectively, these results support a model in which therapy-driven and stochastic events lead to a functionally distinct tumor at GBM recurrence. Our analysis of the genomic, transcriptomic, proteomic and functional genetic landscapes of patient-matched primary and recurrent tumor cells supports parallel tumor-intrinsic mechanisms of treatment resistance which rely on acquisition of immunosuppressive capacity. Not only are recurrent GBM cells burdened by greater stem-like properties and tumorigenic potential, presence of *de novo* driver mutations such as a defective MMR pathway (*MSH6* A1179V and T1219I) may drive hypermutation and shield recurrent GBM cells from the host immune system and anti-PD-1 blockade (Touat et al., 2020). In stark contrast, anti-PD-1 blockade is a tractable therapeutic strategy in other aggressive cancers (i.e. non-small

cell lung cancer, colorectal cancer and melanoma) with a hypermutated profile (Le et al., 2015; McGranahan et al., 2016; Rizvi et al., 2015). In addition, MMR-deficiency in recurrent GBM cells may predispose to a higher mutational burden but, unlike other cancers, these additional mutations may support an immunosuppressive microenvironment.

We observe that MMR-deficient recurrent GBM cells also harbour a deleterious mutation in *PTEN* (H123Y), previously shown to ablate phosphatase activity and prevent PTEN-mediated cell cycle arrest in breast cancer cells (Hlobilkova et al., 2000). In addition, MMR-deficiency and microsatellite instability (MSI) has been associated with truncal *PTEN* loss in gliomas, and likewise, *PTEN* loss occurs in 90% of human MSI endometrial carcinomas (Cancer Genome Atlas Research et al., 2013a; Touat et al., 2020). In addition to MMR deficiency, significant enrichment of *PTEN* mutations at recurrence has been associated with immunosuppressive expression signatures in GBM patients who were classified as non-responders to immune checkpoint blockade in clinical trials with nivolumab and pembrolizumab (Zhao et al., 2019).

Our profiling of GBM recurrence reveals hallmarks not only of resistance to conventional chemoradiotherapy, but also predictive biomarkers of putative resistance to anti-PD-1 therapy. One such example is the novel combination of *de novo* mutations in SWI/SNF components *ARID1A* (Q1364*) and *ARID1B* (P1238S, E647K and P594S) in recurrent tumor cells, which diminish individual genetic vulnerabilities of both genes seen in patient-matched primary tumor cells (Figure S3). Observed recently in endometrial, bladder, esophageal/gastric and biliary cancers (Wang et al., 2020), dual ARID1A/ARID1B loss in GBM may promote dedifferentiation to a stem-like state and hyperproliferation of recurrent tumor cells. ARID1A, encoding a subunit

of the SWI/SNF complex, is the most frequently mutated epigenetic regulator in human cancers, and coincides with treatment-resistant disease in ovarian clear cell carcinoma, colorectal cancer, breast cancer and hepatocellular carcinoma (Jones et al., 2010; Nagarajan et al., 2020). Loss of ARID1A compromises DNA damage repair, contributes to high MSI and tumor mutation burden, and suppresses the immune microenvironment, supporting the view that ARID1A loss may serve as a predictive biomarker for checkpoint blockade efficacy in recurrent GBM (Goswami et al., 2020a).

Aside from the recent report of a patient with widely metastatic post-treatment and IDH-wild-type recurrent GBM (Umphlett et al., 2020), the impact of ARID1A mutations has not been investigated in GBM (likely due to the fact that recurrent GBM samples are infrequently profiled). Loss of ARID1A promotes epithelial-mesenchymal transition, which has been shown to sensitize pancreatic tumors to proteolytic stress (Tomihara et al., 2021), an observation pertinent to the mesenchymal subtype of GBM which is most commonly seen at tumor recurrence, and predicts drug resistance and poor survival of primary GBM patients (Wang et al., 2018b). Our findings support rationally developed therapeutic approaches that reignite the tumor immune microenvironment (Gangoso et al., 2021), prior to targeted immunotherapies.

5.2 Developing therapies specific for recurrent GBM

Altogether, our mutational, proteomic and functional characterization of the remodelled landscape in recurrent GBM reveals novel mechanisms of treatment resistance, warranting therapeutic approaches that exploit synthetic lethal vulnerabilities that emerge at recurrence (**Chapter 2**). By performing the first genome-wide CRISPR-Cas9 gene knockout screens in patient-derived post-treatment recurrent tumor cells, we report an example of a context-specific vulnerability of

PTP4A2. Pharmacological inhibition of PTP4A2 phosphatase activity revealed modulation of axon guidance via ROBO1 as a downstream effector of PTP4A2, further supported by a global enrichment and dependence on ROBO signaling. In fact, our data uncovered and supports a PTP4A2-ROBO1 phosphorylation axis that drives *PTEN*-deficient GBM, warranting further investigation in other *PTEN*-deficient/mutated cancers such as endometrial, prostate and other gliomas (Zehir et al., 2017). To develop a therapeutic approach targeting ROBO signaling, we present evidence supporting the use of an anti-ROBO1 single-domain antibody for treatment of recurrent tumor cells. These findings provide a template for studying recurrence and support development of therapeutic regimens that are informed by therapy-driven or longitudinal shifts in the functional genomic landscape of recurrent tumors.

Although CAR-T cell therapy is a newer adaptation for GBM treatment, advancements to increase its clinical utility are rapidly progressing. In **Chapter 3**, we present a novel CAR-T cell therapy targeting ROBO1 in GBM. We present that ROBO1 expression in enriched in primary and recurrent GBM specimens at the transcript and protein levels, including on the cell surface of brain tumor stem cells (BTSCs). We developed a panel of novel camelid monomeric single-domain antibodies that specifically bind to human ROBO1 with high affinity, and these binders are translatable to an efficacious and ROBO1-specific CAR-T modality. Our study establishes anti-ROBO1 CAR-T cells as a potent immunotherapy for GBM.

In fact, a recent clinical letter outlined administration of B7-H3 CAR T cells to a 56-year-old woman with recurrent GBM, highlighting a potent but short-term anti-tumor response *in situ*, absent of grade 3 or higher toxicities associated with CAR T cell infusion(Tang et al., 2021).

Unfortunately, target antigen heterogeneity was predicted as the reason for treatment failure, as noted previously for CAR T cell therapy targeting EGFRvIII and IL13Rα2(Brown et al., 2016a; O'Rourke et al., 2017). Additionally, novel therapeutic targets for CAR T cell therapy are quickly emerging, including antigens such as the disialoganglioside GD2(Murty et al., 2020), CD70(Jin et al., 2018; Yang et al., 2020), CD133(Vora et al., 2020), carbonic anhydrase IX (CAIX)(Cui et al., 2019), EPHA2(Chow et al., 2013; Yi et al., 2018), podoplanin (PDPN)(Shiina et al., 2016), chondroitin sulfate proteoglycan 4 (CSPG4)(Beard et al., 2014; Geldres et al., 2014), and adhesion molecule L1-CAM (CD171)(Hong et al., 2014). While current trials are focused on targeting single tumor-associated antigens, this increased repertoire of targets will allow multiple antigens to be targeted concurrently to overcome intertumoral heterogeneity as shown by Bielamowicz et al. (2018), who developed trivalent CAR T cells targeting HER2, IL13Rα2 and EphA2. In fact, these trivalent CAR T cells were able to eradicate nearly 100% of tumor cells from multiple GBM samples.

5.3 Concluding remarks

In this thesis, I present a deep interrogation of primary and recurrent GBM at genomic, transcriptomic, proteomic and functional genetic levels. Not only did we learn about the vast differences on all levels at tumor recurrence, but we put forward new therapeutic approaches that specifically leverage vulnerabilities in recurrent GBM. Furthermore, emerging trends towards rational combinatorial therapies are likely to include a systemic reignition of the tumor immune microenvironment. The continued discovery of novel tumor-associated and tumor-specific antigens, paired with the improvement of therapeutic modalities to increase efficacy and reduce toxicity, are necessary for the clinical efficacy of immunotherapies. Overall, a combinatorial

therapy delivered at various stages throughout SoC may reliably improve clinical outcomes in GBM patients.

References

(2021). In Brain tumours (primary) and brain metastases in adults (London).

Abdouh, M., Facchino, S., Chatoo, W., Balasingam, V., Ferreira, J., and Bernier, G. (2009). BMI1 sustains human glioblastoma multiforme stem cell renewal. The Journal of neuroscience : the official journal of the Society for Neuroscience *29*, 8884-8896.

Ahmed, N., Brawley, V., Hegde, M., Bielamowicz, K., Kalra, M., Landi, D., Robertson, C., Gray, T.L., Diouf, O., Wakefield, A.*, et al.* (2017). HER2-Specific Chimeric Antigen Receptor-Modified Virus-Specific T Cells for Progressive Glioblastoma: A Phase 1 Dose-Escalation Trial. JAMA Oncol *3*, 1094-1101.

Ahmed, N., Salsman, V.S., Kew, Y., Shaffer, D., Powell, S., Zhang, Y.J., Grossman, R.G., Heslop, H.E., and Gottschalk, S. (2010). HER2-specific T cells target primary glioblastoma stem cells and induce regression of autologous experimental tumors. Clinical cancer research : an official journal of the American Association for Cancer Research *16*, 474-485.

Alexander, B.M., Ba, S., Berger, M.S., Berry, D.A., Cavenee, W.K., Chang, S.M., Cloughesy, T.F., Jiang, T., Khasraw, M., Li, W.*, et al.* (2018). Adaptive Global Innovative Learning Environment for Glioblastoma: GBM AGILE. Clinical cancer research : an official journal of the American Association for Cancer Research *24*, 737-743.

Alexandrov, L.B., Nik-Zainal, S., Wedge, D.C., Aparicio, S.A., Behjati, S., Biankin, A.V., Bignell, G.R., Bolli, N., Borg, A., Borresen-Dale, A.L.*, et al.* (2013). Signatures of mutational processes in human cancer. Nature *500*, 415-421.

Arbabi Ghahroudi, M., Desmyter, A., Wyns, L., Hamers, R., and Muyldermans, S. (1997). Selection and identification of single domain antibody fragments from camel heavy-chain antibodies. FEBS letters *414*, 521-526.

Arruda, L.B., Sim, D., Chikhlikar, P.R., Maciel, M., Jr., Akasaki, K., August, J.T., and Marques, E.T. (2006). Dendritic cell-lysosomal-associated membrane protein (LAMP) and LAMP-1-HIV-1 gag chimeras have distinct cellular trafficking pathways and prime T and B cell responses to a diverse repertoire of epitopes. J Immunol *177*, 2265-2275.

Bagley, S.J., Desai, A.S., Linette, G.P., June, C.H., and O'Rourke, D.M. (2018). CAR T-cell therapy for glioblastoma: recent clinical advances and future challenges. Neuro-oncology *20*, 1429-1438.

Bagley, S.J., Kothari, S., Rahman, R., Lee, E.Q., Dunn, G.P., Galanis, E., Chang, S.M., Nabors, L.B., Ahluwalia, M.S., Stupp, R.*, et al.* (2022). Glioblastoma Clinical Trials: Current Landscape and Opportunities for Improvement. Clinical cancer research : an official journal of the American Association for Cancer Research *28*, 594-602.

Banelli, B., Carra, E., Barbieri, F., Wurth, R., Parodi, F., Pattarozzi, A., Carosio, R., Forlani, A., Allemanni, G., Marubbi, D.*, et al.* (2015). The histone demethylase KDM5A is a key factor for the resistance to temozolomide in glioblastoma. Cell Cycle *14*, 3418-3429.

Bao, S., Wu, Q., Li, Z., Sathornsumetee, S., Wang, H., McLendon, R.E., Hjelmeland, A.B., and Rich, J.N. (2008). Targeting cancer stem cells through L1CAM suppresses glioma growth. Cancer research *68*, 6043-6048.

Bao, S., Wu, Q., McLendon, R.E., Hao, Y., Shi, Q., Hjelmeland, A.B., Dewhirst, M.W., Bigner, D.D., and Rich, J.N. (2006). Glioma stem cells promote radioresistance by preferential activation of the DNA damage response. Nature *444*, 756-760.

Baral, T.N., MacKenzie, R., and Arbabi Ghahroudi, M. (2013). Single-domain antibodies and their utility. Curr Protoc Immunol *103*, 2 17 11-12 17 57.

Barthel, F.P., Johnson, K.C., Varn, F.S., Moskalik, A.D., Tanner, G., Kocakavuk, E., Anderson, K.J., Abiola, O., Aldape, K., Alfaro, K.D.*, et al.* (2019). Longitudinal molecular trajectories of diffuse glioma in adults. Nature *576*, 112-120.

Basu-Roy, U., Bayin, N.S., Rattanakorn, K., Han, E., Placantonakis, D.G., Mansukhani, A., and Basilico, C. (2015). Sox2 antagonizes the Hippo pathway to maintain stemness in cancer cells. Nature communications *6*, 6411.

Batich, K.A., Mitchell, D.A., Healy, P., Herndon, J.E., 2nd, and Sampson, J.H. (2020). Once, Twice, Three Times a Finding: Reproducibility of Dendritic Cell Vaccine Trials Targeting Cytomegalovirus in Glioblastoma. Clin Cancer Res *26*, 5297-5303.

Batich, K.A., Reap, E.A., Archer, G.E., Sanchez-Perez, L., Nair, S.K., Schmittling, R.J., Norberg, P., Xie, W., Herndon, J.E., 2nd, Healy, P.*, et al.* (2017). Long-term Survival in Glioblastoma with Cytomegalovirus pp65-Targeted Vaccination. Clin Cancer Res *23*, 1898-1909.

Batra, S.K., Castelino-Prabhu, S., Wikstrand, C.J., Zhu, X., Humphrey, P.A., Friedman, H.S., and Bigner, D.D. (1995). Epidermal growth factor ligand-independent, unregulated, cell-transforming potential of a naturally occurring human mutant EGFRvIII gene. Cell Growth Differ *6*, 1251-1259.

Beard, R.E., Zheng, Z., Lagisetty, K.H., Burns, W.R., Tran, E., Hewitt, S.M., Abate-Daga, D., Rosati, S.F., Fine, H.A., Ferrone, S.*, et al.* (2014). Multiple chimeric antigen receptors successfully target chondroitin sulfate proteoglycan 4 in several different cancer histologies and cancer stem cells. Journal for immunotherapy of cancer *2*, 25.

Behan, F.M., Iorio, F., Picco, G., Goncalves, E., Beaver, C.M., Migliardi, G., Santos, R., Rao, Y., Sassi, F., Pinnelli, M.*, et al.* (2019). Prioritization of cancer therapeutic targets using CRISPR-Cas9 screens. Nature *568*, 511-516.

Beier, D., Schulz, J.B., and Beier, C.P. (2011). Chemoresistance of glioblastoma cancer stem cells--much more complex than expected. Molecular cancer *10*, 128.

Bessette, D.C., Qiu, D., and Pallen, C.J. (2008). PRL PTPs: mediators and markers of cancer progression. Cancer Metastasis Rev *27*, 231-252.

Bhat, K.P.L., Balasubramaniyan, V., Vaillant, B., Ezhilarasan, R., Hummelink, K., Hollingsworth, F., Wani, K., Heathcock, L., James, J.D., Goodman, L.D.*, et al.* (2013). Mesenchymal differentiation mediated by NF-kappaB promotes radiation resistance in glioblastoma. Cancer cell *24*, 331-346.

Bielamowicz, K., Fousek, K., Byrd, T.T., Samaha, H., Mukherjee, M., Aware, N., Wu, M.F., Orange, J.S., Sumazin, P., Man, T.K.*, et al.* (2018). Trivalent CAR T cells overcome interpatient antigenic variability in glioblastoma. Neuro-oncology *20*, 506-518.

Blank, C.U., Rozeman, E.A., Fanchi, L.F., Sikorska, K., van de Wiel, B., Kvistborg, P., Krijgsman, O., van den Braber, M., Philips, D., Broeks, A.*, et al.* (2018). Neoadjuvant versus adjuvant ipilimumab plus nivolumab in macroscopic stage III melanoma. Nat Med *24*, 1655-1661.

Bleeker, F.E., Lamba, S., Leenstra, S., Troost, D., Hulsebos, T., Vandertop, W.P., Frattini, M., Molinari, F., Knowles, M., Cerrato, A.*, et al.* (2009). IDH1 mutations at residue p.R132 (IDH1(R132)) occur frequently in high-grade gliomas but not in other solid tumors. Hum Mutat *30*, 7-11.

Bloch, O., Crane, C.A., Fuks, Y., Kaur, R., Aghi, M.K., Berger, M.S., Butowski, N.A., Chang, S.M., Clarke, J.L., McDermott, M.W.*, et al.* (2014). Heat-shock protein peptide complex-96 vaccination for recurrent glioblastoma: a phase II, single-arm trial. Neuro Oncol *16*, 274-279.

Bloch, O., Lim, M., Sughrue, M.E., Komotar, R.J., Abrahams, J.M., O'Rourke, D.M., D'Ambrosio, A., Bruce, J.N., and Parsa, A.T. (2017). Autologous Heat Shock Protein Peptide Vaccination for

Newly Diagnosed Glioblastoma: Impact of Peripheral PD-L1 Expression on Response to Therapy. Clin Cancer Res *23*, 3575-3584.

Brennan, C.W., Verhaak, R.G., McKenna, A., Campos, B., Noushmehr, H., Salama, S.R., Zheng, S., Chakravarty, D., Sanborn, J.Z., Berman, S.H.*, et al.* (2013). The somatic genomic landscape of glioblastoma. Cell *155*, 462-477.

Brock, C.S., Newlands, E.S., Wedge, S.R., Bower, M., Evans, H., Colquhoun, I., Roddie, M., Glaser, M., Brampton, M.H., and Rustin, G.J. (1998). Phase I trial of temozolomide using an extended continuous oral schedule. Cancer Res *58*, 4363-4367.

Brose, K., Bland, K.S., Wang, K.H., Arnott, D., Henzel, W., Goodman, C.S., Tessier-Lavigne, M., and Kidd, T. (1999). Slit proteins bind Robo receptors and have an evolutionarily conserved role in repulsive axon guidance. Cell *96*, 795-806.

Brown, C.E., Aguilar, B., Starr, R., Yang, X., Chang, W.C., Weng, L., Chang, B., Sarkissian, A., Brito, A., Sanchez, J.F.*, et al.* (2018). Optimization of IL13Ralpha2-Targeted Chimeric Antigen Receptor T Cells for Improved Anti-tumor Efficacy against Glioblastoma. Molecular therapy : the journal of the American Society of Gene Therapy *26*, 31-44.

Brown, C.E., Alizadeh, D., Starr, R., Weng, L., Wagner, J.R., Naranjo, A., Ostberg, J.R., Blanchard, M.S., Kilpatrick, J., Simpson, J.*, et al.* (2016a). Regression of Glioblastoma after Chimeric Antigen Receptor T-Cell Therapy. The New England journal of medicine *375*, 2561-2569.

Brown, C.E., Badie, B., Barish, M.E., Weng, L., Ostberg, J.R., Chang, W.C., Naranjo, A., Starr, R., Wagner, J., Wright, C.*, et al.* (2015). Bioactivity and Safety of IL13Ralpha2-Redirected Chimeric Antigen Receptor CD8+ T Cells in Patients with Recurrent Glioblastoma. Clinical cancer research : an official journal of the American Association for Cancer Research *21*, 4062-4072.

Brown, C.E., Warden, C.D., Starr, R., Deng, X., Badie, B., Yuan, Y.C., Forman, S.J., and Barish, M.E. (2013). Glioma IL13Ralpha2 is associated with mesenchymal signature gene expression and poor patient prognosis. PloS one *8*, e77769.

Brown, T.J., Brennan, M.C., Li, M., Church, E.W., Brandmeir, N.J., Rakszawski, K.L., Patel, A.S., Rizk, E.B., Suki, D., Sawaya, R.*, et al.* (2016b). Association of the Extent of Resection With Survival in Glioblastoma: A Systematic Review and Meta-analysis. JAMA Oncol *2*, 1460-1469.

Bruggeman, S.W., Hulsman, D., Tanger, E., Buckle, T., Blom, M., Zevenhoven, J., van Tellingen, O., and van Lohuizen, M. (2007). Bmi1 controls tumor development in an Ink4a/Arf-independent manner in a mouse model for glioma. Cancer cell *12*, 328-341.

Burger, P.C., and Green, S.B. (1987). Patient age, histologic features, and length of survival in patients with glioblastoma multiforme. Cancer *59*, 1617-1625.

Cabrera, A.R., Kirkpatrick, J.P., Fiveash, J.B., Shih, H.A., Koay, E.J., Lutz, S., Petit, J., Chao, S.T., Brown, P.D., Vogelbaum, M.*, et al.* (2016). Radiation therapy for glioblastoma: Executive summary of an American Society for Radiation Oncology Evidence-Based Clinical Practice Guideline. Pract Radiat Oncol *6*, 217-225.

Cancer Genome Atlas Research, N. (2008). Comprehensive genomic characterization defines human glioblastoma genes and core pathways. Nature *455*, 1061-1068.

Cancer Genome Atlas Research, N., Brat, D.J., Verhaak, R.G., Aldape, K.D., Yung, W.K., Salama, S.R., Cooper, L.A., Rheinbay, E., Miller, C.R., Vitucci, M.*, et al.* (2015). Comprehensive, Integrative Genomic Analysis of Diffuse Lower-Grade Gliomas. The New England journal of medicine *372*, 2481-2498.

Cancer Genome Atlas Research, N., Kandoth, C., Schultz, N., Cherniack, A.D., Akbani, R., Liu, Y., Shen, H., Robertson, A.G., Pashtan, I., Shen, R.*, et al.* (2013a). Integrated genomic characterization of endometrial carcinoma. Nature *497*, 67-73.

Cancer Genome Atlas Research, N., Weinstein, J.N., Collisson, E.A., Mills, G.B., Shaw, K.R., Ozenberger, B.A., Ellrott, K., Shmulevich, I., Sander, C., and Stuart, J.M. (2013b). The Cancer Genome Atlas Pan-Cancer analysis project. Nature genetics *45*, 1113-1120.

Chen, C.Y., Hutzen, B., Wedekind, M.F., and Cripe, T.P. (2018). Oncolytic virus and PD-1/PD-L1 blockade combination therapy. Oncolytic Virother *7*, 65-77.

Chen, J., Li, Y., Yu, T.S., McKay, R.M., Burns, D.K., Kernie, S.G., and Parada, L.F. (2012). A restricted cell population propagates glioblastoma growth after chemotherapy. Nature *488*, 522-526.

Cho, H.J., Zhao, J., Jung, S.W., Ladewig, E., Kong, D.S., Suh, Y.L., Lee, Y., Kim, D., Ahn, S.H., Bordyuh, M.*, et al.* (2019). Distinct genomic profile and specific targeted drug responses in adult cerebellar glioblastoma. Neuro-oncology *21*, 47-58.

Choe, J.H., Watchmaker, P.B., Simic, M.S., Gilbert, R.D., Li, A.W., Krasnow, N.A., Downey, K.M., Yu, W., Carrera, D.A., Celli, A.*, et al.* (2021). SynNotch-CAR T cells overcome challenges of specificity, heterogeneity, and persistence in treating glioblastoma. Science translational medicine *13*.

Choi, B.D., Curry, W.T., Carter, B.S., and Maus, M.V. (2018). Chimeric antigen receptor T-cell immunotherapy for glioblastoma: practical insights for neurosurgeons. Neurosurg Focus *44*, E13.

Choi, B.D., Suryadevara, C.M., Gedeon, P.C., Herndon, J.E., 2nd, Sanchez-Perez, L., Bigner, D.D., and Sampson, J.H. (2014). Intracerebral delivery of a third generation EGFRvIII-specific

chimeric antigen receptor is efficacious against human glioma. Journal of clinical neuroscience : official journal of the Neurosurgical Society of Australasia *21*, 189-190.

Choi, B.D., Yu, X., Castano, A.P., Bouffard, A.A., Schmidts, A., Larson, R.C., Bailey, S.R., Boroughs, A.C., Frigault, M.J., Leick, M.B.*, et al.* (2019). CAR-T cells secreting BiTEs circumvent antigen escape without detectable toxicity. Nature biotechnology *37*, 1049-1058.

Chow, K.K., Naik, S., Kakarla, S., Brawley, V.S., Shaffer, D.R., Yi, Z., Rainusso, N., Wu, M.F., Liu, H., Kew, Y.*, et al.* (2013). T cells redirected to EphA2 for the immunotherapy of glioblastoma. Molecular therapy : the journal of the American Society of Gene Therapy *21*, 629-637.

Christensen, B.C., Smith, A.A., Zheng, S., Koestler, D.C., Houseman, E.A., Marsit, C.J., Wiemels, J.L., Nelson, H.H., Karagas, M.R., Wrensch, M.R.*, et al.* (2011). DNA methylation, isocitrate dehydrogenase mutation, and survival in glioma. Journal of the National Cancer Institute *103*, 143-153.

Clarke, M.F., and Fuller, M. (2006). Stem cells and cancer: two faces of eve. Cell *124*, 1111-1115.

Cloughesy, T.F., Mochizuki, A.Y., Orpilla, J.R., Hugo, W., Lee, A.H., Davidson, T.B., Wang, A.C., Ellingson, B.M., Rytlewski, J.A., Sanders, C.M.*, et al.* (2019). Neoadjuvant anti-PD-1 immunotherapy promotes a survival benefit with intratumoral and systemic immune responses in recurrent glioblastoma. Nat Med *25*, 477-486.

Cockle, J.V., Rajani, K., Zaidi, S., Kottke, T., Thompson, J., Diaz, R.M., Shim, K., Peterson, T., Parney, I.F., Short, S.*, et al.* (2016). Combination viroimmunotherapy with checkpoint inhibition to treat glioma, based on location-specific tumor profiling. Neuro-oncology *18*, 518-527.

Colic, M., Wang, G., Zimmermann, M., Mascall, K., McLaughlin, M., Bertolet, L., Lenoir, W.F., Moffat, J., Angers, S., Durocher, D.*, et al.* (2019). Identifying chemogenetic interactions from CRISPR screens with drugZ. Genome Med *11*, 52.

Colman, H., Zhang, L., Sulman, E.P., McDonald, J.M., Shooshtari, N.L., Rivera, A., Popoff, S., Nutt, C.L., Louis, D.N., Cairncross, J.G.*, et al.* (2010). A multigene predictor of outcome in glioblastoma. Neuro-oncology *12*, 49-57.

Contardi, E., Palmisano, G.L., Tazzari, P.L., Martelli, A.M., Fala, F., Fabbi, M., Kato, T., Lucarelli, E., Donati, D., Polito, L.*, et al.* (2005). CTLA-4 is constitutively expressed on tumor cells and can trigger apoptosis upon ligand interaction. Int J Cancer *117*, 538-550.

Couturier, C.P., Ayyadhury, S., Le, P.U., Nadaf, J., Monlong, J., Riva, G., Allache, R., Baig, S., Yan, X., Bourgey, M.*, et al.* (2020). Single-cell RNA-seq reveals that glioblastoma recapitulates a normal neurodevelopmental hierarchy. Nature communications *11*, 3406.

Crane, C.A., Han, S.J., Ahn, B., Oehlke, J., Kivett, V., Fedoroff, A., Butowski, N., Chang, S.M., Clarke, J., Berger, M.S.*, et al.* (2013). Individual patient-specific immunity against high-grade glioma after vaccination with autologous tumor derived peptides bound to the 96 KD chaperone protein. Clin Cancer Res *19*, 205-214.

Cui, J., Zhang, Q., Song, Q., Wang, H., Dmitriev, P., Sun, M.Y., Cao, X., Wang, Y., Guo, L., Indig, I.H.*, et al.* (2019). Targeting hypoxia downstream signaling protein, CAIX, for CAR T-cell therapy against glioblastoma. Neuro-oncology *21*, 1436-1446.

Dalerba, P., Cho, R.W., and Clarke, M.F. (2007). Cancer stem cells: models and concepts. Annual review of medicine *58*, 267-284.

Dallol, A., Krex, D., Hesson, L., Eng, C., Maher, E.R., and Latif, F. (2003). Frequent epigenetic inactivation of the SLIT2 gene in gliomas. Oncogene *22*, 4611-4616.

Dang, L., White, D.W., Gross, S., Bennett, B.D., Bittinger, M.A., Driggers, E.M., Fantin, V.R., Jang, H.G., Jin, S., Keenan, M.C.*, et al.* (2009). Cancer-associated IDH1 mutations produce 2-hydroxyglutarate. Nature *462*, 739-744.

Danson, S.J., and Middleton, M.R. (2001). Temozolomide: a novel oral alkylating agent. Expert review of anticancer therapy *1*, 13-19.

Darmanis, S., Sloan, S.A., Croote, D., Mignardi, M., Chernikova, S., Samghababi, P., Zhang, Y., Neff, N., Kowarsky, M., Caneda, C.*, et al.* (2017). Single-Cell RNA-Seq Analysis of Infiltrating Neoplastic Cells at the Migrating Front of Human Glioblastoma. Cell reports *21*, 1399-1410.

Davidson, T.B., Lee, A., Hsu, M., Sedighim, S., Orpilla, J., Treger, J., Mastall, M., Roesch, S., Rapp, C., Galvez, M.*, et al.* (2019). Expression of PD-1 by T Cells in Malignant Glioma Patients Reflects Exhaustion and Activation. Clin Cancer Res *25*, 1913-1922.

Debinski, W., Gibo, D.M., Hulet, S.W., Connor, J.R., and Gillespie, G.Y. (1999). Receptor for interleukin 13 is a marker and therapeutic target for human high-grade gliomas. Clinical cancer research : an official journal of the American Association for Cancer Research *5*, 985-990.

deCarvalho, A.C., Kim, H., Poisson, L.M., Winn, M.E., Mueller, C., Cherba, D., Koeman, J., Seth, S., Protopopov, A., Felicella, M.*, et al.* (2018). Discordant inheritance of chromosomal and extrachromosomal DNA elements contributes to dynamic disease evolution in glioblastoma. Nature genetics *50*, 708-717.

Dempster, J.M., Pacini, C., Pantel, S., Behan, F.M., Green, T., Krill-Burger, J., Beaver, C.M., Younger, S.T., Zhivich, V., Najgebauer, H.*, et al.* (2019). Agreement between two large pan-cancer CRISPR-Cas9 gene dependency data sets. Nat Commun *10*, 5817.

DeVita, V.T., Jr. (1978). The evolution of therapeutic research in cancer. The New England journal of medicine *298*, 907-910.

Dickinson, R.E., and Duncan, W.C. (2010). The SLIT-ROBO pathway: a regulator of cell function with implications for the reproductive system. Reproduction *139*, 697-704.

Dobin, A., Davis, C.A., Schlesinger, F., Drenkow, J., Zaleski, C., Jha, S., Batut, P., Chaisson, M., and Gingeras, T.R. (2013). STAR: ultrafast universal RNA-seq aligner. Bioinformatics *29*, 15-21.

Dong, Y., Zhang, L., Bai, Y., Zhou, H.M., Campbell, A.M., Chen, H., Yong, W., Zhang, W., Zeng, Q., Shou, W.*, et al.* (2014). Phosphatase of regenerating liver 2 (PRL2) deficiency impairs Kit signaling and spermatogenesis. The Journal of biological chemistry *289*, 3799-3810.

Durocher, Y., Perret, S., and Kamen, A. (2002). High-level and high-throughput recombinant protein production by transient transfection of suspension-growing human 293-EBNA1 cells. Nucleic acids research *30*, E9.

Eckel-Passow, J.E., Lachance, D.H., Molinaro, A.M., Walsh, K.M., Decker, P.A., Sicotte, H., Pekmezci, M., Rice, T., Kosel, M.L., Smirnov, I.V.*, et al.* (2015). Glioma Groups Based on 1p/19q, IDH, and TERT Promoter Mutations in Tumors. The New England journal of medicine *372*, 2499-2508.

Edris, B., Weiskopf, K., Volkmer, A.K., Volkmer, J.P., Willingham, S.B., Contreras-Trujillo, H., Liu, J., Majeti, R., West, R.B., Fletcher, J.A.*, et al.* (2012). Antibody therapy targeting the CD47 protein is effective in a model of aggressive metastatic leiomyosarcoma. Proc Natl Acad Sci U S A *109*, 6656-6661.

Etcheverry, A., Aubry, M., de Tayrac, M., Vauleon, E., Boniface, R., Guenot, F., Saikali, S., Hamlat, A., Riffaud, L., Menei, P.*, et al.* (2010). DNA methylation in glioblastoma: impact on gene expression and clinical outcome. BMC genomics *11*, 701.

Eyupoglu, I.Y., Hore, N., Merkel, A., Buslei, R., Buchfelder, M., and Savaskan, N. (2016). Supra-complete surgery via dual intraoperative visualization approach (DiVA) prolongs patient survival in glioblastoma. Oncotarget *7*, 25755-25768.

Fairhead, M., and Howarth, M. (2015). Site-specific biotinylation of purified proteins using BirA. Methods in molecular biology *1266*, 171-184.

Favero, F., McGranahan, N., Salm, M., Birkbak, N.J., Sanborn, J.Z., Benz, S.C., Becq, J., Peden, J.F., Kingsbury, Z., Grocok, R.J.*, et al.* (2015). Glioblastoma adaptation traced through decline of an IDH1 clonal driver and macro-evolution of a double-minute chromosome. Annals of oncology : official journal of the European Society for Medical Oncology / ESMO *26*, 880-887.

Fecci, P.E., Ochiai, H., Mitchell, D.A., Grossi, P.M., Sweeney, A.E., Archer, G.E., Cummings, T., Allison, J.P., Bigner, D.D., and Sampson, J.H. (2007). Systemic CTLA-4 blockade ameliorates glioma-induced changes to the CD4+ T cell compartment without affecting regulatory T-cell function. Clin Cancer Res *13*, 2158-2167.

Finney, H.M., Akbar, A.N., and Lawson, A.D. (2004). Activation of resting human primary T cells with chimeric receptors: costimulation from CD28, inducible costimulator, CD134, and CD137 in series with signals from the TCR zeta chain. Journal of immunology *172*, 104-113.

Finney, H.M., Lawson, A.D., Bebbington, C.R., and Weir, A.N. (1998). Chimeric receptors providing both primary and costimulatory signaling in T cells from a single gene product. Journal of immunology *161*, 2791-2797.

Francis, J.M., Zhang, C.Z., Maire, C.L., Jung, J., Manzo, V.E., Adalsteinsson, V.A., Homer, H., Haidar, S., Blumenstiel, B., Pedamallu, C.S.*, et al.* (2014). EGFR variant heterogeneity in glioblastoma resolved through single-nucleus sequencing. Cancer discovery *4*, 956-971.

Gangemi, R.M., Griffero, F., Marubbi, D., Perera, M., Capra, M.C., Malatesta, P., Ravetti, G.L., Zona, G.L., Daga, A., and Corte, G. (2009). SOX2 silencing in glioblastoma tumor-initiating cells causes stop of proliferation and loss of tumorigenicity. Stem cells *27*, 40-48.

Gangoso, E., Southgate, B., Bradley, L., Rus, S., Galvez-Cancino, F., McGivern, N., Guc, E., Kapourani, C.A., Byron, A., Ferguson, K.M.*, et al.* (2021). Glioblastomas acquire myeloid-affiliated transcriptional programs via epigenetic immunoediting to elicit immune evasion. Cell.

Gara, R.K., Kumari, S., Ganju, A., Yallapu, M.M., Jaggi, M., and Chauhan, S.C. (2015). Slit/Robo pathway: a promising therapeutic target for cancer. Drug discovery today *20*, 156-164.

Geldres, C., Savoldo, B., Hoyos, V., Caruana, I., Zhang, M., Yvon, E., Del Vecchio, M., Creighton, C.J., Ittmann, M., Ferrone, S.*, et al.* (2014). T lymphocytes redirected against the chondroitin sulfate proteoglycan-4 control the growth of multiple solid tumors both in vitro and in vivo. Clinical cancer research : an official journal of the American Association for Cancer Research *20*, 962-971.

Geraldo, L.H., Xu, Y., Jacob, L., Pibouin-Fragner, L., Rao, R., Maissa, N., Verreault, M., Lemaire, N., Knosp, C., Lesaffre, C.*, et al.* (2021). SLIT2/ROBO signaling in tumor-associated microglia and macrophages drives glioblastoma immunosuppression and vascular dysmorphia. The Journal of clinical investigation *131*.

Gholamin, S., Youssef, O.A., Rafat, M., Esparza, R., Kahn, S., Shahin, M., Giaccia, A.J., Graves, E.E., Weissman, I., Mitra, S.*, et al.* (2020). Irradiation or temozolomide chemotherapy enhances anti-CD47 treatment of glioblastoma. Innate Immun *26*, 130-137.

Goff, S.L., Morgan, R.A., Yang, J.C., Sherry, R.M., Robbins, P.F., Restifo, N.P., Feldman, S.A., Lu, Y.C., Lu, L., Zheng, Z.*, et al.* (2019). Pilot Trial of Adoptive Transfer of Chimeric Antigen Receptor-transduced T Cells Targeting EGFRvIII in Patients With Glioblastoma. Journal of immunotherapy *42*, 126-135.

Goswami, S., Chen, Y., Anandhan, S., Szabo, P.M., Basu, S., Blando, J.M., Liu, W., Zhang, J., Natarajan, S.M., Xiong, L.*, et al.* (2020a). ARID1A mutation plus CXCL13 expression act as

combinatorial biomarkers to predict responses to immune checkpoint therapy in mUCC. Science translational medicine *12*.

Goswami, S., Walle, T., Cornish, A.E., Basu, S., Anandhan, S., Fernandez, I., Vence, L., Blando, J., Zhao, H., Yadav, S.S.*, et al.* (2020b). Immune profiling of human tumors identifies CD73 as a combinatorial target in glioblastoma. Nat Med *26*, 39-46.

Graham, V., Khudyakov, J., Ellis, P., and Pevny, L. (2003). SOX2 functions to maintain neural progenitor identity. Neuron *39*, 749-765.

Harris-Bookman, S., Mathios, D., Martin, A.M., Xia, Y., Kim, E., Xu, H., Belcaid, Z., Polanczyk, M., Barberi, T., Theodros, D.*, et al.* (2018). Expression of LAG-3 and efficacy of combination treatment with anti-LAG-3 and anti-PD-1 monoclonal antibodies in glioblastoma. Int J Cancer *143*, 3201-3208.

Hart, T., Chandrashekhar, M., Aregger, M., Steinhart, Z., Brown, K.R., MacLeod, G., Mis, M., Zimmermann, M., Fradet-Turcotte, A., Sun, S.*, et al.* (2015). High-Resolution CRISPR Screens Reveal Fitness Genes and Genotype-Specific Cancer Liabilities. Cell *163*, 1515-1526.

Hart, T., and Moffat, J. (2016). BAGEL: a computational framework for identifying essential genes from pooled library screens. BMC Bioinformatics *17*, 164.

Hart, T., Tong, A.H.Y., Chan, K., Van Leeuwen, J., Seetharaman, A., Aregger, M., Chandrashekhar, M., Hustedt, N., Seth, S., Noonan, A.*, et al.* (2017). Evaluation and Design of Genome-Wide CRISPR/SpCas9 Knockout Screens. G3 (Bethesda) *7*, 2719-2727.

Haynik, D.M., Roma, A.A., and Prayson, R.A. (2007). HER-2/neu expression in glioblastoma multiforme. Appl Immunohistochem Mol Morphol *15*, 56-58.

Hegi, M.E., Diserens, A.C., Bady, P., Kamoshima, Y., Kouwenhoven, M.C., Delorenzi, M., Lambiv, W.L., Hamou, M.F., Matter, M.S., Koch, A.*, et al.* (2011). Pathway analysis of

glioblastoma tissue after preoperative treatment with the EGFR tyrosine kinase inhibitor gefitinib--a phase II trial. Molecular cancer therapeutics *10*, 1102-1112.

Hegi, M.E., Diserens, A.C., Gorlia, T., Hamou, M.F., de Tribolet, N., Weller, M., Kros, J.M., Hainfellner, J.A., Mason, W., Mariani, L.*, et al.* (2005). MGMT gene silencing and benefit from temozolomide in glioblastoma. The New England journal of medicine *352*, 997-1003.

Heimberger, A.B., Crotty, L.E., Archer, G.E., Hess, K.R., Wikstrand, C.J., Friedman, A.H., Friedman, H.S., Bigner, D.D., and Sampson, J.H. (2003). Epidermal growth factor receptor VIII peptide vaccination is efficacious against established intracerebral tumors. Clin Cancer Res *9*, 4247-4254.

Heimberger, A.B., Hlatky, R., Suki, D., Yang, D., Weinberg, J., Gilbert, M., Sawaya, R., and Aldape, K. (2005). Prognostic effect of epidermal growth factor receptor and EGFRvIII in glioblastoma multiforme patients. Clin Cancer Res *11*, 1462-1466.

Hlobilkova, A., Guldberg, P., Thullberg, M., Zeuthen, J., Lukas, J., and Bartek, J. (2000). Cell cycle arrest by the PTEN tumor suppressor is target cell specific and may require protein phosphatase activity. Experimental cell research *256*, 571-577.

Hodges, T.R., Ott, M., Xiu, J., Gatalica, Z., Swensen, J., Zhou, S., Huse, J.T., de Groot, J., Li, S., Overwijk, W.W.*, et al.* (2017). Mutational burden, immune checkpoint expression, and mismatch repair in glioma: implications for immune checkpoint immunotherapy. Neuro-oncology *19*, 1047-1057.

Hombach, A., Wieczarkowiecz, A., Marquardt, T., Heuser, C., Usai, L., Pohl, C., Seliger, B., and Abken, H. (2001). Tumor-specific T cell activation by recombinant immunoreceptors: CD3 zeta signaling and CD28 costimulation are simultaneously required for efficient IL-2 secretion and can

be integrated into one combined CD28/CD3 zeta signaling receptor molecule. Journal of immunology *167*, 6123-6131.

Hong, H., Stastny, M., Brown, C., Chang, W.C., Ostberg, J.R., Forman, S.J., and Jensen, M.C. (2014). Diverse solid tumors expressing a restricted epitope of L1-CAM can be targeted by chimeric antigen receptor redirected T lymphocytes. Journal of immunotherapy *37*, 93-104.

Hu, H., Li, M., Labrador, J.P., McEwen, J., Lai, E.C., Goodman, C.S., and Bashaw, G.J. (2005). Cross GTPase-activating protein (CrossGAP)/Vilse links the Roundabout receptor to Rac to regulate midline repulsion. Proceedings of the National Academy of Sciences of the United States of America *102*, 4613-4618.

Huang, K., Liu, X., Li, Y., Wang, Q., Zhou, J., Wang, Y., Dong, F., Yang, C., Sun, Z., Fang, C.*, et al.* (2019). Genome-Wide CRISPR-Cas9 Screening Identifies NF-kappaB/E2F6 Responsible for EGFRvIII-Associated Temozolomide Resistance in Glioblastoma. Adv Sci (Weinh) *6*, 1900782.

Hussack, G., Arbabi-Ghahroudi, M., van Faassen, H., Songer, J.G., Ng, K.K., MacKenzie, R., and Tanha, J. (2011). Neutralization of Clostridium difficile toxin A with single-domain antibodies targeting the cell receptor binding domain. The Journal of biological chemistry *286*, 8961-8976.

Imai, C., Mihara, K., Andreansky, M., Nicholson, I.C., Pui, C.H., Geiger, T.L., and Campana, D. (2004). Chimeric receptors with 4-1BB signaling capacity provoke potent cytotoxicity against acute lymphoblastic leukemia. Leukemia *18*, 676-684.

Jackson, C.M., Choi, J., and Lim, M. (2019). Mechanisms of immunotherapy resistance: lessons from glioblastoma. Nature immunology *20*, 1100-1109.

Jacob, F., Salinas, R.D., Zhang, D.Y., Nguyen, P.T.T., Schnoll, J.G., Wong, S.Z.H., Thokala, R., Sheikh, S., Saxena, D., Prokop, S.*, et al.* (2020). A Patient-Derived Glioblastoma Organoid Model and Biobank Recapitulates Inter- and Intra-tumoral Heterogeneity. Cell *180*, 188-204 e122.

Jassal, B., Matthews, L., Viteri, G., Gong, C., Lorente, P., Fabregat, A., Sidiropoulos, K., Cook, J., Gillespie, M., Haw, R.*, et al.* (2020). The reactome pathway knowledgebase. Nucleic acids research *48*, D498-D503.

Ji, N., Zhang, Y., Liu, Y., Xie, J., Wang, Y., Hao, S., and Gao, Z. (2018). Heat shock protein peptide complex-96 vaccination for newly diagnosed glioblastoma: a phase I, single-arm trial. JCI Insight *3*.

Jiang, H., Rivera-Molina, Y., Gomez-Manzano, C., Clise-Dwyer, K., Bover, L., Vence, L.M., Yuan, Y., Lang, F.F., Toniatti, C., Hossain, M.B.*, et al.* (2017). Oncolytic Adenovirus and Tumor-Targeting Immune Modulatory Therapy Improve Autologous Cancer Vaccination. Cancer research *77*, 3894-3907.

Jin, L., Ge, H., Long, Y., Yang, C., Chang, Y.E., Mu, L., Sayour, E.J., De Leon, G., Wang, Q.J., Yang, J.C.*, et al.* (2018). CD70, a novel target of CAR T-cell therapy for gliomas. Neuro-oncology *20*, 55-65.

Johnson, B.E., Mazor, T., Hong, C., Barnes, M., Aihara, K., McLean, C.Y., Fouse, S.D., Yamamoto, S., Ueda, H., Tatsuno, K.*, et al.* (2014). Mutational analysis reveals the origin and therapy-driven evolution of recurrent glioma. Science *343*, 189-193.

Johnson, L.A., Scholler, J., Ohkuri, T., Kosaka, A., Patel, P.R., McGettigan, S.E., Nace, A.K., Dentchev, T., Thekkat, P., Loew, A.*, et al.* (2015). Rational development and characterization of humanized anti-EGFR variant III chimeric antigen receptor T cells for glioblastoma. Science translational medicine *7*, 275ra222.

Jones, S., Wang, T.L., Shih Ie, M., Mao, T.L., Nakayama, K., Roden, R., Glas, R., Slamon, D., Diaz, L.A., Jr., Vogelstein, B.*, et al.* (2010). Frequent mutations of chromatin remodeling gene ARID1A in ovarian clear cell carcinoma. Science *330*, 228-231.

Kaneko, Y., Sakakibara, S., Imai, T., Suzuki, A., Nakamura, Y., Sawamoto, K., Ogawa, Y., Toyama, Y., Miyata, T., and Okano, H. (2000). Musashi1: an evolutionally conserved marker for CNS progenitor cells including neural stem cells. Developmental neuroscience *22*, 139-153.

Keu, K.V., Witney, T.H., Yaghoubi, S., Rosenberg, J., Kurien, A., Magnusson, R., Williams, J., Habte, F., Wagner, J.R., Forman, S.*, et al.* (2017). Reporter gene imaging of targeted T cell immunotherapy in recurrent glioma. Science translational medicine *9*.

Kim, H., and D'Andrea, A.D. (2012). Regulation of DNA cross-link repair by the Fanconi anemia/BRCA pathway. Genes & development *26*, 1393-1408.

Kim, H., Nguyen, N.P., Turner, K., Wu, S., Gujar, A.D., Luebeck, J., Liu, J., Deshpande, V., Rajkumar, U., Namburi, S.*, et al.* (2020). Extrachromosomal DNA is associated with oncogene amplification and poor outcome across multiple cancers. Nature genetics *52*, 891-897.

Kim, H., Zheng, S., Amini, S.S., Virk, S.M., Mikkelsen, T., Brat, D.J., Grimsby, J., Sougnez, C., Muller, F., Hu, J.*, et al.* (2015a). Whole-genome and multisector exome sequencing of primary and post-treatment glioblastoma reveals patterns of tumor evolution. Genome research *25*, 316-327.

Kim, J., Lee, I.H., Cho, H.J., Park, C.K., Jung, Y.S., Kim, Y., Nam, S.H., Kim, B.S., Johnson, M.D., Kong, D.S.*, et al.* (2015b). Spatiotemporal Evolution of the Primary Glioblastoma Genome. Cancer cell *28*, 318-328.

Kim, J.E., Patel, M.A., Mangraviti, A., Kim, E.S., Theodros, D., Velarde, E., Liu, A., Sankey, E.W., Tam, A., Xu, H.*, et al.* (2017). Combination Therapy with Anti-PD-1, Anti-TIM-3, and Focal Radiation Results in Regression of Murine Gliomas. Clin Cancer Res *23*, 124-136.

Kobayashi, M., Bai, Y., Dong, Y., Yu, H., Chen, S., Gao, R., Zhang, L., Yoder, M.C., Kapur, R., Zhang, Z.Y.*, et al.* (2014). PRL2/PTP4A2 phosphatase is important for hematopoietic stem cell self-renewal. Stem cells *32*, 1956-1967.

Koh, H.J., Lee, S.M., Son, B.G., Lee, S.H., Ryoo, Z.Y., Chang, K.T., Park, J.W., Park, D.C., Song, B.J., Veech, R.L.*, et al.* (2004). Cytosolic NADP+-dependent isocitrate dehydrogenase plays a key role in lipid metabolism. The Journal of biological chemistry *279*, 39968-39974.

Koka, V., Potti, A., Forseen, S.E., Pervez, H., Fraiman, G.N., Koch, M., and Levitt, R. (2003). Role of Her-2/neu overexpression and clinical determinants of early mortality in glioblastoma multiforme. Am J Clin Oncol *26*, 332-335.

Kong, S., Sengupta, S., Tyler, B., Bais, A.J., Ma, Q., Doucette, S., Zhou, J., Sahin, A., Carter, B.S., Brem, H.*, et al.* (2012). Suppression of human glioma xenografts with second-generation IL13R-specific chimeric antigen receptor-modified T cells. Clinical cancer research : an official journal of the American Association for Cancer Research *18*, 5949-5960.

Korber, V., Yang, J., Barah, P., Wu, Y., Stichel, D., Gu, Z., Fletcher, M.N.C., Jones, D., Hentschel, B., Lamszus, K.*, et al.* (2019). Evolutionary Trajectories of IDH(WT) Glioblastomas Reveal a Common Path of Early Tumorigenesis Instigated Years ahead of Initial Diagnosis. Cancer cell *35*, 692-704 e612.

Korotkevich, G., Sukhov, V., and Sergushichev, A. (2020). Fast gene set enrichment analysis. bioRxiv.

Krenciute, G., Krebs, S., Torres, D., Wu, M.F., Liu, H., Dotti, G., Li, X.N., Lesniak, M.S., Balyasnikova, I.V., and Gottschalk, S. (2016). Characterization and Functional Analysis of scFv-based Chimeric Antigen Receptors to Redirect T Cells to IL13Ralpha2-positive Glioma. Molecular therapy : the journal of the American Society of Gene Therapy *24*, 354-363.

Krenciute, G., Prinzing, B.L., Yi, Z., Wu, M.F., Liu, H., Dotti, G., Balyasnikova, I.V., and Gottschalk, S. (2017). Transgenic Expression of IL15 Improves Antiglioma Activity of IL13Ralpha2-CAR T Cells but Results in Antigen Loss Variants. Cancer immunology research *5*, 571-581.

Kuhnol, C., Herbarth, M., Foll, J., Staege, M.S., and Kramm, C. (2013). CD137 stimulation and p38 MAPK inhibition improve reactivity in an in vitro model of glioblastoma immunotherapy. Cancer Immunol Immunother *62*, 1797-1809.

Kumar, A., Boyle, E.A., Tokita, M., Mikheev, A.M., Sanger, M.C., Girard, E., Silber, J.R., Gonzalez-Cuyar, L.F., Hiatt, J.B., Adey, A.*, et al.* (2014). Deep sequencing of multiple regions of glial tumors reveals spatial heterogeneity for mutations in clinically relevant genes. Genome biology *15*, 530.

Lacroix, M., Abi-Said, D., Fourney, D.R., Gokaslan, Z.L., Shi, W., DeMonte, F., Lang, F.F., McCutcheon, I.E., Hassenbusch, S.J., Holland, E.*, et al.* (2001). A multivariate analysis of 416 patients with glioblastoma multiforme: prognosis, extent of resection, and survival. J Neurosurg *95*, 190-198.

Langmead, B., Trapnell, C., Pop, M., and Salzberg, S.L. (2009). Ultrafast and memory-efficient alignment of short DNA sequences to the human genome. Genome biology *10*, R25.

Lapointe, S., Perry, A., and Butowski, N.A. (2018). Primary brain tumours in adults. Lancet *392*, 432-446.

Lathia, J.D., Gallagher, J., Heddleston, J.M., Wang, J., Eyler, C.E., Macswords, J., Wu, Q., Vasanji, A., McLendon, R.E., Hjelmeland, A.B.*, et al.* (2010). Integrin alpha 6 regulates glioblastoma stem cells. Cell stem cell *6*, 421-432.

Le, D.T., Uram, J.N., Wang, H., Bartlett, B.R., Kemberling, H., Eyring, A.D., Skora, A.D., Luber, B.S., Azad, N.S., Laheru, D.*, et al.* (2015). PD-1 Blockade in Tumors with Mismatch-Repair Deficiency. The New England journal of medicine *372*, 2509-2520.

Lee, G., Auffinger, B., Guo, D., Hasan, T., Deheeger, M., Tobias, A.L., Kim, J.Y., Atashi, F., Zhang, L., Lesniak, M.S.*, et al.* (2016). Dedifferentiation of Glioma Cells to Glioma Stem-like Cells By Therapeutic Stress-induced HIF Signaling in the Recurrent GBM Model. Molecular cancer therapeutics *15*, 3064-3076.

Lee, J., Kotliarova, S., Kotliarov, Y., Li, A., Su, Q., Donin, N.M., Pastorino, S., Purow, B.W., Christopher, N., Zhang, W.*, et al.* (2006). Tumor stem cells derived from glioblastomas cultured in bFGF and EGF more closely mirror the phenotype and genotype of primary tumors than do serum-cultured cell lines. Cancer cell *9*, 391-403.

Lee, J.K., Wang, J., Sa, J.K., Ladewig, E., Lee, H.O., Lee, I.H., Kang, H.J., Rosenbloom, D.S., Camara, P.G., Liu, Z.*, et al.* (2017). Spatiotemporal genomic architecture informs precision oncology in glioblastoma. Nature genetics *49*, 594-599.

Lee, S.H., Jo, S.H., Lee, S.M., Koh, H.J., Song, H., Park, J.W., Lee, W.H., and Huh, T.L. (2004). Role of NADP+-dependent isocitrate dehydrogenase (NADP+-ICDH) on cellular defence against oxidative injury by gamma-rays. International journal of radiation biology *80*, 635-642.

Lee, Y., Kim, K.H., Kim, D.G., Cho, H.J., Kim, Y., Rheey, J., Shin, K., Seo, Y.J., Choi, Y.S., Lee, J.I.*, et al.* (2015). FoxM1 Promotes Stemness and Radio-Resistance of Glioblastoma by Regulating the Master Stem Cell Regulator Sox2. PloS one *10*, e0137703.

Lenoir, W.F., Lim, T.L., and Hart, T. (2018). PICKLES: the database of pooled in-vitro CRISPR knockout library essentiality screens. Nucleic acids research *46*, D776-D780.

Li, F., Lv, B., Liu, Y., Hua, T., Han, J., Sun, C., Xu, L., Zhang, Z., Feng, Z., Cai, Y.*, et al.* (2018). Blocking the CD47-SIRPalpha axis by delivery of anti-CD47 antibody induces antitumor effects in glioma and glioma stem cells. Oncoimmunology *7*, e1391973.

Li, Y.M., Suki, D., Hess, K., and Sawaya, R. (2016). The influence of maximum safe resection of glioblastoma on survival in 1229 patients: Can we do better than gross-total resection? J Neurosurg *124*, 977-988.

Li, Z., Bao, S., Wu, Q., Wang, H., Eyler, C., Sathornsumetee, S., Shi, Q., Cao, Y., Lathia, J., McLendon, R.E.*, et al.* (2009). Hypoxia-inducible factors regulate tumorigenic capacity of glioma stem cells. Cancer cell *15*, 501-513.

Liau, L.M., Ashkan, K., Tran, D.D., Campian, J.L., Trusheim, J.E., Cobbs, C.S., Heth, J.A., Salacz, M., Taylor, S., D'Andre, S.D.*, et al.* (2018). First results on survival from a large Phase 3 clinical trial of an autologous dendritic cell vaccine in newly diagnosed glioblastoma. J Transl Med *16*, 142.

Liau, L.M., Black, K.L., Prins, R.M., Sykes, S.N., DiPatre, P.L., Cloughesy, T.F., Becker, D.P., and Bronstein, J.M. (1999). Treatment of intracranial gliomas with bone marrow-derived dendritic cells pulsed with tumor antigens. J Neurosurg *90*, 1115-1124.

Lim, M., Ye, X., Piotrowski, A.F., Desai, A.S., Ahluwalia, M.S., Walbert, T., Fisher, J.D., Desideri, S., Belcaid, Z., Jackson, C.*, et al.* (2019). Updated phase I trial of anti-LAG-3 or anti-CD137 alone and in combination with anti-PD-1 in patients with recurrent GBM. Journal of Clinical Oncology *37*, 2017-2017.

Lin, M.D., Lee, H.T., Wang, S.C., Li, H.R., Hsien, H.L., Cheng, K.W., Chang, Y.D., Huang, M.L., Yu, J.K., and Chen, Y.H. (2013). Expression of phosphatase of regenerating liver family genes during embryogenesis: an evolutionary developmental analysis among Drosophila, amphioxus, and zebrafish. BMC Dev Biol *13*, 18.

Liu, J., Blake, S.J., Yong, M.C., Harjunpaa, H., Ngiow, S.F., Takeda, K., Young, A., O'Donnell, J.S., Allen, S., Smyth, M.J.*, et al.* (2016a). Improved Efficacy of Neoadjuvant Compared to Adjuvant Immunotherapy to Eradicate Metastatic Disease. Cancer Discov *6*, 1382-1399.

Liu, L., Li, W., Geng, S., Fang, Y., Sun, Z., Hu, H., Liang, Z., and Yan, Z. (2016b). Slit2 and Robo1 expression as biomarkers for assessing prognosis in brain glioma patients. Surg Oncol *25*, 405-410.

Louis, D.N., Perry, A., Reifenberger, G., von Deimling, A., Figarella-Branger, D., Cavenee, W.K., Ohgaki, H., Wiestler, O.D., Kleihues, P., and Ellison, D.W. (2016). The 2016 World Health Organization Classification of Tumors of the Central Nervous System: a summary. Acta neuropathologica *131*, 803-820.

Louis, D.N., Perry, A., Wesseling, P., Brat, D.J., Cree, I.A., Figarella-Branger, D., Hawkins, C., Ng, H.K., Pfister, S.M., Reifenberger, G.*, et al.* (2021). The 2021 WHO Classification of Tumors of the Central Nervous System: a summary. Neuro-oncology *23*, 1231-1251.

Lyratzopoulos, G., Abel, G.A., McPhail, S., Neal, R.D., and Rubin, G.P. (2013). Measures of promptness of cancer diagnosis in primary care: secondary analysis of national audit data on patients with 18 common and rarer cancers. British journal of cancer *108*, 686-690.

MacLeod, G., Bozek, D.A., Rajakulendran, N., Monteiro, V., Ahmadi, M., Steinhart, Z., Kushida, M.M., Yu, H., Coutinho, F.J., Cavalli, F.M.G.*, et al.* (2019). Genome-Wide CRISPR-Cas9 Screens

Expose Genetic Vulnerabilities and Mechanisms of Temozolomide Sensitivity in Glioblastoma Stem Cells. Cell reports *27*, 971-986 e979.

Mair, B., Tomic, J., Masud, S.N., Tonge, P., Weiss, A., Usaj, M., Tong, A.H.Y., Kwan, J.J., Brown, K.R., Titus, E.*, et al.* (2019). Essential Gene Profiles for Human Pluripotent Stem Cells Identify Uncharacterized Genes and Substrate Dependencies. Cell reports *27*, 599-615 e512.

Mair, M.J., Kiesel, B., Feldmann, K., Widhalm, G., Dieckmann, K., Wohrer, A., Mullauer, L., Preusser, M., and Berghoff, A.S. (2021). LAG-3 expression in the inflammatory microenvironment of glioma. J Neurooncol *152*, 533-539.

Manoranjan, B., Chokshi, C., Venugopal, C., Subapanditha, M., Savage, N., Tatari, N., Provias, J.P., Murty, N.K., Moffat, J., Doble, B.W.*, et al.* (2020). A CD133-AKT-Wnt signaling axis drives glioblastoma brain tumor-initiating cells. Oncogene *39*, 1590-1599.

Manoranjan, B., Wang, X., Hallett, R.M., Venugopal, C., Mack, S.C., McFarlane, N., Nolte, S.M., Scheinemann, K., Gunnarsson, T., Hassell, J.A.*, et al.* (2013). FoxG1 interacts with Bmi1 to regulate self-renewal and tumorigenicity of medulloblastoma stem cells. Stem cells *31*, 1266-1277.

Mansfield, A.S., Nevala, W.K., Lieser, E.A., Leontovich, A.A., and Markovic, S.N. (2013). The immunomodulatory effects of bevacizumab on systemic immunity in patients with metastatic melanoma. Oncoimmunology *2*, e24436.

Mao, D.D., Gujar, A.D., Mahlokozera, T., Chen, I., Pan, Y., Luo, J., Brost, T., Thompson, E.A., Turski, A., Leuthardt, E.C.*, et al.* (2015). A CDC20-APC/SOX2 Signaling Axis Regulates Human Glioblastoma Stem-like Cells. Cell reports *11*, 1809-1821.

Maude, S.L., Frey, N., Shaw, P.A., Aplenc, R., Barrett, D.M., Bunin, N.J., Chew, A., Gonzalez, V.E., Zheng, Z., Lacey, S.F.*, et al.* (2014). Chimeric antigen receptor T cells for sustained remissions in leukemia. The New England journal of medicine *371*, 1507-1517.

Mazor, T., Pankov, A., Johnson, B.E., Hong, C., Hamilton, E.G., Bell, R.J.A., Smirnov, I.V., Reis, G.F., Phillips, J.J., Barnes, M.J., *et al.* (2015). DNA Methylation and Somatic Mutations Converge on the Cell Cycle and Define Similar Evolutionary Histories in Brain Tumors. Cancer cell *28*, 307-317.

McBrayer, S.K., Mayers, J.R., DiNatale, G.J., Shi, D.D., Khanal, J., Chakraborty, A.A., Sarosiek, K.A., Briggs, K.J., Robbins, A.K., Sewastianik, T., *et al.* (2018). Transaminase Inhibition by 2-Hydroxyglutarate Impairs Glutamate Biosynthesis and Redox Homeostasis in Glioma. Cell *175*, 101-116 e125.

McCarthy, D.J., Chen, Y., and Smyth, G.K. (2012). Differential expression analysis of multifactor RNA-Seq experiments with respect to biological variation. Nucleic acids research *40*, 4288-4297.

McGranahan, N., Furness, A.J., Rosenthal, R., Ramskov, S., Lyngaa, R., Saini, S.K., Jamal-Hanjani, M., Wilson, G.A., Birkbak, N.J., Hiley, C.T., *et al.* (2016). Clonal neoantigens elicit T cell immunoreactivity and sensitivity to immune checkpoint blockade. Science *351*, 1463-1469.

McQueeney, K.E., Salamoun, J.M., Burnett, J.C., Barabutis, N., Pekic, P., Lewandowski, S.L., Llaneza, D.C., Cornelison, R., Bai, Y., Zhang, Z.Y., *et al.* (2018). Targeting ovarian cancer and endothelium with an allosteric PTP4A3 phosphatase inhibitor. Oncotarget *9*, 8223-8240.

Mertsch, S., Schmitz, N., Jeibmann, A., Geng, J.G., Paulus, W., and Senner, V. (2008). Slit2 involvement in glioma cell migration is mediated by Robo1 receptor. Journal of neuro-oncology *87*, 1-7.

Meyer, M., Reimand, J., Lan, X., Head, R., Zhu, X., Kushida, M., Bayani, J., Pressey, J.C., Lionel, A.C., Clarke, I.D., *et al.* (2015). Single cell-derived clonal analysis of human glioblastoma links functional and genomic heterogeneity. Proceedings of the National Academy of Sciences of the United States of America *112*, 851-856.

Meyers, R.M., Bryan, J.G., McFarland, J.M., Weir, B.A., Sizemore, A.E., Xu, H., Dharia, N.V., Montgomery, P.G., Cowley, G.S., Pantel, S.*, et al.* (2017). Computational correction of copy number effect improves specificity of CRISPR-Cas9 essentiality screens in cancer cells. Nature genetics *49*, 1779-1784.

Miao, H., Choi, B.D., Suryadevara, C.M., Sanchez-Perez, L., Yang, S., De Leon, G., Sayour, E.J., McLendon, R., Herndon, J.E., 2nd, Healy, P.*, et al.* (2014). EGFRvIII-specific chimeric antigen receptor T cells migrate to and kill tumor deposits infiltrating the brain parenchyma in an invasive xenograft model of glioblastoma. PloS one *9*, e94281.

Mitchell, D.A., Batich, K.A., Gunn, M.D., Huang, M.N., Sanchez-Perez, L., Nair, S.K., Congdon, K.L., Reap, E.A., Archer, G.E., Desjardins, A.*, et al.* (2015). Tetanus toxoid and CCL3 improve dendritic cell vaccines in mice and glioblastoma patients. Nature *519*, 366-369.

Mitchell, D.A., Cui, X., Schmittling, R.J., Sanchez-Perez, L., Snyder, D.J., Congdon, K.L., Archer, G.E., Desjardins, A., Friedman, A.H., Friedman, H.S.*, et al.* (2011). Monoclonal antibody blockade of IL-2 receptor alpha during lymphopenia selectively depletes regulatory T cells in mice and humans. Blood *118*, 3003-3012.

Mitchell, D.A., Xie, W., Schmittling, R., Learn, C., Friedman, A., McLendon, R.E., and Sampson, J.H. (2008). Sensitive detection of human cytomegalovirus in tumors and peripheral blood of patients diagnosed with glioblastoma. Neuro Oncol *10*, 10-18.

Moody, C.L., and Wheelhouse, R.T. (2014). The medicinal chemistry of imidazotetrazine prodrugs. Pharmaceuticals *7*, 797-838.

Morton, A.R., Dogan-Artun, N., Faber, Z.J., MacLeod, G., Bartels, C.F., Piazza, M.S., Allan, K.C., Mack, S.C., Wang, X., Gimple, R.C.*, et al.* (2019). Functional Enhancers Shape Extrachromosomal Oncogene Amplifications. Cell *179*, 1330-1341 e1313.

Murty, S., Haile, S.T., Beinat, C., Aalipour, A., Alam, I.S., Murty, T., Shaffer, T.M., Patel, C.B., Graves, E.E., Mackall, C.L.*, et al.* (2020). Intravital imaging reveals synergistic effect of CAR T-cells and radiation therapy in a preclinical immunocompetent glioblastoma model. Oncoimmunology *9*, 1757360.

Nagane, M., Coufal, F., Lin, H., Bogler, O., Cavenee, W.K., and Huang, H.J. (1996). A common mutant epidermal growth factor receptor confers enhanced tumorigenicity on human glioblastoma cells by increasing proliferation and reducing apoptosis. Cancer Res *56*, 5079-5086.

Nagarajan, S., Rao, S.V., Sutton, J., Cheeseman, D., Dunn, S., Papachristou, E.K., Prada, J.G., Couturier, D.L., Kumar, S., Kishore, K.*, et al.* (2020). ARID1A influences HDAC1/BRD4 activity, intrinsic proliferative capacity and breast cancer treatment response. Nature genetics *52*, 187-197.

Neftel, C., Laffy, J., Filbin, M.G., Hara, T., Shore, M.E., Rahme, G.J., Richman, A.R., Silverbush, D., Shaw, M.L., Hebert, C.M.*, et al.* (2019). An Integrative Model of Cellular States, Plasticity, and Genetics for Glioblastoma. Cell *178*, 835-849 e821.

Newcomb, E.W., Lukyanov, Y., Kawashima, N., Alonso-Basanta, M., Wang, S.C., Liu, M., Jure-Kunkel, M., Zagzag, D., Demaria, S., and Formenti, S.C. (2010). Radiotherapy enhances antitumor effect of anti-CD137 therapy in a mouse Glioma model. Radiat Res *173*, 426-432.

Nguemgo Kouam, P., Rezniczek, G.A., Kochanneck, A., Priesch-Grzeszkowiak, B., Hero, T., Adamietz, I.A., and Buhler, H. (2018). Robo1 and vimentin regulate radiation-induced motility of human glioblastoma cells. PloS one *13*, e0198508.

Nobusawa, S., Lachuer, J., Wierinckx, A., Kim, Y.H., Huang, J., Legras, C., Kleihues, P., and Ohgaki, H. (2010). Intratumoral patterns of genomic imbalance in glioblastomas. Brain Pathol *20*, 936-944.

Norden, A.D., Korytowsky, B., You, M., Kim Le, T., Dastani, H., Bobiak, S., and Singh, P. (2019). A Real-World Claims Analysis of Costs and Patterns of Care in Treated Patients with Glioblastoma Multiforme in the United States. J Manag Care Spec Pharm *25*, 428-436.

Noushmehr, H., Weisenberger, D.J., Diefes, K., Phillips, H.S., Pujara, K., Berman, B.P., Pan, F., Pelloski, C.E., Sulman, E.P., Bhat, K.P.*, et al.* (2010). Identification of a CpG island methylator phenotype that defines a distinct subgroup of glioma. Cancer cell *17*, 510-522.

Nutt, C.L., Mani, D.R., Betensky, R.A., Tamayo, P., Cairncross, J.G., Ladd, C., Pohl, U., Hartmann, C., McLaughlin, M.E., Batchelor, T.T.*, et al.* (2003). Gene expression-based classification of malignant gliomas correlates better with survival than histological classification. Cancer research *63*, 1602-1607.

O'Rourke, D.M., Nasrallah, M.P., Desai, A., Melenhorst, J.J., Mansfield, K., Morrissette, J.J.D., Martinez-Lage, M., Brem, S., Maloney, E., Shen, A.*, et al.* (2017). A single dose of peripherally infused EGFRvIII-directed CAR T cells mediates antigen loss and induces adaptive resistance in patients with recurrent glioblastoma. Science translational medicine *9*.

Ohno, M., Ohkuri, T., Kosaka, A., Tanahashi, K., June, C.H., Natsume, A., and Okada, H. (2013). Expression of miR-17-92 enhances anti-tumor activity of T-cells transduced with the anti-EGFRvIII chimeric antigen receptor in mice bearing human GBM xenografts. Journal for immunotherapy of cancer *1*, 21.

Omuro, A., Vlahovic, G., Lim, M., Sahebjam, S., Baehring, J., Cloughesy, T., Voloschin, A., Ramkissoon, S.H., Ligon, K.L., Latek, R.*, et al.* (2018). Nivolumab with or without ipilimumab in patients with recurrent glioblastoma: results from exploratory phase I cohorts of CheckMate 143. Neuro Oncol *20*, 674-686.

Orzan, F., De Bacco, F., Crisafulli, G., Pellegatta, S., Mussolin, B., Siravegna, G., D'Ambrosio, A., Comoglio, P.M., Finocchiaro, G., and Boccaccio, C. (2017). Genetic Evolution of Glioblastoma Stem-Like Cells From Primary to Recurrent Tumor. Stem cells *35*, 2218-2228.

Ostrom, Q.T., Cioffi, G., Waite, K., Kruchko, C., and Barnholtz-Sloan, J.S. (2021). CBTRUS Statistical Report: Primary Brain and Other Central Nervous System Tumors Diagnosed in the United States in 2014-2018. Neuro-oncology *23*, iii1-iii105.

Ostrom, Q.T., Gittleman, H., Xu, J., Kromer, C., Wolinsky, Y., Kruchko, C., and Barnholtz-Sloan, J.S. (2016). CBTRUS Statistical Report: Primary Brain and Other Central Nervous System Tumors Diagnosed in the United States in 2009-2013. Neuro-oncology *18*, v1-v75.

Ozawa, T., Riester, M., Cheng, Y.K., Huse, J.T., Squatrito, M., Helmy, K., Charles, N., Michor, F., and Holland, E.C. (2014). Most human non-GCIMP glioblastoma subtypes evolve from a common proneural-like precursor glioma. Cancer cell *26*, 288-300.

Padfield, E., Ellis, H.P., and Kurian, K.M. (2015). Current Therapeutic Advances Targeting EGFR and EGFRvIII in Glioblastoma. Front Oncol *5*, 5.

Park, J., Shim, J.K., Yoon, S.J., Kim, S.H., Chang, J.H., and Kang, S.G. (2019). Transcriptome profiling-based identification of prognostic subtypes and multi-omics signatures of glioblastoma. Scientific reports *9*, 10555.

Parsons, D.W., Jones, S., Zhang, X., Lin, J.C., Leary, R.J., Angenendt, P., Mankoo, P., Carter, H., Siu, I.M., Gallia, G.L.*, et al.* (2008). An integrated genomic analysis of human glioblastoma multiforme. Science *321*, 1807-1812.

Patel, A.P., Tirosh, I., Trombetta, J.J., Shalek, A.K., Gillespie, S.M., Wakimoto, H., Cahill, D.P., Nahed, B.V., Curry, W.T., Martuza, R.L.*, et al.* (2014). Single-cell RNA-seq highlights intratumoral heterogeneity in primary glioblastoma. Science *344*, 1396-1401.

Pessina, F., Navarria, P., Cozzi, L., Ascolese, A.M., Simonelli, M., Santoro, A., Clerici, E., Rossi, M., Scorsetti, M., and Bello, L. (2017). Maximize surgical resection beyond contrast-enhancing boundaries in newly diagnosed glioblastoma multiforme: is it useful and safe? A single institution retrospective experience. Journal of neuro-oncology *135*, 129-139.

Phillips, H.S., Kharbanda, S., Chen, R., Forrest, W.F., Soriano, R.H., Wu, T.D., Misra, A., Nigro, J.M., Colman, H., Soroceanu, L.*, et al.* (2006). Molecular subclasses of high-grade glioma predict prognosis, delineate a pattern of disease progression, and resemble stages in neurogenesis. Cancer cell *9*, 157-173.

Pituch, K.C., Miska, J., Krenciute, G., Panek, W.K., Li, G., Rodriguez-Cruz, T., Wu, M., Han, Y., Lesniak, M.S., Gottschalk, S.*, et al.* (2018). Adoptive Transfer of IL13Ralpha2-Specific Chimeric Antigen Receptor T Cells Creates a Pro-inflammatory Environment in Glioblastoma. Molecular therapy : the journal of the American Society of Gene Therapy *26*, 986-995.

Platten, M., Bunse, L., Wick, A., Bunse, T., Le Cornet, L., Harting, I., Sahm, F., Sanghvi, K., Tan, C.L., Poschke, I.*, et al.* (2021). A vaccine targeting mutant IDH1 in newly diagnosed glioma. Nature *592*, 463-468.

Prolo, L.M., Li, A., Owen, S.F., Parker, J.J., Foshay, K., Nitta, R.T., Morgens, D.W., Bolin, S., Wilson, C.M., Vega, L.J.*, et al.* (2019). Targeted genomic CRISPR-Cas9 screen identifies MAP4K4 as essential for glioblastoma invasion. Scientific reports *9*, 14020.

Puchalski, R.B., Shah, N., Miller, J., Dalley, R., Nomura, S.R., Yoon, J.G., Smith, K.A., Lankerovich, M., Bertagnolli, D., Bickley, K.*, et al.* (2018). An anatomic transcriptional atlas of human glioblastoma. Science *360*, 660-663.

Qazi, M.A., Vora, P., Venugopal, C., Adams, J., Singh, M., Hu, A., Gorelik, M., Subapanditha, M.K., Savage, N., Yang, J.*, et al.* (2018). Cotargeting Ephrin Receptor Tyrosine Kinases A2 and

A3 in Cancer Stem Cells Reduces Growth of Recurrent Glioblastoma. Cancer research *78*, 5023-5037.

Qazi, M.A., Vora, P., Venugopal, C., McFarlane, N., Subapanditha, M.K., Murty, N.K., Hassell, J.A., Hallett, R.M., and Singh, S.K. (2016). A novel stem cell culture model of recurrent glioblastoma. Journal of neuro-oncology *126*, 57-67.

Reardon, D.A. (2006). Phase II study of pembrolizumab or pembrolizumab plus bevacizumab for recurrent glioblastoma (rGBM) patients. Journal of Clinical Oncology *36*.

Reardon, D.A. (2017). ATIM-12. PHASE 2 STUDY TO EVALUATE THE CLINICAL EFFICACY AND SAFETY OF MEDI4736 (DURVALUMAB [DUR]) IN PATIENTS WITH BEVACIZUMAB (BEV)-REFRACTORY RECURRENT GLIOBLASTOMA (GBM). Neuro Oncol *19*.

Reardon, D.A., Brandes, A.A., Omuro, A., Mulholland, P., Lim, M., Wick, A., Baehring, J., Ahluwalia, M.S., Roth, P., Bahr, O.*, et al.* (2020a). Effect of Nivolumab vs Bevacizumab in Patients With Recurrent Glioblastoma: The CheckMate 143 Phase 3 Randomized Clinical Trial. JAMA Oncol *6*, 1003-1010.

Reardon, D.A., Desjardins, A., Vredenburgh, J.J., O'Rourke, D.M., Tran, D.D., Fink, K.L., Nabors, L.B., Li, G., Bota, D.A., Lukas, R.V.*, et al.* (2020b). Rindopepimut with Bevacizumab for Patients with Relapsed EGFRvIII-Expressing Glioblastoma (ReACT): Results of a Double-Blind Randomized Phase II Trial. Clin Cancer Res *26*, 1586-1594.

Reardon, D.A., Gokhale, P.C., Klein, S.R., Ligon, K.L., Rodig, S.J., Ramkissoon, S.H., Jones, K.L., Conway, A.S., Liao, X., Zhou, J.*, et al.* (2016). Glioblastoma Eradication Following Immune Checkpoint Blockade in an Orthotopic, Immunocompetent Model. Cancer Immunol Res *4*, 124-135.

Reimand, J., Kull, M., Peterson, H., Hansen, J., and Vilo, J. (2007). g:Profiler--a web-based toolset for functional profiling of gene lists from large-scale experiments. Nucleic acids research *35*, W193-200.

Reinartz, R., Wang, S., Kebir, S., Silver, D.J., Wieland, A., Zheng, T., Kupper, M., Rauschenbach, L., Fimmers, R., Shepherd, T.M., *et al.* (2017). Functional Subclone Profiling for Prediction of Treatment-Induced Intratumor Population Shifts and Discovery of Rational Drug Combinations in Human Glioblastoma. Clinical cancer research : an official journal of the American Association for Cancer Research *23*, 562-574.

Reitman, Z.J., Duncan, C.G., Poteet, E., Winters, A., Yan, L.J., Gooden, D.M., Spasojevic, I., Boros, L.G., Yang, S.H., and Yan, H. (2014). Cancer-associated isocitrate dehydrogenase 1 (IDH1) R132H mutation and d-2-hydroxyglutarate stimulate glutamine metabolism under hypoxia. The Journal of biological chemistry *289*, 23318-23328.

Reitman, Z.J., Jin, G., Karoly, E.D., Spasojevic, I., Yang, J., Kinzler, K.W., He, Y., Bigner, D.D., Vogelstein, B., and Yan, H. (2011). Profiling the effects of isocitrate dehydrogenase 1 and 2 mutations on the cellular metabolome. Proceedings of the National Academy of Sciences of the United States of America *108*, 3270-3275.

Rhee, J., Buchan, T., Zukerberg, L., Lilien, J., and Balsamo, J. (2007). Cables links Robo-bound Abl kinase to N-cadherin-bound beta-catenin to mediate Slit-induced modulation of adhesion and transcription. Nature cell biology *9*, 883-892.

Rhee, J., Mahfooz, N.S., Arregui, C., Lilien, J., Balsamo, J., and VanBerkum, M.F. (2002). Activation of the repulsive receptor Roundabout inhibits N-cadherin-mediated cell adhesion. Nature cell biology *4*, 798-805.

Rickman, D.S., Bobek, M.P., Misek, D.E., Kuick, R., Blaivas, M., Kurnit, D.M., Taylor, J., and Hanash, S.M. (2001). Distinctive molecular profiles of high-grade and low-grade gliomas based on oligonucleotide microarray analysis. Cancer research *61*, 6885-6891.

Ritchie, M.E., Phipson, B., Wu, D., Hu, Y., Law, C.W., Shi, W., and Smyth, G.K. (2015). limma powers differential expression analyses for RNA-sequencing and microarray studies. Nucleic acids research *43*, e47.

Rius-Rocabert, S., Garcia-Romero, N., Garcia, A., Ayuso-Sacido, A., and Nistal-Villan, E. (2020). Oncolytic Virotherapy in Glioma Tumors. Int J Mol Sci *21*.

Rizvi, N.A., Hellmann, M.D., Snyder, A., Kvistborg, P., Makarov, V., Havel, J.J., Lee, W., Yuan, J., Wong, P., Ho, T.S.*, et al.* (2015). Cancer immunology. Mutational landscape determines sensitivity to PD-1 blockade in non-small cell lung cancer. Science *348*, 124-128.

Roh, T.H., Kang, S.G., Moon, J.H., Sung, K.S., Park, H.H., Kim, S.H., Kim, E.H., Hong, C.K., Suh, C.O., and Chang, J.H. (2019). Survival benefit of lobectomy over gross-total resection without lobectomy in cases of glioblastoma in the noneloquent area: a retrospective study. J Neurosurg *132*, 895-901.

Romani, M., Pistillo, M.P., and Banelli, B. (2018). Epigenetic Targeting of Glioblastoma. Front Oncol *8*, 448.

Sadelain, M., Brentjens, R., and Riviere, I. (2013). The basic principles of chimeric antigen receptor design. Cancer discovery *3*, 388-398.

Sahebjam, S., Forsyth, P.A., Tran, N.D., Arrington, J.A., Macaulay, R., Etame, A.B., Walko, C.M., Boyle, T., Peguero, E.N., Jaglal, M.*, et al.* (2021). Hypofractionated stereotactic re-irradiation with pembrolizumab and bevacizumab in patients with recurrent high-grade gliomas: results from a phase I study. Neuro Oncol *23*, 677-686.

Salamoun, J.M., McQueeney, K.E., Patil, K., Geib, S.J., Sharlow, E.R., Lazo, J.S., and Wipf, P. (2016). Photooxygenation of an amino-thienopyridone yields a more potent PTP4A3 inhibitor. Organic & biomolecular chemistry *14*, 6398-6402.

Sampson, J.H., Aldape, K.D., Archer, G.E., Coan, A., Desjardins, A., Friedman, A.H., Friedman, H.S., Gilbert, M.R., Herndon, J.E., McLendon, R.E.*, et al.* (2011). Greater chemotherapy-induced lymphopenia enhances tumor-specific immune responses that eliminate EGFRvIII-expressing tumor cells in patients with glioblastoma. Neuro Oncol *13*, 324-333.

Sampson, J.H., Archer, G.E., Mitchell, D.A., Heimberger, A.B., Herndon, J.E., 2nd, Lally-Goss, D., McGehee-Norman, S., Paolino, A., Reardon, D.A., Friedman, A.H.*, et al.* (2009). An epidermal growth factor receptor variant III-targeted vaccine is safe and immunogenic in patients with glioblastoma multiforme. Mol Cancer Ther *8*, 2773-2779.

Sampson, J.H., Choi, B.D., Sanchez-Perez, L., Suryadevara, C.M., Snyder, D.J., Flores, C.T., Schmittling, R.J., Nair, S.K., Reap, E.A., Norberg, P.K.*, et al.* (2014). EGFRvIII mCAR-modified T-cell therapy cures mice with established intracerebral glioma and generates host immunity against tumor-antigen loss. Clinical cancer research : an official journal of the American Association for Cancer Research *20*, 972-984.

Sampson, J.H., Heimberger, A.B., Archer, G.E., Aldape, K.D., Friedman, A.H., Friedman, H.S., Gilbert, M.R., Herndon, J.E., 2nd, McLendon, R.E., Mitchell, D.A.*, et al.* (2010). Immunologic escape after prolonged progression-free survival with epidermal growth factor receptor variant III peptide vaccination in patients with newly diagnosed glioblastoma. J Clin Oncol *28*, 4722-4729.

Sampson, J.H., Maus, M.V., and June, C.H. (2017). Immunotherapy for Brain Tumors. Journal of clinical oncology : official journal of the American Society of Clinical Oncology *35*, 2450-2456.

Sanai, N., Polley, M.Y., McDermott, M.W., Parsa, A.T., and Berger, M.S. (2011). An extent of resection threshold for newly diagnosed glioblastomas. J Neurosurg *115*, 3-8.

Sarkaria, J.N., Hu, L.S., Parney, I.F., Pafundi, D.H., Brinkmann, D.H., Laack, N.N., Giannini, C., Burns, T.C., Kizilbash, S.H., Laramy, J.K.*, et al.* (2018). Is the blood-brain barrier really disrupted in all glioblastomas? A critical assessment of existing clinical data. Neuro-oncology *20*, 184-191.

Schafer, N., Gielen, G.H., Rauschenbach, L., Kebir, S., Till, A., Reinartz, R., Simon, M., Niehusmann, P., Kleinschnitz, C., Herrlinger, U.*, et al.* (2019). Longitudinal heterogeneity in glioblastoma: moving targets in recurrent versus primary tumors. J Transl Med *17*, 96.

Schalper, K.A., Rodriguez-Ruiz, M.E., Diez-Valle, R., Lopez-Janeiro, A., Porciuncula, A., Idoate, M.A., Inoges, S., de Andrea, C., Lopez-Diaz de Cerio, A., Tejada, S.*, et al.* (2019). Neoadjuvant nivolumab modifies the tumor immune microenvironment in resectable glioblastoma. Nat Med *25*, 470-476.

Schumacher, T., Bunse, L., Pusch, S., Sahm, F., Wiestler, B., Quandt, J., Menn, O., Osswald, M., Oezen, I., Ott, M.*, et al.* (2014). A vaccine targeting mutant IDH1 induces antitumour immunity. Nature *512*, 324-327.

Schupper, A.J., Baron, R.B., Cheung, W., Rodriguez, J., Kalkanis, S.N., Chohan, M.O., Andersen, B.J., Chamoun, R., Nahed, B.V., Zacharia, B.E.*, et al.* (2021). 5-Aminolevulinic acid for enhanced surgical visualization of high-grade gliomas: a prospective, multicenter study. J Neurosurg, 1-10.

Schuster, J., Lai, R.K., Recht, L.D., Reardon, D.A., Paleologos, N.A., Groves, M.D., Mrugala, M.M., Jensen, R., Baehring, J.M., Sloan, A.*, et al.* (2015). A phase II, multicenter trial of rindopepimut (CDX-110) in newly diagnosed glioblastoma: the ACT III study. Neuro Oncol *17*, 854-861.

Seeger, M., Tear, G., Ferres-Marco, D., and Goodman, C.S. (1993). Mutations affecting growth cone guidance in Drosophila: genes necessary for guidance toward or away from the midline. Neuron *10*, 409-426.

Sheline, G.E. (1977). Radiation therapy of brain tumors. Cancer *39*, 873-881.

Shiina, S., Ohno, M., Ohka, F., Kuramitsu, S., Yamamichi, A., Kato, A., Motomura, K., Tanahashi, K., Yamamoto, T., Watanabe, R.*, et al.* (2016). CAR T Cells Targeting Podoplanin Reduce Orthotopic Glioblastomas in Mouse Brains. Cancer immunology research *4*, 259-268.

Singh, S.K., Clarke, I.D., Terasaki, M., Bonn, V.E., Hawkins, C., Squire, J., and Dirks, P.B. (2003). Identification of a cancer stem cell in human brain tumors. Cancer research *63*, 5821-5828.

Singh, S.K., Hawkins, C., Clarke, I.D., Squire, J.A., Bayani, J., Hide, T., Henkelman, R.M., Cusimano, M.D., and Dirks, P.B. (2004). Identification of human brain tumour initiating cells. Nature *432*, 396-401.

Skiriute, D., Vaitkiene, P., Saferis, V., Asmoniene, V., Skauminas, K., Deltuva, V.P., and Tamasauskas, A. (2012). MGMT, GATA6, CD81, DR4, and CASP8 gene promoter methylation in glioblastoma. BMC Cancer *12*, 218.

Snuderl, M., Fazlollahi, L., Le, L.P., Nitta, M., Zhelyazkova, B.H., Davidson, C.J., Akhavanfard, S., Cahill, D.P., Aldape, K.D., Betensky, R.A.*, et al.* (2011). Mosaic amplification of multiple receptor tyrosine kinase genes in glioblastoma. Cancer cell *20*, 810-817.

Sockolosky, J.T., Dougan, M., Ingram, J.R., Ho, C.C., Kauke, M.J., Almo, S.C., Ploegh, H.L., and Garcia, K.C. (2016). Durable antitumor responses to CD47 blockade require adaptive immune stimulation. Proc Natl Acad Sci U S A *113*, E2646-2654.

Son, M.J., Woolard, K., Nam, D.H., Lee, J., and Fine, H.A. (2009). SSEA-1 is an enrichment marker for tumor-initiating cells in human glioblastoma. Cell stem cell *4*, 440-452.

Sottoriva, A., Spiteri, I., Piccirillo, S.G., Touloumis, A., Collins, V.P., Marioni, J.C., Curtis, C., Watts, C., and Tavare, S. (2013). Intratumor heterogeneity in human glioblastoma reflects cancer evolutionary dynamics. Proceedings of the National Academy of Sciences of the United States of America *110*, 4009-4014.

Squibb, B.M. (2020). Bristol Myers Squibb Announces Update on Phase 3 CheckMate -548 Trial Evaluating Patients with Newly Diagnosed MGMT-Methylated Glioblastoma Multiforme (Princeton, NJ: Bristol Myers Squibb).

Stupp, R., Hegi, M.E., Mason, W.P., van den Bent, M.J., Taphoorn, M.J., Janzer, R.C., Ludwin, S.K., Allgeier, A., Fisher, B., Belanger, K.*, et al.* (2009). Effects of radiotherapy with concomitant and adjuvant temozolomide versus radiotherapy alone on survival in glioblastoma in a randomised phase III study: 5-year analysis of the EORTC-NCIC trial. The Lancet Oncology *10*, 459-466.

Stupp, R., Mason, W.P., van den Bent, M.J., Weller, M., Fisher, B., Taphoorn, M.J., Belanger, K., Brandes, A.A., Marosi, C., Bogdahn, U.*, et al.* (2005). Radiotherapy plus concomitant and adjuvant temozolomide for glioblastoma. The New England journal of medicine *352*, 987-996.

Subramanian, A., Tamayo, P., Mootha, V.K., Mukherjee, S., Ebert, B.L., Gillette, M.A., Paulovich, A., Pomeroy, S.L., Golub, T.R., Lander, E.S.*, et al.* (2005). Gene set enrichment analysis: a knowledge-based approach for interpreting genome-wide expression profiles. Proceedings of the National Academy of Sciences of the United States of America *102*, 15545-15550.

Suva, M.L., Rheinbay, E., Gillespie, S.M., Patel, A.P., Wakimoto, H., Rabkin, S.D., Riggi, N., Chi, A.S., Cahill, D.P., Nahed, B.V.*, et al.* (2014). Reconstructing and reprogramming the tumor-propagating potential of glioblastoma stem-like cells. Cell *157*, 580-594.

Szerlip, N.J., Pedraza, A., Chakravarty, D., Azim, M., McGuire, J., Fang, Y., Ozawa, T., Holland, E.C., Huse, J.T., Jhanwar, S.*, et al.* (2012). Intratumoral heterogeneity of receptor tyrosine kinases EGFR and PDGFRA amplification in glioblastoma defines subpopulations with distinct growth factor response. Proceedings of the National Academy of Sciences of the United States of America *109*, 3041-3046.

Tang, X., Wang, Y., Huang, J., Zhang, Z., Liu, F., Xu, J., Guo, G., Wang, W., Tong, A., and Zhou, L. (2021). Administration of B7-H3 targeted chimeric antigen receptor-T cells induce regression of glioblastoma. Signal Transduct Target Ther *6*, 125.

Tang, Z., Li, C., Kang, B., Gao, G., Li, C., and Zhang, Z. (2017). GEPIA: a web server for cancer and normal gene expression profiling and interactive analyses. Nucleic acids research *45*, W98-W102.

Toledo, C.M., Ding, Y., Hoellerbauer, P., Davis, R.J., Basom, R., Girard, E.J., Lee, E., Corrin, P., Hart, T., Bolouri, H.*, et al.* (2015). Genome-wide CRISPR-Cas9 Screens Reveal Loss of Redundancy between PKMYT1 and WEE1 in Glioblastoma Stem-like Cells. Cell reports *13*, 2425-2439.

Tomihara, H., Carbone, F., Perelli, L., Huang, J.K., Soeung, M., Rose, J.L., Robinson, F.S., Lissanu Deribe, Y., Feng, N., Takeda, M.*, et al.* (2021). Loss of ARID1A Promotes Epithelial-Mesenchymal Transition and Sensitizes Pancreatic Tumors to Proteotoxic Stress. Cancer research *81*, 332-343.

Touat, M., Li, Y.Y., Boynton, A.N., Spurr, L.F., Iorgulescu, J.B., Bohrson, C.L., Cortes-Ciriano, I., Birzu, C., Geduldig, J.E., Pelton, K.*, et al.* (2020). Mechanisms and therapeutic implications of hypermutation in gliomas. Nature *580*, 517-523.

Umphlett, M., Shea, S., Tome-Garcia, J., Zhang, Y., Hormigo, A., Fowkes, M., Tsankova, N.M., and Yong, R.L. (2020). Widely metastatic glioblastoma with BRCA1 and ARID1A mutations: a case report. BMC Cancer *20*, 47.

Urwyler, O., Izadifar, A., Vandenbogaerde, S., Sachse, S., Misbaer, A., and Schmucker, D. (2019). Branch-restricted localization of phosphatase Prl-1 specifies axonal synaptogenesis domains. Science *364*.

Vaddepally, R.K., Kharel, P., Pandey, R., Garje, R., and Chandra, A.B. (2020). Review of Indications of FDA-Approved Immune Checkpoint Inhibitors per NCCN Guidelines with the Level of Evidence. Cancers (Basel) *12*.

Vargas Lopez, A.J. (2021). Glioblastoma in adults: a Society for Neuro-Oncology (SNO) and European Society of Neuro-Oncology (EANO) consensus review on current management and future directions. Neuro-oncology *23*, 502-503.

Venugopal, C., Hallett, R., Vora, P., Manoranjan, B., Mahendram, S., Qazi, M.A., McFarlane, N., Subapanditha, M., Nolte, S.M., Singh, M.*, et al.* (2015). Pyrvinium Targets CD133 in Human Glioblastoma Brain Tumor-Initiating Cells. Clinical cancer research : an official journal of the American Association for Cancer Research *21*, 5324-5337.

Venugopal, C., Li, N., Wang, X., Manoranjan, B., Hawkins, C., Gunnarsson, T., Hollenberg, R., Klurfan, P., Murty, N., Kwiecien, J.*, et al.* (2012). Bmi1 marks intermediate precursors during differentiation of human brain tumor initiating cells. Stem cell research *8*, 141-153.

Verhaak, R.G., Hoadley, K.A., Purdom, E., Wang, V., Qi, Y., Wilkerson, M.D., Miller, C.R., Ding, L., Golub, T., Mesirov, J.P.*, et al.* (2010). Integrated genomic analysis identifies clinically relevant subtypes of glioblastoma characterized by abnormalities in PDGFRA, IDH1, EGFR, and NF1. Cancer cell *17*, 98-110.

von Roemeling, C.A., Wang, Y., Qie, Y., Yuan, H., Zhao, H., Liu, X., Yang, Z., Yang, M., Deng, W., Bruno, K.A.*, et al.* (2020). Therapeutic modulation of phagocytosis in glioblastoma can activate both innate and adaptive antitumour immunity. Nat Commun *11*, 1508.

Vora, P., Venugopal, C., Salim, S.K., Tatari, N., Bakhshinyan, D., Singh, M., Seyfrid, M., Upreti, D., Rentas, S., Wong, N.*, et al.* (2020). The Rational Development of CD133-Targeting Immunotherapies for Glioblastoma. Cell stem cell *26*, 832-844 e836.

Waitkus, M.S., Pirozzi, C.J., Moure, C.J., Diplas, B.H., Hansen, L.J., Carpenter, A.B., Yang, R., Wang, Z., Ingram, B.O., Karoly, E.D.*, et al.* (2018). Adaptive Evolution of the GDH2 Allosteric Domain Promotes Gliomagenesis by Resolving IDH1(R132H)-Induced Metabolic Liabilities. Cancer research *78*, 36-50.

Walker, M.D., Strike, T.A., and Sheline, G.E. (1979). An analysis of dose-effect relationship in the radiotherapy of malignant gliomas. Int J Radiat Oncol Biol Phys *5*, 1725-1731.

Walter, F.M., Penfold, C., Joannides, A., Saji, S., Johnson, M., Watts, C., Brodbelt, A., Jenkinson, M.D., Price, S.J., Hamilton, W.*, et al.* (2019). Missed opportunities for diagnosing brain tumours in primary care: a qualitative study of patient experiences. Br J Gen Pract *69*, e224-e235.

Wang, D., Aguilar, B., Starr, R., Alizadeh, D., Brito, A., Sarkissian, A., Ostberg, J.R., Forman, S.J., and Brown, C.E. (2018a). Glioblastoma-targeted CD4+ CAR T cells mediate superior antitumor activity. JCI Insight *3*.

Wang, J., Cazzato, E., Ladewig, E., Frattini, V., Rosenbloom, D.I., Zairis, S., Abate, F., Liu, Z., Elliott, O., Shin, Y.J.*, et al.* (2016). Clonal evolution of glioblastoma under therapy. Nature genetics *48*, 768-776.

Wang, Q., Hu, B., Hu, X., Kim, H., Squatrito, M., Scarpace, L., deCarvalho, A.C., Lyu, S., Li, P., Li, Y.*, et al.* (2018b). Tumor Evolution of Glioma-Intrinsic Gene Expression Subtypes Associates with Immunological Changes in the Microenvironment. Cancer cell *33*, 152.

Wang, Q., Hu, B., Hu, X., Kim, H., Squatrito, M., Scarpace, L., deCarvalho, A.C., Lyu, S., Li, P., Li, Y.*, et al.* (2017). Tumor Evolution of Glioma-Intrinsic Gene Expression Subtypes Associates with Immunological Changes in the Microenvironment. Cancer cell *32*, 42-56 e46.

Wang, Z., Chen, K., Jia, Y., Chuang, J.-C., Sun, X., Lin, Y.-H., Celen, C., Li, L., Huang, F., Liu, X.*, et al.* (2020). Dual ARID1A/ARID1B loss leads to rapid carcinogenesis and disruptive redistribution of BAF complexes. Nature Cancer *1*, 909-922.

Watkins, S., Robel, S., Kimbrough, I.F., Robert, S.M., Ellis-Davies, G., and Sontheimer, H. (2014). Disruption of astrocyte-vascular coupling and the blood-brain barrier by invading glioma cells. Nature communications *5*, 4196.

Wei, S.C., Duffy, C.R., and Allison, J.P. (2018). Fundamental Mechanisms of Immune Checkpoint Blockade Therapy. Cancer discovery *8*, 1069-1086.

Weller, M., Butowski, N., Tran, D.D., Recht, L.D., Lim, M., Hirte, H., Ashby, L., Mechtler, L., Goldlust, S.A., Iwamoto, F.*, et al.* (2017). Rindopepimut with temozolomide for patients with newly diagnosed, EGFRvIII-expressing glioblastoma (ACT IV): a randomised, double-blind, international phase 3 trial. The Lancet Oncology *18*, 1373-1385.

Weller, M., van den Bent, M., Preusser, M., Le Rhun, E., Tonn, J.C., Minniti, G., Bendszus, M., Balana, C., Chinot, O., Dirven, L.*, et al.* (2021). EANO guidelines on the diagnosis and treatment of diffuse gliomas of adulthood. Nature reviews Clinical oncology *18*, 170-186.

Wen, P.Y., Weller, M., Lee, E.Q., Alexander, B.M., Barnholtz-Sloan, J.S., Barthel, F.P., Batchelor, T.T., Bindra, R.S., Chang, S.M., Chiocca, E.A.*, et al.* (2020). Glioblastoma in adults: a

Society for Neuro-Oncology (SNO) and European Society of Neuro-Oncology (EANO) consensus review on current management and future directions. Neuro-oncology *22*, 1073-1113.

Whitfield, B.T., and Huse, J.T. (2022). Classification of adult-type diffuse gliomas: Impact of the World Health Organization 2021 update. Brain Pathol, e13062.

Willingham, S.B., Volkmer, J.P., Gentles, A.J., Sahoo, D., Dalerba, P., Mitra, S.S., Wang, J., Contreras-Trujillo, H., Martin, R., Cohen, J.D.*, et al.* (2012). The CD47-signal regulatory protein alpha (SIRPa) interaction is a therapeutic target for human solid tumors. Proc Natl Acad Sci U S A *109*, 6662-6667.

Wills, M.R., Carmichael, A.J., Mynard, K., Jin, X., Weekes, M.P., Plachter, B., and Sissons, J.G. (1996). The human cytotoxic T-lymphocyte (CTL) response to cytomegalovirus is dominated by structural protein pp65: frequency, specificity, and T-cell receptor usage of pp65-specific CTL. J Virol *70*, 7569-7579.

Wong, K., Ren, X.R., Huang, Y.Z., Xie, Y., Liu, G., Saito, H., Tang, H., Wen, L., Brady-Kalnay, S.M., Mei, L.*, et al.* (2001). Signal transduction in neuronal migration: roles of GTPase activating proteins and the small GTPase Cdc42 in the Slit-Robo pathway. Cell *107*, 209-221.

Wu, W., Wong, K., Chen, J., Jiang, Z., Dupuis, S., Wu, J.Y., and Rao, Y. (1999). Directional guidance of neuronal migration in the olfactory system by the protein Slit. Nature *400*, 331-336.

Yan, H., Parsons, D.W., Jin, G., McLendon, R., Rasheed, B.A., Yuan, W., Kos, I., Batinic-Haberle, I., Jones, S., Riggins, G.J.*, et al.* (2009). IDH1 and IDH2 mutations in gliomas. The New England journal of medicine *360*, 765-773.

Yang, M., Tang, X., Zhang, Z., Gu, L., Wei, H., Zhao, S., Zhong, K., Mu, M., Huang, C., Jiang, C.*, et al.* (2020). Tandem CAR-T cells targeting CD70 and B7-H3 exhibit potent preclinical activity against multiple solid tumors. Theranostics *10*, 7622-7634.

Yi, Z., Prinzing, B.L., Cao, F., Gottschalk, S., and Krenciute, G. (2018). Optimizing EphA2-CAR T Cells for the Adoptive Immunotherapy of Glioma. Mol Ther Methods Clin Dev *9*, 70-80.

Yiin, J.J., Hu, B., Jarzynka, M.J., Feng, H., Liu, K.W., Wu, J.Y., Ma, H.I., and Cheng, S.Y. (2009). Slit2 inhibits glioma cell invasion in the brain by suppression of Cdc42 activity. Neuro-oncology *11*, 779-789.

Ypsilanti, A.R., Zagar, Y., and Chedotal, A. (2010). Moving away from the midline: new developments for Slit and Robo. Development *137*, 1939-1952.

Yu, G., Wang, L.G., Han, Y., and He, Q.Y. (2012). clusterProfiler: an R package for comparing biological themes among gene clusters. OMICS *16*, 284-287.

Yu, K., Hu, Y., Wu, F., Guo, Q., Qian, Z., Hu, W., Chen, J., Wang, K., Fan, X., Wu, X.*, et al.* (2020). Surveying brain tumor heterogeneity by single-cell RNA-sequencing of multi-sector biopsies. Natl Sci Rev *7*, 1306-1318.

Zbinden, M., Duquet, A., Lorente-Trigos, A., Ngwabyt, S.N., Borges, I., and Ruiz i Altaba, A. (2010). NANOG regulates glioma stem cells and is essential in vivo acting in a cross-functional network with GLI1 and p53. The EMBO journal *29*, 2659-2674.

Zehir, A., Benayed, R., Shah, R.H., Syed, A., Middha, S., Kim, H.R., Srinivasan, P., Gao, J., Chakravarty, D., Devlin, S.M.*, et al.* (2017). Mutational landscape of metastatic cancer revealed from prospective clinical sequencing of 10,000 patients. Nature medicine *23*, 703-713.

Zeng, J., See, A.P., Phallen, J., Jackson, C.M., Belcaid, Z., Ruzevick, J., Durham, N., Meyer, C., Harris, T.J., Albesiano, E.*, et al.* (2013). Anti-PD-1 blockade and stereotactic radiation produce long-term survival in mice with intracranial gliomas. Int J Radiat Oncol Biol Phys *86*, 343-349.

Zhang, J., Liu, X., Bell, A., To, R., Baral, T.N., Azizi, A., Li, J., Cass, B., and Durocher, Y. (2009). Transient expression and purification of chimeric heavy chain antibodies. Protein Expr Purif *65*, 77-82.

Zhang, J., Sai, K., Wang, X.L., Ye, S.Q., Liang, L.J., Zhou, Y., Chen, Z.J., Hu, W.M., and Liu, J.M. (2020). Tim-3 Expression and MGMT Methylation Status Association With Survival in Glioblastoma. Front Pharmacol *11*, 584652.

Zhang, M., Hutter, G., Kahn, S.A., Azad, T.D., Gholamin, S., Xu, C.Y., Liu, J., Achrol, A.S., Richard, C., Sommerkamp, P.*, et al.* (2016). Anti-CD47 Treatment Stimulates Phagocytosis of Glioblastoma by M1 and M2 Polarized Macrophages and Promotes M1 Polarized Macrophages In Vivo. PLoS One *11*, e0153550.

Zhang, X., Chen, W., Fan, J., Wang, S., Xian, Z., Luan, J., Li, Y., Wang, Y., Nan, Y., Luo, M.*, et al.* (2018a). Disrupting CD47-SIRPalpha axis alone or combined with autophagy depletion for the therapy of glioblastoma. Carcinogenesis *39*, 689-699.

Zhang, X., Fan, J., Wang, S., Li, Y., Wang, Y., Li, S., Luan, J., Wang, Z., Song, P., Chen, Q.*, et al.* (2017). Targeting CD47 and Autophagy Elicited Enhanced Antitumor Effects in Non-Small Cell Lung Cancer. Cancer Immunol Res *5*, 363-375.

Zhang, X., Wang, S., Nan, Y., Fan, J., Chen, W., Luan, J., Wang, Y., Liang, Y., Li, S., Tian, W.*, et al.* (2018b). Inhibition of autophagy potentiated the anti-tumor effects of VEGF and CD47 bispecific therapy in glioblastoma. Appl Microbiol Biotechnol *102*, 6503-6513.

Zhao, J., Chen, A.X., Gartrell, R.D., Silverman, A.M., Aparicio, L., Chu, T., Bordbar, D., Shan, D., Samanamud, J., Mahajan, A.*, et al.* (2019). Immune and genomic correlates of response to anti-PD-1 immunotherapy in glioblastoma. Nature medicine *25*, 462-469.

Zheng, H., Ying, H., Yan, H., Kimmelman, A.C., Hiller, D.J., Chen, A.J., Perry, S.R., Tonon, G., Chu, G.C., Ding, Z.*, et al.* (2008). p53 and Pten control neural and glioma stem/progenitor cell renewal and differentiation. Nature *455*, 1129-1133.